CEPC New Physics Potentials

Prepared for the CEPC BSM white paper

CEPC BSM Physics Study Group

CONTRIBUTORS (TO BE UPDATED)

ABSTRACT (XUAI, ZHEN)

Circular Electron Positron Collider (CEPC) is a large-scale, next-generation collider facility that can probe electroweak scale physics in a new and comprehensive manner, through copious productions of the Higgs, Z, and W bosons and its upgradable to run above the $t\bar{t}$ threshold. Beyond high-precision the Standard Model (SM) measurements, CEPC has also a great potential for direct beyond the SM (BSM) physics searches. This document describes the corresponding BSM physics potential at CEPC.

CONTENTS

I. EXECUTIVE SUMMARY (ZHAO LI)

Discovered in 2012 by the ATLAS and CMS Collaborations at the Large Hadron Collider (LHC), the Higgs boson is crucial to the Standard Model (SM). Exploring into Higgs precision measurements is essential for improving our understanding of crucial phenomena, such as the origins of the electroweak scale, the characteristics of the electroweak phase transition, and the reasons behind the matter-antimatter imbalance in the universe. Furthermore, the Higgs boson serves as a gateway to exploring unknown aspects of physics, including dark matter and its dark sector, heavy sterile neutrinos, among other areas. Each of the new phenomena may guide us to certain new mechanics beyond the SM. As shown in Fig.1, for instance, the investigation on the electroweak symmetry breaking and the origin of elementary mass may reveal the supersymmetric extension or more complicated Higgs potential with additional Higgs bosons. An electron-positron Higgs factory, in comparison to the LHC, offers vital and complementary insights that could significantly broaden our comprehension of this mysterious particle and contribute to resolving the aforementioned fundamental questions. Consequently, it is considered a top priority among the various future collider projects proposed.

Circular Electron-Positron Collider (CEPC) is a proposed high-energy lepton collider, aimed at operating across multiple center of mass energies. This facility is designed as a versatile platform for exploring the physics beyond what the SM currently explains. It is anticipated to play a crucial role in investigating exotic Higgs boson decays and other particle phenomena, potentially revealing new knowledge about the new physics, e.g. supersymmetry (SUSY) and dark sectors of physics. Moreover, the CEPC's advanced capabilities are set to facilitate detailed investigations into light electroweakinos and sleptons, elements vital for a better understanding of SUSY. These studies are expected to complement those at the LHC, offering fresh perspectives on the search for new physics. The collider also promises a conducive setting for exploring dark matter candidates and particles within the dark sector, which could revolutionize our comprehension of the universe. Additionally, CEPC is also capable of detecting particles with long lifetimes, offering insights into critical issues like neutrino mass and the origins of matter over antimatter. The CEPC will examine flavor-changing processes, highly indicative of new physics, providing indirect evidence that could challenge or confirm theories extending beyond the SM. BSM studies at CEPC also help to

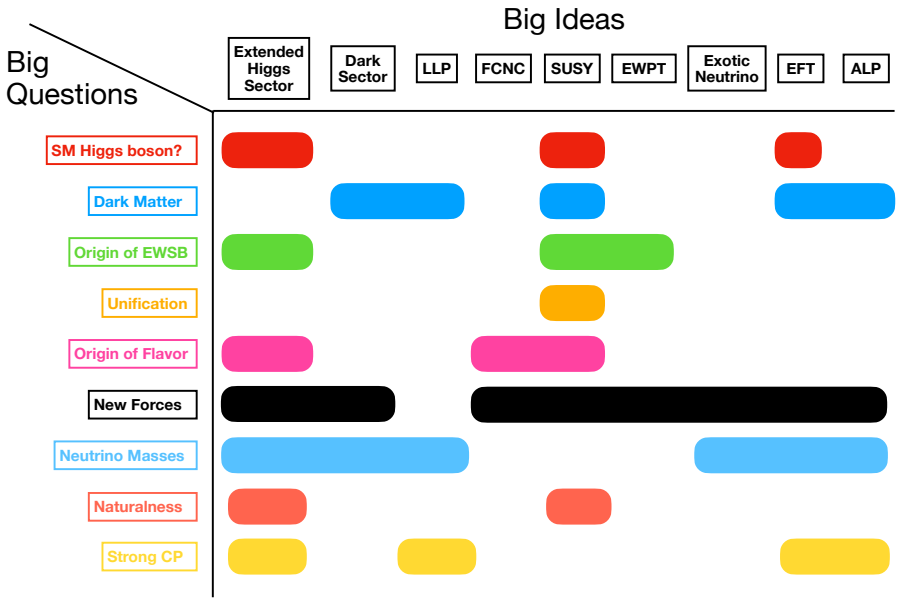

FIG. 1: Overlap between the questions and ideas.

probe the nature of the electroweak phase transition, a phenomenon crucial to our understanding of the universe and the asymmetry between matter and antimatter. Beyond the above, CEPC is set to contribute significantly to the study of neutrino properties, potentially linking to broader theories of leptogenesis and dark matter. New physics searches at CEPC can also explore a spectrum of unconventional scenarios, such as axion-like particles and variations in lepton behavior, with extensive implications for physics beyond the SM. The data collected by the CEPC will be vital for comprehensive analyses, refining and narrowing down the possibilities within various theoretical frameworks, including the Standard Model Effective Field Theory (SMEFT), Two-Higgs-Doublet Model (2HDM), and supersymmetry.

In summary, the CEPC stands as a groundbreaking advancement in particle physics, ready to reveal new particles and interactions that could fundamentally alter our understanding of the universe. With its high-precision measurements, clean experimental conditions, and flexibility in energy levels, CEPC emerges as a powerful instrument for pushing the boundaries of our knowledge in particle physics and addressing some of the most challenging questions in the field.

II. INTRODUCTION (YU GAO)

The Higgs boson is central to many mysteries of the Standard Model (SM) of particle physics, such as the scale of the electroweak unification, the nature of the electroweak phase transition, the flavor structure of fermions and so on. The Higgs field is also deeply connected with many fundamental phenomena beyond the Standard Model, such as the asymmetry of matter and anti-matter in the Universe, the presence of dark matter and dark energy, and the mechanism for cosmic inflation. The 2012 discovery of the Higgs boson completed the last piece in the jigsaw puzzle of the SM's fundamental particle spectrum, and it offers an extremely powerful probe for Higgs boson related mysteries and phenomena. A Higgs factory that can measure the properties of the Higgs boson to an unprecedented precision is vital for this exploration.

The LHC has so far served as a powerful Higgs factory. The high luminosity run of the LHC (HL-LHC) is projected to ultimately produce 100 million Higgs bosons. However, proton-proton collision has large backgrounds and theoretical/systematical uncertainties, and the typical accuracy of the Higgs property at the HL-LHC are expected to be limited to a few percent [1].

In comparison to the LHC, an electron-positron colliders will have significant advantages in Higgs boson measurements. An electron-positron collider is by nature free of QCD backgrounds. The ratio of the Higgs signal versus the SM background is about 7-8 orders of magnitude higher than that at the HL-LHC. An electron-positron collider can product precise and manipulable initial states that help to determine the the Higgs boson's decay width and its couplings. Several future electron-positron colliders have been proposed, including the International Linear Collider (ILC) [2], the Compact Linear Collider (CLIC) [3], the Future Circular Collider (FCC) [4], and the Circular Electron Positron Collider (CEPC) [5, 6]. At the same time, a number of alternative possibilities are under consideration, e.g. a 125 GeV Muon collider [7], C3 [8], ReliC [9], CERC [10], etc.

The CEPC is proposed by the High Energy Physics community immediately after the Higgs boson was discovered. The CEPC working group initially kicked off in September of 2013. In the year 2015, the CEPC working group presented the pre-CDR [5, 6] as the first milestone of CEPC study. Intensive R&D and physics study in the following years led to the 2018 delivery of the CEPC Conceptual Design Report (CDR) [11], reporting no show-

stoppers identified for this gigantic machine. In 2023, the Accelerator TDR was released[12], demonstrating that technology is ready for construction.

The CEPC is designed to host a main circular ring with a total circumference of 100 kilometers. The facility is designed to operate at several benchmark center-of-mass energies: $E_{\mathrm{CM}} = 91.2$ GeV as a Z factory, $E_{\mathrm{CM}} \simeq 160$ GeV for W boson pair production threshold and $E_{\mathrm{CM}} = 240$ GeV as a Higgs factory. The CEPC center-of-mass energy is capable of upgrading to 360 GeV, enabling $t\bar{t}$ pair production. Considering future upgrades, the collider's underground tunnel will have sufficient room to host both the CEPC and the SPPC [13].

The CEPC CDR envisioned the collider to operate with two main detectors. A ten-year nominal operation plan delivers the total integrated luminosities of 16, 2.6, and 5.6 ab^{-1} for Z-pole, WW, and Higgs factory runs, respectively. In terms of event yield, the CEPC will produce approximately one trillion Z bosons, 100 million W bosons, and over one million Higgs bosons. In addition, billions of bottom quarks, charm quarks, and tau-leptons will also be produced via Z boson decays, making the CEPC also a B-factory and a tau-charm factory.

At this date, the CEPC accelerator study has entered the Technical Design Report (TDR) phase, supervised by CEPC International Advisory Committee (IAC). Essential technologies in the core accelerator systems are being developed and validated, including high-quality Superconducting Radio-Frequency (SRF) systems, Machine-Detector Interface (MDI), high precision magnets for the booster and collider rings, vacuum systems, and so on. Several accelerator prototypes have been produced and validated, achieving or surpassing the required performances. These developments result in an updated nominal run plan for the CEPC, shown in Figure 2. Currently, the CEPC Study group is moving forward toward a project approval around the year 2027.

The CEPC adopts a phased strategy for achieving both its construction and performance goals. The baseline target will be operating at the center-of-mass energy from the Z pole up to 240 GeV, with the maximal synchrotron radiation power per beam at 30 MW. After upgrading the power supply and the heat load capability of the cooling system, the maximal synchrotron radiation power per beam will increase from 30 MW to 50 MW, increasingly the instantaneous luminosity linearly. Ultimately, the center-of-mass energy can raise to 360 GeV by increasing the RF cavities.

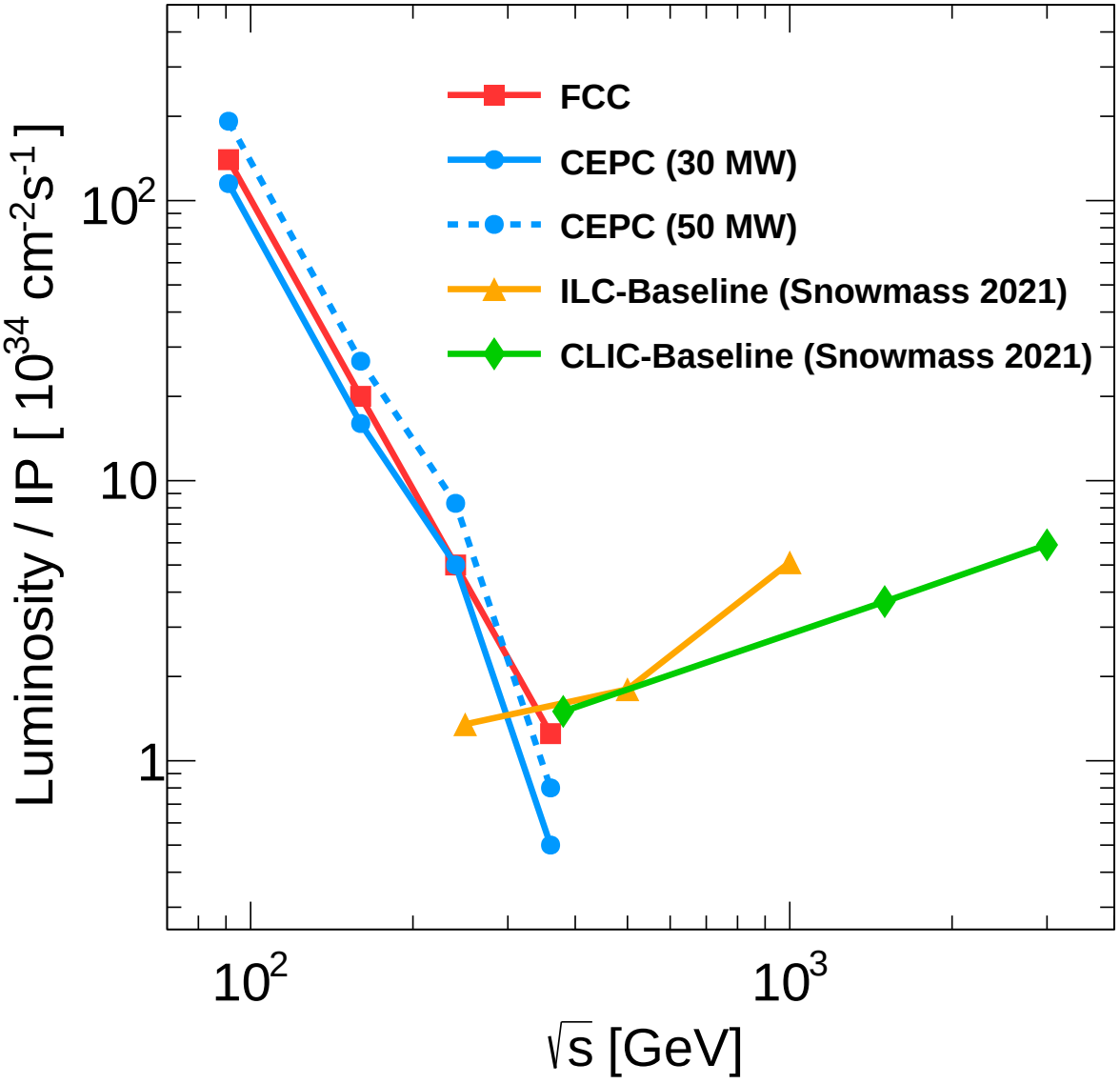

FIG. 2: The updated run plan of the CEPC, with the baseline and upgrade shown in solid and dashed blue curves, respectively. The run plans for several other proposals of the e^+e^- colliders are also shown for comparison. See [14] for details.

A new data-taking scenario is also being developed from the upgraded performance of the CEPC accelerator, emphasizing on the scientific goals of a Higgs and Z factory, as summarized in Table I. The study aims at ten years of data-taking at $E_{\rm CM} = 240$ GeV with two interaction points (IPs), accumulating 20 ab^{-1} worth of integrated luminosity and producing 4 million Higgs bosons. It also plans to operate for at least two years near the Z

Operation mode	Z factory	WW threshold	Higgs factory	$t\bar{t}$
$\sqrt{s}$ (GeV)	91.2	160	240	360
Run time (year)	2	1	10	5
Instantaneous luminosity ($10^{34}cm^{-2}s^{-1}$, per IP)	191.7	26.6	8.3	0.83
Integrated luminosity (ab^{-1}, 2 IPs)	100	6	20	1
Event yields	3×10^{12}	1×10^{8}	4×10^{6}	5×10^{5}

TABLE I: Nominal CEPC operation scheme, and the physics yield, of four different modes. See [14] for details.

pole with an integrated luminosity of 100 ab^{-1}. About one year will be devoted to the WW threshold scan, providing MeV level accuracy on the W boson mass and decay width. After the high energy upgrade, the CEPC will be operated for at least five years at a 360 GeV center-of-mass energy with a 1 ab^{-1} integrated luminosity. About 500 thousand $t\bar{t}$ events and 150 thousand inclusive Higgs events will be produced during this run. In addition, a possible expansion to 4 interaction points is also under active investigation, so that the collision statistics can potentially be further enhanced.

The CEPC Physics study groups have continued to explore the scientific potential, focusing on a wide range of physics topics, including Higgs precision measurements, precise electroweak measurements, flavor physics, QCD-related measurements, and new physics searches. Physics studies identified a handful of critical detector requirements, quantified its impact on different physics benchmarks, and brought up clear performance goals for the CEPC detector design. To name a few, such requirements include the separation of final state particles, precise reconstruction of energy/momentum for different species of final state particles, the identification of physics objects in high-multiplicity events, good calibration of beam energy and instant luminosity, and so on. With these demands from physics study, the CEPC detector group dedicated a series of detector R&D programs to the optimization between achieving physics requirements and leveraging the latest detector technology.

The main body of this white paper is dedicated to the new physics potential at the

FIG. 3: A cartoon of new physics involvement at the CEPC.

CEPC. A broad range of new physics topics will be covered, and our goal is to explore the kaleidoscope of new physics models, and specify their search strategy and projected discovery potential at the CEPC. Fig. 3 shows a cartoon of the major new physics studies in this white paper, and detailed reviews will be presented in the following sections.

Aiming at SM electroweak test as a central task, the CEPC is designed with world-leading performance in the precision measurement of the Higgs potential. Beyond the Standard Model searches can benefit immensely from the CEPC's precision in measuring the decay of the Higgs boson, Z boson and the top quark. Section provides a comprehensive review of exotic $h/Z/t$ decay sensitivities at the CEPC and the expected sensitivity on non-SM Higgs potentials. Supersymmetry, dark sector motivated signals, and the decay channels yielding long-lived particles are emphasized as benchmark scenarios of particular interest. Cross-check measurements on potential Higgs-like hints from existing LHC results are also discussed.

Supersymmetry provides an elegant framework to answer the SM's gauge hierarchy problem and has been extensively searched for by existing colliders. The CEPC offers search

windows on many SUSY scenarios that are difficult for higher energy hadronic collisions. In Section VII, we present the studies on the CEPC's direct search sensitivity on less massive SUSY electroweakinos and charged sleptons, where robust improvements on existing limits can be expected. It is also shown that SUSY-induced exotic channels with large missing energy and a diphoton signal yield strong limits on multi-TeV selectrons, much heavier than the CEPC center-of-mass energy. Relatively light sleptons are of strong interest due to their potential role in explaining the recent muon $g-2$ excess, and their synergy with the CEPC sensitivity is discussed in detail. The projected limits from ILC/CLIC SUSY search are also included for comparison.

Dark sector and dark matter can be revealed via searches involving missing momentum, and dark sector models with leptonic and electroweak connections to the SM are of particular interest. The CEPC is designed with state-of-art detectors and will offers excellent reconstruction of missing energy/momentum. In Section V, we present the recent process on selected dark matter/sector models and their studies for the designed high luminosity at Z-pole, Higgs-factory and 360 GeV runs of the CEPC. The projected sensitivities have been provided for a number of such models, e.g. lepton-portal dark sectors, neutrino and electromagnetically interacting dark particles, leptophilic dark matter, visible in Z-decays, etc.

Long-lived particles (LLPs) have risen to a heated collider search target recently. The LLP scenario typically features a massive BSM particle with a much prolonged lifetime due to its near-degenerate mass to another particle, or highly suppressed couplings, and it can leave a novel signal inside the collider's detectors. In Section VI, we first briefly review the computation methodology for LLP production, and then we proceed to discuss the projected sensitivities with the main detector, proposed far detectors, and the beam dump. LLPs are predicted in many BSM theories, and LLP searches during Higgs and Z boson decay are important benchmark scenarios at the CEPC. Dedicated sensitivity studies are presented for supersymmetry, vector-like lepton extended models, axion-like particles, extra neutral gauge bosons, etc.

The Z-pole run of CEPC can produce large samples of flavored hadrons and leptons, such as B, D mesons and τ leptons, which offer a powerful measurement of new physics with flavored couplings. A more comprehensive review of CEPC's flavor physics is presented in a dedicated white paper. In Section VIII of this document we summarize the CEPC's

potential in new physics search via flavor portal. Important BSM search aspects include potential corrections to the Cabibbo–Kobayashi–Maskawa matrix, testing the presence of flavor-changing neutral current, violation of lepton flavor universality, etc. Precision testing on the flavor symmetries of the SM can test new physics effects from a high energy scale. We include recent studies on charged lepton flavor violation, b, c-hadron decays, and the search for light BSM degree of freedom during flavor transitions.

Encouraged by progress in gravitational wave observations, high-energy phase transitions during the Early Universe gained much popularity in recent years. The nature of the electroweak phase transition sensitively depends on the details of the Higgs potential, and the future colliders test of the CEPC offers a unique cross-check on our Universe's early phase-transition history. One of the essential questions to answer is whether the transition is a cross-over like in the vanilla SM, or it may undergo a more violent process, esp. type-I transition with bubble formation and contribute nontrivially to the cosmic baryon asymmetry, stochastic gravitational wave background, etc. It is shown that the CEPC's precision can test Higgs potentials that generate visible signals for future gravitational wave experiments. In Section IX we list the crucial measurements for electroweak phase transition, including the Zh production cross-section, Higgs decay width, and its decay branching ratios, which are very sensitive to new physics corrections to the Higgs potential.

Neutrino oscillation provides a clear indication of physics beyond the Standard Model, such as the seesaw mechanism. The precision of the CEPC will offer powerful tests for the underlying neutrino models. Section X discusses the CEPC's advantage in neutrino-related searches and the potential connection to leptogenesis. Relevant scenarios include the heavy neutrino search at the CEPC's main/far detectors and the beam dump, promptly decaying heavy neutrinos with high lepton multiplicity and visible lepton-number violation, active-sterile neutrino transition and non-standard effective neutrino interactions.

In addition, the CEPC features a unique opportunity for even more exotic physics searches. In particular, the low hadronic background and high sensitivity to soft leptons, photons, and jets empower careful investigation of exotic physical processes with high lepton multiplicity, or those that require good lepton reconstruction, energy resolution, and flavor recognition. Section XI discusses how exotic models involving lepton and photon interactions can benefit from such capability. For instance, the characteristic Chern-Simons term involving photons and axion-like particles can be probed to high precision at the CEPC. At

Tera-Z and Higgs factory runs, the rare decay of the Higgs boson and electroweak gauge boson can be of particular interest. The high design luminosity at these runs offers a powerful probe into right-handed neutrino, extended scalars, exotic lepton models, etc. Noticeably the high sensitivity with leptons also empowers precision tests on the SM lepton interactions, such as the dipole moment of μ and τ leptons, effective non-standard neutrino interactions. These measurements provide a complementary test of underlying BSM theory, generating large corrections to lepton form factors. In addition, strong interest in quantum entanglement has started to emerge in collider physics. Section XI also includes newly completed analyses on its application in leptonic Higgs boson decays.

Recent developments in global fitting techniques, like GAMBIT, etc., greatly strengthen our ability to navigate through vast new physics model spaces. Global fits maximize data's theoretical output by efficiently analyzing and comparing a large number of different models. This powerful computation capability can quickly identify models or parameter spaces with the highest priority, making robust references for theory interpretation. In Section XII, we include recent global-fitting analyses for well-motivated SMEFT, 2HDM and SUSY models, based on the CEPC's design specifics at Z-pole, Higgs factory and $t\bar{t}$ runs.

III. DESCRIPTION OF CEPC FACILITY, NOMINAL LUMINOSITY AND TYPICAL DETECTOR PERFORMANCE (MANQI)

A. Key Collider Features

CEPC Accelerator provides an instant luminosity range from XX - XX at center-of-mass energy of 91 to 240 GeV, in its nominal operation plan - with 10 years of data taking at Higgs mode, 2 years at Z, and 1 year for the W threshold scan, CEPC could deliver 4 million Higgs boson, 4 Tera Z boson, and Gigas of W boson.

According to the CEPC CDR [11] (Change to TDR), the beam energy spread could typically be controlled to the level of 0.1%. This, together with a detector that can reconstruct precisely the hadronic events – allowing for precise determination of missing energy/momentum – thus enables relevant physics measurements with high precision; for instance, tagging leptonic heavy quark decay and searching for dark matter candidates in hadronic events, especially at the Z factory mode.

Operation mode	Z factory	WW threshold	Higgs factory	$t\bar{t}$
$\sqrt{s}$ (GeV)	91.2	160	240	360
Beam size σ_x (μm)	6	13	15	39
Beam size σ_y (μm)	0.035	0.042	0.036	0.113
Bunch length (total, mm)	8.7	4.9	3.9	2.9
Crossing angle at IP (mrad)		33		

TABLE II: Beam size, bunch length, and crossing angle at different operation modes of the CEPC [14].

The CEPC uses a nano beam scenario and therefore the typical beam spot sizes are of order μm in the x direction, order nm in the y direction, and correspondingly of order a few hundred μm in the z direction. The beam sizes at different operation modes of the CEPC are summarized in Table II. The accelerator could stabilize the collision area with a typical size of order μm in the transverse direction and of order $\sim \mathcal{O}(100)$ μm along the beam direction. The spatial uncertainty of the interaction point could therefore be limited, enabling high precision measurements with τ final states – for example, in dark matter searches with $Z \to \tau^+\tau^-$ events at Z factory.

B. Key Detector Features

In general, the CEPC detector would have a large acceptance with a solid angle coverage of at least $|\cos\theta| < 0.99$. This detector would also have a low energy/momentum threshold at the 100 MeV level in order to record and recognize low energy objects that characterize certain hadron decays, *e.g.*, soft photons and pions generated from excited heavy hadrons, as well as some low energy hadrons that are essential for understanding relevant QCD processes [15].

To efficiently separate signal events from background, it is essential to identify the relevant physics objects and to precisely reconstruct their properties – especially their energy/momentum. For a Tera-Z detector, a typical benchmark is to reconstruct the interme-

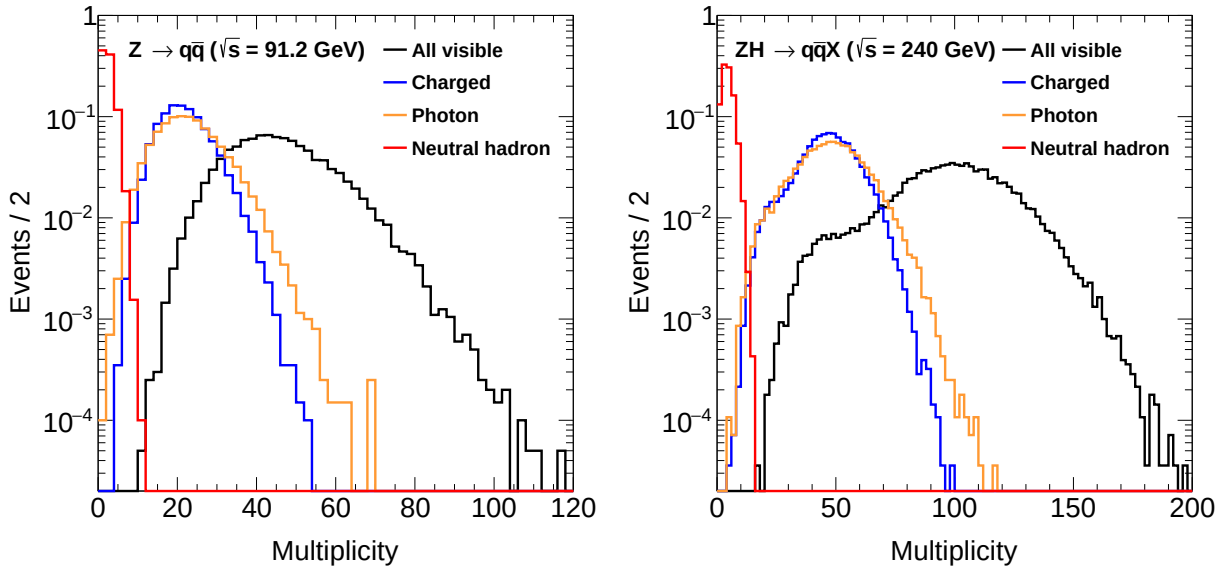

FIG. 4: Multiplicities of different types of final state particles in $Z \to q\bar{q}$ (91.2 GeV) and $Z(\to q\bar{q})H(\to$ inclusive) (240 GeV) events.

diate particles, such as $\pi^0 \to \gamma\gamma$, $K^0_S \to \pi^+\pi^-$, $\phi \to K^+K^-$, $\Lambda \to p\pi^-$, etc, inside hadronic Z events. A more challenging case would be to identify the decay products of a target heavy flavor hadron which may decay into $\mathcal{O}(10)$ particles with a complicated and rich decay cascading order inside a jet. These decay products include not only charged final state particles (leptons and charged hadrons), but also photons, neutral hadrons, and the missing energy/momentum induced by neutrinos. A hadronic Z event could has upto 100 final state particles, as shown in Figure 4. To successfully separate and reconstruct the relevant final state particles of the target particle is a key challenge for the measurements performed in hadronic Z events, and it is necessary to employ the particle flow method [16, 17], which emphasizes the separation of final state particles and has been proven capable of providing better reconstruction of both the hadronic system and of the missing energy/momentum.

In addition, good intrinsic resolution of sub-detectors, (*i.e.*, momentum reconstruction by the tracker and energy measurement by the calorimeter), is always critical for flavor physics measurements. It not only leads to the precise reconstruction of physics properties such as particle masses, but also significantly reduces the combinatory background especially present in physics measurements with narrow resonances. In particular, determining how to achieve an excellent electromagnetic (EM) energy resolution with a particle flow oriented high-granularity calorimeter is indeed challenging but necessary for the flavor physics program,

since photons and neutral pions are common decay products in many fundamental flavor physics measurements. The benchmark analysis of CKM angle α measurement via $B \to \pi\pi$ [18] suggests an EM resolution of order $\mathcal{O}(3\%/\sqrt{E})$ in order to fulfill the requirement of 3σ separation between B^0 and B_s^0 with a 30 MeV B-meson mass resolution.

Most of the flavor physics measurements are relevant to hadronic events, especially di-jet events at the Z pole. It is essential to identify the origin of a jet, i.e., to determine whether it is originated from a quark, an anti-quark, or even a gluon. The jet origin identification [19], to a certain extend, shall be regarded as a natural extension of jet flavor tagging, quark-gluon jet separation, and jet charge measurements, which is indispensable in flavor physics measurements such as CKM and CP violation measurements.

A successful flavor physics program also needs a high efficiency/purity PID. An efficient PID not only suppresses the combinatory background induced by misidentified particles, but also separates decays with similar topologies in final states, such as $B^0_{(s)} \to \pi^+\pi^-$, $B^0_{(s)} \to K^+K^-$, and $B^0_{(s)} \to K^\pm\pi^\pm$ [20]. A decent PID is also critical for the jet origin identification [19, 21] and relevant physics measurements such as the Higgs rare/exotic decay measurement [19]. The benchmark analysis of $B_s \to \phi\nu\bar{\nu}$ [22] shows that a relative sensitivity of BR($B_s \to \phi\nu\bar{\nu}$) less than 2% at a Tera-Z collider requires a $3\,\sigma$ K/π separation for the identification of charged hadrons, see the left panel of Figure 5. This requirement can be addressed by multiple PID technologies. For instance, the CEPC baseline detector can separate different species of hadrons using dE/dx information measured by TPC and TOF information provided by either an dedicated TOF device, or combining TOF and ECAL together. Detector optimization study[23] suggests that dE/dx needs to reach 3% with combination of a TOF resolution of 50 ps to statisfy this PID requirement. In addition, the dN/dx technology proposed by drift chamber of IDEA concept [24] is promising to further improve the PID performance.

A high-precision and low-material vertex system is vital for the CEPC flavor physics program. Precise vertex measurements provide pivotal information to distinguish the species of the initial quark that fragments into a jet, namely the jet origin identification. Precise vertex information is also critical for determining the decay time or lifetime of heavy flavor hadrons with high precision. To match the characteristic timescales such as those of $B_s - \bar{B}_s$ mixing ($\sim$ 56 fs), of D_s decay ($\sim$ 500 fs), and of τ decay ($\sim$ 290 fs), the lifetime resolution is required to reach order $\mathcal{O}(10)$ fs. This accurate lifetime measurement also benefits flavor

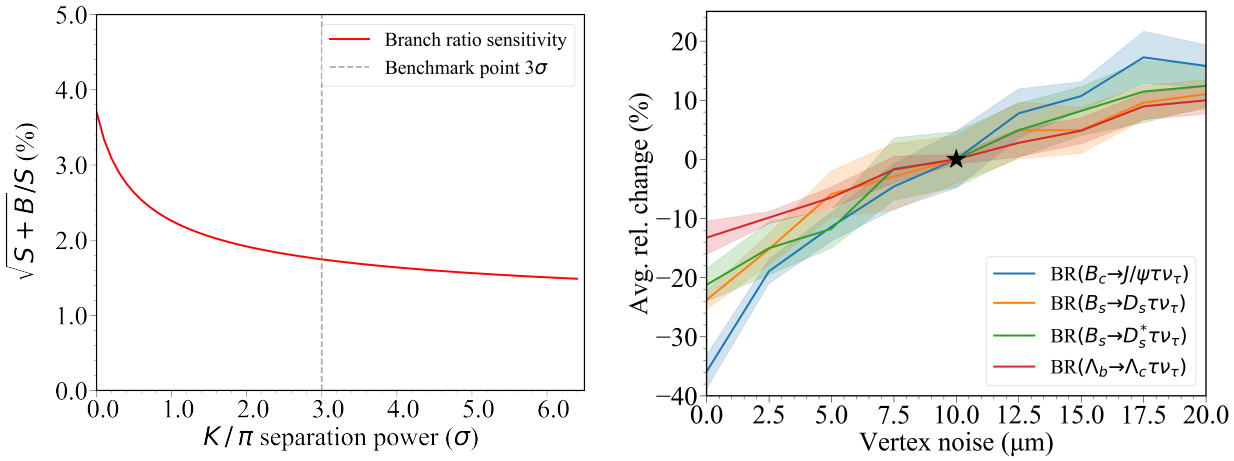

FIG. 5: **LEFT:** Sensitivity of measuring BR($B_s \to \phi\nu\bar{\nu}$) as a function of PID performance, parameterized by the K/π separation power [22]. **RIGHT:** Precision variance of measuring BR($H_b \to H_c\tau\nu_\tau$) as a function of detector vertex noise [25], with stared reference point set by a vertex noise of 10 μm.

tagging and time-dependent CP violation measurements. In addition, a high-performance vertex system can provide a precise reconstruction of the secondary vertices that characterize some heavy flavor hadron decays, such as the example shown in Figure 6. Such a system can also help to suppress the background, especially from the IP. One concrete application can be the measurements of FCCC-mediated BR($H_b \to H_c\tau\nu_\tau$), where the H_b reconstruction can significantly rely on the determination of the H_c decay vertex and the measurement of the muon track originating from the τ decay [25]. As shown in the right panel of Figure 5, the reduced noise of vertex system can uniformly benefit these measurements, yielding an improvement in precision of $\mathcal{O}(10\%)$ level.

The above-mentioned requirements are also highly beneficial for physics programs at higher center-of-mass energies, *i.e.* the 160 GeV W^+W^- threshold scan, the 240 GeV Higgs run, and the 360 GeV top operation. On top of their core physics programs, such as W mass and precise Higgs/top properties measurements, the data samples and key detector features also support an intensive flavor physics program, see Section **??**.

To address these physics requirements, intensive efforts on detector conceptual design, on physics performance study, and on key technology R&D have been performed. We refer to two benchmark detector concepts in this white paper. These concepts are used in the simulations in this manuscript, providing reference performance for relevant physics potential

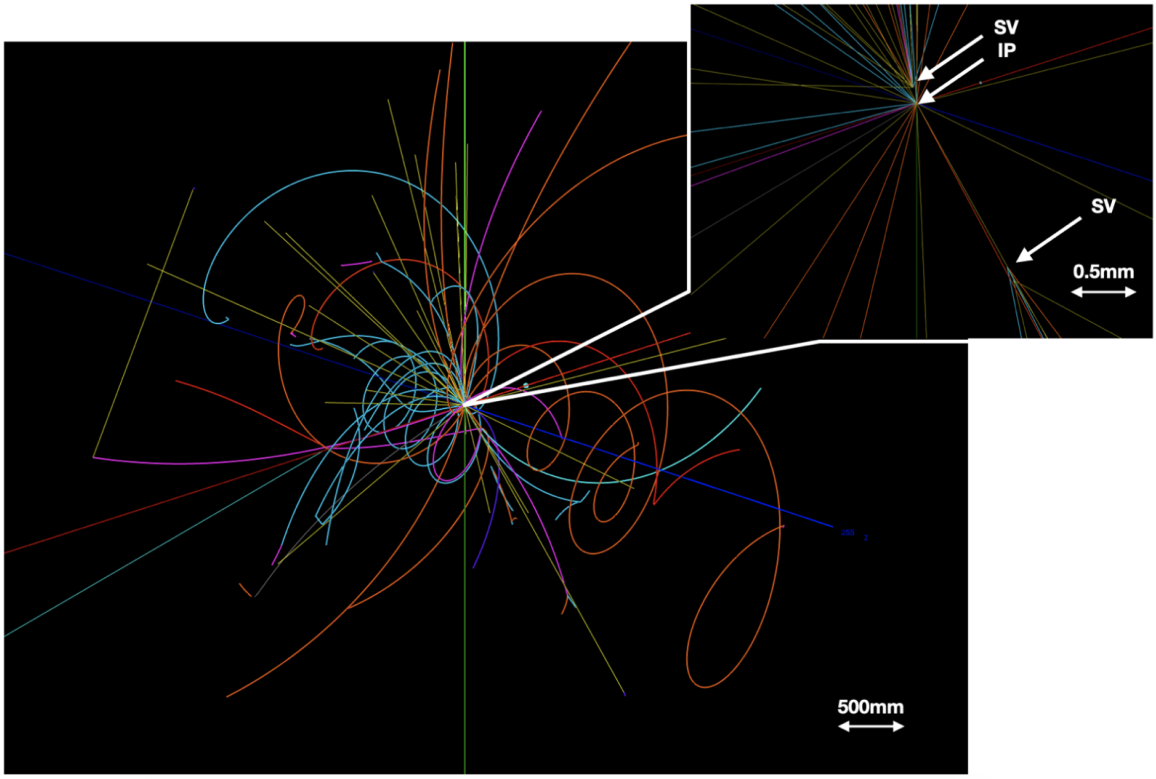

FIG. 6: Display of a $Z \to b\bar{b}$ event with typical secondary vertices (SV).**This figure looks dark. Shall we use a brighter one?**

studies.

The starting point of our discussion is the CEPC baseline detector as delineated in its CDR study [11]. Guided by the particle flow principle, the CEPC baseline design features a high-precision tracking system, a high-granularity calorimeter system, and a high magnetic field. Shown in detail in Figure 7, the CEPC baseline detector consists, from inside to outside, of a silicon pixel vertex detector, a silicon tracker, a time projection chamber (TPC), a silicon-tungsten sampling EM calorimeter (Si-W ECAL), a steel-glass resistive plate chambers sampling hadronic calorimeter (SDHCAL), a superconducting solenoid providing a magnetic field of 3 Tesla, and a flux return yoke embedded with a muon detector. Additionally, the Si-W ECAL could also be instrumented with a few timing layers to enable time-of-flight (TOF) measurements with precision of 50 ps or even better [11, 27].

Alongside the CEPC baseline detector, an alternative detector concept known as IDEA (Innovative Detector for Electron-positron Accelerator) [26] is also utilized in various studies

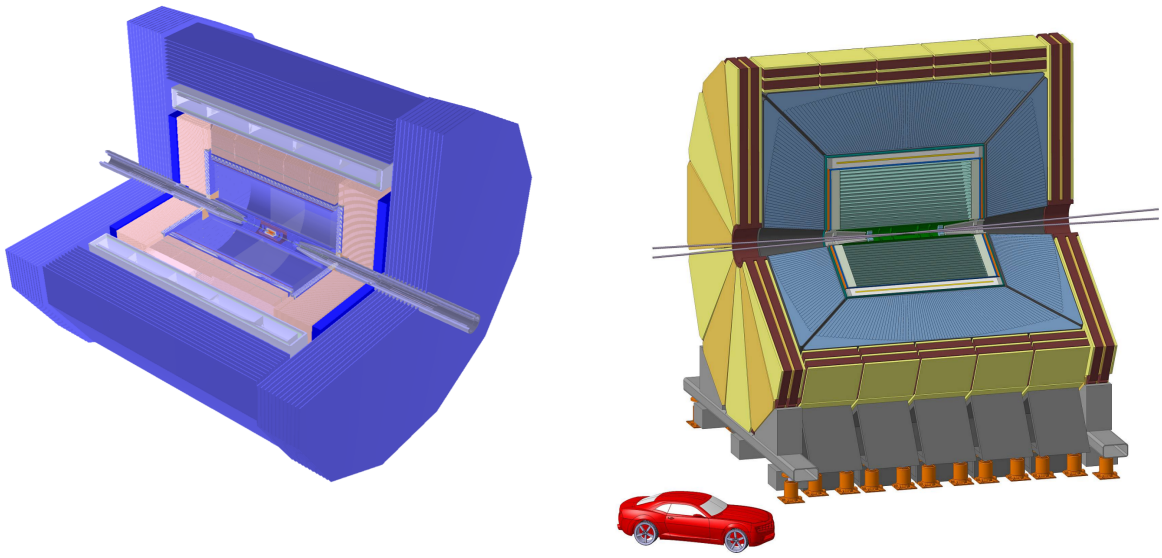

FIG. 7: Schematic layouts of the CEPC baseline detector [11] (left) and the IDEA detector [26] (right).

covered in this white paper. The IDEA detector also serves as a reference detector for the FCC-*ee* project. In comparison to the CEPC baseline detector, the IDEA detector incorporates a dual readout calorimeter system to attain superior energy resolution for both EM and hadronic showers. Moreover, the IDEA detector operates with a reduced magnetic field of 2 Tesla while compensating for this reduction by offering a larger tracking volume. The overall structure of the IDEA detector can be seen in Figure 7.

By virtue of the particle flow oriented design, the CEPC baseline detector performs well in efficient tracking, lepton identification, and precise reconstruction of hadronic systems. These excellent features of the CEPC baseline detector provide a solid basis for flavor physics studies. The achieved performance of the CEPC baseline detector during its CDR phase is summarized in Table III. Notably, the baseline tracking system demonstrates an efficiency close to 100% and a relative momentum resolution approaching $\mathcal{O}(10^{-3})$ for individual tracks with momenta exceeding 1 GeV within the barrel region, as illustrated in Figure 8. As depicted in left panel of Figure 9, the baseline photon energy resolution is $17\%/\sqrt{E} \oplus 1\%$, achieved by the sampling Si-W ECAL, which features the high granularity critical for particle flow reconstruction. In terms of PID performance, the CEPC baseline design achieves a K/π separation better than 2σ in the momentum range up to 20 GeV by effectively combining TOF and dE/dx information, as shown in Figure 10. The inclusive $Z \to q\bar{q}$ sample exhibits

Item	Baseline [11]	Objective	Comments
	Basic Performance		
Acceptance	$\lvert\cos\theta\rvert < 0.99$ [11]		
Threshold	200 MeV [28, 29]	100 MeV	For tracks & photons
Beam energy spread	$\mathcal{O}(0.1\%)$ [11]		
Tracker momentum resolution	$\mathcal{O}(0.1\%)$ [11]		
ECAL energy resolution	$17\%/\sqrt{E} \oplus 1\%$ [11]	$3\%/\sqrt{E}$ [18]	
HCAL energy resolution	$60\%/\sqrt{E} \oplus 1\%$ [11]		
Vertex resolution	10–200 μm [11]		
Jet energy resolution	3–5% [11, 30]		For 20–100 GeV
$\ell - \pi$ mis-ID	$< 1\%$ [31]		In jet, $\lvert\vec{p}\rvert > 2$ GeV
$\pi - K$ separation	$> 2\sigma$ [11]	$> 3\sigma$ [22]	In jet, $\lvert\vec{p}\rvert > 1$ GeV, TOF+dE/dx
	Flavor Physics Benchmarks (Depending on the Above)		
$\sigma(m_{H,W,Z})$	3.7% [11]		Hadronic decays
b-jet efficiency×purity	$\sim 70\%$ [11]		In Z hadronic decays
c-jet efficiency×purity	$\sim 40\%$ [11]		In Z hadronic decays
b-jet charge tagging $\epsilon_{\text{eff}} = \epsilon(1-2\omega)^2$	-	15–25% [21, 32]	For B_s
π^0 efficiency×purity	$\gtrsim 70\%$ [29]	$\gtrsim 80\%$ [18]	In Z hadronic decays, $\lvert\vec{p}_{\pi^0}\rvert > 5$ GeV
K_S^0, Λ , D efficiency	60%-85% [33]		In Z hadronic decays, all tracks
τ efficiency×purity	70% [34]		In $WW \to \tau\nu q\bar{q}'$, inclusive
τ mis-ID	$\mathcal{O}(1\%)$ [34]		In $WW \to \tau\nu q\bar{q}'$, inclusive

TABLE III: Summary of detector performance of the CEPC baseline detector and some objectives for flavor physics benchmarks.

an overall $K^{\pm}$ identification efficiency and purity exceeding 95% [23]. Regarding hadronic systems, the CEPC baseline detector attains a boson mass resolution (BMR) better than 4% for hadronically decaying W, Z, and Higgs bosons, as illustrated in right panel of Figure 9. This not only enables a separation exceeding $2\,\sigma$ between W and Z bosons in their hadronic decays, but also enhances the precision of missing energy/momentum measurements, which are vital for flavor physics investigations.

Following the completion of the CEPC CDR, there are still ongoing research efforts focused on the detector design to further optimize the baseline performance parameters and to cater to the requirements for the CEPC flavor physics program. These optimization efforts primarily concentrate on three key aspects: EM energy resolution, PID performance, and jet charge measurements. To address the demand for improved separation of B^0 and B_s^0 with EM final states, a significantly enhanced EM energy resolution of $3\%/\sqrt{E}$ [18] is pursued, as

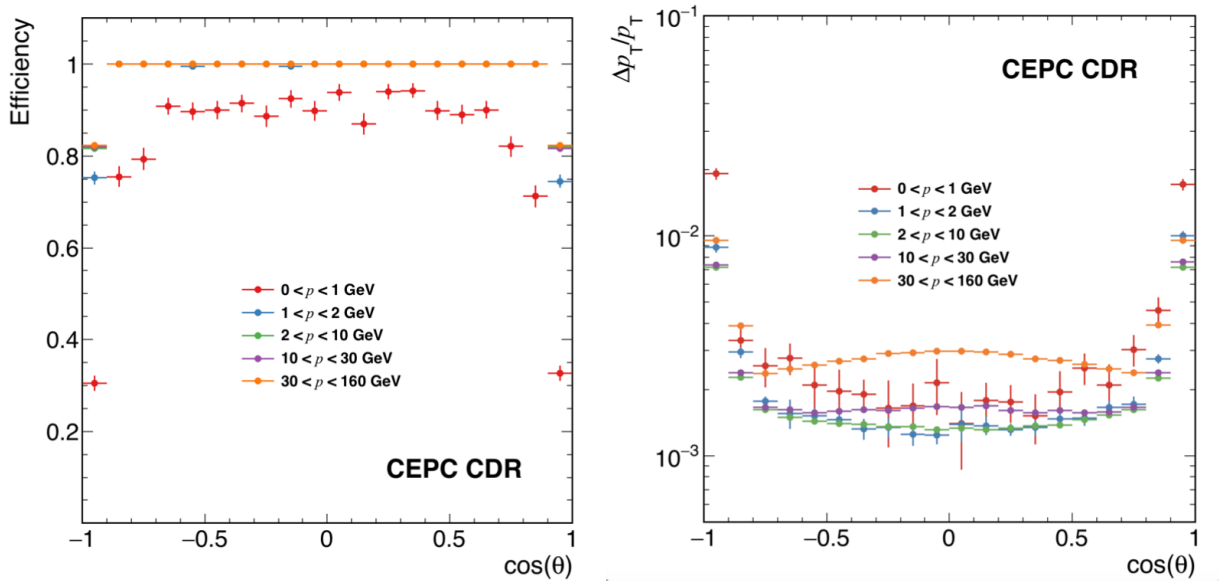

FIG. 8: Single track reconstruction efficiency (left) and momentum resolution (right) of the CEPC baseline detector [11].

compared to the baseline resolution of $17\%/\sqrt{E}\oplus 1\%$ shown in left panel of Figure 9. Accompanying this resolution enhancement, a corresponding photon energy threshold of 100 MeV is envisioned. To attain this level of EM resolution while maintaining compatibility with PFA performance, novel concepts for high-resolution and high-granularity crystal ECAL designs have been proposed [35–37], and relevant R&D studies [38] are progressing. For PID performance, a K/π separation better than 3 σ is suggested. This improved PID capability can be achieved by combining various techniques, including TOF [39, 40], dE/dx [23, 41], and dN/dx [24] measurements. The performance of jet charge measurement is typically characterized by the effective tagging efficiency (power) $\epsilon_{\rm eff} \equiv \epsilon_{\rm tag}(1-2\omega)^2$, where $\epsilon_{\rm tag}$ is the flavor tagging efficiency and ω is the wrong tagging fraction. The study [21] develops a Leading Particle Jet Charge method (LPJC) and combines it with a Weighted Jet Charge (WJC) method to form a Heavy Flavor Jet Charge method (HFJC). This study evaluates the effective tagging power for c/b jets at the CEPC Z pole operation and finds it to be 39%/20%. Additionally, by implementing benchmark IP cuts of 0.02/0.04 mm to distinguish the origin of the leading charged particle (whether from the decay of the leading heavy hadron or QCD fragmentation), the effective tagging power for c/b jets was found to be 39.0%/26.8%. Furthermore, a dedicated b-jet charge tagging algorithm developed

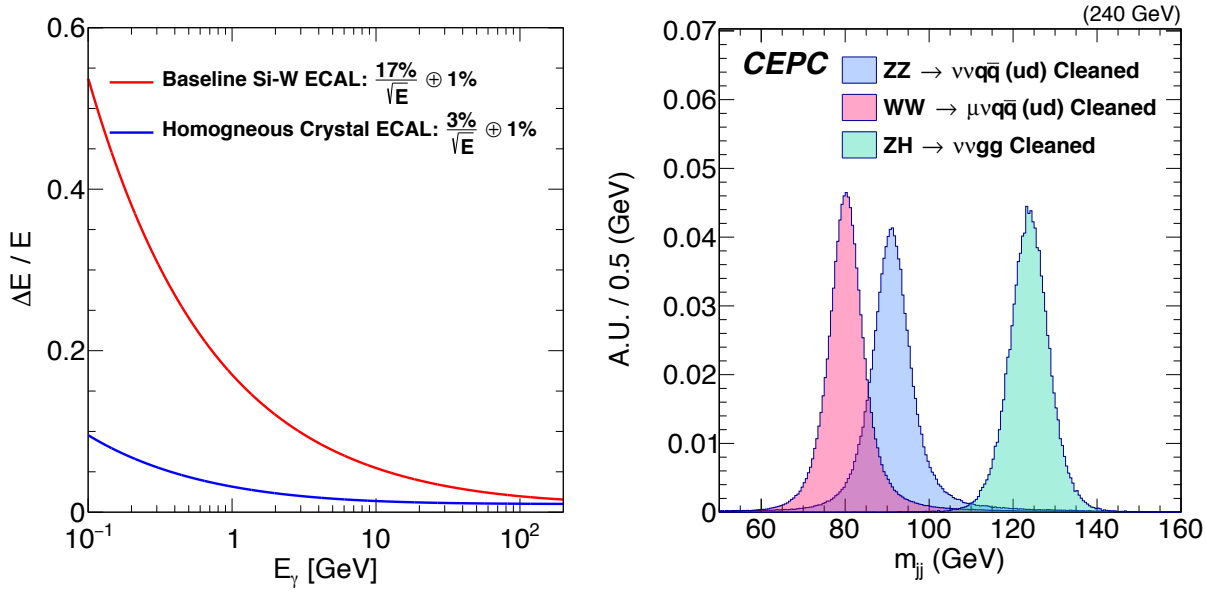

FIG. 9: **LEFT:** Comparison of the CEPC baseline photon energy resolution achieved by the sampling Si-W ECAL [11] and expected photon energy resolution of homogeneous crystal ECAL. **RIGHT** Reconstructed boson masses of cleaned $\nu\bar{\nu}q\bar{q}$, $l\nu q\bar{q}$, and $\nu\bar{\nu}H,\ H \to gg$ events [30].

specifically for the study of $B_s^0 \to J/\psi\phi$ at the CEPC [32] achieved an effective tagging power of 20%. Consequently, a range of $\epsilon_{\text{eff}} \in [15, 25]\%$ is determined for the future b-jet charge tagging power at the Tera-Z. These advancements in performance parameters are also summarized in Table III.

In addition, the conceptual detector of CEPC has a large geometric acceptance, a decent performance in identifying final state particles, especially charged hadrons, as well as a precise low-material vertex system located close to the interaction point. These detector properties are of great significance in the identification of jet origins. Furthermore, recent advancements in machine learning algorithms, such as the ParticleNet algorithm [42] developed in the CMS experiments, provide necessary tools for this multi-category identification. Through full simulated sample of Higgs/Z to di-jet processes with CEPC conceptual detector, ParticleNet can simultaneously identify $b/\bar{b}$, $c/\bar{c}$, and $s/\bar{s}$ quarks with flavor tagging efficiencies of 90%, 80%, and 60%, respectively [19]. Meanwhile, the misidentification rate for jet charge can be controlled at 18%, 7%, and 16%, correspondingly. The corresponding performance is shown in Figure 11.

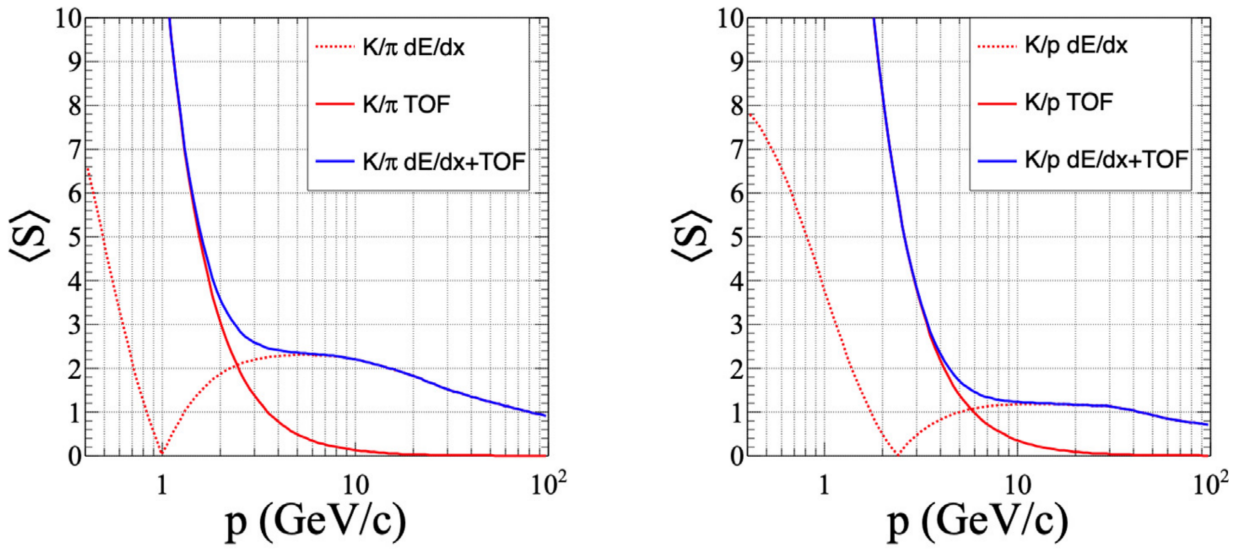

FIG. 10: Separation power of K/π (left) and K/p (right) using different techniques [23].

IV. EXOTIC HIGGS POTENTIAL AND EXOTIC HIGGS/Z/TOP DECAYS (YAQUAN, ZHAO)

A. Introduction

The exploration of novel physics phenomena may manifest through the exotic decay channels of the Higgs boson, Z boson and top quark. Especially, it may explain the dynamics of generic Higgs portal or some exotic effective operators. The research effort devoted to investigating Higgs/Z/top exotic decays will effectively improve the precision of the coupling measurements for relevant particles and will constitute an indispensable element of the scientific agenda for the prospective Higgs factories. These capacities could be significantly enhanced with the introduction of cutting-edge machine learning technologies [43, 44]. In the following sections, we will review some representative investigations for the relevant exotic decays.

B. Model-independent Sensitivity to Exotic Higgs decays

A comprehensive assessment of the sensitivity of lepton colliders to exotic decay channels of the Higgs boson into various final states was presented in Ref. [45], with a particular emphasis on the channels that face considerable challenges at hadron Colliders. The findings

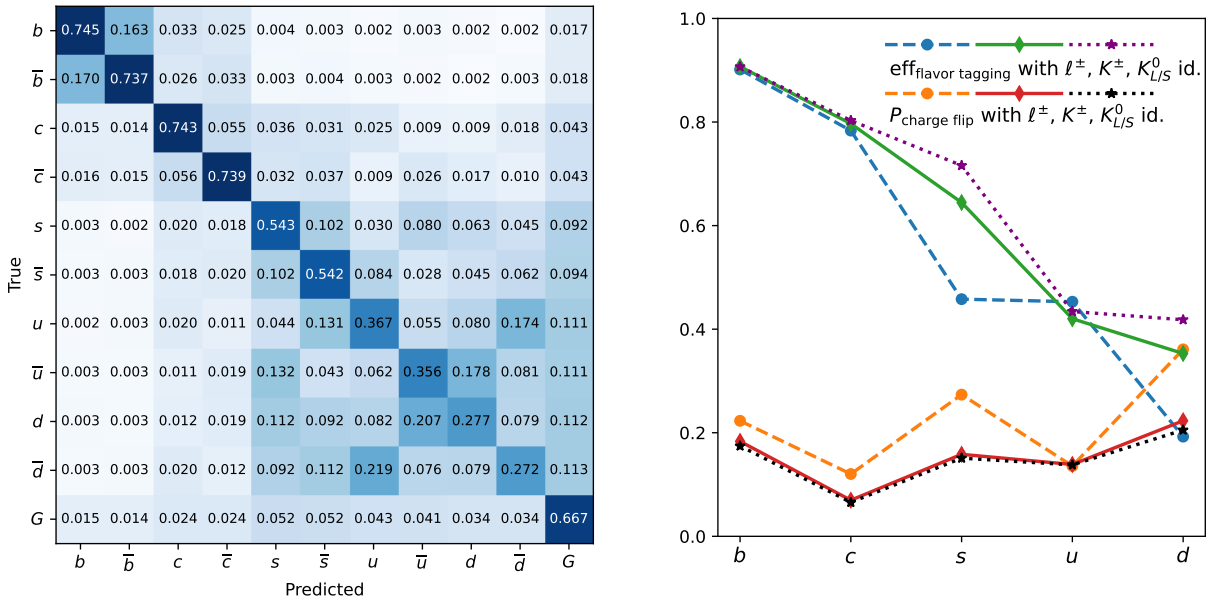

FIG. 11: Jet origin identification performance [19] of full simulated Higgs/Z to di-jet processes with CEPC conceptual detector. **LEFT:** The confusion matrix M_{11} with perfect identification of leptons and charged hadrons. **RIGHT:** Jet flavor tagging efficiency and charge flip rate for S vs. U or D with identification of leptons, plus identification of charged hadrons and neutral kaons.

of the investigation indicate that lepton colliders exhibit notable potential for sensitivity in the discussed decay channels. The present analysis is concentrated on the two-body Higgs decays into BSM particles, denoted as X_i, through the decay process $h \to X_1 X_2$. These particles are permitted to undergo further decays, potentially resulting in four-body final states at most. The cascade decay modes are systematically categorized into four distinct cases, as illustrated in Fig. 12. A broad class of the underlying BSM theoretical frameworks, including but not limited to singlet scalar extensions, two-Higgs-doublet models, SUSY models, various Higgs portals, and gauge extensions of the SM, as referenced in [45–48], provide the theoretical impetus for the exploration of these exotic decay channels.

At the CEPC 240 GeV, the predominant mechanism for the Higgs boson production is the associated production with a Z boson. The decay of the Z boson into detectable final states facilitates the identification of the Higgs boson via the recoil mass method. Implementing a selection criterion centered around the peak of the recoil mass significantly reduces background processes from SM processes. Several channels have been investigated in Ref.[45].

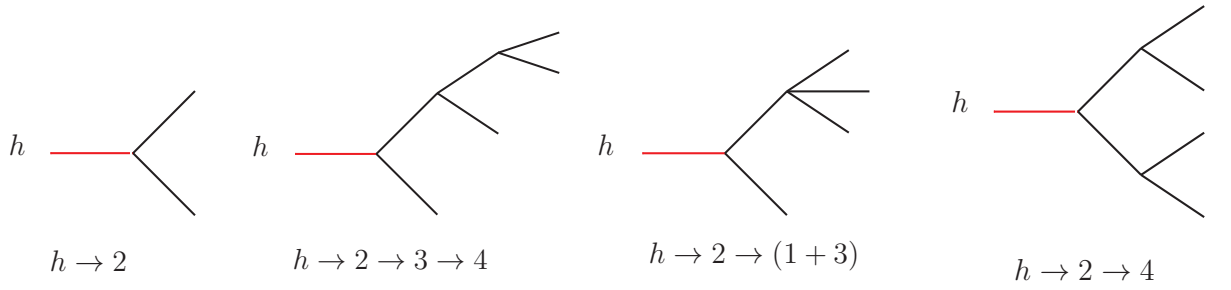

FIG. 12: Representative topologies of the Higgs exotic decays (from Ref.[45]).

The results of which are shown in Fig. 13. The analysis provides the projected exclusion limits at the 95% C.L. for the CEPC with an integrated luminosity of 20 ab^{-1}. Additionally, the forecasted sensitivities for the LHC represented by gray bars are included. The projections for the LHC are based on the most current sensitivity estimates. However, several of these projections are either non-existent or notably conservative. More contemporaneous investigations, such as those presented in Ref. [49] concerning the decay $h \to 4\tau$, and Ref. [50] about the decay $h \to 4b$, have shown the consistency of these sensitivity projections.

The LHC is expected to impose stringent constraints on a large number of decay channels that involve muons, electrons, and photons. In the context of the more formidable channels that are dependent on the detection of jets, heavy quarks, and tau leptons, the prospective enhancements in sensitivity compared to current LHC projections span from

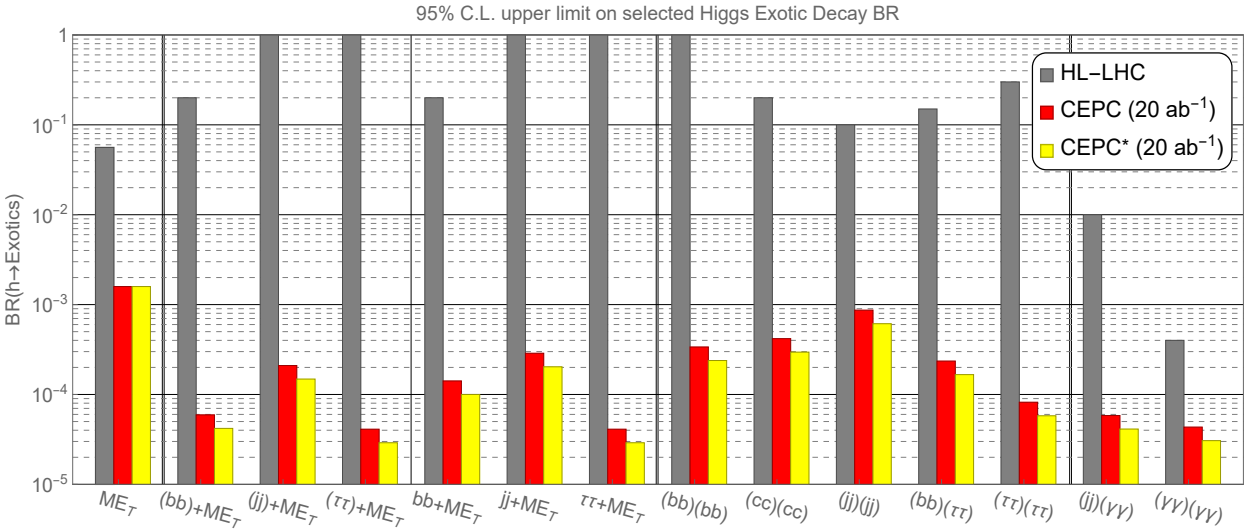

FIG. 13: The 95% C.L. upper limit on selected Higgs exotic decay branching fractions at HL-LHC and CEPC, based on Ref [45].

Decay channel	Upper limit on the branching ratio at 95% C.L.			
	HL-LHC	CEPC	ILC	FCC-ee
ME_T	0.056	0.0028	0.0025	0.005
$(b\bar{b})+\mathrm{ME}_T$	0.2	1×10^{-4}	2×10^{-4}	5×10^{-5}
$(jj)+\mathrm{ME}_T$	-	5×10^{-4}	5×10^{-4}	2×10^{-4}
$(\tau\tau)+\mathrm{ME}_T$	1	8×10^{-4}	1×10^{-3}	3×10^{-4}
$b\bar{b}+\mathrm{ME}_T$	0.2	3×10^{-4}	4×10^{-4}	1×10^{-4}
$jj+\mathrm{ME}_T$	-	5×10^{-4}	7×10^{-4}	2×10^{-4}
$\tau\tau+\mathrm{ME}_T$	-	8×10^{-4}	1×10^{-3}	3×10^{-4}
$(b\bar{b})(b\bar{b})$	0.2	4×10^{-4}	9×10^{-4}	3×10^{-4}
$(c\bar{c})(c\bar{c})$	0.2	8×10^{-4}	1×10^{-3}	3×10^{-4}
$(jj)(jj)$	0.1	1×10^{-3}	2×10^{-3}	7×10^{-4}
$(b\bar{b})(\tau\tau)$	0.15	4×10^{-4}	6×10^{-4}	2×10^{-4}
$(\tau\tau)(\tau\tau)$	$0.2 \sim 0.4$	1×10^{-4}	2×10^{-4}	5×10^{-5}
$(jj)(\gamma\gamma)$	0.01	1×10^{-4}	2×10^{-4}	3×10^{-5}
$(\gamma\gamma)(\gamma\gamma)$	4×10^{-4}	1×10^{-4}	1×10^{-4}	3×10^{-5}

TABLE IV: The projection of upper limits at 95% C.L. on selected exotic decay branching ratios for various channels at the HL-LHC is compared to those at various lepton colliders, as shown in Figure 13.

one to four orders of magnitude. This substantial improvement is attributed to the reduced QCD background and the effectiveness of Higgs boson identification through the recoil mass method that is expected to be employed at forthcoming lepton collider facilities. Specifically, for exotic decays of the Higgs boson without missing energy, the anticipated improvements in detection sensitivity range between two to three orders of magnitude. An exception is noted for the $(\gamma\gamma)(\gamma\gamma)$ decay channel, which is projected to enhance merely one order of magnitude. This particular channel at the LHC benefits from the ability to reconstruct the Higgs boson mass from the final state particles, which significantly aids in the discrimination between signal and background. Moreover, decay channels involving electrons, muons, and photons, which are considered to be relatively clean signatures at the LHC, stand to gain

from the higher statistics that will be provided by the HL-LHC, thereby utilizing the higher event counts to improve statistical precision. Table IV summarises the upper limit on the branching ratios for different channels for the HL-LHC, CEPC, ILE and FCC-ee.

C. Exotic Higgs potential

The exotic Higgs potential is often realized through the extension of the SM Higgs potential, leading to the SM-s model. This model is a minimal theoretical extension that introduces a new scalar particle, typically denoted as s, which can mix with the Higgs boson. The Lagrangian for this extension is given by:

$$\mathcal{L} = \mathcal{L}_{\text{kin}} + \frac{\mu_s^2}{2}S^2 - \frac{\lambda_s}{4!}S^4 - \frac{\kappa}{2}S^2|H|^2 + \mu^2|H|^2 - \lambda|H|^4, \tag{1}$$

where $\mathcal{L}_{\text{kin}}$ represents the kinetic terms, μ_s^2 and λ_s are parameters associated with the new scalar s, κ describes the mixing between s and the Higgs boson H, and μ^2 and λ are the mass and self-coupling parameters of the Higgs boson, respectively.

The SM-s model is driven by theoretical interests such as naturalness, which tackles the hierarchy problem between the Higgs mass and the Planck scale; potential interactions with dark matter, possibly linking the visible and dark sectors of the universe; and the electroweak phase transition, which could influence the early universe's dynamics and baryon asymmetry.

The new scalar s can lead to exotic Higgs decays, such as $h \to ss$, which are not present in the SM. These decays are of particular interest because they could provide evidence for physics beyond the SM and help resolve some of the current puzzles in particle physics.

At the LHC, detecting the decay $h \to ss$ is challenging due to significant background processes. However, the projected sensitivity of the HL-LHC for the $bb\tau\tau$ final state is $\text{Br}(h \to ss) < 2.8 \times 10^{-2}$ according to CMS projections [51]. At the future electron-positron colliders, the sensitivity for the $bbbb$ final state is much more promising.[45] With at least three b-tagged jets required in the final state, the b-tagging efficiency can be conservatively chosen to be 80%, and the charm mis-tagging rate and the light flavor mis-tagging rate can be set to be 9% and 1%, respectively. As shown in Fig. 14, the future lepton collider with 5 ab^{-1} integrated luminosity can exclude branching fractions of $h \to ss \to (\bar{b}b)(\bar{b}b)$ down to $3 \times 10^{-4} \sim 4 \times 10^{-4}$, in the range of mediator mass 20 GeV $< m_s <$ 60 GeV.

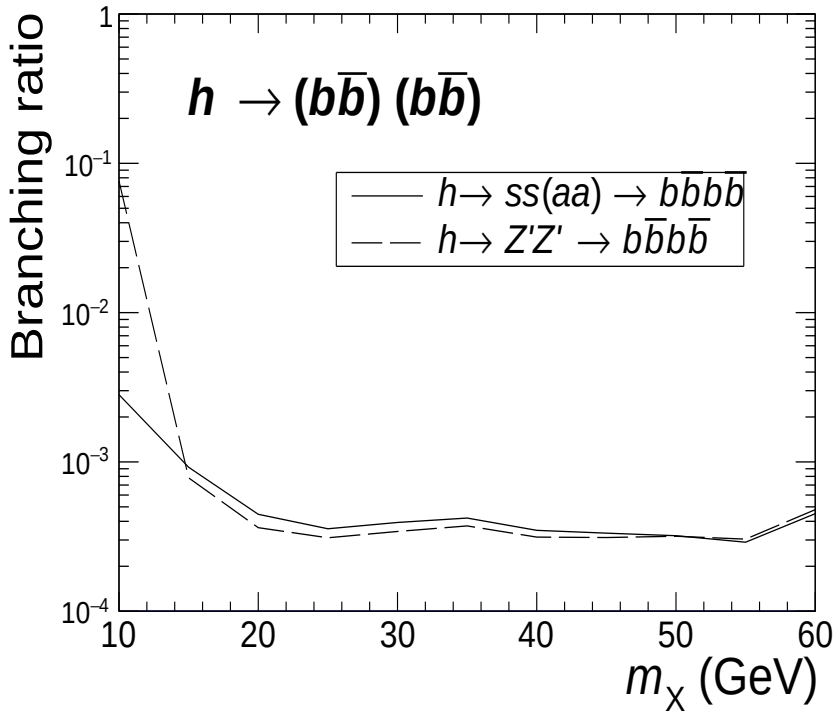

FIG. 14: The 95% C.L. exclusive bound on Br($h \to (\bar{b}b)(\bar{b}b)$), based on Ref. [45].

The enhanced sensitivity at electron-positron colliders is attributed to their cleaner experimental environment and the precision can be significantly improved with high statistics in the next-generation facilities. This makes them ideal for studying rare processes and searching for new physics, such as the exotic Higgs decays discussed here.

D. Higgs exotic decays in supersymmetry

Numerous supersymmetric extensions of the Standard Model have the potential to produce the exotic decay channels of the Higgs boson. In recent years, the next-to-minimal supersymmetric standard model (NMSSM) and its slightly modified version, semi-constrained NMSSM (scMSSM) have drawn considerable interest as a framework for probing the properties of the Higgs boson. In particular, a comprehensive analysis has been undertaken to execute two primary investigations on the exotic decays of the Higgs boson at the CEPC.

First, there has been a concerted effort to clarify the nature of the invisible decay channels of the 125 GeV SM-like Higgs boson into potential dark matter (DM) candidates, specifically

into pairs of the lightest neutralinos $h \to \tilde{\chi}_1^0\tilde{\chi}_1^0$ [52–54]. Theoretical predictions suggest the existence of four distinct funnel-annihilation processes for the lightest supersymmetric particle (LSP) $\tilde{\chi}_1^0$, corresponding to intermediate states h_2, Z, h_1, and a_1. The composition of the LSP is constrained to either a singlino-dominant or a higgsino-dominant form. In the scenario where the LSP is predominantly singlino, it is supposed to achieve the observed dark matter relic density. As shown in Fig.15, the branching fraction for the Higgs boson's invisible decay is expected to be minimal, giving a challenge for detection at the CEPC. Nevertheless, this decay channel falls within the detection capabilities of the forthcoming LUX-ZEPLIN (LZ) 7-ton experiment, particularly in the regime of spin-dependent (SD) interactions. Conversely, a higgsino-dominant LSP is predicted to yield an insufficient relic density and is associated with a substantial branching fraction for the Higgs invisible decay, leaving it in the investigation capability of the CEPC.

Second, investigations have been directed towards the decay of the Higgs boson into lighter CP-odd or CP-even Higgs states, with particular attention given to the processes $h_2 \to a_1a_1$, $h_1 \to a_1a_1$, and $h_2 \to h_1h_1$ manifesting in final states comprising four bottom quarks ($4b$), four jets ($4j$), a pair of bottom quarks and a pair of tau leptons ($2b2\tau$), and four tau leptons (4τ) respectively [55]. Three distinct scenarios are compared and their relative sensitivities are evaluated in the context of detecting these exotic Higgs decay modes at the HL-LHC as well as at forthcoming lepton colliders, including the CEPC. The predominant mechanism for the production of the SM-like Higgs boson is identified as the Zh channel. Empirical findings suggest that the most efficient strategy for the detection of these exotic decays at the CEPC would be via the 4τ channel, with the requisite minimum integrated luminosity for potential discoveries being as modest as 0.26 fb^{-1}. Table V encapsulates the requisite minimum integrated luminosities for the detection of these exotic Higgs decays across various experimental setups, including the HL-LHC, CEPC, FCC-ee, and ILC. The analysis indicates that the luminosity threshold requisite for discovery at the CEPC is comparable to that of the FCC-ee, highlighting the competitive potential of these facilities in the search for new physics phenomena.

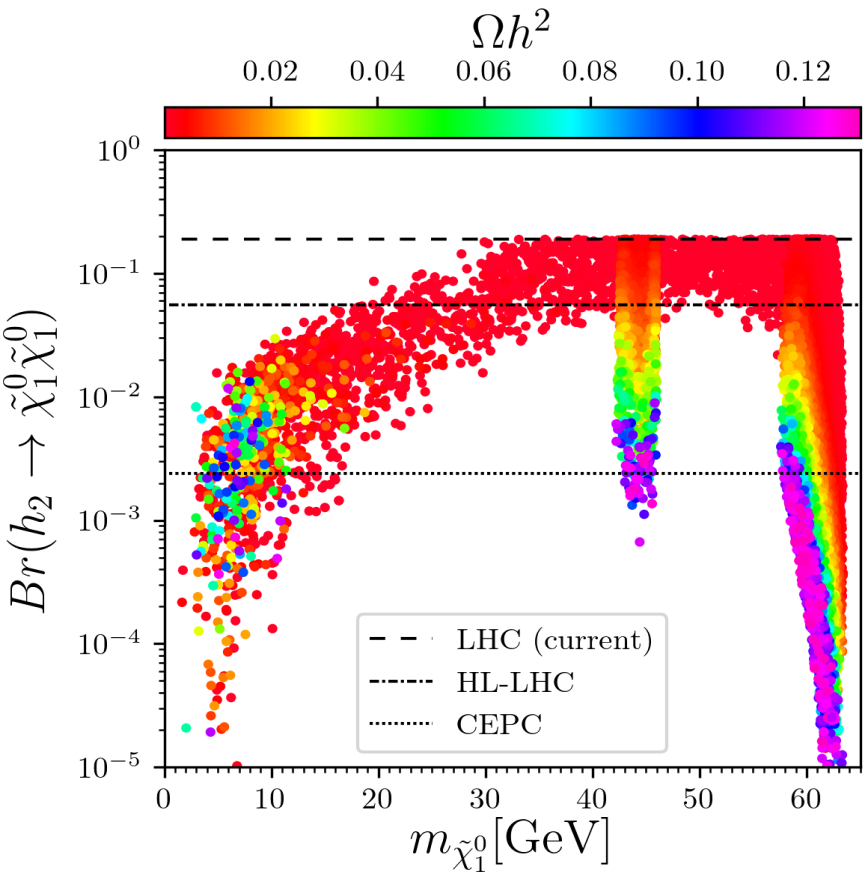

FIG. 15: The surviving samples projected in the invisible branching ratio $Br(h \to \tilde{\chi}_1^0\tilde{\chi}_1^0)$ versus $m_{\tilde{\chi}_1^0}$ planes, with colors indicating the relic density Ωh^2.The dashed, dot-dashed and dotted line shows the current upper limit 19% of the invisible Higgs decay [56], the future detection accuracy of that at HL-LHC 5.6% [45] and CEPC 0.24% [57] respectively.

E. Exotic Decays via Dark Sector

1. *Higgs Exotic Decays via Dark Sector*

Within the framework of the lepton portal dark matter model, the relic abundance is determined by the portal coupling involving the majorana fermion DM candidate χ, the singlet charged scalar mediator $S^{\pm}$, and the SM right-handed lepton [58]. The incorporation of the scalar portal interaction not only leads to a significant enhancement of the detection capabilities at the LHC through the $gg \to h^\star \to S^+S^-$ process but also induces novel signal channels, including exotic decay processes and the coupling deviations of the Higgs boson. These aspects yield promising prospects for the exploration and detailed examination of the

Deacy Mode	Future colliders			
	HL-LHC	CEPC	FCC-ee	ILC
$(b\bar{b})(b\bar{b})$	650fb^{-1}(@II)	0.42fb^{-1}(@III)	0.41fb^{-1}(@III)	0.31fb^{-1}(@II)
$(jj)(jj)$	-	21fb^{-1}(@II)	18fb^{-1}(@II)	25fb^{-1}(@II)
$(\tau^+\tau^-)(\tau^+\tau^-)$	-	0.26fb^{-1}(@III)	0.22fb^{-1}(@III)	0.31fb^{-1}(@III)
$(b\bar{b})(\tau^+\tau^-)$	1500fb^{-1}(@II)	4.6fb^{-1}(@II)	3.6fb^{-1}(@II)	4.4fb^{-1}(@II)
$(\mu^+\mu^-)(\tau^+\tau^-)$	1000fb^{-1}(@II)	-	-	-

TABLE V: The minimum integrated luminosity for discovering the exotic Higgs decay at the future colliders, where the "@I, II, III" means the three different scenarios. Scenario I: h_2 is SM-like Higgs, and the light scalar a_1 is CP-odd; Scenario II: h_1 is SM-like Higgs, and the light scalar a_1 is CP-odd; Scenario III: h_2 is SM-like Higgs, and the light scalar h_1 is CP-even.

model.

The experimental results from the LEP have excluded the existence of a charged scalar $S^{\pm}$ with a mass m_S below 100 GeV, thus negating the possibility of the on-shell decay $h \to S^+S^-$. Nevertheless, in the event that the mass of the dark matter candidate χ, m_χ, is less than half the mass of the Higgs boson, $m_h/2 \approx 62.5$ GeV, the portal coupling λ_{HS} may activate the exotic decay processes such as the three- or four-body decays $h \to S^{\pm}\ell^{\mp}\chi$ or $h \to \ell^{\pm}\chi\ell^{\mp}\chi$. These decays are mediated by either one or two virtual $S^{\pm}$, depending on whether m_S is less than m_h. The decay rates for these processes are directly proportional to $y_\ell^2\lambda_{HS}^2$ or $y_\ell^4\lambda_{HS}^2$. This relationship presents an innovative method for probing the parameters λ_{HS} and y_ℓ. By calibrating y_ℓ to the theoretical value y_ℓ^{th}, which is derived from the requisite relic abundance, one may deduce constraints on the λ_{HS} coupling for a given set of mass parameters (m_S,m_χ).

For a certain integrated luminosity, it is feasible to derive constraints on the branching ratio $Br(h \to S^{\pm(*)}S^{\mp(*)} \to \ell^+\chi\ell'^-\chi)$. These constraints can subsequently be converted into upper bounds for λ_{HS}, relying on the determination of y_ℓ through the conditions imposed by the DM relic abundance, as illustrated in the left panel of Fig. 16. An apparent discontinuity in the depicted curves around $m_S = 125$ GeV corresponds to a transition in the available phase space, shifting from a three-body to a four-body decay mechanism. In conclusion, the

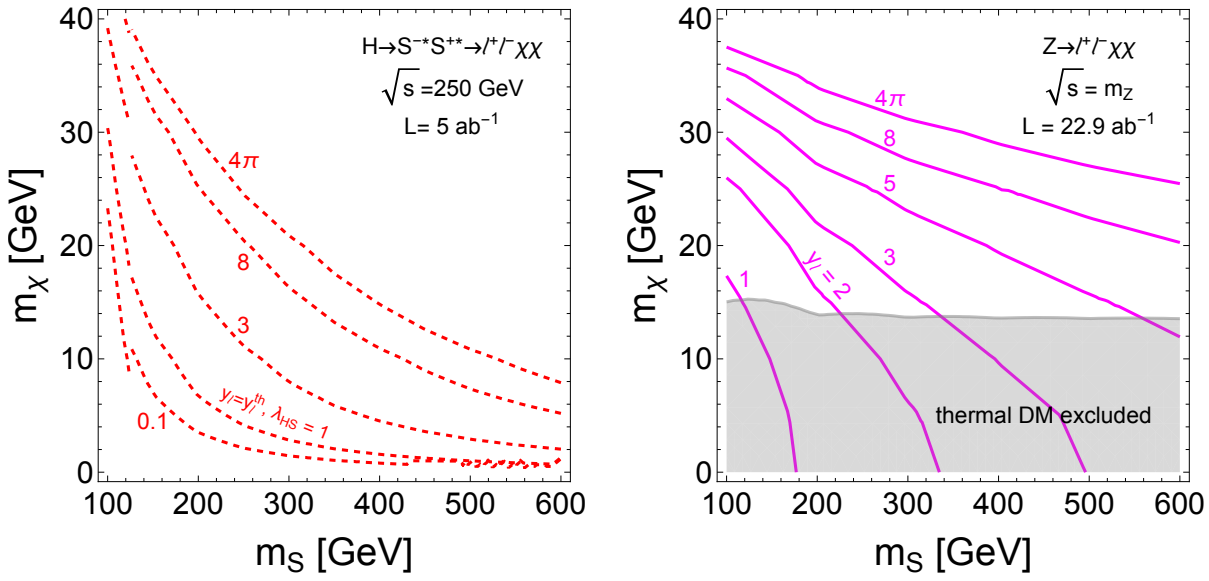

FIG. 16: These two plots come from Ref. [58]. Left: The 95% confidence level (C.L.) constraint on the coupling combination λ_{HS} as contours resulting from the exotic decay $h \to S^{\pm(*)}S^{\mp *} \to \ell^+\chi\ell'^-\chi$. The lepton portal coupling y_ℓ is fixed at $y_\ell^{\rm th}$, representing the value required to achieve the correct DM relic abundance. Right: The 95% C.L. constraint contours for y_ℓ in the exotic decay $Z \to \ell^+\chi\ell'^-\chi$. The grey shaded region indicates the parameter space that can be excluded if $y_\ell = y_\ell^{\rm th}$.

future CEPC is anticipated to impose stringent constraint on the interaction strengths for scenarios with a relatively light DM candidate, $m_\chi \lesssim 30$ GeV, and a mediator scalar mass m_S within the sub-TeV scale.

Another example is the Higgs decay into a dark shower, i.e., a shower of dark-sector particles, which can be bosons or be fermions, for example, composite neutrinos [59]. These can either decay promptly or be long-lived and their decay back to visible SM particles can be either hadronic or leptonic. The process is motivated by generic considerations of hidden sector strong dynamics. It also appears in the discussion of neutral naturalness [60]. Current studies have been focusing on the Higgs decays into a pair of twin glueballs [61–66], but this is only a subclass of the generic Higgs decays into these final states. This dark shower channel is also motivated by the class of models with a large number of light scalars [67], e.g., NNaturalness [68], electroweak scale as a trigger [69], and delayed or non-restored electroweak symmetry [70–73].

2. Z Exotic Decays via Dark Sector

Besides the exotic decays of the SM Higgs boson, the exotic decay of the Z boson constitutes an additional prospect for the investigation beyond the SM physics [74]. To refine the precision in measuring SM parameters, the forthcoming CEPC will include the operation at the Z resonance [11, 75], a regime that could potentially yield an enormous quantity of Z bosons, ranging from Giga (10^9) to Tera (10^{12}).

Notably, within the context of the model under consideration [58], there exists an exotic decay mode $Z \to \ell^+\chi\ell'^-\chi$, which results in a final state characterized by a pair of leptons accompanied by missing energy. This decay channel is mediated by two distinct types of Feynman diagrams: the first involves a pair of virtual $S^\pm$ particles via the ZS^+S^- vertex, while the second proceeds via a single virtual $S^\pm$ that emerges from the $Z\ell^+\ell^-$ vertex, with the scalar S coupling to one of the leptons. Given the assumption that the charged scalar $S^\pm$ possesses a mass exceeding 100 GeV, thereby surpassing the mass of any other particle involved, the decay width is predominantly governed by the second diagram type. This decay width exhibits a dependence that is proportional to $y_\ell^4 m_S^{-4}$.

In the right panel of Fig. 16, the 95% C.L. constraint on the branching ratio for the exotic decay mode is approximately $\mathrm{Br}(Z \to e^-e^+\chi\chi) \lesssim 10^{-9}$ for the Tera Z scenario. However, it is known that this upper bound is sensitive to the mass parameters m_χ and m_S. In the right panel of Fig. 16, the 95% C.L. upper limit on y_ℓ is represented by the region above the magenta contours. This constraint is compared with the requirement for y_ℓ^{th} derived from thermal relic considerations. It becomes apparent that, under the Tera Z framework, DM candidates with a mass of $m_\chi \lesssim 13$ GeV are excluded by the search for the exotic decay $Z \to e^-e^+\chi\chi$, as theoretically y_ℓ^{th} exceeds the derived limit from the Z exotic decay. The exclusion zone is illustrated in gray and denoted as "thermal DM excluded". This constraint serves as a supplementary bound for scenarios with large scalar mass m_S, compared with the constraints imposed by the LHC, which are not predicated on the on-shell production of S. Moreover, considering that both the decay width for the exotic decay and the DM annihilation cross-section are proportional to $y_\ell^4 m_S^{-4}$, the exclusion boundary can be extended horizontally to substantially high values of m_S. Consequently, this provides a robust constraint for the DM model.

Besides the specific exotic Z decay channel above, Ref. [74] have studied a broad range of

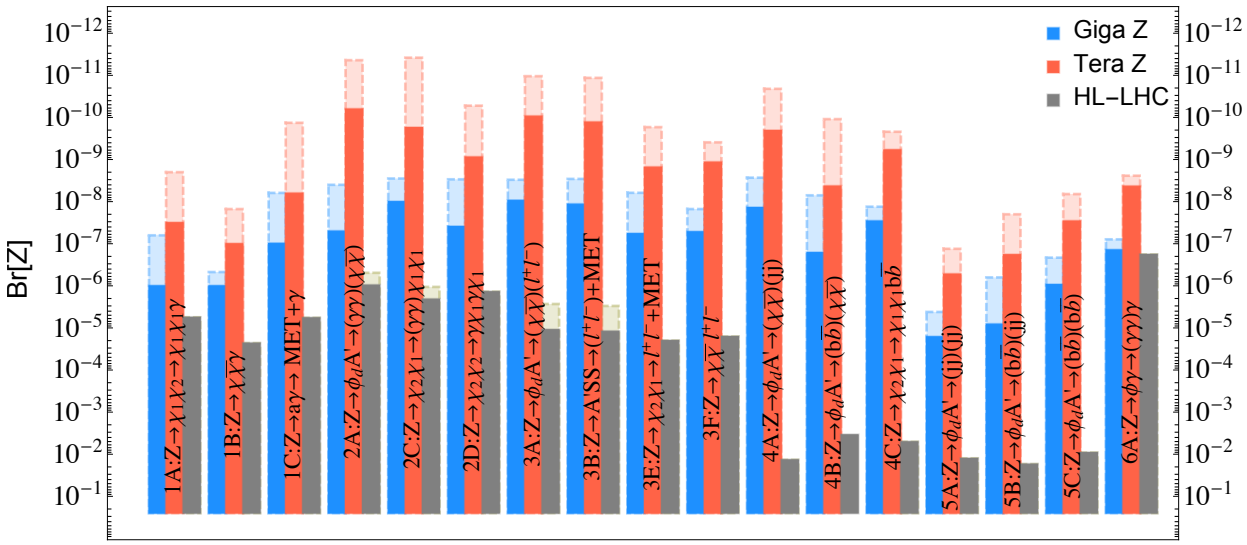

FIG. 17: The reach for the branching ratio of various exotic Z decay modes at the future Z-factories (Giga Z and Tera Z) and the HL-LHC at 13 TeV with $\mathcal{L} = 3$ ab^{-1} [74]. The sensitivities, in general, generally also depend on model parameters, such as the masses of the mediator and dark matter. The dark-colored regions with solid boundaries represent the reach for the worst case in the parameter space, while the lighter regions with dashed boundaries indicate reach in the best case.

dark sector models and model-independent exotic Z decay channels at future e^+e^- colliders with the Giga Z and Tera Z options. Four general categories of dark sector models have been included: Higgs portal dark matter, vector portal dark matter, inelastic dark matter and axion-like particles. Focusing on channels motivated by the dark sector models, an independent model study of the sensitivities of Z-factories is also carried out. The results are compared with the reach of high luminosity LHC (HL-LHC). The final states of the exotic decays are categorized according to the number of resonances and possible topologies. The projected reach for those channels is shown in Fig. 17. In comparison with the HL-LHC, the future Z-factories can be more sensitive to many interesting decay modes. The exotic Z decay summary table is given here.

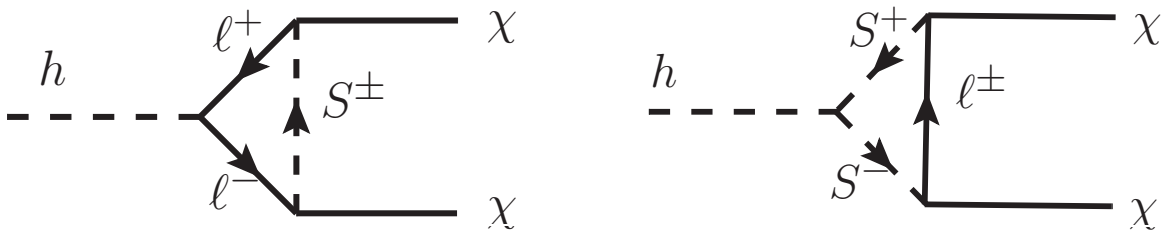

FIG. 18: The one-loop induced Higgs invisible decay (from Ref.[58]). The cross-diagrams for Majorana fermion χ are not shown here but are included in the calculation.

F. Higgs exotic invisible decays

The Higgs invisible decay $h \to \chi\chi$ is induced by the two Feynman diagrams at one-loop level listed in Fig. 18, and is similar to the Higgs to neutralinos decay in the SUSY models [76–79]. Due to the small lepton mass, usually the first diagram is negligible.

The most stringent constraint on the branching ratio for the invisible decay of the Higgs boson is $Br(h \to \text{inv}) < 13\%$, ascertained by the ATLAS Run-II with an integrated luminosity of 139 fb^{-1} [80]. Projected advancements at the HL-LHC anticipate an enhanced sensitivity for the detection of invisible Higgs decay, with expectations set around 3.5% [81]. Furthermore, at the future e^+e^- colliders such as the CEPC, the sensitivity could potentially be refined to approximately 0.3% [11].

Anticipated data from forthcoming collider experiments can set limits on $y_\ell^2\lambda_{HS}$, depending on the scalar mass m_S and the DM candidate mass m_χ. In the left panel of Fig. 19, one can observe the sensitivity contours for $y_\ell^2\lambda_{HS}$ corresponding to the LHC (brown), the HL-LHC (blue), and the CEPC (red). The dashed and solid lines represent $y_\ell^2\lambda_{HS} = 1$ and $y_\ell^2\lambda_{HS} = 10$, respectively. It is shown that the prospective e^+e^- collider exhibits superior sensitivity in comparison to the hadron collider alternatives.

Turning to the right panel of Fig. 19, the Yukawa coupling y_ℓ is calibrated to its thermal value y_ℓ^{th}, which is requisite for satisfying the DM relic abundance criteria. By fixing the values of m_S and m_χ, the future sensitivity to λ_{HS} can be extrapolated utilizing the projected CEPC sensitivity for the invisible Higgs decay branching ratio, $Br(h \to \text{inv}) = 0.3\%$. The resulting sensitivity contours are illustrated accordingly. A notable characteristic is the reduction in sensitivity to λ_{HS} for m_χ values below 6 GeV, attributable to the decay width's leading order term in the small m_χ expansion being linearly dependent on m_χ. As m_χ

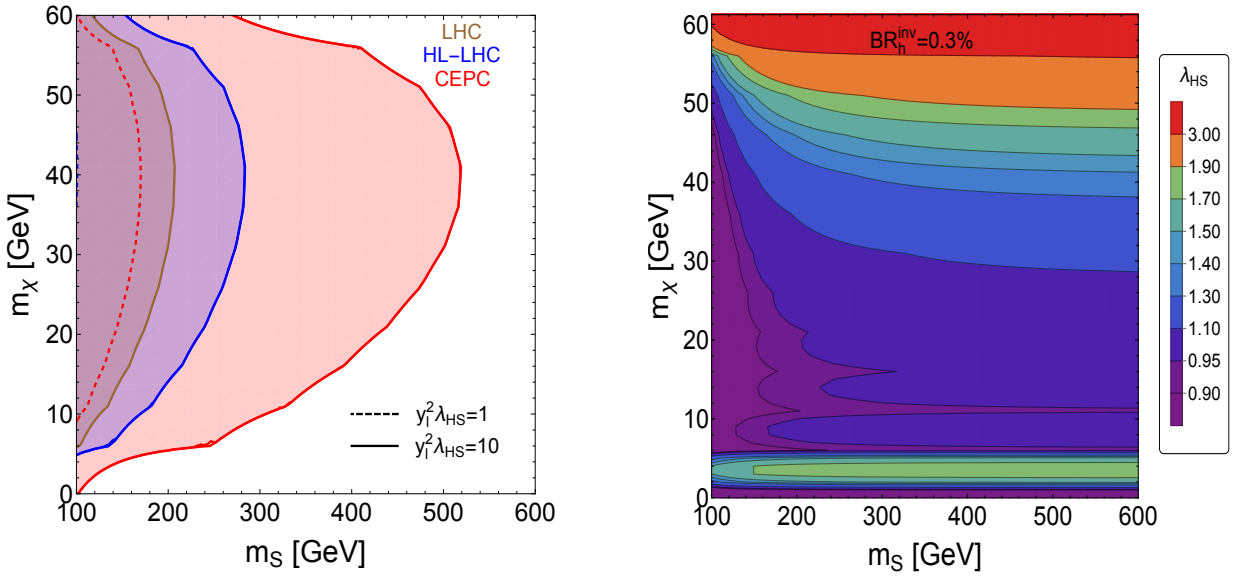

FIG. 19: These two plots come from Ref.[58]. Left: the Higgs invisible decay as a probe for the combination $y_\ell^2\lambda_{HS}$ at different colliders. Right: the CEPC sensitivity $\mathrm{Br}(h \to \mathrm{inv}) < 0.3\%$ can set bounds on λ_{HS} if we fix $y_\ell = y_\ell^{\mathrm{th}}$ from the relic abundance requirement.

diminishes further, the thermal value y_ℓ^{th} increases to compensate the annihilation cross-section, thereby restoring and even enhancing the sensitivity to λ_{HS}. Consequently, the optimal sensitivity for λ_{HS} is achieved in regions of small m_S and moderate m_χ.

G. Decays into Long-Lived Particles

1. *Higgs exotic decays into Long-Lived Particles*

The CEPC is proposed to be a key facility in the search for new physics, particularly through the examination of Higgs boson decays into long-lived particles (LLPs). A recent comprehensive study has shed light on several key areas that could potentially improve our understanding of the universe's fundamental particles and interactions.

The research [82] has investigated the possibility of neutrally charged LLPs being produced through the exotic decay of the Higgs boson. By analyzing the process $e^+e^- \to ZH$, where the Z boson decays inclusively and the Higgs boson further decays into LLPs (X_1 and X_2), the study has employed advanced machine learning techniques to analyze an integrated

luminosity of 20 ab^{-1}. These LLPs can decay into either a neutrino pair or a quark-antiquark pair, leading to distinct final states that were identified using Convolutional Neural Networks (CNN) and Graph Neural Networks (GNN). The findings have provided constraints on the branching ratio of Higgs boson decay to LLPs, offering a new observation on the Higgs boson's decay characteristics.

Furthermore, the study [83] has explored the production of long-lived scalar particles from Higgs exotic decays at the CEPC. The signal process involves a Higgsstrahlung event, followed by the decay of the Higgs boson into a new long-lived scalar boson X, which subsequently decays into a pair of quarks. This research has considered the Higgs bosons produced at CEPC, providing sensitivities to the branching ratio of $h \to XX$ and interpreting the results within the framework of the Higgs-portal Hidden Valley model and neutral-naturalness models.

The investigation [84] into displaced-vertex signatures of scalar LLPs pair-produced from exotic Higgs decays has also been a significant focus. The study has examined two theoretical models, including a Higgs-portal model that predicts a very light scalar boson h_s, which decays into a pair of muons or pions, and a neutral-naturalness model that predicts the lightest mirror glueball with a mass of $\mathcal{O}(10)$ GeV. These models have been analyzed for their distinctive signatures at colliders, providing a comprehensive understanding of the potential LLP signatures.

Additionally, the study [85] has addressed the sensitivity reach to massive LLPs within the context of the Hidden Valley model, where the Higgs boson decays into two long-lived Hidden-Valley particles that subsequently decay into b-quarks. The research has also investigated the sensitivity to long-lived dark photons produced in Higgsstrahlung events via the Higgs portal, $h \to \gamma_D\gamma_D$. The high statistical significance data generation at the CEPC, combined with the advanced analysis techniques, is expected to provide a more precise measurement of the Higgs boson's decay width, surpassing current measurements at the LHC. More detailed discussions can be found in Sec.VI.

2. Z exotic decays into Long Lived Particles

At the CEPC, the high-luminosity Z-boson factory provides a unique opportunity to investigate Long-Lived Particles (LLPs) from Z-boson exotic decays.

The study [86] examines the sensitivity of the CEPC to the decay of Z-bosons into long-lived lightest neutralinos (denoted as $\tilde{\chi}_1^0$) within the context of R-parity-violating supersymmetry. The lightest neutralino is predominantly bino-like with minor Higgsino components. The research emphasizes the $\lambda'_{ijk} L_i \cdot Q_j \bar{D}_k$ operators, particularly the $\lambda'_{112} L_1 \cdot Q_1 \bar{D}_2$ operator, which leads to the decay of the lightest neutralino into SM particles via a scalar-fermion exchange. For specific conditions, the lightest neutralino becomes long-lived, allowing it to travel a macroscopic distance before decaying.

Besides, the sensitivity estimation is provided for the CEPC in terms of contour curves on a plane of model parameters $\lambda'_{112}/m^2_{\tilde{f}}$ versus $m_{\tilde{\chi}_1^0}$. It shows that for a branching ratio $\mathrm{Br}(Z \to \tilde{\chi}_1^0 \tilde{\chi}_1^0)$ of 10^{-3} and a neutralino mass of approximately 40 GeV, the model parameter $\lambda'_{112}/m^2_{\tilde{f}}$ can be probed down to about 1.5×10^{-14} (3.9×10^{-14}) GeV^{-2} at the CEPC with a center-of-mass energy of $\sqrt{s} = 91.2$ GeV and integrated luminosities of 150 (16) ab^{-1}.

Additionally, the study [87] discusses the investigation of axion-like particles (ALPs) coupled to charged leptons in Z-boson decays at CEPC. The ALPs are assumed to have very long lifetimes and behave as missing energy. The study analyzes the signal process $e^- e^+ \to \mu^- \mu^+ a$ and considers various background sources. Sensitivity reaches are presented for different integrated luminosities.

Lastly, the study [88] addresses the sensitivity of different experiments to Z-boson decays to a pair of long-lived neutralinos in R-parity-violating supersymmetry. Assuming a negligible background, it presents the sensitivity reaches of different far detector (FD) designs at the CEPC for a branching ratio of $Z \to \tilde{\chi}_1^0 \tilde{\chi}_1^0$ equal to 10^{-3}. It also compares these sensitivity reaches with those of the main detector (MD) and other experiments.

Overall, at the CEPC, the potential to probe BSM physics by studying Z-boson exotic decays could offer insights into long-lived particles and their properties. More detailed discussions can be found in Sec.VI.

H. The 95 GeV Higgs boson at the CEPC

CMS and ATLAS have performed searches for scalar di-photon resonances using LHC Run 1 and 2 data. CMS observed a local excess with $2.8\,\sigma$ significance at 95.3 GeV in the Run 1 result. Recently, results based on the full Run 2 data set at 13 TeV showed a local excess of $2.9\,(1.7)\,\sigma$ at 95.4 GeV at CMS [89] (ATLAS) [90]. Using both ATLAS and CSM Run 2 results, and neglecting possible correlations, in Ref. [91] a combined signal strength of $\mu_{\gamma\gamma}^{\rm exp} = 0.24^{+0.09}_{-0.08}$ was obtained, corresponding to an excess of $3.1\,\sigma$. LEP reported a local $2.3\,\sigma$ excess in the $e^+e^- \to Z(\phi \to b\bar{b})$ searches [92], consistent with a scalar resonance with a mass of about 95.4 GeV and a signal strength of $\mu_{bb}^{\rm exp} = 0.117 \pm 0.057$ [93, 94]. Here we consider the possiblity that these excesses arise from the production of a single new particle – a possible first sign of BSM physics in the Higgs sector.

In Refs. [91, 95] it was demonstrated that the extension of the 2HDM by a complex singlet, the S2HDM [96], can give a perfect description of these excesses, while being in agreement with LHC BSM Higgs searches and LHC Higgs rate measurements. The S2HDM represents a template for a broad class of models where a mostly gauge-singlet scalar particle, h_{95}, obtains its couplings to fermions and gauge bosons via the mixing with the SM-like Higgs boson at 125 GeV. In Ref. [95] it was also demonstrated that a future e^+e^- collider operating at 250 GeV could determine the couplings of h_{125} to a sufficiently high precision to find deviations w.r.t. a SM Higgs boson (see Fig. 20 left) and thus test the proposed scenario. Despite the suppressed couplings of the possible state at 95.4 GeV compared to h_{125}, a future e^+e^- Higgs factory could produce h_{95} in large numbers (see e.g. Ref. [97]) and determine its properties with high precision (see Fig. 20 right).

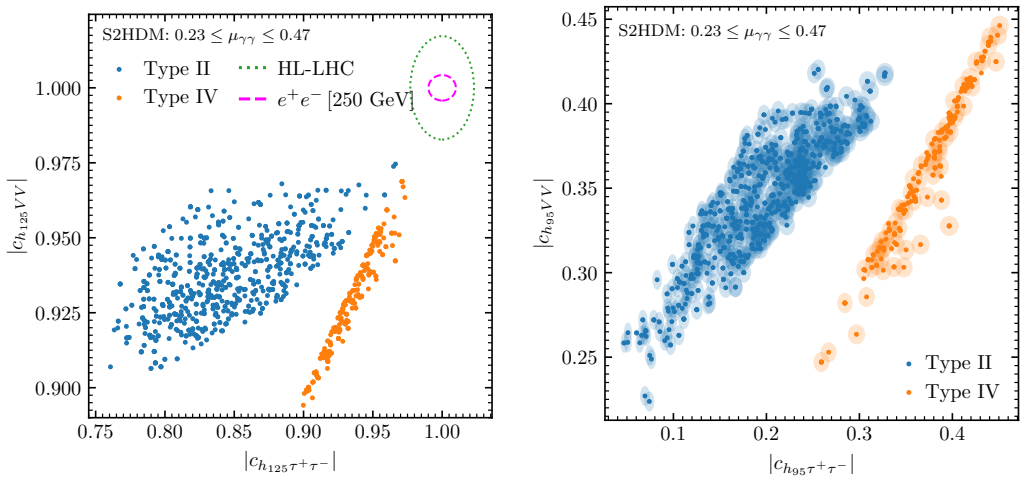

FIG. 20: S2HDM parameter points passing the applied constraints for the di-photon and $b\bar{b}$ signal strengths. (For the di-photon signal strength a slightly higher value as $\mu_{\gamma\gamma}^{\text{exp}}$ were used, as in Ref. [95], which is not expected to change the results in a qualitative way.) Blue (orange) points correspond to the S2HDM type II (IV). Left: $(|c_{h_{125}\tau^+\tau^-}|, |c_{h_{125}VV}|)$ plane. The green dotted and the magenta dashed ellipses indicate the projected experimental precision of the coupling measurements at the HL-LHC [98] and a future e^+e^- collider operating at 250 GeV and assuming 2 ab^{-1} of integrated luminosity [99], respectively, with their centers located at the SM values. Right: $(|c_{h_{95}\tau^+\tau^-}|, |c_{h_{95}VV}|)$ plane (where $c_{h_{95}xx}$ denotes the coupling strength relative to the SM Higgs-boson coupling). The shaded ellipses around the dots indicate the projected experimental precision with which the couplings of h_{95} could be measured at a future e^+e^- collider, which we evaluated according to Ref. [100]. Here $c_{h_{95}xx}(c_{h_{125}xx})$ denotes the coupling strength of $h_{95}(h_{125})$ relative to the SM Higgs-boson coupling.

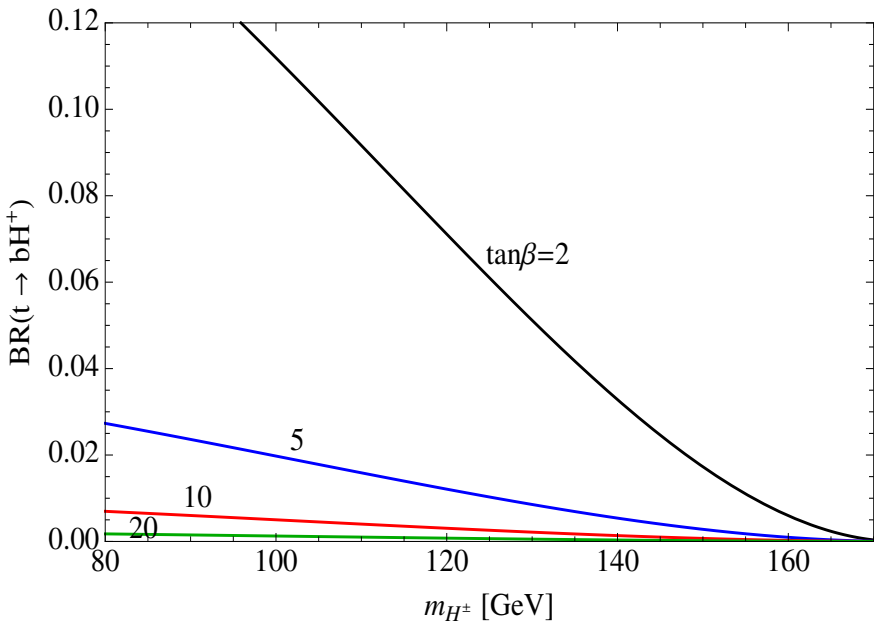

FIG. 21: Br($t \to bH^+$) for $\tan\beta = 2$ (black), 5 (blue), 10 (red), 20 (green). The t decay into H^+ is larger for smaller $m_{H^\pm}$ and smaller $\tan\beta$, from Ref.[101].

I. Top quark exotic decays

In the context of the dark force model, as outlined in Ref.[101], the decay of a top quark into a charged Higgs boson via the process $t \to bH^+$ is a significant opportunity for exploring new physics, particularly if the charged Higgs is relatively light. This charged Higgs, in turn, is proposed to predominantly decay into dark gauge bosons (Z's), which are key components of the dark sector. Consequently, future experimental data, potentially from the CEPC operating at 350 GeV, could potentially observe the decay chain $t \to bH^+ \to bW^+ + Z's$.

Direct calculations demonstrate that for a charged Higgs mass of $m_{H^\pm} = 140$ GeV, the branching ratio for the top quark decay into a charged Higgs, Br $(t \to bH^+)$, is approximately between 0.03 and 0.0003, within the parameter range of $\tan\beta = 2 - 20$, as shown in Fig.21. This range of branching ratios indicates that even a small proportion of top quark decays could produce a detectable number of Z' bosons at high-energy collider experiments.

The detection of such exotic decays depends on the precise measurement of the top quark's mass and decay width. It is highlighted that the present large uncertainty in the top quark decay width (around 25%) leaves room for new decay modes that could originate from physics beyond the SM. Moreover, it underscores that the top quark's short lifetime

Source	m_{top} precision (MeV)	
	Optimistic	Conservative
Statistics	9	9
Theory	8	24
Quick scan	2	2
α_S	17	17
Top width	10	10
Experimental efficiency	5	44
Background	2	14
Beam energy	2	2
Luminosity spectrum	3	6
Total	24	57

TABLE VI: The expected statistical and systematical uncertainties of the top quark mass measurement in optimistic and conservative scenarios at CEPC, from Ref. [102]

and its decay before forming hadrons make it an ideal candidate for probing new physics.

A study of top quark mass measurements is presented at the $t\bar{t}$ threshold based on CEPC [102]. A centre-of-mass energy scan near two times the top quark mass is performed, and the measurement precision of top quark mass, width and α_S are evaluated using the $t\bar{t}$ production rates. Realistic scan strategies at the threshold are discussed to maximise the sensitivity to the measurements individually and simultaneously in the CEPC scenarios, assuming a total luminosity limited to 100 fb^{-1}. With the optimal scan for individual property measurements, the top quark mass precision is expected to be 9 MeV, the top quark width precision is expected to be 25 MeV and α_S can be measured at a precision of 0.00034, considering only the statistical uncertainty. Taking into account the systematic uncertainties from theory, width, α_S, experimental efficiency, background subtraction, beam energy and luminosity spectrum, the top quark mass can be measured at a precision of 24 MeV optimistically and 57 MeV conservatively at CEPC, as shown in Tab. VI.

J. Summary

This chapter explores the potential for discovering new physics through exotic decay channels of the Higgs boson, Z boson, and top quark, emphasizing their significance in understanding physics BSM and electroweak interactions. The CEPC is highlighted as a powerful facility for probing these decays and shedding light on unexplored aspects of particle physics. Exotic decays of Higgs, Z bosons, and top quarks provide a crucial window into novel physics, often associated with Higgs portal models or exotic effective operators. These decays are vital for precision measurements at future Higgs factories and could benefit from machine learning technologies that enhance data analysis and exotic signal detection.

Lepton colliders like the CEPC are particularly well-suited for detecting Higgs boson decays into BSM particles, such as X_1 and X_2, which may undergo further decays into multiple particle final states. Four distinct decay categories are considered. The recoil mass method used at lepton colliders allows for better separation of signal from background, compared to hadron colliders like the LHC. CEPC's projected sensitivity of the decay branching ratio enhancements is expected to outperform the LHC by orders of magnitude, especially for channels that do not involve missing energy. The potential of the SM-s model, where a new scalar particle (s) mixes with the Higgs boson, is discussed. This theoretical framework addresses issues like naturalness and dark matter interactions, which tackle the hierarchy problem. One notable decay, $h \to ss$, which is difficult to detect at the LHC, can be studied more effectively at the CEPC due to its cleaner experimental environment and greater sensitivity. Supersymmetric extensions, such as the NMSSM and scMSSM, are examined for their ability to generate exotic Higgs decays, including invisible decays into dark matter candidates like neutralinos. The CEPC's capabilities in probing such decays, particularly final states like $h_1 \to 4\tau$, exceed those of the HL-LHC with only 0.26 fb^{-1}.

The chapter also discusses Higgs decays into dark-sector particles, such as long-lived particles (LLPs), which could decay into visible SM particles after traveling significant distances. Lepton colliders, like the CEPC, operating at high luminosity, are ideal for exploring these decays. Potential exotic decays of the Z boson into LLPs are also covered, highlighting the unique capabilities of future Z factories (e.g., Giga Z, Tera Z) in detecting such processes. Invisible Higgs decays, potentially into dark matter candidates, are another focus. Current constraints from the LHC could be improved significantly at the CEPC, where sensitivities

to invisible decays are expected to be an order of magnitude higher than at the HL-LHC. The possibility of detecting LLPs through exotic Higgs decays at the CEPC is further explored. Advanced machine learning techniques, such as convolutional and graph neural networks, offer promising constraints on the branching ratios for these decays. The detection of LLPs in both Higgs and Z boson decays is examined, providing a path for future investigations into these elusive particles. Additionally, the potential existence of a 95 GeV scalar boson is discussed, as suggested by excesses observed in CMS and ATLAS data from Run 1 and Run 2 of the LHC. This possible BSM particle, described within the S2HDM model, represents a gauge-singlet scalar that mixes with the SM Higgs boson. The CEPC could provide precise measurements to confirm or refute the presence of such a particle. Finally, exotic decays of the top quark, such as $t \to bH^+$, where the charged Higgs decays into dark-sector particles like dark gauge bosons, are discussed. The CEPC, particularly at higher energies, presents an opportunity to detect these decays and investigate new physics related to the top quark's interactions with the dark sector.

Overall, the CEPC offers extensive opportunities to explore exotic decays and probe BSM physics through precision measurements and improved detection capabilities, positioning it as a critical tool for advancing particle physics.

V. DARK MATTER AND DARK SECTOR (JIA, XIAOPING, YONGCHAO, BHUPAL)

There is substantial evidence for the existence of Dark Matter (DM) from astrophysical and cosmological observations. However, its particle nature remains unknown and is awaiting for exploration. Conventional dark matter candidates, such as Weakly Interacting Massive Particles (WIMPs), have significant couplings to Standard Model particles, which enable the thermal freeze-out mechanism and result in the correct relic abundance [103, 104]. This has motivated searches for DM at high-energy hadron and lepton colliders, aiming to produce DM particles directly. These searches target both heavy DM particles up to the TeV scale and lighter ones down to the GeV scale. Collider searches offer a complementary cross-check to direct and indirect search experiments. A recent comprehensive review of DM phenomenology can be found in Ref. [105] and the review of DM collider phenomenology can be found in Ref. [106].

Recently, a new class of models has garnered significant attention within the scientific community, proposing that DM does not directly couple to SM particles but resides in a "dark sector" (or "hidden sector") [107]. The dark sector interacts with the SM through portal particles, which could have tiny couplings to the SM sector to evade the null results from the direct detection, but still could provide the DM right relic abundance. Thus, for these interactions to enable secluded annihilation for DM relic abundance, the mass of the portal particles must be smaller than that of the DM particles. Due to their feeble coupling and low mass, these portal particles are ideal targets for searches at the luminosity frontier. Electron-positron colliders such as CEPC and FCC-ee, which function as high-luminosity W, Z, and Higgs boson factories and offer cleaner experimental environments compared to hadron colliders, are well-suited to search for these feebly interacting portal particles [11, 108]. For example, the CEPC can search for exotic decays related to the dark sector in both Z and Higgs decay events, as discussed in Sec. IV E. Additionally, the CEPC is capable of searching for various DM particles, including those predicted by supersymmetric models, scalar portals, lepton portals, and gauge mixing portals. It can also investigate DM particles with millicharge, electromagnetic form factors, and those described by effective field theory (EFT) frameworks. The simplified models typically used in the LHC new physics searches can be found in Ref. [109].

The phenomenology studies of DM and dark sector particles at the lepton colliders have been performed intensively recently. In this section, we will refer to previous study results in Refs. [11, 108] and focus exclusively on recent progress in the following benchmark scenarios to highlight the capabilities of CEPC. We categorize DM and dark sector models based on their portal connections to SM, specifically: (A) Scalar portal, (B) Fermion portal, (C) Vector portal, and (D) DM within the EFT framework. In the last subsection (E), we discuss a scenario where dark matter does not require a portal but is instead directly charged under Standard Model gauge interactions. We also examine how the loop effects of this DM influence electroweak and Higgs precision observables, providing constraints on this specific model. Note that the Axion portal is specifically discussed in the later section More Exotics XI. For each of these models, we discuss the sensitivity of the CEPC. A summary of the sensitivity for each model, along with corresponding figures and references, is summarized in Table VII for readers convenience.

Portal	Effective operator	$\sqrt{s}$ [GeV]	$\mathcal{L}[ab^{-1}]$	Sensitivity of CEPC (HL-LHC)	Figs.	Ref.
Scalar	$\lambda_{HP}\lvert H\rvert^2 S^2 \to$ scalar mixing $\sin\theta$	250	5	invisible S, $\sin\theta \approx 0.03$ (0.20 global-fits)	22	[110]
Fermion	$y_\ell \bar{\chi}_L S^\dagger \ell_R$ + H.c.	250	5	covering 100 GeV $< m_S <$ 170 GeV	23	[58]
	$\kappa \Phi \overline{q'_L} \ell_R$ + H.c. (dark QCD)	250	5	$m_\Phi \sim 10$ TeV for $c\tau_{\rm darkpion} \in [1, 10^3]$ cm (Null)	25	[111]
	$y\Phi \bar{F}_L \ell_R$ + H.c.	240	5.6	$y\theta_L \in [10^{-11},\ 10^{-7}]$ ($\lesssim 10^{-8} - 10^{-9}$)	26	[112]
Vector	$A'_\mu \left(e\epsilon J^\mu_{\rm em} + g_D \bar{\chi}\gamma^\mu \chi\right)$	250	5	$\epsilon \sim 10^{-3}$ for $g_D = e$ and $m_{A'} < 125$ GeV ($\epsilon \sim 0.02$)	27, 28	[110]
	$\varepsilon A_\mu \bar{\chi}\gamma^\mu \chi$, (millicharge DM)	250	5	$\epsilon \sim 0.1$ for $m_\chi \sim 50$ GeV	29	[113]
		91.2	2.6	$\epsilon \sim 0.02$ for $m_\chi \sim 5$ GeV		
		160	16	$\epsilon \sim 0.5$ for $m_\chi \sim 10$ GeV		
	$\frac{1}{2}\mu_\chi \bar{\chi}\sigma^{\mu\nu}\chi F_{\mu\nu} + \frac{i}{2} d_\chi \bar{\chi}\sigma^{\mu\nu}\gamma^5 \chi F_{\mu\nu}$	91.2	100	$\mu_\chi, d_\chi \sim 4 \times 10^{-7}$ (4×10^{-6})μ_B for $m_\chi < 25$ GeV	30	[114]
	$-a_\chi \bar{\chi}\gamma^\mu\gamma^5 \chi \partial^\nu F_{\mu\nu} + b_\chi \bar{\chi}\gamma^\mu \chi \partial^\nu F_{\mu\nu}$	240	20	$a_\chi, b_\chi \sim 10^{-6}$ (2×10^{-6}) GeV^{-2} for $m_\chi < 80$ GeV		
EFT	$\frac{1}{\Lambda^2}\sum_i \left(\bar{\chi}\gamma_\mu(1-\gamma_5)\chi\right)\left(\bar{\ell}\gamma^\mu(1-\gamma_5)\ell\right)$	250	5	$\Lambda_i \sim 2$ TeV ($m_\chi = 0$) (Null)	31	[115]
	$\frac{1}{\Lambda_A^2}\bar{\chi}\gamma_\mu\gamma_5\chi\bar{\ell}\gamma^\mu\gamma_5\ell$	250	5	$\Lambda_A \sim 1.5$ TeV (Null)	32	[113]
	$\sum_i \frac{1}{\Lambda_i^2}\left(\bar{e}\Gamma_\mu e\right)\left(\bar{\nu}_L\Gamma^\mu\chi_L\right)$ + H.c. $\Gamma_\mu = 1, \gamma_5, \gamma_\mu, \gamma_\mu\gamma_5, \sigma_{\mu\nu}$	240	20	$\Lambda_i \sim 1$ TeV ($m_\chi = 0$) (Null)	33	[116]

TABLE VII: Recent results from the CEPC study on dark sector signals. The first column lists the signal signatures, the second column presents the corresponding relevant operators, the third and fourth columns provide the center-of-mass energy and the integrated luminosity. The fifth column presents the sensitivity to the coupling, suppression scale, or branching ratios at the CEPC. Where relevant HL-LHC sensitivities are available, they are shown in parentheses or shown with Null meaning HL-LHC constraints do not apply. The final two columns provide the corresponding figures in this draft and references for the readers' convenience.

A. Scalar portal

The scalar portal means the DM interact with SM particles via SM scalars, such as Higgs. Thus, hidden sector particles can be associated with the production of Z and H bosons at the CEPC. Ref. [110] studied the reach of an ultraviolet (UV) model, the Double Dark Portal model, at the CEPC with $\sqrt{s} = 250/500$ GeV and $\mathcal{L} = 5\,\text{ab}^{-1}$. This model includes both gauge boson and scalar portals; in the scalar portal, there is a new dark sector scalar S with mixing angle $\sin\alpha$ to the SM Higgs. The scalar mixing can lead to the associated production with the SM Higgs H_0 boson: $\tilde{Z}S$, where the tilde denotes the particles in their mass eigenstates. In this channel, we considered the leptonic decay of the Z boson and the dark scalar S decay into dark matter χ, resulting in a final state of dilepton plus missing energy $\bar{\ell}\ell + \not{E}$. We show the exclusion sensitivities of this channel in Fig. 22, which provides

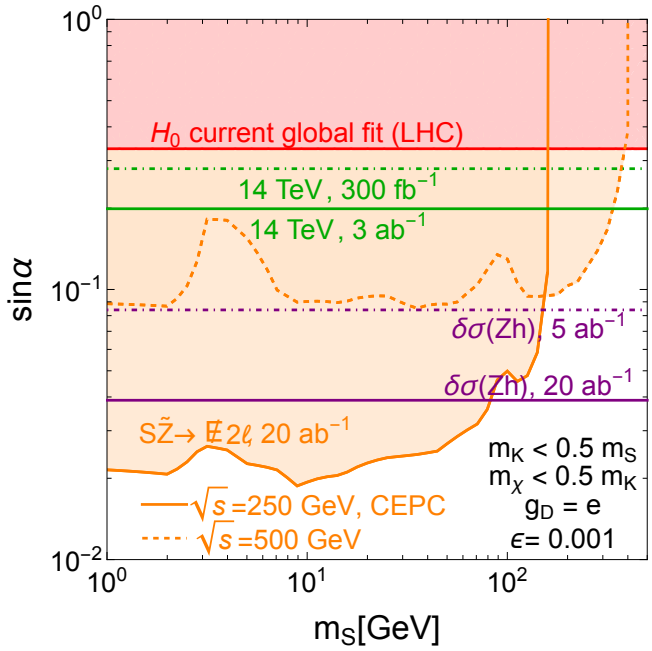

FIG. 22: Exclusion reach for the dark scalar and the SM Higgs mixing from the $\tilde{Z}S$, $\tilde{Z} \to \ell^+\ell^-$ search in the recoil mass distribution for invisible S decays in the $\sin\alpha$ vs. m_S plane using $5\,\text{ab}^{-1}$ of e^+e^- data at $\sqrt{s} = 250$ GeV or 500 GeV in orange shaded region. The purple lines come from the precision measurement of Zh cross-section at CEPC with 5ab^{-1} and 10ab^{-1}. For other constraints, see Ref. [110] for details.

the limits in the 2D parameter space of $\sin\alpha$-m_S for the dark scalar. The phenomenology for the vector portal in this model is presented in Section V C 1.

B. Fermion portal

Traditional WIMP DM generally come across a conflict between direct detection limit and relic abundance because they come from the same interaction and processes. In order to solve this conflict, many WIMP models carefully arrange the interactions to suppress the signals for direct and indirect detection [117]. For instance, direct detection signals can be tuned to couple to nuclear spin, or be suppressed by small momentum transfer or low velocity of dark matter. Indirect detection signals can be p-wave suppressed by configuring the initial dark matter pair state to have an angular momentum quantum number $L = 1$ or by being chirally suppressed. Therefore, collider searches become crucial and complementary, as the DM produced at colliders typically moves at velocities close to the speed of light, rendering

the low dark matter velocity suppression ineffective. In this section, we will explore three critical models that have been studied in recent researches.

1. *Lepton portal DM*

One relevant fermion portal example for the CEPC is the lepton portal DM model [118], in which a Majorana DM candidate, denoted as χ, couples to the SM right-handed leptons ℓ_R via a complex charged scalar mediator S through Yukawa-type coupling $y_\ell \bar{\chi}_L \ell_R S^\dagger$. Recently, Ref. [58] have studied the collider phenomenology and the interplay with the gravitational wave (GW) astronomy in an extension of the lepton portal DM model. The masses of DM and mediator S, as well as the lepton coupling y_ℓ and the Higgs portal coupling λ_{HS}, which related to the operator $\lambda_{HS}(S^*S)(H^\dagger H)$, can be probed at the CEPC via the pair production of mediators $e^+e^- \to S^{\pm(*)}S^\mp \to \ell^+\chi\ell'^-\chi$, exotic decays of the Higgs or Z boson, $h/Z \to S^{\pm(*)}S^{\mp(*)} \to \ell^+\chi\ell'^-\chi$ and $h \to \chi\chi$, and the Higgs couplings, including $h\ell^+\ell^-$, $h\gamma\gamma$ and hZZ. In the left and middle panels of Fig. 23, we show the constraints of CEPC at 240 GeV with 5 ab^{-1} from the pair production of mediators $e^+e^- \to S^{\pm(*)}S^\mp$ with the dark scalar subsequently decay into $S^\mp \to \ell^\mp\chi$.

In addition to the collider signals, the model might trigger a first-order phase transition in the early Universe, provided that the mediator mass parameter μ_S^2 is negative, and the Higgs portal coupling λ_{HS} is large enough. Therefore, the first-order phase transition can induce significant gravitational wave signal, which can probe the parameter space of the scalar potential couplings.

On the other hand, the scalar S can mediate 1-loop diagram with the same Higgs portal coupling, which modifies the Higgs decay process, such as $h \to \chi\chi$ invisible channel and $h \to \ell^+\ell^-$ leptonic channels. For invisible channel $h \to \chi\chi$, the partial decay width is given as

$$\Gamma(h \to \chi\bar{\chi}) = \frac{g_{h\chi\chi}^2 m_h}{8\pi}\left(1 - \frac{4m_\chi^2}{m_h^2}\right)^{\frac{3}{2}}, \quad g_{h\chi\chi} \approx -\frac{y_\ell^2 \lambda_{HS} m_\chi v}{16\pi^2 m_S^2} + \mathcal{O}\left(m_S^{-3}\right). \tag{2}$$

Given the Higgs invisible BR sensitivity for HL-LHC around 3.5% [81] and CEPC around 0.3% [11], we show the sensitivity reach for HL-LHC and CEPC on the coupling $\lambda_{\rm HS} y_\ell^2$ as 2D function of m_S and m_χ in the right panel of Fig. 23. For example, with $m_\chi = 40$ GeV and $m_S = 200$ GeV, the corresponding constraints for HL-LHC and CEPC are $\lambda_{\rm HS} y_\ell^2 < 1.84$

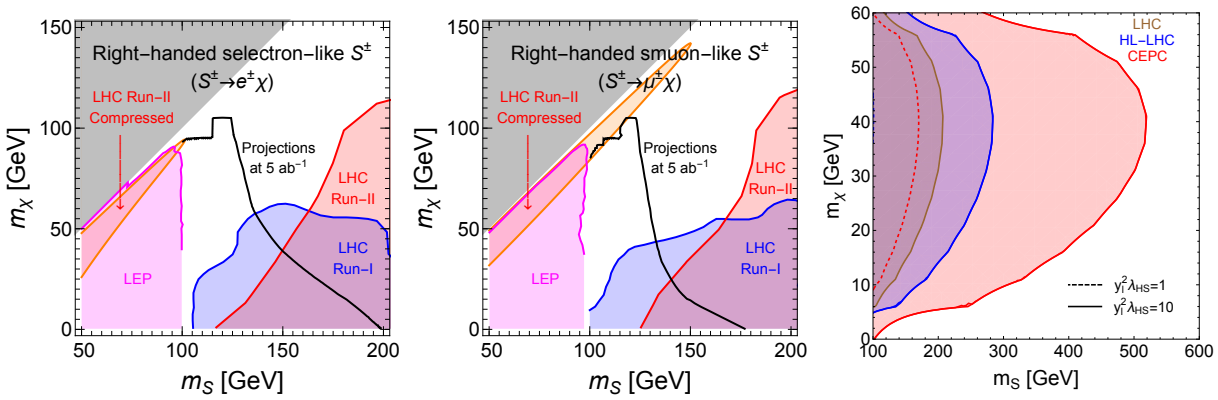

FIG. 23: Left and middle panels: the current constraints for right-handed selectron-like and right-handed smuon-like scalar S in the dark matter mass $m_{\rm DM}$ and dark scalar mass m_S 2D plane [58]. The shaded regions are exclusions from previous experiments. The black lines are projections for the CEPC reach at 5 ab^{-1} from the Drell-Yan process $e^+e^- \to S^{\pm(*)}S^{\mp}$ with the further dark scalar decay $S^{\mp} \to \ell^{\mp}\chi$. The sensitivity for m_S larger than $\sqrt{s}/2 = 120$ GeV are due to the inclusion of off-shell S^* contributions. Right panel: the sensitivity reach for HL-LHC and CEPC on the coupling $\lambda_{\rm HS}y_\ell^2$ as 2D function of m_S and m_χ for HL-LHC and CEPC [58].

and < 0.54, respectively.

In Fig. 24, we show the LISA sensitivity projections and the CEPC projections for comparison, where we have assumed the leptonic coupling y_ℓ has been fixed by the relic abundance requirement. Therefore, we can directly compare the LISA and CEPC projections on the Higgs portal coupling $\lambda_{\rm HS}$, where the overlap of the parameter space reachable by the two probes can be used for crosschecking. The procedure of Ref. [58] can be generalized to other leptophilic WIMP models that are difficult to be probed in the direct and indirect detections, especially the models with scalar DM and/or mediators in which a first-order phase transition may happen.

2. Asymmetric DM

In addition to DM, the observed baryon asymmetry of the Universe (BAU) is also a main puzzle in cosmology and particle physics. Current measurements show that the abundance of baryon and DM are roughly at the same order of magnitude ($\Omega_{\rm DM} \simeq 5\Omega_{\rm B}$) [119, 120].

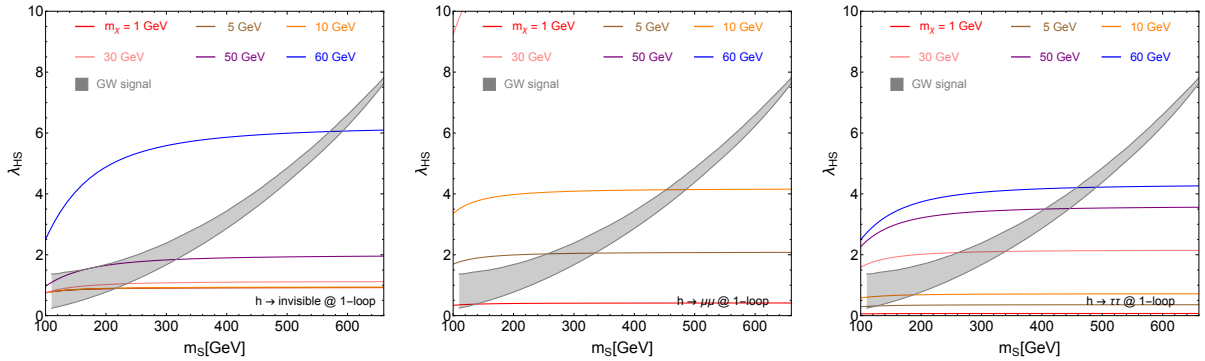

FIG. 24: Figure from Ref. [58], the interplay between GW detection and future e^+e^- collider searches. The gray shaded region is the LISA detectable parameter space. We have assumed the leptonic coupling y_ℓ has been fixed by the relic abundance requirement. From left to right, the sensitivities for λ_{HS} are shown from future CEPC precision measurements, in which the region above a given m_χ (corresponding to a colored line) can be probed.

This coincidence provides the motivation to consider the so-called "asymmetric DM" (ADM) model [121–124].

A new ADM model has been proposed and studied in [111]. In this model, the dark sector is charged under a dark QCD, SU(3)′, and the mass of DM is generated via the dark confinement (so our DM is actually a "dark baryon"). Furthermore, to generate dark and visible asymmetry simultaneously, we introduce a scalar mediator (labeled as Φ) that is charged under dark SU(3)′ and SM $\mathrm{U(1)_Y}$. Mediator Φ couples to dark quark (labeled as q') and SM right-hand leptons, and thus provide a portal for us to search for.

The Lagrangian related to collider search is

$$\mathcal{L} \supset \bar{q}'(\not{D} - m_{q'})q' + (D_\mu\Phi)^\dagger(D^\mu\Phi) - m_\Phi^2\Phi^\dagger\Phi - \frac{1}{4}G'^{\mu\nu}G'_{\mu\nu} - (\kappa\Phi\bar{q'}_L l_R + h.c.) \ , \qquad (3)$$

where $G'^{\mu\nu}$ is the field strength of dark gluon. Mediator Φ can be produced in pairs at LHC via the Hyper charge it carries. Then Φ decays to a SM lepton and a dark quark q'. While on CEPC, $q'\bar{q}'$ can be produced directly via a t-channel Φ. Due to the dark confinement, q' will hadronize to a cluster of dark mesons (labeled as π'). Dark meson π' (long-lived) will decay to lepton pair via the Φ portal, and leave displaced vertex inside detector. Fig. 25 (left) shows the predicted signal process on CEPC for illustration. The study shows that CEPC has the ability to cover a large parameter space of this model, see Fig. 25 (right). The mass of mediator can be excluded up to $\mathcal{O}(10)$ TeV, if the proper lifetime of dark pion

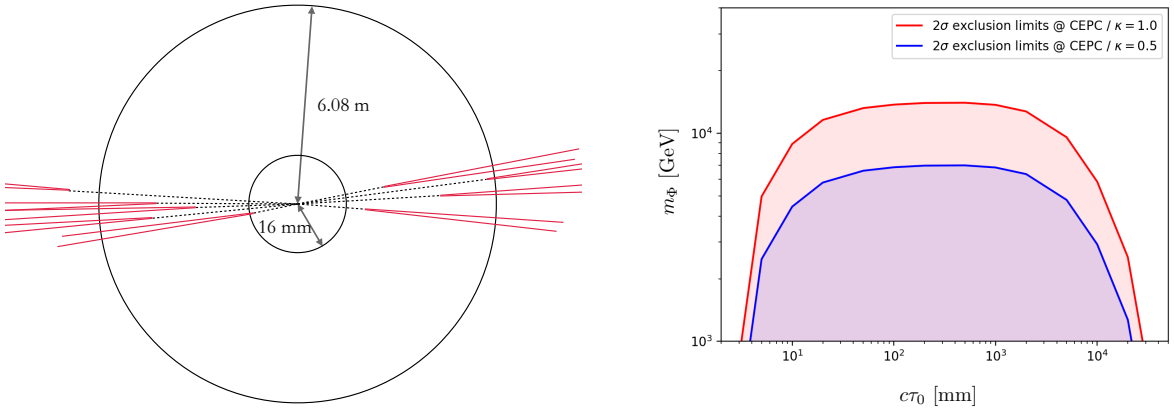

FIG. 25: Left: An illustration of the signal process at CEPC. Detector is represented by two circles. Black dotted lines and red solid lines are dark pions and muons, respectively. Right: 2 σ exclusion limits on the mediator mass m_Φ as a function of the dark pion proper decay length, with coupling κ fixed to 0.5 and 1.0 respectively. The HL-LHC can only provide very weak constraints on heavy Φ, thus are not shown here [111].

π' is between 10 mm and 10 m. This bound is stronger than the limit from current ATLAS displaced lepton jet search result [125].

3. *Long-lived dark scalar*

Recently, vector-like leptons (VLL) as a simple extension to the standard model have attracted widespread attention both in theory and experiments. The VLL model can include an additional dark sector scalar ϕ, mediating the heavy vector-like lepton $F^\pm$ mixing with the first SM lepton generation [112]. The relevant Lagrangian in the mass basis at leading order reads:

$$\begin{aligned}\mathcal{L}_{\text{int}} \supset\ & \bar{F}(i\partial_\mu - eA_\mu + e\tan\theta_W Z_\mu)\gamma^\mu F - m_F\bar{F}F - m_\ell\bar{\ell}\ell \\ & + \frac{1}{2}\frac{e}{\sin\theta_W\cos\theta_W}\theta_L Z_\mu(\bar{F}_L\gamma^\mu\ell_L + \text{h.c.}) - \frac{e}{\sqrt{2}\sin\theta_W}\theta_L(W^+_\mu\bar{\nu}_L\gamma^\mu F_L + \text{h.c.}) \\ & - y\phi\left(\bar{F}_L\ell_R + \bar{\ell}_R F_L + \theta_R\bar{F}F - \theta_L\bar{\ell}\ell\right),\end{aligned} \tag{4}$$

where the mixing parameters $\theta_{L/R}$ hold the relation $\theta_L \simeq \frac{m_\ell}{m_F}\tan\theta_R \ll \theta_R$. Ref. [112] focuses on the parameter space $m_F > m_\phi \gg m_\ell$ and $m_F > 200\,\text{GeV}$ to avoid constraints from multilepton and Z boson searches. In this case, the scalar ϕ can only decay to a lepton pair $\bar{\ell}\ell$, but this decay is suppressed by the mass ratio $(m_\ell/m_F)^2$, thus ϕ can naturally be

long-lived.

Regarding CEPC, one requires the lepton in Eq. (4) to be an electron. Therefore, the electron-positron collider can produce a pair of dark scalars $\phi\phi$ by exchanging $F^{\pm}$ via the t channel, followed by subsequent decays into a pair of e^+e^- particles. Since the CEPC has a center of mass energy much smaller than the LHC, the direct production of the heavy VLL F is not possible.

If ϕ is long-lived, its decay to an electron pair can lead to a displaced vertex (DV) signature. Since there are two ϕ scalars, there could be one displaced vertex without specifying where the other ϕ decays, leading to the inclusive displaced vertex (iDV) signature. It is also possible that both ϕ scalars decay in the inner tracker, allowing the reconstruction of two DVs from di-electrons.

The corresponding sensitivities for the iDV and 2DV at future CEPC are studied in Ref. [112] and shown in Fig. 26, where the number of signal events $N = 3$ is plotted. Compared to HL-LHC searches, the DV searches at CEPC can effectively probe low-mass m_ϕ but are less capable of detecting larger masses due to the lower center-of-mass energy of CEPC. In comparison with the dilepton plus missing energy searches at the LHC, which exclude very small coupling combinations $y\theta_L$, CEPC shows complementary sensitivity for intermediate $y\theta_L \in [10^{-11}, 10^{-7}]$.

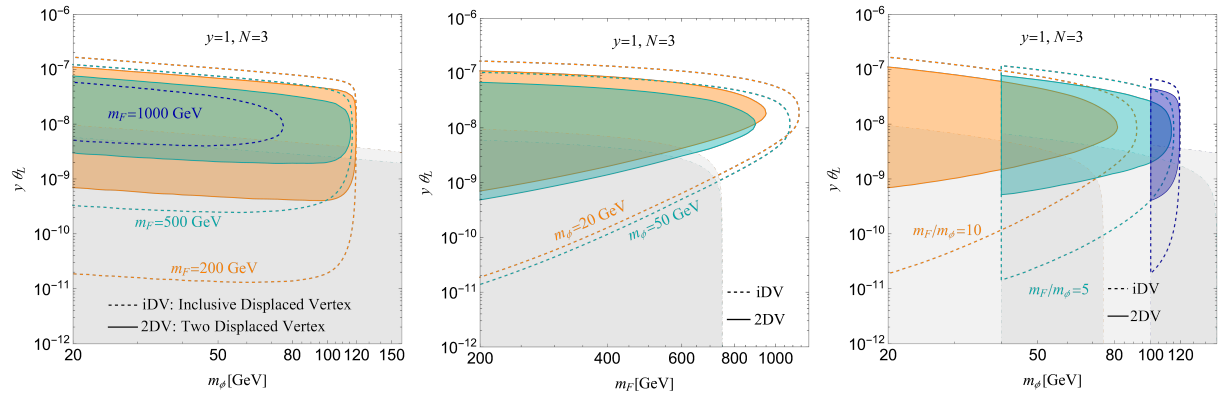

FIG. 26: The expected 95% C.L. sensitivities at the Higgs factory of CEPC for the long-lived scalar case are shown as a function of the scalar or vector-like lepton mass m_ϕ or m_F for $\mathcal{L} = 5.6$ ab^{-1} and $\sqrt{s} = 240$ GeV. The coupling y is the Yukawa coupling for the lepton portal term and θ_L is the mixing angle for left-handed SM lepton with the heavy left-handed F The sensitivities for different masses of the vector-like lepton m_F and the scalar m_ϕ are shown with different colors. The sensitivities from iDV (inclusive displaced vertex) and 2DV (two displaced vertex) search strategies are indicated with dashed lines without color shading and with solid lines with color shading, respectively. Moreover, the gray-shaded regions represent the constraints from LHC dilepton and missing energy or transverse momentum searches, with the corresponding colors as boundaries for different masses.

C. Vector portal

In general, the SM vector portal for DM involve the neutral mediators, the Z boson and the photon (γ), consistent with the fact that DM is neutral. In this section, we will consider these cases separately.

1. Dark sector particles from gauge boson associate productions

In the Double Dark Portal model, the vector portal features a new $U(1)'$ vector gauge boson K with kinetic mixing parameter ϵ, with the fermionic dark matter χ coupling to the $U(1)'$ vector [110]. These new gauge portal interactions can lead to the following associated production with the SM Z boson: $\tilde{Z}\tilde{K}$ and $\gamma\tilde{K}$. For the $\tilde{Z}\tilde{K}$ channel, we considered the

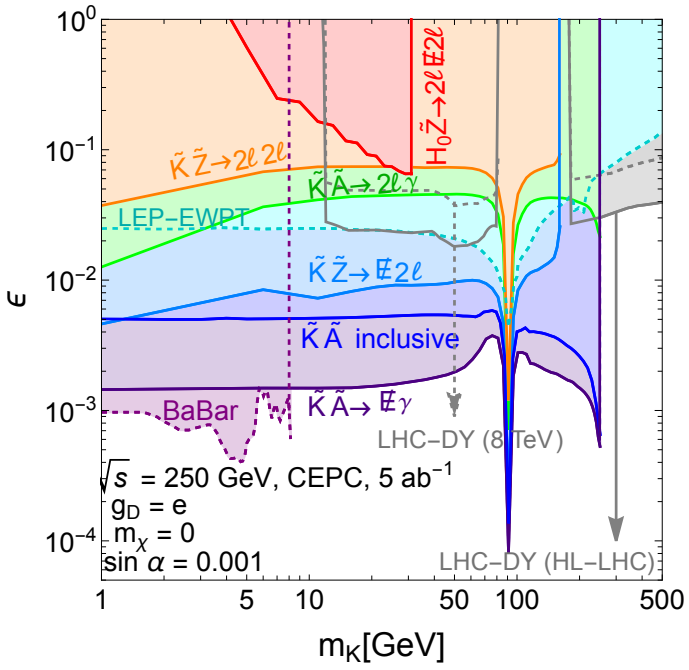

FIG. 27: Projected exclusion regions at CEPC in the ϵ vs. m_K plane from multiple complementary searches of $\tilde{K}$ production are shown in solid lines. The 3 ab^{-1} HL-LHC projection for Drell-Yan constraints is also depicted as a solid line. For other constraints, see Ref. [110] for details.

following decays: one where $\tilde{Z} \to \bar{\ell}\ell$ and $\tilde{K} \to \bar{\chi}\chi$, resulting in dileptons plus missing energy; and another where $\tilde{Z} \to \bar{\ell}\ell$ and $\tilde{K} \to \bar{\ell}\ell$, resulting in a four-lepton final state. For the $\gamma\tilde{K}$ channel, we considered several decays: first, using the recoil mass method to look for $\tilde{K}$ inclusive decay; second, $\tilde{K} \to \bar{\ell}\ell$, resulting in dileptons plus one photon final state; and third, $\tilde{K} \to \bar{\chi}\chi$, resulting in a mono-photon final state.

The corresponding exclusion sensitivities of these channels are shown in Fig. 27, which provide the limits in the 2D parameter space ϵ-m_K for the dark vector. In Fig. 28, we compare the collider sensitivity with dark matter detection and indirect detection experiments, as well as the relic abundance requirement. We emphasize that the collider constraint is not sensitive to the coupling between the DM and the mediator, as long as the invisible decay of the dark photon dominates. Therefore, the reach of a future e^+e^- collider will complement and potentially supersede that of dark matter searches.

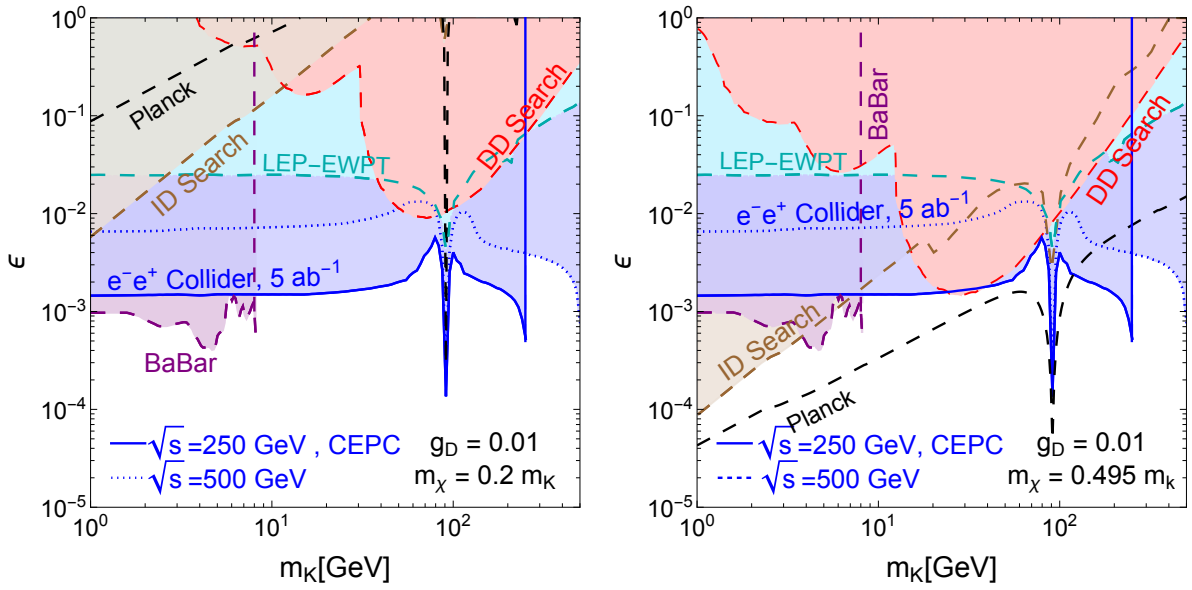

FIG. 28: The reach of direct detection (red), indirect detection (brown), and searches at e^+e^- colliders (blue) in the ϵ vs. m_K plane from [110]. We fix $g_D = 0.01$, $m_\chi = 0.2m_K$ (left panel) and $m_\chi = 0.495m_K$ (right panel). We also show the contours where χ satisfies the relic density measurement by the Planck collaboration as black dashed lines. Existing constraints from LEP electroweak precision measurements (LEP-EWPT) and the BaBar search for the $\tilde{K}$ invisible decay (BaBar) are also included.

2. Millicharge DM

The CEPC can shed light on the particle properties of dark matter (DM), which currently remain elusive despite the overwhelming evidence from cosmology and astrophysical measurements. Recently, Ref. [113] investigated the capability of CEPC in probing the parameter space of millicharged DM. The monophoton signature at CEPC, which arises when a pair of DM particles is produced in association with a photon, is shown to be capable of significantly improving DM constraints, offering a promising avenue to decipher the mysteries of dark matter [113].

The 95% CL upper bound from the monophoton channel at CEPC on millicharged DM is shown in Fig. 29. The interaction Lagrangian of this model is given by:

$$\mathcal{L} = e\varepsilon A_\mu \bar{\chi}\gamma^\mu \chi, \tag{5}$$

where χ is the Dirac DM, A_μ is the photon, e is the electromagnetic coupling strength,

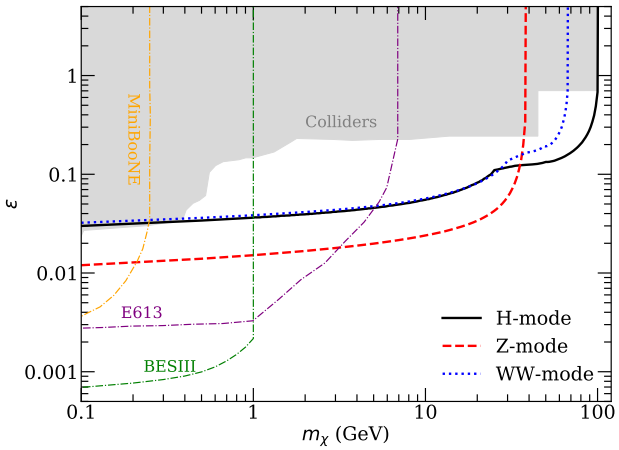

FIG. 29: Expected 95% CL constraints on the millicharge ε in the three CEPC running modes. Also shown are other constraints/sensitivities on millicharged particles [126–129].

and ε is the millicharge. Sensitivities are computed for the following three CEPC running modes: 5.6 ab^{-1} data in the H-mode, 16 ab^{-1} data in the WW-mode, and 2.6 ab^{-1} data in the Z-mode. The Z and H modes have the best sensitivity for DM below and above 40 GeV, respectively. The constrains on the millicharge in the mass range of 1-100 GeV can be probed by CEPC, with an improvement factor of nearly one order of magnitude compared to previous collider bounds.

3. Dark sector particles with EM form factors

Primary importance for our understanding of elementary interactions is shedding light on the dark sector states. Recently, Ref. [114] investigated the sensitivity of CEPC on the dark states with electromagnetic form factors for magnetic dipole moments (MDM) and electric dipole moments (EDM) at mass-dimension 5, and anapole moment (AM) and charge radius interaction (CR) at mass-dimension 6.

In Ref. [114], the fermionic dark state χ may have the effective interactions with the hypercharge gauge boson field B_μ [130, 131], and the interactions can be written with electromagnetic field strength tensor $F_{\mu\nu} \equiv \partial_\mu A_\nu - \partial_\nu A_\mu$ and Z gauge field strength tensor

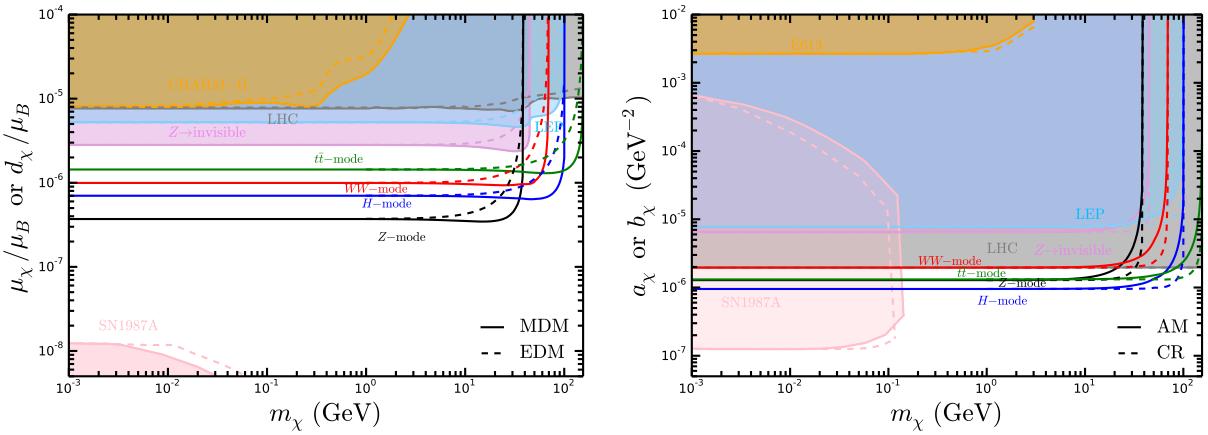

FIG. 30: The expected 95% C.L. exclusion limits on the electromagnetic form factors for mass-dimension 5 operators (**Left**) through MDM (solid) and EDM (dashed), and for mass-dimension 6 operators (**Right**) through AM (solid) and CR interaction (dashed) in the four CEPC running modes [114]. The landscape of current leading constraints are also shown with shaded regions, exploiting from terrestrial experiments, such as proton-beam experiments CHARM-II or E613 [132], monophoton searches and Z-boson invisible decay at LEP and monojet searches at LHC [131], and astrophysics supernovae SN 1987A [133].

$Z_{\mu\nu} \equiv \partial_\mu Z_\nu - \partial_\nu Z_\mu$ as

$$\begin{aligned}\mathcal{L}_\chi = &\frac{1}{2}\mu_\chi \bar{\chi}\sigma^{\mu\nu}\chi F_{\mu\nu} + \frac{i}{2}d_\chi \bar{\chi}\sigma^{\mu\nu}\gamma^5\chi F_{\mu\nu} - a_\chi \bar{\chi}\gamma^\mu\gamma^5\chi\partial^\nu F_{\mu\nu} + b_\chi \bar{\chi}\gamma^\mu\chi\partial^\nu F_{\mu\nu} \\ &+ \frac{1}{2}\mu_\chi^Z \bar{\chi}\sigma^{\mu\nu}\chi Z_{\mu\nu} + \frac{i}{2}d_\chi^Z \bar{\chi}\sigma^{\mu\nu}\gamma^5\chi Z_{\mu\nu} - a_\chi^Z \bar{\chi}\gamma^\mu\gamma^5\chi\partial^\nu Z_{\mu\nu} + b_\chi^Z \bar{\chi}\gamma^\mu\chi\partial^\nu Z_{\mu\nu}.\end{aligned} \tag{6}$$

Here $\mathcal{C}_\chi^Z = -\mathcal{C}_\chi \sin\theta_W$ with $\mathcal{C}_\chi = \mu_\chi$, d_χ, a_χ, b_χ, and θ_W denotes Weinberg angle. μ_χ and d_χ are the dimensional coefficients of the mass-dimension 5 MDM and EDM interactions, expressed in units of the Bohr magneton μ_B, and $\sigma_{\mu\nu} \equiv i[\gamma^\mu, \gamma^\nu]/2$; a_χ and b_χ are the dimensional coefficients of the mass-dimension 6 AM and CR interactions.

The dark states χ can be produced from the process $e^+e^- \to \gamma/Z \to \chi\bar{\chi}$ at CEPC. In order to probe the dark state at CEPC, one should consider $\chi\bar{\chi}$ pair production associated with a hard photon radiated from the initial state electron or positron ($e^+e^- \to \chi\bar{\chi}\gamma$), i.e., the typical monophoton signature.

Fig. 30 shows the 95% C.L. upper bounds at CEPC via the monophoton channel on the electromagnetic form factors for mass-dimension 5 operators through MDM (solid) and EDM (dashed) on the left , and for mass-dimension 6 operators through AM (solid) and

CR interaction (dashed) on the right. The limits are obtained using 20 ab^{-1} data in the H-mode, 6 ab^{-1} data in the WW-mode, 100 ab^{-1} data in the Z-mode, and 1 ab^{-1} data in the $t\bar{t}$-mode. The Z-mode has the best sensitivity on the light dark states for mass-dimension 5 operators MDM with $m_\chi \lesssim 35$ GeV, and EDM with $m_\chi \lesssim 25$ GeV, which can probe the couplings down to about $3.7 \times 10^{-7}\,\mu_B$. The HL-LHC projection with 25% systematic error can probe MDM and EDM operators down to $4 \times 10^{-6}\,\mu_B$, thus CEPC can provide better sensitivity of about one order. The H-mode has the best sensitivity on the the light dark states for mass-dimension 6 operators AM with $m_\chi \lesssim 63$ GeV, and CR with $m_\chi \lesssim 89$ GeV, and the corresponding couplings can be probed down to about 1.3×10^{-6} GeV^{-2} and 9.8×10^{-7} GeV^{-2} respectively. Furthermore, one finds that CEPC can explore the previously untouched parameter region for both mass-dimension 5 and mass-dimension 6 operators of dark states in the future.

D. DM in EFT framework

1. *Leptophilic DM*

Most of the existing experimental constraints on DM crucially rely on its interactions with nucleons, and can therefore be largely evaded if the DM predominantly interacts with the SM leptons, but not quarks at tree-level. Such *leptophilic* DM (LDM) arises naturally in many BSM scenarios [134–155], some of which could even explain various existing experimental anomalies, such as the muon anomalous magnetic moment [156], DAMA/LIBRA annual modulation [157], anomalous cosmic ray positron excess [158–161], the galactic center gamma-ray excess [162], and XENON1T electron excess [163]. Dedicated searches for LDM in direct detection [164–166] and beam dump [167, 168] experiments have also been discussed.

Lepton colliders provide an ideal testing ground for the direct production of LDM and its subsequent detection via either mono-photon [113, 115, 169–179] or mono-Z [115, 180–183] signatures. Here we will discuss the CEPC sensitivities to LDM in the monophoton channel following a model-independent EFT approach [115]. See also Refs. [173, 176, 184–194] for earlier works on collider searches for DM in the EFT framework. Here we assume the LDM to be fermionic and only show the results for the dimension-6 operators of vector-axialvector

(V-A) type for illustration. Within the minimal EFT approach, the only relevant degrees of freedom are the DM mass m_χ and an effective cut-off scale Λ which determines the strength of the four-Fermi operator given by

$$\mathcal{L}_{\rm eff} = \frac{1}{\Lambda^2} \sum_j \left(\overline{\chi}\Gamma^j_\chi \chi\right) \left(\overline{\ell}\Gamma^j_\ell \ell\right) \,, \tag{7}$$

where $\Gamma^\mu_\chi = (c^\chi_V + c^\chi_A\gamma_5)\,\gamma^\mu$ and $\Gamma_{e\mu} = (c^e_V + c^e_A\gamma_5)\,\gamma_\mu$ for V-A type. For simplicity, we will also set $c^\chi_V = c^\chi_A = c^e_V = c^e_A = 1$. For other choices of the couplings, our results for the sensitivity on Λ can be easily scaled accordingly. Note that the EFT results are valid as long as $\Lambda > \max\{\sqrt{s}, 3m_\chi\}$ [195].

Our results for the mono-photon case $e^+e^- \to \chi\overline{\chi}\gamma$ are shown in Fig. 31. The different solid contours correspond to different CEPC operation modes as given in Table I. The details of background estimations, signal selection and cut-based analysis can be found in Ref. [115]. The various shaded regions are excluded by direct detection (XENON1T [196], PANDAX-4T [197]), indirect detection (Fermi-LAT [198], AMS [199]), astrophysics (SN1987A [200]) and cosmology (CMB [198]) constraints. Along the dot-dashed line, the observed DM relic density is reproduced for a thermal DM assuming only DM-electron effective coupling. From Fig. 31, it is clear that CEPC can probe new LDM parameter space, especially in the low DM mass range (for $m_\chi \lesssim 10$ GeV).

Fig. 32 shows the 95% CL lower bound on the new physics scale for one of the effective field theory interactions of DM in Ref. [113]. The interaction Lagrangian in this case is given by:

$$\mathcal{L} = \frac{1}{\Lambda_A^2}\bar{\chi}\gamma_\mu\gamma_5\chi\bar{\ell}\gamma^\mu\gamma_5\ell, \tag{8}$$

where χ is the Dirac DM, ℓ are charged leptons, and Λ_A is the new physics scale. The H-mode yields the most stringent constraints on Λ_A. The three modes of CEPC are expected to lead to better limits in the DM mass range of $m_\chi \lesssim (10-25)$ GeV than Xenon1T [201], under the assumption that Λ_A takes the same value for charged leptons and quarks.

2. Interplay of dark particles with neutrinos

Interactions between dark matter (DM) and standard model (SM) particles have been extensively studied through direct detection methods [202–204], indirect detection techniques

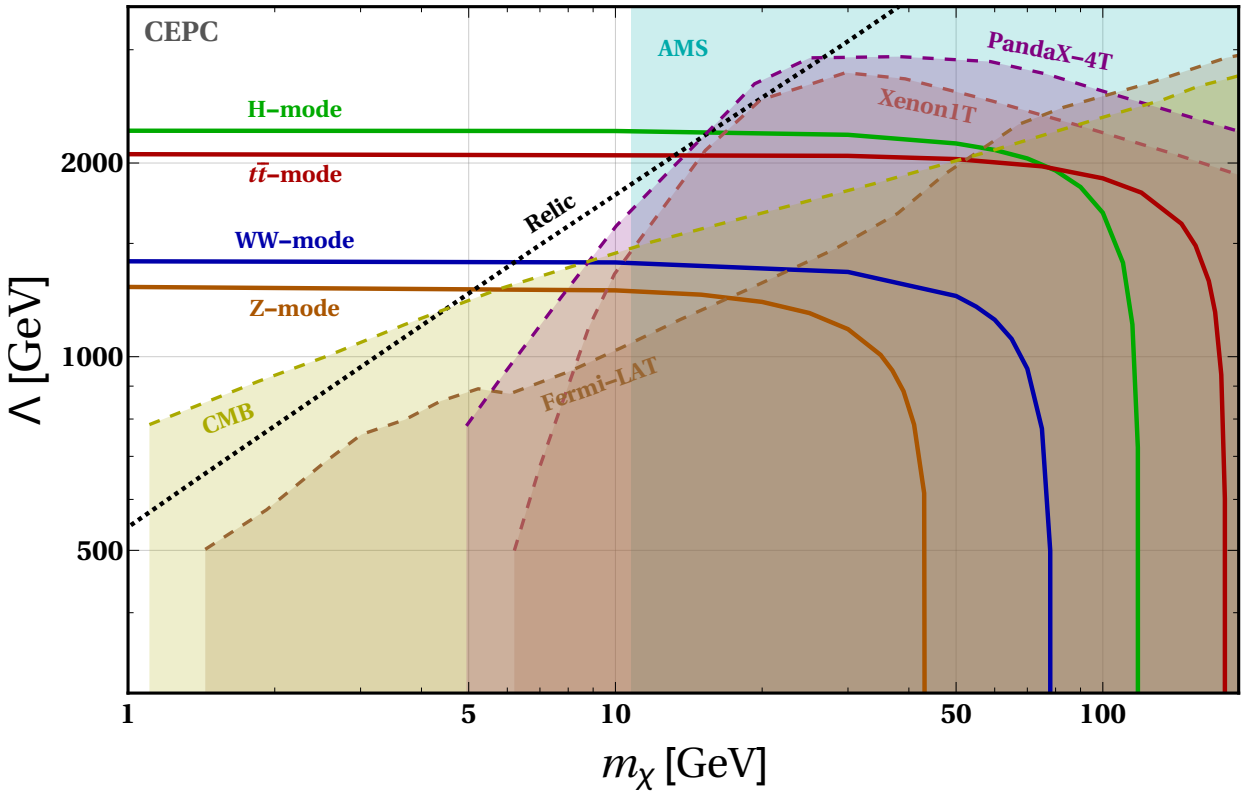

FIG. 31: The 3σ sensitivity contours in the mono-photon channel for the LDM with V-A operator structure with unpolarized e^+e^- beams and different CEPC operation modes as given in Table I. The various shaded regions are excluded by direct detection (XENON1T [196], PANDAX-4T [197]), indirect detection (Fermi-LAT [198], AMS [199]), astrophysics (SN1987A [200]) and cosmology (CMB [198]) constraints. Along the dot-dashed line, the observed DM relic density is reproduced for a thermal DM assuming only DM-electron effective coupling. Figure updated from Ref. [115] for CEPC.

[205–207], and collider searches [106, 192, 208, 209]. The null results and stringent constraints on the couplings have led to the postulation of a dark sector comprising particles with varying mass scales and feeble couplings to the SM.

One advantage of collider detection is the ability to search for heavy particles as long as their mass, m_χ, is less than or equal to $\sqrt{s}$. Thus, colliders can probe not only the true DM particles that persist today but also any DS particles that can be directly generated. Additionally, most constraints focus on the DM coupling with nucleons and, consequently, quarks. Collider searches offer a tunable environment to distinguish between the leptophilic and hadrophilic natures of DM.

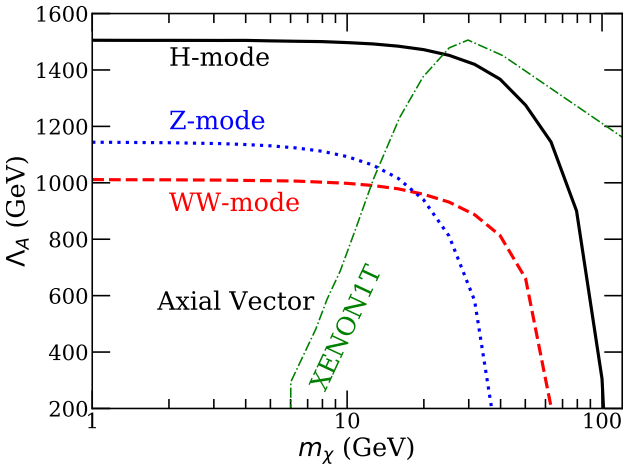

FIG. 32: Expected 95% CL constraints on Λ_A in the three CEPC running modes. Also shown are the Xenon1T constraints on Λ_A [201].

Ref. [116] focuses on absorption operators that couple a dark fermion with neutrinos and charged electrons/positrons. The study examines mono-photon and electron-positron pair productions associated with missing energy (a neutrino and a dark sector fermion) at future e^+e^- colliders such as CEPC, FCC-ee, ILC, and CLIC [116]. The findings indicate that mono-photon searches prevail at CEPC and ILC, while $e^+e^- + \not{E}$ dominates at CLIC. The combined sensitivity can reach well above 1 TeV at CEPC/FCC-ee and ILC, and can further extend to 30 TeV at CLIC.

Figure 33 shows astrophysical X/γ-ray observations and cosmological constraints for sub-MeV absorption dark matter [210], demonstrating that collider searches are actually more sensitive. For a heavy dark fermion ($m_\chi > 2m_e$), the collider probe is generally weaker than astrophysical and cosmological constraints due to the increased decay width. However, this is only true when the dark fermion is assumed to be the genuine DM. The astrophysical and cosmological constraints can be relaxed by the presence of a large number of particles in the DS. In this sense, collider searches provide a complementary approach to addressing either light or heavy dark fermions.

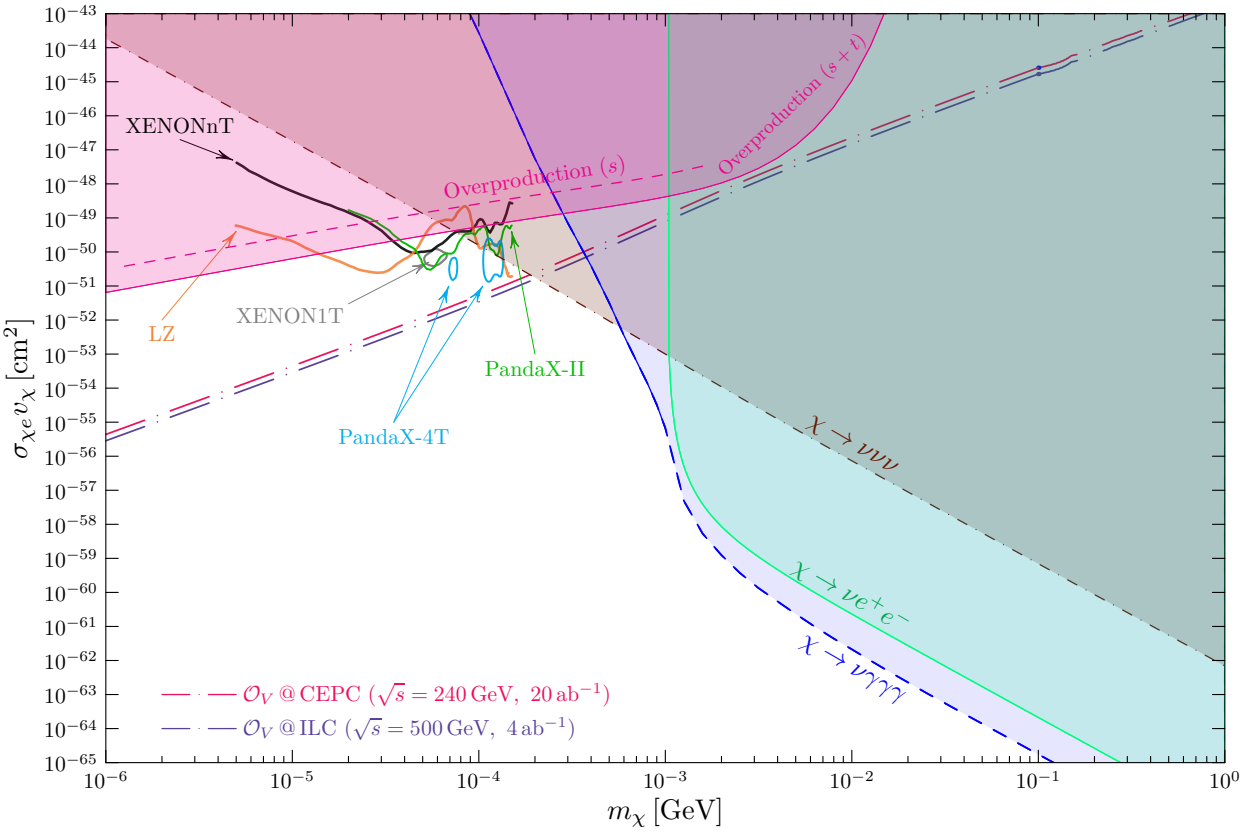

FIG. 33: Constraints on the fermionic absorption DM from direct detection experiments (PandaX-II, PandaX-4T, XENONnT, and LZ), cosmology, astrophysics, and the projected sensitivities at the future lepton colliders (CEPC, ILC, and CLIC) [116].

E. Dark matter and its loop effects at CEPC

Because of the limited center-of-mass energy, the massive particles present in dark matter (DM) models could hardly be directly produced at the CEPC. Nevertheless, the precise measurements of electroweak phenomena at the CEPC offer a propitious avenue for indirect detection of these particles via loop effects. Specifically, the CEPC is well-suited for the examination of DM models featuring supplementary electroweak multiplets.

A number of studies have been performed on this topic [211–219], with a particular emphasis on two models [214, 220–222]: the singlet-doublet dark matter (SDDM) and doublet-triplet dark matter (DTDM) models. These two models can be regarded as the generalizations of electroweak sectors with proper UV completion. For instance, the SDDM and DTDM models are similar to the bino-Higgsino and Higgsino-wino sectors in SUSY models. The SDDM model features one singlet Weyl spinor with a Majorana mass term

of $-m_s SS/2$, alongside two doublet Weyl spinors possessing opposite $U(1)_Y$ charges and a mass term of $-m_D \epsilon_{ij} D_1^j D_2^j$. Within this model, there exist two new Yukawa couplings $y_1 S D_1^i H_i - y_2 S D_2^i H_i^\dagger$, where H_i denotes the SM Higgs doublet. The DTDM model involves one triplet and two doublet Weyl spinors. Both models are characterized by four independent parameters: two mass parameters and two Yukawa couplings. After electroweak symmetry breaking, the Yukawa terms induces the mixing of states. The lightest neutral particle potentially serves as a candidate for DM.

The new particles introduced in these models have the potential to influence various electroweak phenomena at the CEPC, including Higgs decays [217, 218], oblique parameters [212, 214, 216], and production of electroweak particles, such as $e^+e^- \to \mu^+\mu^-$, ZZ, W^+W^-, and $Z\gamma$, through loop effects [213, 215, 219]. Notably, the CEPC, renowned as a Higgs factory, possesses a robust capacity to scrutinize these effects by means of measuring the Zh associated production with a remarkable precision of 0.5% [217–219]. To quantify the impact of new physics models on the Zh production cross section, we define a deviation parameter $\Delta\sigma/\sigma_0 \equiv |\sigma_{\rm NP} - \sigma_{\rm SM}|/\sigma_{\rm SM}$. Another promising avenue for the detection of new particles in the dark sector is the diphoton decay of the Higgs boson. For this process, we define a deviation $\Delta\Gamma/\Gamma_0 \equiv |\Gamma_{\rm NP} - \Gamma_{\rm SM}|/\Gamma_{\rm SM}$ for this process. In the left panel of Fig. 34, we display the parameter regions in the DTDM model for $y_1 = y_2 = 1$ with notable deviations $\Delta\sigma/\sigma_0 > 0.5\%$ for the Zh production and $\Delta\Gamma/\Gamma_0 > 9.4\%$ for the Higgs diphoton decay at the CEPC with an integrated luminosity of 5 ab^{-1}.

In the right panel of Fig. 34, we display the parameter regions excluded by the observed DM relic density [223] and the LZ searches for DM-nucleon spin-independent scattering [224]. It is important to highlight that the exploration of the parameter space at the CEPC can serve as a valuable complement to other DM detection experiments, as illustrated in Fig. 34. Despite the inclusion of DM within the electroweak multiplets, the interactions between DM particles and nucleons may be suppressed in certain parameter regions, leading to what is commonly referred as "blind spots" for direct detection [225, 226]. Within the framework of the DTDM model, a global custodial symmetry emerges in the scenario where $y_1 = y_2$ [214, 222], resulting in a null coupling between DM and the Z boson, thereby yielding vanishing spin-dependent scattering. Furthermore, when $m_D < m_T$, the condition of $y_1 = y_2$ gives rise to a null coupling between DM and the Higgs boson, resulting in vanishing spin-independent scattering. The SDDM model exhibits similar characteristics to the DTDM

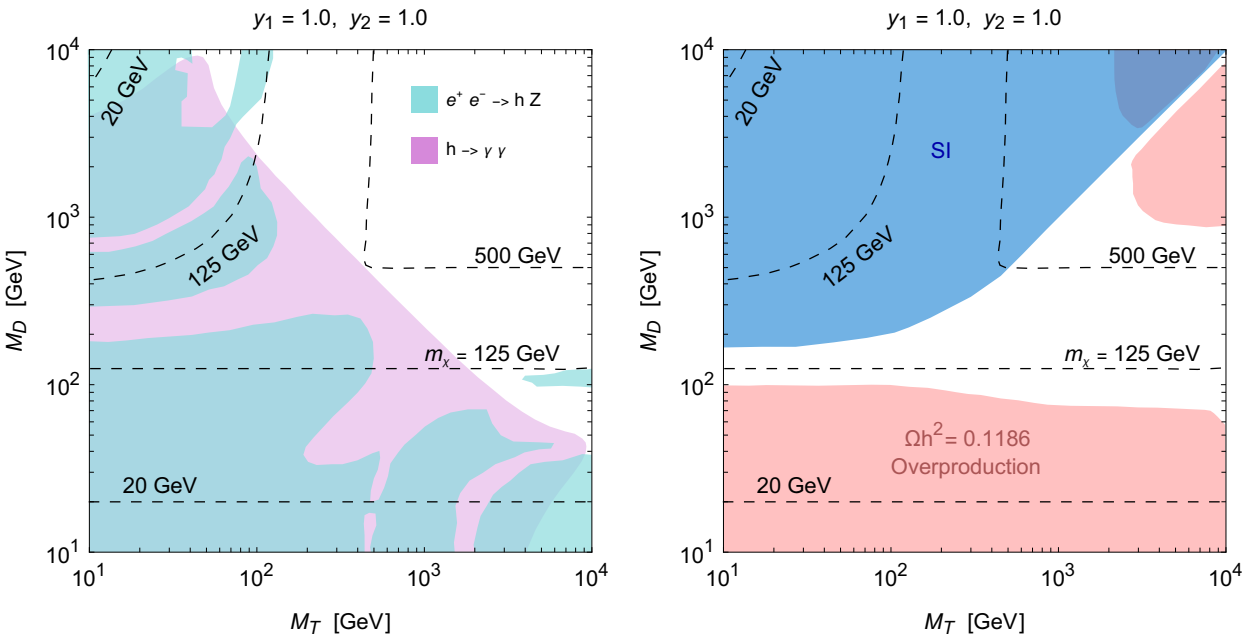

FIG. 34: Left panel: CEPC sensitives in the DTDM model with $y_1 = y_2 = 1$. The blue and purple regions represent the deviations $\Delta\sigma/\sigma_0$ for the Zh production and $\Delta\Gamma/\Gamma_0$ for the Higgs diphoton decay above 0.5% and 9.4%, respectively. Right panel: constraints from other DM detection experiments. The blue and red regions denote the parameter regions excluded by the direct detection of DM-nucleon spin-independent scattering and DM relic density, respectively.

model.

F. Summary

In this section, we explore the capabilities of the CEPC in searching for DM through various interaction portals, including the scalar portal, the fermion portal, the vector portal, and EFT operators. The clean experimental environment and clear center-of-mass energy of CEPC provide distinct advantages over the HL-LHC for certain DM searches. Specifically, as summarized in Figure 35, the CEPC exhibits improved sensitivity by approximately one order of magnitude compared to HL-LHC in the cases of scalar, fermion, and vector portals, as well as in the investigation of the magnetic dipole moment (MDM) and electric dipole moment (EDM). These enhancements originate from the reduction of background noise and targeted searches such as Higgs and Z bosons. In contrast, the HL-LHC demon-

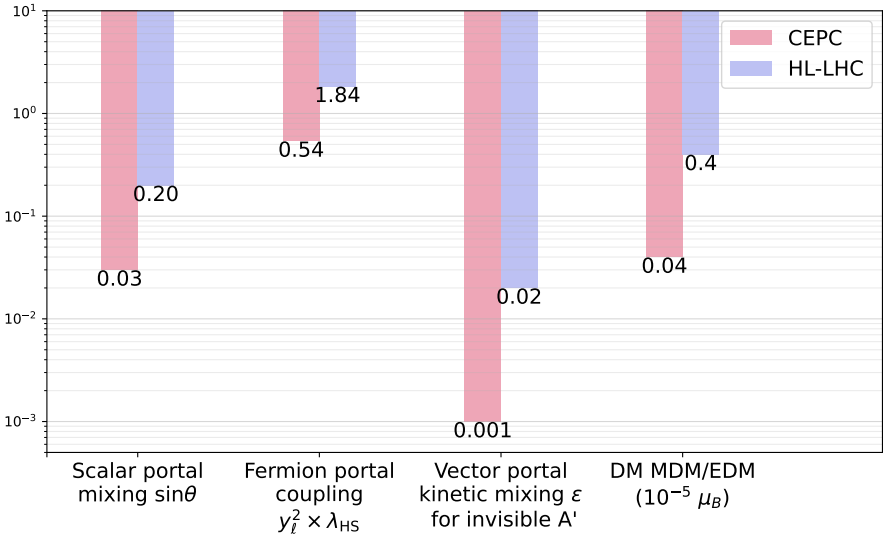

FIG. 35: The sensitivities for scalar, fermion, and vector portals, as well as dark matter magnetic dipole moment and electric dipole moment operators for CEPC and HL-LHC.

strates superior sensitivity for direct search of heavy particles due to its larger cross sections from hadronic collisions, allowing significant production of dark matter signals from their decay. Overall, this comparative analysis shows the strengths of CEPC in probing specific DM models and highlights the importance of utilizing its unique attributes to advance our understanding of the interactions between dark matter and SM particles.

VI. LONG-LIVED PARTICLE SEARCHES (XIANG CHEN, LIANG LI, YING-NAN MAO, KECHEN WANG, ZEREN SIMON WANG)

A. Introduction

Recent years have witnessed a surge of interest in new fundamental particles with a relatively long lifetime which are predicted in many theoretical incarnations of physics beyond the Standard Model (BSM) and are often dubbed "long-lived particles" (LLPs). Such particles are supposed to become long-lived, for various reasons including feeble couplings to other particles, phase space suppression, approximate symmetry, and heavy mediators. Moreover, LLPs can resolve multiple fundamental problems of the Standard Model (SM) such as the non-vanishing neutrino mass, dark matter, baryogenesis, and naturalness. Ex-

amples include heavy neutral leptons, dark photons, axion-like particles, and dark Higgs bosons (see, for instance, Refs. [227–231] for reviews of different models predicting LLPs). On the other hand, at colliders such as the LHC, searches for heavy new particles have been going on, with no concrete discovery except stringent lower bounds on the mass of these particles such as squarks at $2-3$ TeV [232–236]; this situation has also shifted much attention in the community towards other BSM signatures including those asociated with the LLPs [237–241]. For these reasons, collider searches for LLPs are becoming an increasingly important approach to probing BSM physics.

While the LHC has observed the SM Higgs boson in 2012 [242, 243], entered the Run 3 phase recently, and is expected to complete its high-luminosity stage by mid-2030s, intensive discussion concerning the next-generation high-energy colliders has never ceased since decades ago. Such discussion mainly centers around these colliders' potential in discovering new fundamental particles and interactions. These future collider-experiments include the Circular Electron Positron Collider (CEPC) in China [11, 12, 244–246], the International Linear Collider (ILC) in Japan [247–251], and the Future Circular Collider (FCC) [4, 252–254] and the Compact Linear Collider (CLIC) [255, 256] at CERN. The ILC and CLIC would be linear electron-positron colliders, while both the CEPC and the FCC in its initial stage, called the FCC-ee, would be operated as circular colliders of electron and positron beams. These future colliders would be running at the center-of-mass (CM) energies ranging from about 91.2 GeV at the Z-pole, 240-250 GeV as a Higgs factory, 160 GeV as a W-boson factory, 350 GeV as a top-quark factory, to even higher energies up to the TeV scale. The corresponding gauge and Higgs bosons are thus produced in a clean environment (i.e. with only little background contamination). We note that for the Higgs-factory mode at the CM energy of 240 GeV, sensitivities shown in this section usually correspond to the integrated luminosity of 5.6 ab^{-1} for the CEPC, and the upgraded luminosity of 20 ab^{-1} can lead to stronger discovery sensitivities.

Compared to hadron colliders such as the LHC, the high-energy electron-positron colliders usually have higher integrated luminosities and looser trigger conditions. This allows for not only precision measurements of the SM particles and parameters, but also searches for new particles including LLPs e.g. via rare (electroweak) decays of the SM particles such as the Z- and Higgs bosons. Since the e^-e^+ colliders have definite colliding-parton energies, recoil strategy can be adopted in collider searches. Phenomenological studies on their sensitivities

to LLPs have been performed extensively; see e.g. Ref. [257] for recent reviews of LLP experiments at the proposed FCC-ee collider. These works have considered not only the default detector located at the interaction point (IP), dubbed "*main detector*" (MD) or "*near detector*" (ND) in this work, but also the proposed external detectors (or "*far detectors*" (FDs) away from the IP), for searching for LLPs. Moreover, beam-dump experiments have also been suggested for construction at future e^-e^+ colliders, aiming primarily at finding new exotic states with a long lifetime. We note that the LLPs produced at the IP of beam-energy-symmetric e^-e^+ colliders tend to travel along the transverse direction in the laboratory frame, while at pp colliders the LLPs often employ a large boost in the forward/longitudinal direction as a result of the proton's parton distribution.

In Table VIII, we summarize results from recent CEPC's studies on LLPs. In the table, the first column lists the types of the LLPs; the second column presents the corresponding signal signature; the third and fourth columns provide the center-of-mass energy and the integrated luminosity; the fifth column indicates the considered main detector (MD) or far detectors (FD3 or LAYCAST); the sixth column shows sensitivities on the couplings, suppression scales, branching ratios, or production cross sections with assumptions of the LLP's mass (m), lefetime (τ) and others; the last two column provide the references. Check the main text for the meanings of symbols and abbreviations.

This section is organized as follows. In Sec. VI B we present a computation procedure of LLP signal-event rates at colliders. Then in Sec. VI C, Sec. VI D, and Sec. VI E, we review LLP studies and summarize their results at main detectors, proposed far detectors, and possible beam-dump experiments, respectively, for future high-energy e^-e^+ colliders. Finally, we conclude in Sec. VI F with a summary and an outlook.

B. Computation of LLP signal-event rates

In this section, we present and discuss a simplified and widely used computation procedure of the theory-predicted signal-event rates of the LLP.

As shown in Fig. 36, we assume that the LLP is produced (essentially) at the IP of a collider, and travels a macroscopic distance with a constant velocity[261] before decaying into SM or other new particles. The survival probability of the LLP after traveling a distance D can be estimated with the exponential decay law $P(D) = e^{-D/\lambda}$, where λ is the LLP's

LLP Type	Signal Signature	$\sqrt{s}$ [GeV]	$\mathcal{L}$ [ab^{-1}]	Detector	Sensitivities on parameters [Assumptions]	Figs.	Refs.
New scalar particles (X)	$Z(\to \text{incl.})\, h(\to XX)$, $X \to q\bar{q}/\nu\bar{\nu}$	240	20	MD	$\text{Br}(h \to XX) \sim 10^{-6}$ [$m \in (1, 50)$ GeV, $\tau \in (10^{-3}, 10^{-1})$ ns]	38	[82]
	$Z(\to \text{incl.})\, h(\to XX)$, $X \to \text{incl.}$	240	5.6	MD	$\text{Br}(h \to XX) \sim 3 \times 10^{-6}$ [$m = 0.5$ GeV, $c\tau \sim 5 \times 10^{-3}$ m]	50	[88]
				FD3	$\text{Br}(h \to XX) \sim 7 \times 10^{-5}$ [$m = 0.5$ GeV, $c\tau \sim 1$ m]	50	[88]
				LAYCAST	$\text{Br}(h \to XX) \sim 5 \times 10^{-6}$ [$m = 0.5$ GeV, $c\tau \sim 10^{-1}$ m]	50	[258]
RPV-SUSY neutralinos ($\tilde{\chi}_1^0$)	$Z \to \tilde{\chi}_1^0\tilde{\chi}_1^0$, $\tilde{\chi}_1^0 \to \text{incl.}$	91.2	150	MD	$\lambda'_{112}/m_{\tilde{f}}^2 \in (2 \times 10^{-14}, 10^{-8})$ GeV^{-2} [$m \sim 40$ GeV, $\text{Br}(Z \to \tilde{\chi}_1^0\tilde{\chi}_1^0) = 10^{-3}$]	44	[88]
				FD3	$\lambda'_{112}/m_{\tilde{f}}^2 \in (10^{-14},\ 10^{-9})$ GeV^{-2} [$m \sim 40$ GeV, $\text{Br}(Z \to \tilde{\chi}_1^0\tilde{\chi}_1^0) = 10^{-3}$]	51	[88]
				LAYCAST	$\lambda'_{112}/m_{\tilde{f}}^2 \in (7 \times 10^{-15},\ 10^{-9})$ GeV^{-2} [$m \sim 40$ GeV, $\text{Br}(Z \to \tilde{\chi}_1^0\tilde{\chi}_1^0) = 10^{-3}$]	51	[258]
ALPs (a)	$Z^{(*)} \to \mu^-\mu^+ a$	91	150	MD	$f_a/C_{\mu\mu}^A \lesssim 950$ GeV	45	[87]
	$e^+e^- \to \gamma\, a$, $a \to \gamma\gamma$	91.2	150	MD	$C_{\gamma\gamma}/\Lambda \sim 10^{-3}$ TeV^{-1} [$C_{\gamma Z} = 0$, $m \sim 2$ GeV]	52	[258]
				FD3	$C_{\gamma\gamma}/\Lambda \sim 6 \times 10^{-3}$ TeV^{-1} [$C_{\gamma Z} = 0$, $m \sim 0.3$ GeV]	52	[259]
				LAYCAST	$C_{\gamma\gamma}/\Lambda \sim 2 \times 10^{-3}$ TeV^{-1} [$C_{\gamma Z} = 0$, $m \sim 0.7$ GeV]	52	[258]
Hidden valley particles (π_V^0)	$Z\, h(\to \pi_V^0\pi_V^0)$, $\pi_V^0 \to b\bar{b}$	350	1.0	MD	$\sigma(h) \times \text{BR}(h \to \pi_v^0\pi_v^0) \sim 10^{-4}$ pb [$m \in (25, 50)$ GeV, $\tau \sim 10^2$ ps]	42	[260]
Dark photons (γ_D)	$Z(\to q\bar{q})\, h(\to \gamma_D\gamma_D)$, $\gamma_D \to \ell^-\ell^+/q\bar{q}$	250	2.0	MD	$\text{Br}(h \to \gamma_D\gamma_D) \sim 10^{-5}$, [$m \in (5, 10)$ GeV, $\tau \sim 10^2$ ps, $\epsilon \in (10^{-6}, 10^{-7})$]	43	[85]

TABLE VIII: Summary of results from recent CEPC's studies on LLPs. The first column lists the types of the LLPs; the second column presents the corresponding signal signature; the third and fourth columns provide the center-of-mass energy and the integrated luminosity; the fifth column indicates the considered main detector (MD) or far detectors (FD3 or LAYCAST); the sixth column shows sensitivities on the couplings, suppression scales, branching ratios, or production cross sections with assumptions of the LLP's mass (m), lefetime (τ) and others; the last two column provide the references. Check the main text for the meanings of symbols and abbreviations.

boosted decay length in the laboratory frame. Considering the effect of special relativity, λ can be calculated as

$$\lambda = \beta\gamma\, c\tau = \frac{p}{E}\frac{E}{m}\, c\tau = \frac{p}{m}\, c\tau \ , \tag{9}$$

where c is the speed of light, while p, E, and m are the magnitude of the three-momentum

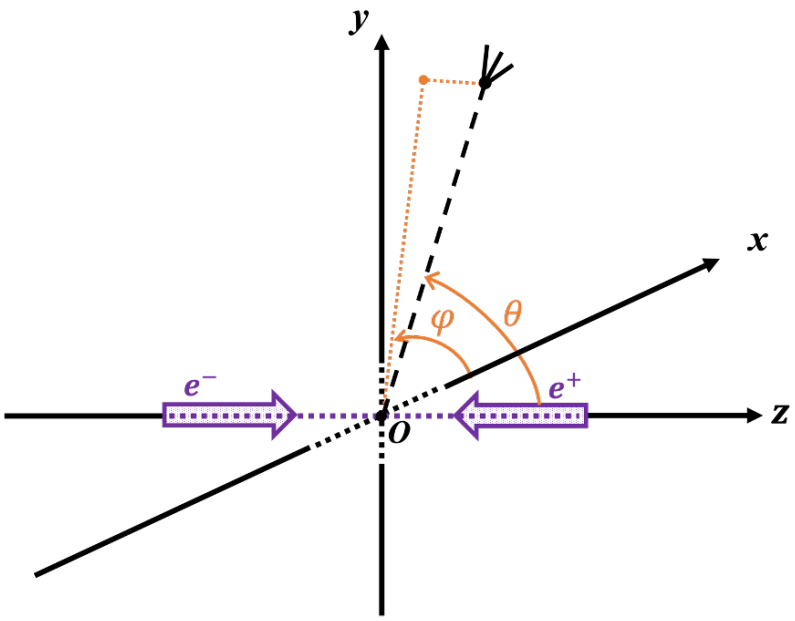

FIG. 36: Sketch of the production and decay of a LLP at electron-positron colliders.

$\vec{p}$, energy, and mass of the LLP, respectively. $\beta = p/E$ and $\gamma = E/m$ are the speed and boost factor of the LLP, and τ is the LLP's lifetime in its rest frame and can be predicted from theoretical model parameters. With the knowledge of the boosted decay length of an LLP denoted with the index i, it is then possible to compute its decay probability inside the fiducial volume (f.v.) of a detector, if the moving direction of the LLP points towards it,

$$P[(\text{LLP})_i \text{ in f.v.}] = e^{\left(-D_i^e/\lambda_i\right)} - e^{\left(-D_i^l/\lambda_i\right)} \ , \tag{10}$$

where D_i^e (D_i^l) is the distance from the IP to the point on the detector surface where the LLP would enter (leave) the detector if not having decayed beforehand, and λ_i is the LLP's boosted decay length. Note that $D_i^e < D_i^l$ by definition. Obviously, $P[(\text{LLP})_i \text{ in f.v.}] = 0$, if the LLP travels outside the fiducial volume's window. In practice, the cylindrical/azimuthal symmetry, if (approximately) present for the relative position and orientation between the detector and the IP, can be made use of since the LLP kinematic distribution in the azimuthal angle is almost always homogeneous, as an overall factor applied to the right-hand side of Eq. (10). Taking advantage of the azimuthal symmetry allows for obtaining robust results with fewer MC simulation events required.

In a phenomenological analysis, the average decay probability of an LLP in a detector's fiducial volume, $\langle P[\text{LLP in f.v.}]\rangle$, is often required in order to predict the signal-event rates.

To achieve sufficient precision in the prediction, it is usually required to perform Monte Carlo (MC) simulation, unless the signal-event kinematics can be analytically derived. We thus compute $\langle P[\text{LLP in f.v.}]\rangle$ with

$$\langle P[\text{LLP in f.v.}]\rangle = \frac{1}{N_{\text{LLP}}^{\text{MC}}} \sum_{i=1}^{N_{\text{LLP}}^{\text{MC}}} P[(\text{LLP})_i \text{ in f.v.}] \ . \tag{11}$$

Here, $N_{\text{LLP}}^{\text{MC}}$ labels the total number of the LLPs generated with the MC simulation program, and $P[(\text{LLP})_i$ in f.v.] is obtained with Eq. (10).

We can therefore express the expected signal-event number with,

$$N_{\text{LLP}}^{\text{exp}} = N_{\text{LLP}}^{\text{prod}} \cdot \langle P[\text{LLP in f.v.}]\rangle \cdot \text{Br}(\text{LLP} \to \text{vis}) \cdot \epsilon_{\text{det}} \ , \tag{12}$$

where $N_{\text{LLP}}^{\text{prod}} = \sigma_{\text{LLP}}^{\text{prod}} \cdot \mathcal{L}$ is the total number of the LLPs produced at the collider and is determined by the LLP's production cross section $\sigma_{\text{LLP}}^{\text{prod}}$ and the collider's integrated luminosity $\mathcal{L}$. It is important that the kinematic cuts (if there is any) to which $N_{\text{LLP}}^{\text{prod}}$ corresponds should be aligned with those imposed in the MC simulations for computing $\langle P[\text{LLP in f.v.}]\rangle$. $\text{Br}(\text{LLP} \to \text{vis})$ is the branching ratio of LLP decaying into visible products. ϵ_{det} denotes the detector efficiency for the visible final state. For simplicity, we do not include the possible dependence of ϵ_{det} on the momentum, energy, or production position of the final-state particles from LLP decays. Further, LLP searches often impose cut selections on observables typical for LLP decay products, such as requiring a large transverse impact parameter. If such selections and detector efficiencies specific for LLPs are to be imposed, it is required to simulate the LLP decays with correct decay BRs including the decay positions handled by the MC simulation tool used.

Eq. (12) depends in a complicated way on not only the collider setups including the detector's design but also the theoretical model parameters such as the LLP's mass and its couplings to other particles. The LLP production cross section, $\sigma_{\text{LLP}}^{\text{prod}}$, is affected by both the collider beam energies and the coupling(s) inducing the LLP's production, and $\mathcal{L}$ reflects linearly the volume of the collected data. To compute the average decay probability in the detector's fiducial volume, $\langle P[\text{LLP in f.v.}]\rangle$, we should take into account the detector's geometry such as its position, shape, and volume, as well as the LLP's kinematics determined by beam energies, LLP mass, as well as its proper lifetime which further depends on its mass and decay couplings. The visible decay branching ratio $\text{Br}(\text{LLP} \to \text{vis.})$ can be predicted by the LLP's mass and sometimes also its decay couplings' strengths. Finally, the detector

efficiency $\epsilon_{\rm det}$ can often be modeled as a function of the LLP's energy and travelling direction, and is essentially determined by the detector's design.

In the large decay-length limit (which is usually of the most interest in LLP studies) such that the boosted decay length λ of the LLP is mostly dominant over the distance between the IP and the detector, the right-hand side of Eq. (10) can be expanded and as a result, the LLP decay probabilities in the fiducial volume and hence the signal-event number $N_{\rm LLP}^{\rm exp}$ become essentially, to the first order, proportional to $\Delta D = D_i^l - D_i^e$ times an overall factor accounting for the proportion of the generated LLPs travelling inside the window/solid-angle coverage of the detector. Assuming a fixed ΔD, the MD has the advantage of a huge solid-angle coverage compared to a FD, which can be offset, in principle, by building a FD with a large volume depending on its distance to the IP and the available space. However, for a FD, it is possible to implement shielding measures such as rock and lead in the space between the IP and the FD, thus removing potential background sources that would weaken the sensitivity reach especially for the MD. For beam-dump experiments, a boost of the LLP in the forward direction should be exploited and thus increasing the length of the detector can linearly strengthen the signal-event rates.

We note that advanced neural networks, trained using deep learning techniques to exploit the distinct LLP signatures and topologies, can further differentiate signals from SM backgrounds, especially in a clean environment provided by lepton colliders. Ref. [82] demonstrates that LLP searches can reach their full physics potential by harnessing the power of machine learning (ML). The LLP signal efficiency with an ML-based approach can increase significantly compared to traditional selection-based methods, while maintaining a background-free environment.

We conclude the section with a brief discussion on typical potential background sources for LLP searches at colliders. Although in general collider searches for LLPs suffer from relatively few background sources compared to prompt searches, there remain several typical origins of background events [238, 241]. Particle collisions induce scattering processes that produce certain SM particles that have a relatively long lifetime such as charm and bottom mesons, leading to collider signatures similar to those of BSM LLPs. Non-collision background sources include material interactions with SM particles, fake tracks and DVs, detector noise, and cosmic-ray muons. While the SM irreducible background events can often be simulated in a reliable way, the non-collision type of background sources can usually

be estimated only with non-traditional methods such as data-driven approaches, especially for the MD experiments. For FD and beam-dump experiments, the large space available between the IP/beam dump and the detector can often allow for installation of shielding, removing some of these backgrounds to a large extent such as long-lived SM particles. In practice, in many phenomenological analysis on collider searches for LLPs, in particular in the context of FD or beam-dump experiments, the assumption of zero background event is often made, expecting novel experimental strategies and methods, as well as instrumented apparatus such as shielding with lead or rock, can remove essentially all the background events.

C. Studies with the main detector

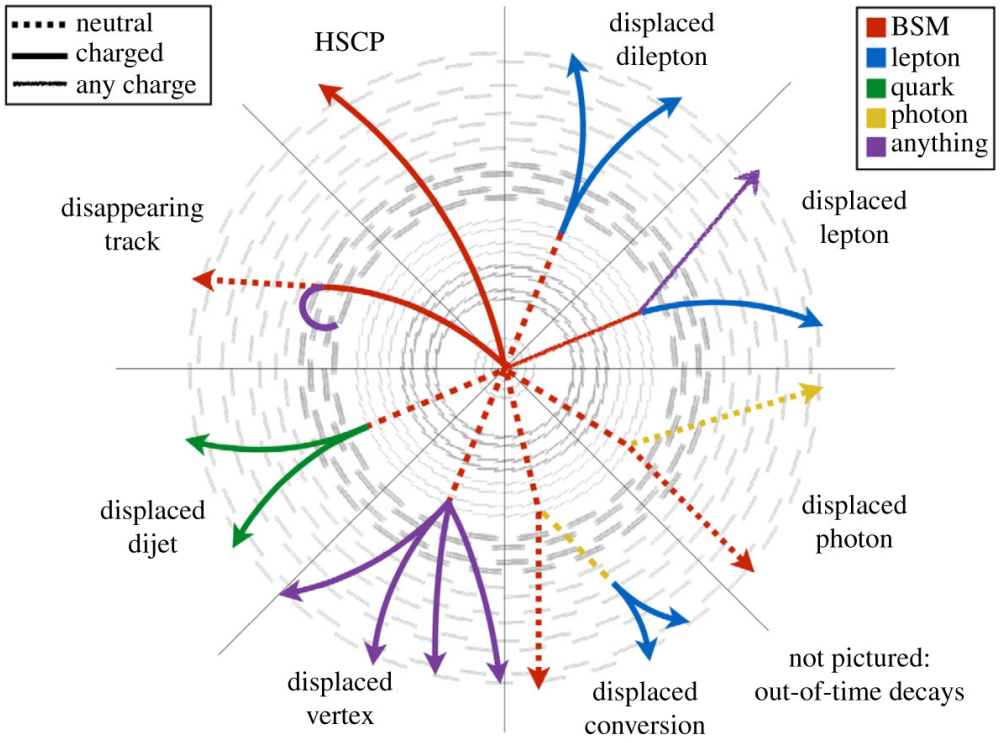

FIG. 37: Typical LLP signatures at the MD of a collider. Taken from Ref. [239].

LLPs can manifest themselves via different signatures at the MD of a collider. This is illustrated in Fig. 37 extracted from Ref. [239]. Charged LLPs, if not too soft, can leave a visible track inside the MD. For example, heavy stable charged particles (HSCPs) can travel through the whole detector without decaying, leaving a complete track. Similarly, a charged

LLP can decay inside the MD into charge-neutral or soft charged final states, resulting in a disappearing track. Neutral LLPs often couple only very feebly with SM particles, so that they do not interact with the detector material. If they leave the MD without decaying, they appear simply as missing energy or transverse momentum, and can only be searched for if they are produced in association with visible objects. However, if they decay inside the MD but with a macroscopic distance from the IP, exotic signatures can arise including displaced vertex, displaced leptons, displaced jets, and non-pointing photons.

In the rest of this section, we review past LLP studies with the MD at future high-energy electron-positron colliders, which cover various theoretical models and collider signatures. LLP studies related to the flavor physics are discussed in Sec. VIII. Sensitivity results for long-lived heavy neutral leptons, doubly-charged scalars in seesaw models, electrophilic axion-like particles (eALPs) are presented in Sec. X A 1, Sec. X D, Sec. XI A, respectively.

1. *Higgs boson decays*

LLPs can be produced from exotic decays of the Higgs boson, c.f. Sec. IV G 1. Recent studies are summarized as follows.

New scalar particles:

Ref. [82] performs a search for neutrally charged LLPs (X_1, X_2) produced via the rare decay of the Higgs boson. The signal process is $e^+e^- \to ZH(Z \to \text{inclusive}, H \to X_1 + X_2)$ at $\sqrt{s} = 240$ GeV. X_1 and X_2 can each decay into a $\nu\bar{\nu}$ pair or a $q\bar{q}$ pair, resulting in final states with either two jets (type-I signal) or four jets (type-II signal) [262]. The study is conducted using full simulation MC samples corresponding to an integrated luminosity of 20.0 ab^{-1} and about 4×10^6 Higgs bosons. Both Convolutional Neural Networks (CNN) and Graph Neural Networks (GNN) have been trained using full MC signal and background samples. The results of two neural networks agree with each other.

Figure 38 shows constraints on the branching ratio of Higgs boson decay to LLPs. For the two LLPs signal types, a parameter $\epsilon_V := \frac{BR(X\to\nu\bar{\nu})}{BR(X\to q\bar{q})}$ is defined. In the case of Type I and Type II signal yields having a fixed ratio, a value of 0.2 is set and a one-dimensional 95% Confidence Level upper limit on $\mathcal{B}(H \to \text{LLPs})$ is derived and shown in Figure 38a). In the case of Type I and Type II signal yields having a floating ratio ϵ_V with an allowed range of 10^{-6} and 100, a one-dimensional 95% Confidence Level upper limit on $\mathcal{B}(H \to \text{LLPs})$

is derived and shown in Figure 38b). In the fixed ratio case, the upper limit results have significantly smaller uncertainties than the floating ratio case. The best upper limit result in the fix ratio case is 1.2×10^{-6} on $\mathcal{B}(H \to \text{LLPs})$ with a statistics of 4×10^6 Higgs bosons.

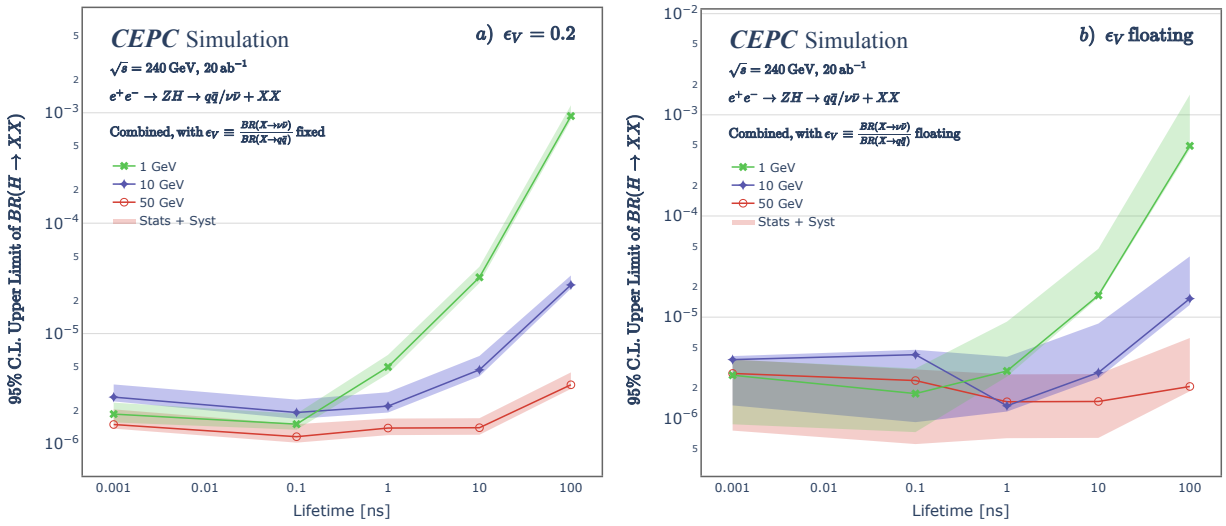

FIG. 38: (Color online) 95% C.L. upper limit on the branching ratio (BR) for the Higgs boson (H) decay into pairs of LLPs (X_1X_2) via $e^+e^- \to ZH$, where ϵ_V is the ratio $\frac{BR(X\to\nu\bar{\nu})}{BR(X\to q\bar{q})}$. **a)**: a fixed ratio $\epsilon_V = 0.2$, **b)**: a floating ϵ_V. The shaded areas indicate statistical and systematic uncertainties combined. Taken from Ref. [82].

Ref. [83] investigates long-lived scalar particles produced from exotic Higgs-boson decays at the CEPC and FCC-ee. The signal process is Higgsstrahlung $e^-e^+ \to hZ$ at $\sqrt{s} = 250$ GeV, followed with $h \to XX$ and $Z \to (\ell^-\ell^+)$, where $\ell = e, \mu$ and X is the long-lived new scalar boson. X is assumed to be produced at the IP and is required to decay inside the inner tracker into a pair of quarks, leading to displaced hadronic final states. The X particle is required to decay at a position with a distance larger than 3 cm (5 µm) to the IP, for the "long lifetime" ("large mass") analysis. Further, this displacement distance is required to be within the outer radius of the tracker which is 1.81 (2.14) m for the CEPC (FCC-ee) detector. The dominant SM background processes, $e^-e^+ \to hZ \to (b\bar{b})(\ell^+\ell^-)$ and $e^-e^+ \to ZZ \to (b\bar{b})(\ell^+\ell^-)$, are investigated and selection cuts are imposed in order to eliminate such background. The numbers of Higgs bosons produced at both CEPC and FCC-ee are considered to be 1.1×10^6. In addition to forecasting sensitivities to the branching ratio of $h \to XX$ as shown in Fig. 39, results are also interpreted in the parameter space of

theory models including the Higgs-portal Hidden Valley model and various incarnations of neutral-naturalness models.

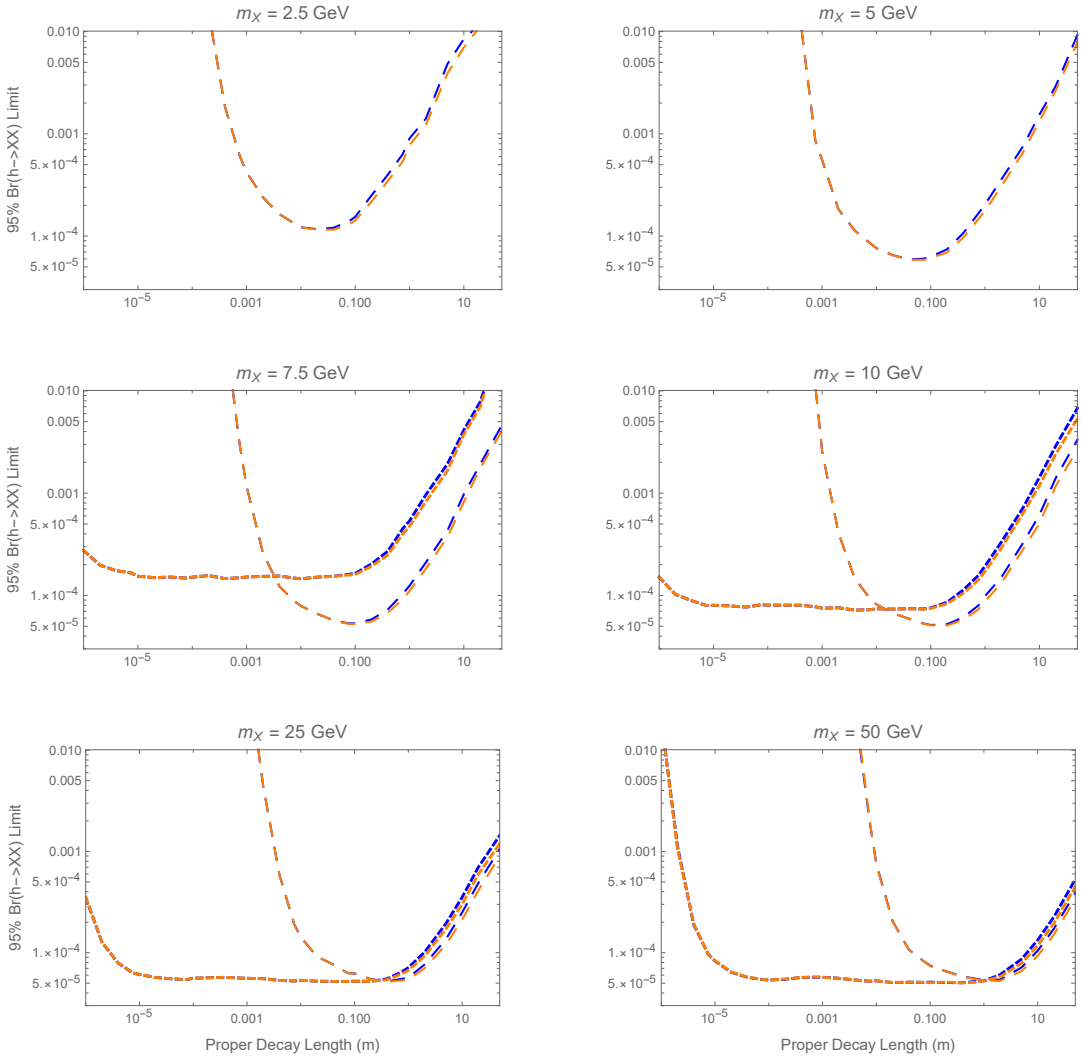

FIG. 39: Projected 95% $h \to XX$ branching ratio limits as a function of proper decay length for a variety of X masses. Blue lines are for CEPC and orange lines are for FCC-ee, and where only one is visible they overlap. The larger dashes are the 'long lifetime' analysis and the smaller dashes are the 'large mass' analysis. Taken from Ref. [83].

Ref. [84] studies displaced-vertex signatures of scalar LLPs pair-produced from exotic Higgs decays at the CEPC and FCC-ee with CM energy $\sqrt{s} = 240$ GeV and an integrated luminosity $\mathcal{L}_h = 5.6$ ab^{-1}. These charge-neutral LLPs decay into a pair of leptons or quarks at the partonic level. Two theoretical models are investigated: a Higgs-portal model and a neutral-naturalness model. These two models feature two representative mass ranges for

scalar LLPs, corresponding to different characteristic signatures at colliders.

The Higgs-portal model includes a very light scalar boson, h_s, in the sub-GeV mass regime, stemming from a singlet scalar field appended to the SM. Such a light scalar LLP decays into a pair of muons or pions, giving rise to a distinctive signature of collimated muon-jet or pion-jet, thanks to the sub-GeV mass. Thus, for this model, the signal process is $h \to h_s h_s, h_s \to \mu^-\mu^+, \pi^-\pi^+$ where the SM Higgs boson h is produced in Higgsstrahlung process. For the dimuon decay of h_s, displaced muons are detected in either the inner tracker (IT) detector or muon spectrometer (MS). Further, for h_s decays into a pair of charged pions, displaced vertices are considered to be reconstructed in the IT, HCAL, or MS. The background is assumed to be negligible after event selections on the opening angle of the LLP decay products are imposed, and 95% C.L. sensitivity reaches are presented in terms of three-signal-event contour curves in the plane spanned by the h_s mass and the Higgs bosons mixing angle θ, for two benchmark choices of the new scalar-single field's vacuum expectation value (vev) $\langle\chi\rangle = 10, 100$ GeV.

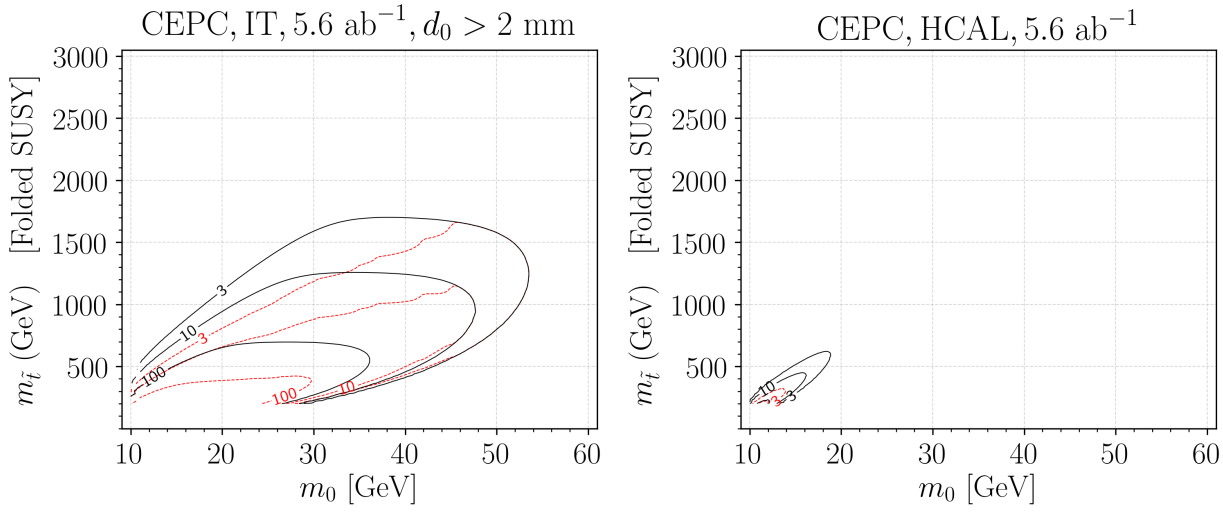

FIG. 40: Sensitivity reaches of log10(N_{signal}) at the CEPC for the Folded SUSY model. The black(red) curves correspond to $\kappa = \kappa_{\max}(\kappa = \kappa_{\min})$. Taken from Ref. [84].

On the other hand, the neutral-naturalness model, e.g. folded supersymmetry, predicts the lightest mirror glueball 0^{++} of mass $\mathcal{O}(10)$ GeV, leading to displaced decays with a large transverse impact parameter because of the relatively large mass. The mirror glueball in the mass range of $\mathcal{O}(10)$ GeV dominantly decays into a pair of b-jets, which is taken to be the signal channel. Thus, for this model, the signal process is $h \to 0^{++}0^{++}, 0^{++} \to b\bar{b}$.

Two major background processes are taken into account: $e^-e^+ \to ZZ \to (\ell^+\ell^-, jj)(b\bar{b})$ and $e^-e^+ \to Zh \to (\ell^+\ell^-, jj)(b\bar{b})$, in which the $b\bar{b}$ pair comes from prompt Z-boson's or SM Higgs boson's decay. Sensitivity reaches are shown in Fig. 40 in terms of the contour curves with different numbers of signal events, in the $(m_0, m_{\tilde{t}})$ plane, where $m_{\tilde{t}}$ is the stop mass, for two possible parameterizations of κ, which is a parameter taking into account the effect of the glueball hadronization and nonperturbative mixing effects between the excited glueball states and the SM Higgs boson.

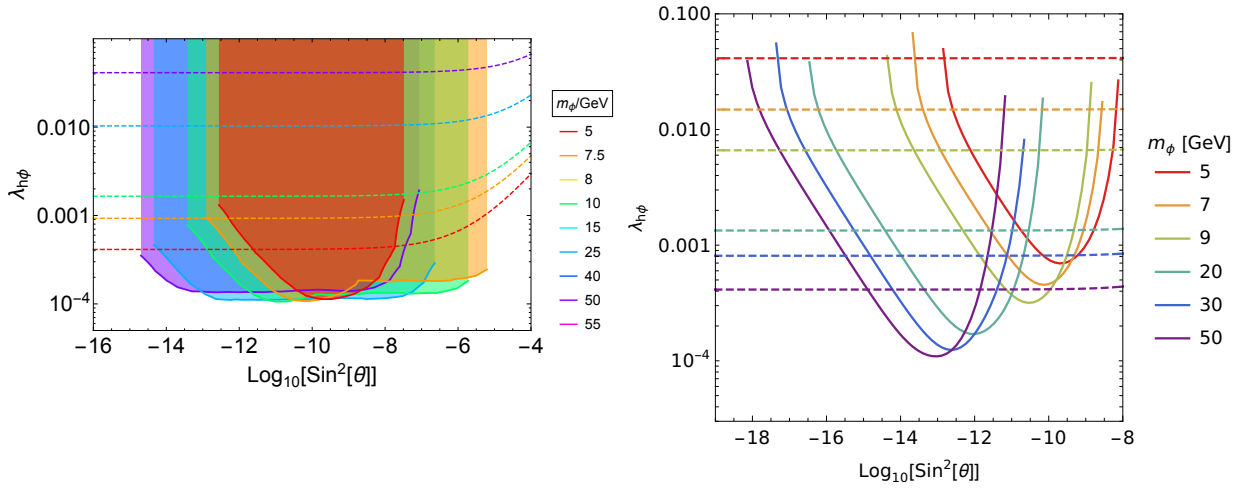

FIG. 41: Top: bounds on $\lambda_{h\phi}$ and $\sin^2\theta$ for various singlet masses arising from searches for displaced jets in Higgs decays at the FCC-ee with $\sqrt{s} = 240$ GeV and integrated luminosity $\mathcal{L}_h = 5$ ab^{-1}; the dashed lines show the upper naturalness limit $\lambda_{h\phi}^{\max} = m_\phi^2/v^2 + 4\pi m_\phi \sin\theta/v$. Bottom: bounds on $\lambda_{h\phi}$ and $\sin^2\theta$ for various singlet masses arising from searches for delayed jets in Higgs decays; the dashed lines show the upper naturalness limit $\lambda_{h\phi}^{\max}$ of for each mass. Since physics is the same, sensitivities can be interpreted as the results at the CEPC.Taken from Ref. [263].

Ref. [263] computes collider sensitivities to long-lived singlet scalar particles produced from SM Higgs-boson decays, $h \to \phi\phi$, considering signatures of invisible decays, displaced and delayed jets, and coupling fits of untagged decays. Results from the searches of displaced and delayed jets are shown in Fig. 41 for FCC-ee with $\sqrt{s} = 240$ GeV and integrated luminosity $\mathcal{L}_h = 5$ ab^{-1}. Results for invisible decays are also given in this study. Since physics is the same, sensitivities can be interpreted as the results at the CEPC.

Hidden valley particles:

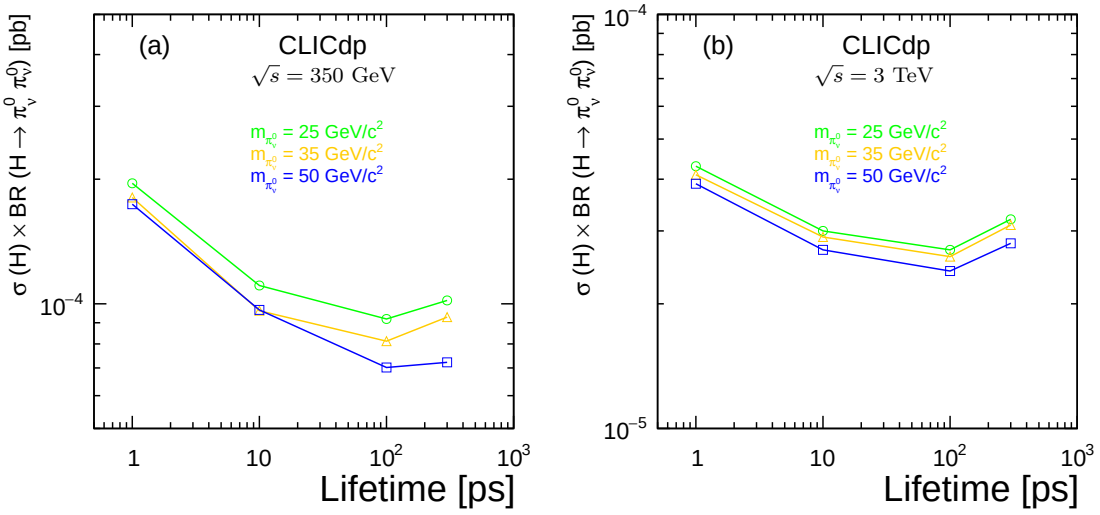

FIG. 42: Expected 95% CL cross-section upper limits on the $\sigma(H) \times BR(H \to \pi_v^0 \pi_v^0)$, within the model [264], for three different π_v^0 masses: 25 GeV (green), 35 GeV (yellow), 50 GeV (blue), as a function of π_v^0 lifetime for $\sqrt{s} = 350$ GeV (a) and $\sqrt{s} = 3$ TeV (b). Since physics is the same, sensitivities can be interpreted as the results at the CEPC with upgraded CM energies.Taken from Ref. [260].

Ref. [260] works on the sensitivity reach to massive LLPs using the ILD detector at CLIC with $\sqrt{s} = 350$ GeV and 3 TeV, and an integrated luminosity of 1 ab^{-1} and 3 ab^{-1}, respectively. The study is in the context of the Hidden Valley model. In this work, two long-lived Hidden-Valley particles are pair produced from the SM Higgs boson decays, and subsequently decay into b-quarks, i.e. $h \to \pi_V^0 \pi_V^0 \to (b\bar{b})(b\bar{b})$, providing four b-jets in the final state. At $\sqrt{s} = 350$ GeV, Higgs bosons are dominantly produced from the Higgsstrahlung process ($e^- e^+ \to Zh$), while at $\sqrt{s} = 3$ TeV, the dominant production channel is the WW-fusion ($e^- e^+ \to \nu\bar{\nu}h$). Signal samples with π_v^0 lifetimes from 1 to 300 ps, masses between 25 and 50 GeV, and the parent Higgs mass of 126 GeV, are generated, while background samples of $q\bar{q}$, $q\bar{q}\nu\bar{\nu}$, $q\bar{q}q\bar{q}$, $q\bar{q}q\bar{q}\nu\bar{\nu}$ are generated, with additional samples of $t\bar{t}$ and WWZ for $\sqrt{s} = 350$ GeV. The observables based on reconstructed displaced vertices are input for performing multivariate analysis and reducing the SM background. Sensitivity results are presented for the production cross-section ($\sigma(h) \times \mathrm{BR}(h \to \pi_v^0 \pi_v^0)$) as a function of the LLP's

lifetime for three different π_v^0 masses: 25, 35, 50 GeV. We reproduce them in Fig. 42.

Dark photons:

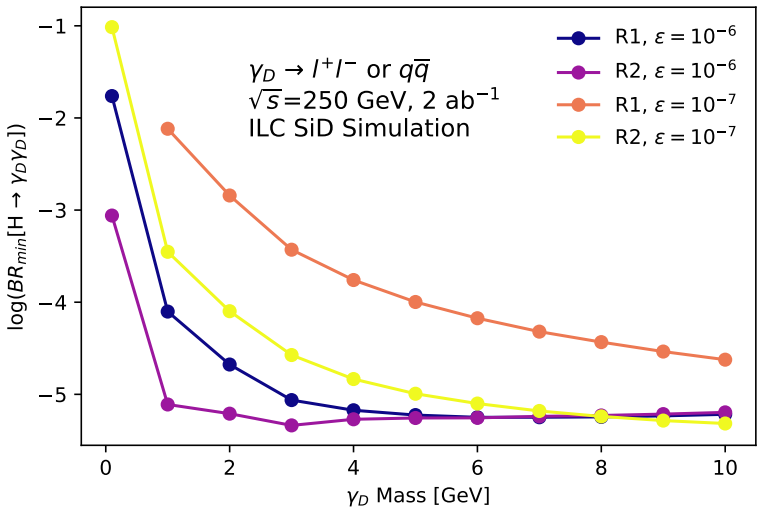

FIG. 43: The minimum branching ratio $H \to \gamma_D\gamma_D$ to which SiD will be sensitive for $\sqrt{s} = 250$ GeV and 2 ab^{-1}, when both leptonic and hadronic decays are reconstructed within the regions $R1$ and $R2$, for $\epsilon = 10^{-6}, 10^{-7}$. Since physics is similar, sensitivities can be interpreted as the results at the CEPC with the same CM energy and integrated luminosity. Taken from Ref. [85].

Ref. [85] studies sensitivity to long-lived dark photons produced in Higgsstrahlung events via the Higgs portal, $h \to \gamma_D\gamma_D$, with the Silicon Detector (SiD) at ILC. The considered signal process is $e^-e^+ \to Zh \to (q\bar{q})\,(\gamma_D\gamma_D), \gamma_D \to \ell^-\ell^+/q\bar{q}$ at $\sqrt{s} = 250$ GeV with an integrated luminosity of 2 ab^{-1} for each of two polarization cases $e_L^-e_R^+$ and $e_R^-e_L^+$ at nominal ILC TDR polarization fractions, and 80% electron polarization and 30% positron polarization, respectively. The following SM background processes are considered and generated: 2-fermion states $e^-e^+ \to f\bar{f}$, 3-fermion states $e\gamma \to eZ, \nu W \to 3f$, and 4-fermion states $e^-e^+ \to WW, e\nu W, ZZ, eeZ, \nu\bar{\nu}Z \to 4f$. Two requirements for fiducial regions "$R1$" and "$R2$" are taken into account. It is found that the requirement of a displaced vertex formed from tracks with measurably large impact parameter in the clean ILC event environment likely suppresses background events to a negligible level. Assuming no background with the selections outlined in the study, baseline sensitivities on the minimal branching ratio $h \to \gamma_D\gamma_D$ as a function of γ_D mass are presented in Fig. 43 for several choices of the kinetic

mixing parater ϵ. Additionally, this study also presents the first full simulation of LLPs for SiD. Since physics is similar, sensitivities can be interpreted as the results at the CEPC with the same CM energy and integrated luminosity.

2. *Z-boson decays*

Future lepton colliders such as the CEPC and FCC-ee would run as high-luminosity Z-boson factories, which offer a unique opportunity to study LLPs from rare Z-boson decays, c.f. Sec. IV G 2. Recent studies are summarized as follows.

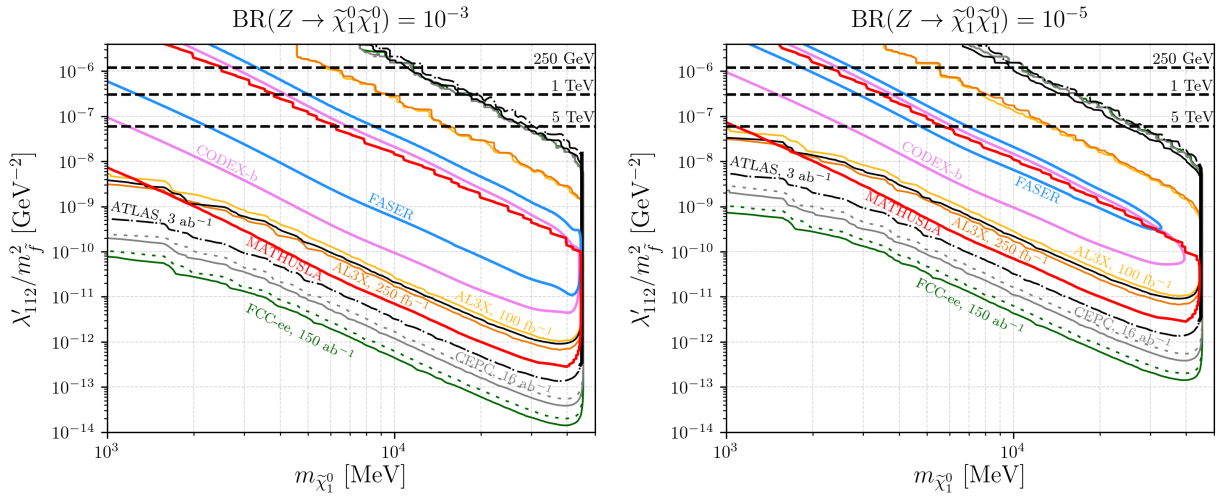

FIG. 44: The sensitivity estimate of the CEPC (grey) and the FCC-ee (green) presented in the 2D plane of $\lambda'_{112}/m^2_{\tilde{f}}$ vs. $m_{\tilde{\chi}_1^0}$ assuming BR($Z \to \tilde{\chi}_1^0\tilde{\chi}_1^0$) = 10^{-3} (left) and 10^{-5} (right), respectively. The solid contour curves correspond to three decay events in the fiducial volume when considering all decay modes of $\tilde{\chi}_1^0$, while the dashed lines include only visible/charged decay modes ($K^{(*)\pm}e^{\mp}$, e^-us or $e^+\bar{u}\bar{s}$). The estimates for experiments at the LHC: AL3X, CODEX-b, FASER and MATHUSLA, are reproduced from Refs. [265, 266]. The ATLAS results correspond to HL-LHC for $\sqrt{s}$ = 14 TeV and 3 ab^{-1} integrated luminosity. The black horizontal dashed lines correspond to the current RPV bounds on the single coupling λ'_{112} [267] for three different degenerate sfermion masses $m_{\tilde{f}}$ = 250 GeV, 1 TeV, and 5 TeV as labelled. Taken from Ref. [86].

Ref. [86] considers the physics scenario where the long-lived lightest neutralino pair $\tilde{\chi}_1^0\tilde{\chi}_1^0$

is produced from Z-decays in the context of the R-parity-violating supersymmetry model. The lightest neutralino $\tilde{\chi}_1^0$ is dominantly bino-like with small Higgsino components. The study focuses on the $\lambda'_{ijk} L_i \cdot Q_j \bar{D}_k$ operators, and $\lambda'_{112}\ L_1 \cdot Q_1 \bar{D}_2$ is chosen to be the only nonvanishing RPV operator, which leads to the lightest neutralino decays to SM particles via a sfermion exchange. For $m_{\tilde{\chi}_1^0} < m_Z/2$ and small λ' couplings, the lightest neutralino becomes long-lived and decays after having travelled a macroscopic distance. The signal process is $Z \to \tilde{\chi}_1^0 \tilde{\chi}_1^0,\ \tilde{\chi}_1^0 \to e^{\mp} K^{(*)\pm}/e^{\mp} jj$ at $\sqrt{s} = 91.2$ GeV. The fiducial volume of the detectors is considered as the inner detector consisting of the vertex detector and the tracker. This choice is conservative and ensures that the electrons produced from the neutralino decays could be reconstructed. The signal events require at least one neutralino decaying inside the inner detector, while the other could decay either inside or outside the inner detector.

The background is assumed to be negligible, and sensitivity reaches are presented in terms of three-signal-event contour curves on the model parameters. Fig. 44 shows the sensitivity estimate of the CEPC (grey) and the FCC-ee (green) in the 2D plane of $\lambda'_{112}/m^2_{\tilde{f}}$ vs. $m_{\tilde{\chi}_1^0}$ for two different benchmark values of BR($Z \to \tilde{\chi}_1^0 \tilde{\chi}_1^0$), respectively. The analyses indicates that when assuming Br($Z \to \tilde{\chi}_1^0 \tilde{\chi}_1^0$) $= 10^{-3}$ and $m_{\tilde{\chi}_1^0} \sim 40$ GeV, the model parameter $\lambda'_{112}/m^2_{\tilde{f}}$ can be probed down to as low as $\sim 1.5 \times 10^{-14}$ (3.9×10^{-14}) GeV^{-2} at the FCC-ee (CEPC) with CM energy $\sqrt{s} = 91.2$ GeV and 150 (16) ab^{-1} integrated luminosity. Sensitivity results are compared with the projected sensitivity reaches of the ATLAS experiment at the HL-LHC [268] and the proposed LHC experiments with far detectors (AL3X [269], CODEX-b [270], FASER [271], and MATHUSLA [230]). Ref. [87] probes axion-like particles (ALPs) coupled to charged leptons in leptonic decays of the Z-boson at CEPC and FCC-ee. The ALPs are assumed to have very long lifetime, travel through the main detector, and behave as missing energy. The signal process is $e^- e^+ \to Z^{(*)} \to \ell^- \ell^+ a$ at $\sqrt{s} = 91$ GeV. This study analyzes the signal process of $e^- e^+ \to \mu^- \mu^+ a$, and considers background sources including $\tau^+ \tau^-$, $\mu^+ \mu^- \nu \bar{\nu}$, and $\mu^+ \mu^- \gamma$ (where γ gets undetected). Fig. 45, extracted from Ref. [87], presents sensitivity reaches in terms of the contour curves in the $f_a/C^A_{\mu\mu}$ vs. m_a plane for various integrated luminosities of 50, 100 and 150 ab^{-1}. Limits based on the ALP contribution to the anomalous magnetic moment of the muon are also shown together. The sensitivity reaches for the ALP with a large coupling to photons and negative $C^A_{\mu\mu}$ are also derived in this study.

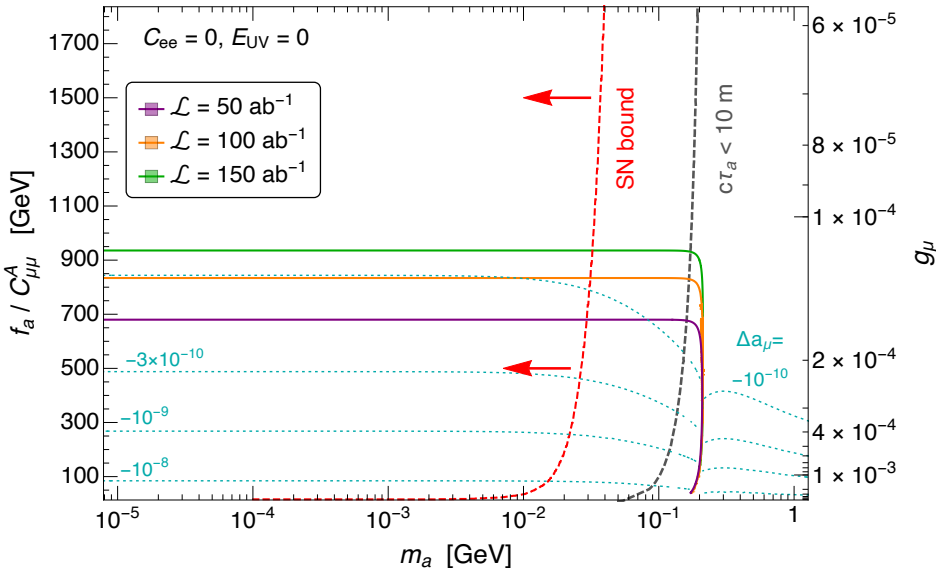

FIG. 45: Prospected CEPC/FCC-ee 95% CL exclusion on the (m_a, $f_a/C^A_{\mu\mu}$) plane for a muonic ALP ($C^A_{ee} = 0$, $E_{\rm UV} = 0$) with different assumptions for the integrated luminosity $\mathcal{L}$, as indicated. On the right side of the dashed grey line the proper decay length of the ALP is $c\tau_a < 10$ m. The region to the left of the red dashed line is excluded by SN1987A data, according to the analysis in [272]. The dotted cyan contours show the ALP contribution to the anomalous magnetic moment of the muon, $\Delta a_\mu \equiv (g-2)_\mu/2$. Taken from Ref. [87].

3. *Supersymmetry (SUSY)*

Ref. [273] reviews studies on LLPs at the ILC and CLIC in the context of SUSY models. The long-lived next-to-lightest supersymmetric particle (NLSP) is the stau $\tilde{\tau}$, and the lightest supersymmetric particle (LSP) is the gravitino $\tilde{G}$ or axino $\tilde{a}$. The signal includes both the 2-body decay process $\tilde{\tau} \to \tau\tilde{G}/\tau\tilde{a}$ and 3-body decay process $\tilde{\tau} \to \gamma\tau\tilde{G}/\gamma\tau\tilde{a}$.

Ref. [274] studies the SUSY scenario at the ILC where the gravitino $\tilde{G}$ is the LSP and a charged stau $\tilde{\tau}$ is the long-lived, metastable NLSP. The signal process is $\tilde{\tau} \to \tau\tilde{G}$. In the analyses, stau detection and measurement principle consists of several steps: identify a $\tilde{\tau}$ and determine its mass from kinematics; follow the track until it is trapped inside the detector; observe the stopping point until a decay $\tilde{\tau} \to \tau\tilde{G}$ is triggered by a large energy release uncorrelated to beam collisions; record the decay time to determine the $\tilde{\tau}$ lifetime; finally, measure the τ recoil energy to get the gravitino mass. The case study assumes the

ILC running at $\sqrt{s} = 500$ GeV and an integrated luminosity $\mathcal{L} = 100$ fb^{-1}.

Ref. [275] investigates the prospects of observing lepton flavour violation at future e^-e^+ and e^-e^- linear colliders in scenarios where the gravitino $\tilde{G}$ is the LSP, and the long-lived stau $\tilde{\tau}$ is the NLSP. Since the NLSP can only decay gravitationally into gravitinos and charged leptons, the decay rate is very suppressed and the NLSP could traverse several layers of the vertex detector before decaying or even being stopped and trapped in it. The signals of lepton flavor violation would consist of two heavily ionizing tracks owing to the long-lived staus accompanied by two or four charged leptons. The signals consist of multi-lepton final states with two heavily ionizing charged tracks produced by the long-lived staus. The numerical analyses are performed at the ILC with $\sqrt{s} = 500$ GeV and an integrated luminosity of 500 fb^{-1} assuming the beams are unpolarized. The sensitivity reaches to lepton flavor violation are presented and compared with the present and future constraints on lepton flavor violation stemming from the non-observation of rare leptonic decays.

4. Vector-like leptons with scalar

Ref. [112] considers vector-like leptons (VLLs) $F^\pm$ as a simple extension to the SM, with an accompanying scalar particle ϕ at future electron-positron colliders. Assuming $F^\pm$ and ϕ mix only with the first-generation SM leptons, the authors focus on CEPC with CM energy 240 GeV. The scalar particle ϕ is long-lived; it is pair produced and subsequently decays into e^-e^+. Employing the inner tracker for reconstructing the displaced vertex and applying appropriate event-selection cuts to suppress background from the SM Z- and Higgs bosons' prompt decays, the analysis finds good performance of CEPC for $m_\phi < 70$ GeV and $m_F < 1$ TeV. Details of this study can be found in Sec. V B 3.

D. Studies with far detectors

It has been well accepted among the high-energy-physics community that at colliders such as LHC, besides the traditional MD installed at the IP, FDs, can also be constructed for operation away from the IP by up to $\mathcal{O}(100)$ m. When the decay lengths of LLPs are very long (e.g. $\lambda \gtrsim \mathcal{O}(100)$ m), they can have a sizable probability to travel through the MD, acting as missing energy. In this case, a far detector could have a better chance to observe

their decay processes if λ of the LLPs falls roughly around its distance to the IP, and could reconstruct the information of time, position, energy, momentum, mass, etc. Moreover, the large space between the FD and the IP allows for sufficient shielding which can effectively remove background sources. Therefore, in principle, such far detectors can enhance the discovery potential for LLPs with very long decay lengths.

1. *Far detectors at hadron colliders*

	ANUBIS	FASER	FASER2
IP	ATLAS	ATLAS	ATLAS
int. lumi. [fb^{-1}]	3000	150	3000
	FACET	MATHUSLA	AL3X
IP	CMS	CMS	ALICE
int. lumi. [fb^{-1}]	3000	3000	100, 250
	CODEX-b	MoEDAL-MAPP1	MoEDAL-MAPP2
IP	LHCb	LHCb	LHCb
int. lumi. [fb^{-1}]	300	30	300

TABLE IX: Summary table of the LLP FDs at the LHC, listing the associated interaction point and the projected integrated luminosity.

Two classes of FDs are currently operating or have been proposed at the LHC. The first class is a series of detectors that are composed of dense materials such as tungsten or liquid argon as targets and mainly purposed for detecting high-energy active neutrinos originating from the LHC IPs through neutrino-nucleus deep inelastic scattering. Among them, SND@LHC [277, 278] and FASERν [279, 280] are collecting data during the LHC Run 3. AdvSND [281, 282], FASERν2 [281, 283, 284], and FLArE-10/100 [281, 285] would be further upgraded experiments and have been proposed to be running during the high-luminosity LHC (HL-LHC) era at the proposed Forward Physics Facility (FPF) [281]. These FPF experiments would be installed in the very forward direction on/off-axis, about 600 meters away from the ATLAS IP.

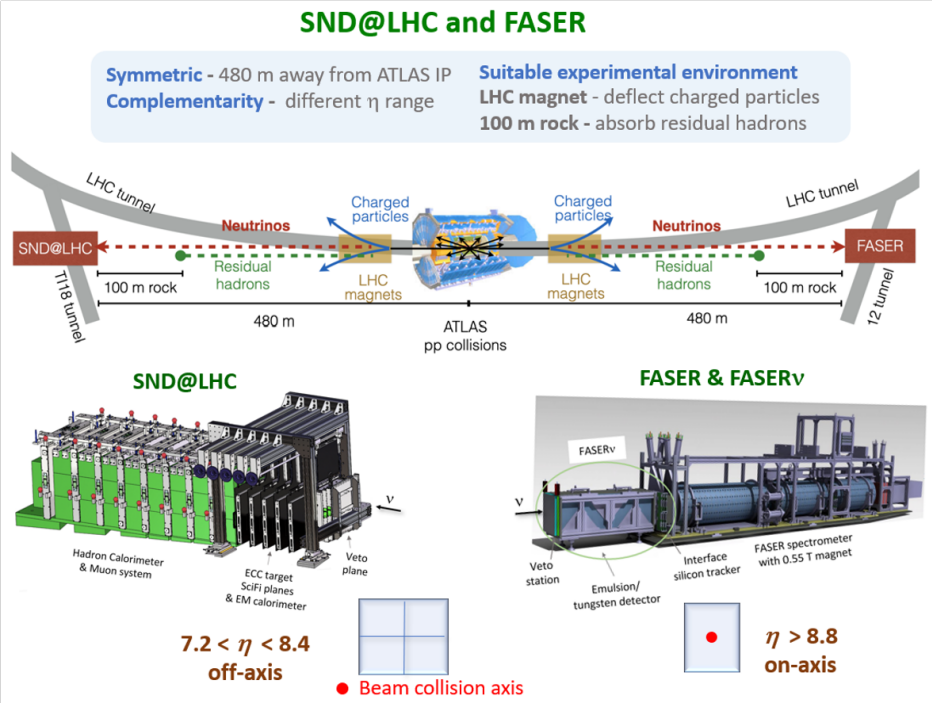

FIG. 46: Schematic pictures of the SND@LHC, FASERν, and FASER experiments. Taken from Ref. [276].

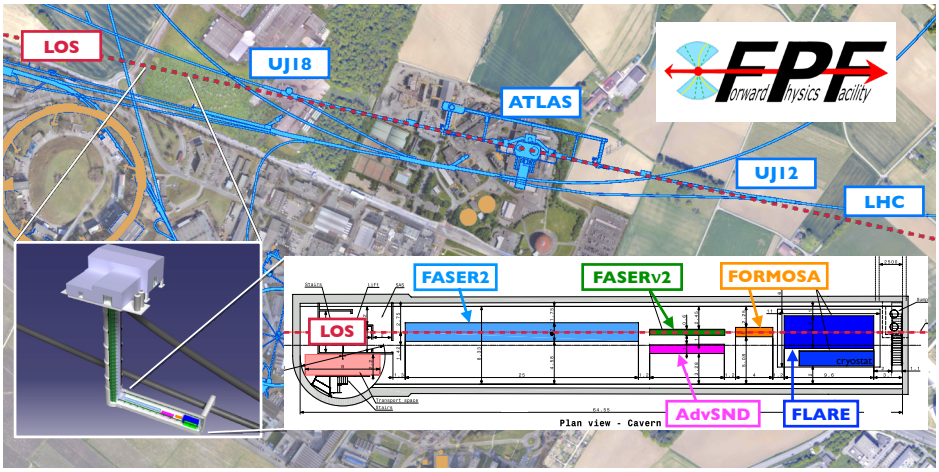

FIG. 47: The preferred location for the FPF, a proposed new cavern for the HL-LHC era. The FPF will be 65 m-long and 8.5 m-wide and will house a diverse set of experiments to explore the many physics opportunities in the far-forward region. Taken from Ref. [281].

Another type of FDs at the LHC aim primarily at searching for displaced decays of LLPs into charged final-state particles. These experiments include and FASER and FASER2 [271, 286, 287], MATHUSLA [230, 288, 289], ANUBIS [290], AL3X [269], FACET [291], CODEX-

b [270, 292], MoEDAL-MAPP1 and MAPP2 [293, 294], which suggest to install auxilliary detectors at positions $\mathcal{O}(5-500)$ m away from the IPs of the ATLAS, CMS, or LHCb experiments. For example, FASER is a small cylindrical detector installed right behind FASERν and is currently operating during Run 3. FASER2 would be the upgraded program of FASER, installed at FPF with a distance of 620 m from the ATLAS IP. Alternatively, in one of the service shafts above the ATLAS IP, another detector called ANUBIS has been suggested to be constructed; it also has a cylindrical shape but faces vertically. MATHUSLA has been proposed to be constructed about $\sim$ 100 m above the CMS IP, with a mostly empty decay volume monitored by trackers for reconstruction of LLP decays into charged particles. In the forward direction of the CMS IP, FACET has been brought up to be placed surrounding the beam pipe. In the vicinity of the ALICE IP, AL3X has been suggested. Finally, for the LHCb IP, some far-detector proposals currently exist: CODEX-b, MoEDAL-MAPP1 and MAPP2. For a summary of these detectors including their geometries and corresponding integrated luminosities, see e.g. Refs. [291, 295, 296]. We list these LLP FDs in Table IX including their associated interaction point and the integrated luminosity. In Fig. 46, schematic pictures of SND@LHC, FASERν, and FASER, extracted from Ref. [276], are also shown, and in Fig. 47 the location of the FPF is illustrated together with the setup of the experiments proposed to be hosted there, reproduced from Ref. [281].

2. Proposed far detectors at lepton colliders

Besides at the LHC, FDs for detecting LLPs have also been proposed for operation at future e^-e^+ colliders, with the potential of enhancing the sensitivity reach to LLPs [88, 297, 298]. In particular, Ref. [88] firstly proposes the installation of FAr Detectors at the Electron Positron Collider (FADEPC) and investigates their basic designs and the corresponding discovery potentials for LLPs in several theoretical scenarios.

For planning the construction of FDs, since the tunnel of the LHC has already been constructed, there is little free space that could be utilized. However, for future e^-e^+ colliders the situation is more optimistic and open; as their construction plan is still under development, there is large freedom in the geometry and location of such FDs to be deployed. Therefore, it is both important and practical to start to design such FDs already now, so that it would be possible to have them built during the construction of the main experiment.

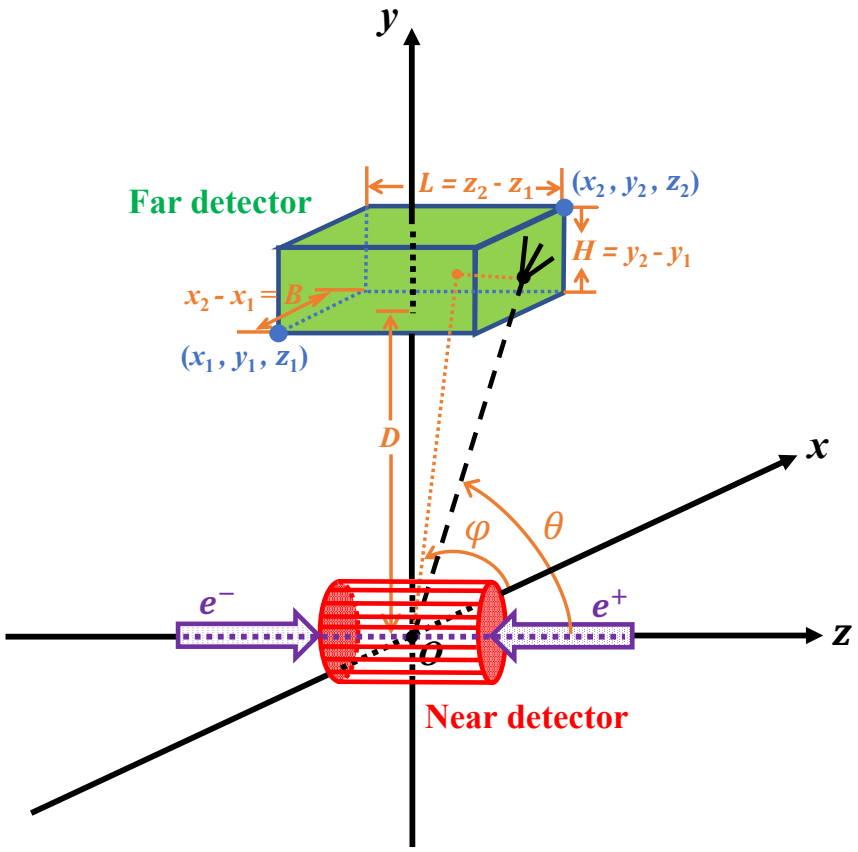

FIG. 48: The sketch displays the main detector (near detector, abbreviated as ND) and an example far detector. The dashed line indicates that one LLP is produced at the IP, travels through the main detector and decay insider the far detector. Taken from Ref. [88].

Further, at the LHC with proton-proton collisions, owing to the parton distributions in the protons, there is typically a large boost in the very forward direction for the LLPs, and as a result, all the proposed FD experiments there should have some longitudinal distance from the IP. However, it is a different case for symmetrical electron-positron colliders, where the LLPs produced would tend to travel in the transverse direction. Given the difference in the LLP kinematics between the LHC and future high-energy electron-positron colliders, as well as the currently large freedom for locating both the experimental hall and the FDs, we argue that auxiliary FDs at future e^-e^+ colliders could play a unique role in searching for LLPs. Fig. 48 from Ref. [88] is the sketch of an example FD at future e^-e^+ colliders. The coordinate system is set up as follows: the origin O is the IP; the injected electron and positron beams travel along the z axis, while the $+z$ direction is defined as the electron beam outgoing direction; the vertical and horizontal axes orthogonal to the z-axis are set to

be y- and x-axes, respectively; the $+y$ direction are chosen to be upward. The red cylinder enclosing the IP depicts the main detector (near detector, abbreviated as ND), while the green cuboid illustrates a far detector located with a distance from the IP. The distance of the FD to the IP is labeled with D.

Refs. [88, 259] consider various locations and geometrical setups of far detectors (FD1–FD8) at future e^-e^+ colliders and investigate their potentials for discovering LLPs in the physics scenarios including exotic Higgs decays, the lightest neutralinos in the R-parity-violating supersymmetry (RPV-SUSY), heavy neutral leptons, and axion-like particles. Besides, to compare discovery sensitivities between the FDs and NDs, Ref. [88] also derives sensitivity reach to the LLPs at the NDs of future e^-e^+ colliders and LHC FD experiments such as AL3X, CODEX-b, and MATHUSLA100. For the NDs at future e^-e^+ colliders, the CEPC's baseline detector setup are chosen. For the FDs at future e^-e^+ colliders, their shapes are assumed as cuboid and the locations of the FDs are $\sim 5 - 100$ m away in the transverse direction from the IP. For example, the FD1 design in this study is about $5 - 10$ m from the IP and employs a volume of 5×10^3 m^3. It can be placed inside the experiment hall if the hall is big enough, or in a cavern or shaft near the experiment hall. The volume of the other FD designs is large, and they are $50 - 100$ m from the IP. Ref. [88] finds that for searching for LLPs, FDs at future lepton colliders can extend and complement the sensitivity reaches of the default MD and the present and future LHC experiments. In particular, for the theoretical models considered, a MATHUSLA-sized far detector would give a modest improvement compared to the case with a main detector only at future lepton colliders.

Inspired by the previous proof-of-principle study [297], recently Ref. [258] propose a similar tracker detector, named as the LAYered CAvern Surface Tracker (LAYCAST), to be installed on the wall and ceiling of the main cavern at future electron-positron colliders such as CEPC and FCC-ee. The fiducial volume is taken to be the space between the main detector and the cavern's surface. The setup of LAYCAST is shown in Fig. 49, where the coordinate system is the same as in Fig. 48. The shape of the experimental hall is simplified into a cuboid. Considering that the floor of the experiment hall cannot be installed owing to load bearing and other reasons, the LAYCAST would be mounted on the roof surface and four vertical walls of the experimental hall. The LLPs produced at the IP, if decaying inside the main detector, can potentially be observed therein via the decay products. If they traverse the main detector and decay before reaching the cavern's inner surface, they

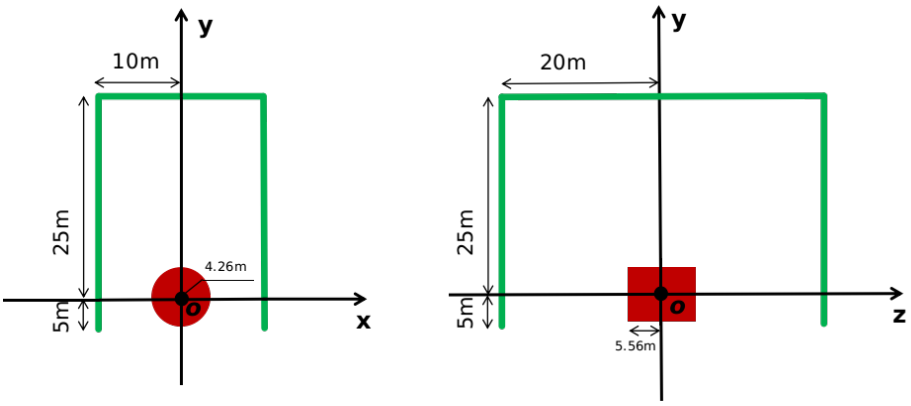

FIG. 49: The left and right plots show section views of the experimental setup in the xOy and yOz planes, respectively. In the plots, the red cylinder enclosing the coordinate origin represents the main detector of CEPC/FCC-ee. The green area depicts the proposed new far detector, LAYCAST, in the shape of a thin layer to be instrumented on the cavern surface. Take from Ref. [258].

may be detected by the LAYCAST experiment. Recent LLP studies with various FDs are summarized as follows. Sensitivity results for long-lived heavy neutral leptons are presented in Sec. X A 2.

3. Higgs boson decays

Refs. [88, 258] study a pair of long-lived light scalars X produced from the SM Higgs boson decays, $h \to XX$, at $\sqrt{s} = 240$ GeV. The total number of the SM Higgs bosons produced at either the CEPC or FCC-ee is specified as $N_h = 1.14 \times 10^6$ with an integrated luminosity $\mathcal{L} = 5.6$ ab^{-1}. Sensitivity results in terms of 3-signal-event contour curves are presented, corresponding to 95% C.L. limits with zero background events. Besides, sensitivity results in terms of 20-signal-event contour curves for LAYCAST are also presented, corresponding to 95% C.L. limits with about 100 background events, to estimate the effect of non-zero background. Fig. 50, extracted from Refs. [88, 258], shows sensitivity reaches in the branching ratio Br($h \to XX$) vs. proper decay length $c\tau$ plane for the the light scalar mass $m_X = 0.5$ GeV. Sensitivity reaches for $m_X = 10$ GeV are also given in Ref. [88, 258].

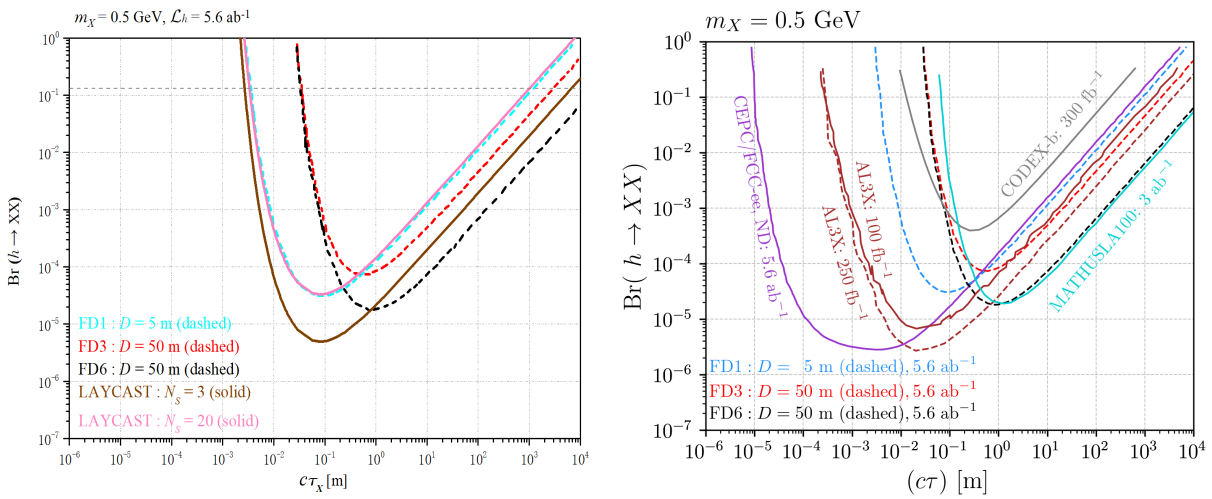

FIG. 50: Left: Sensitivity reaches of the CEPC/FCC-ee's far detectors FD1, FD3, FD6 and LAYCAST in the Br($h \to XX$) vs. $c\tau$ plane for $m_X = 0.5$ GeV. Right: Sensitivity reaches of the CEPC/FCC-ee's far detectors FD1, FD3, FD6, compared with predictions for the CEPC/FCC-ee's main detector (near detector, abbreviated as ND) and for AL3X, CODEX-b and MATHUSLA100. Taken from Ref. [88, 258].

4. $Z-$boson decays

Ref. [88, 258] consider Z-boson decays to a pair of long-lived neutralinos in the RPV-SUSY, $Z \to \tilde{\chi}_1^0\tilde{\chi}_1^0$, at $\sqrt{s} = 91.2$ GeV. The lightest neutralino is mostly bino with tiny components of Higgsinos. In the analyses, the total number of the Z-bosons produced at the CEPC is specified as $N_Z^{\rm CEPC} = 7.0 \times 10^{11}$ corresponding to a total integrated luminosity of $\mathcal{L}_Z^{\rm CEPC} = 16$ ab^{-1}, while $N_Z^{\rm FCC-ee} = 5.0 \times 10^{12}$ corresponding to $\mathcal{L}_Z^{\rm FCC\text{-}ee} = 150$ ab^{-1}. Sensitivity results in terms of 3-signal-event contour curves are presented, corresponding to 95% C.L. limits with vanishing background. Besides, sensitivity results in terms of 20-signal-event contour curves for LAYCAST are also presented, corresponding to 95% C.L. limits with about 100 background events, to estimate the effect of non-zero background. Fig. 51 is reproduced from Ref. [88, 258], and it show sensitivity reaches of different FD designs assuming Br($Z \to \tilde{\chi}_1^0\tilde{\chi}_1^0$) $= 10^{-3}$ for $m_{\tilde{\chi}_1^0} \ll m_Z/2$. Sensitivity reaches of both the FDs and NDs at the CEPC/FCC-ee with different integrated luminosities of $\mathcal{L} = 16$, 150, and 750 ab^{-1}, are also presented and compared in Ref. [88, 258].

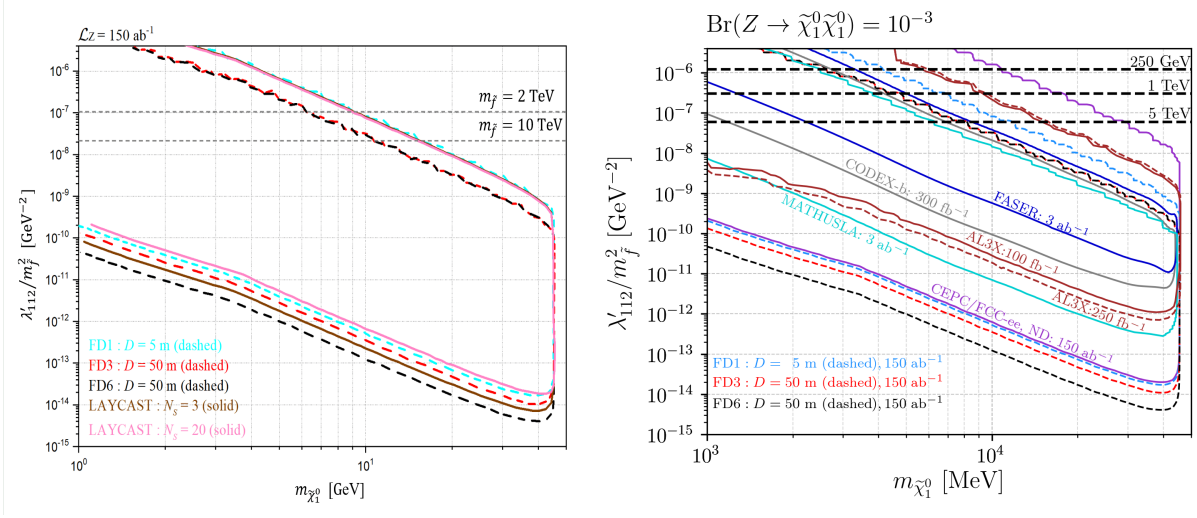

FIG. 51: Sensitivity reaches of different experiments assuming $\mathrm{Br}(Z \to \tilde{\chi}^0_1\tilde{\chi}^0_1) = 10^{-3}$. Left: results of the CEPC/FCC-ee's far detectors FD1, FD3, FD6 and LAYCAST in the $\lambda'_{112}/m^2_{\tilde{f}}$ vs. $m_{\tilde{\chi}^0_1}$ plane. Right: results of the CEPC/FCC-ee's far detectors FD1, FD3, FD6, compared with predictions for the CEPC/FCC-ee's main detector (near detector, abbreviated as ND) and other experiments. Taken from Ref. [88, 258].

5. *Axion-like particles*

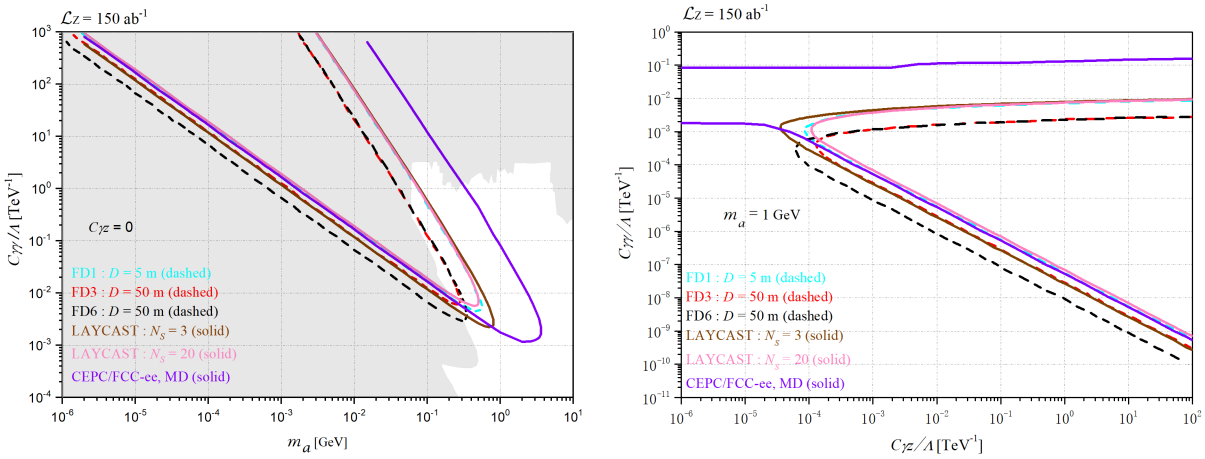

FIG. 52: Left: when $C_{\gamma Z} = 0$, sensitivity reaches of representative far detectors FD1, FD3, FD6, LAYCAST and the CEPC/FCC-ee's main detector (MD) with integrated luminosity $\mathcal{L}_Z = 150$ ab^{-1} in the $C_{\gamma\gamma}/\Lambda$ vs. m_a plane. Right: when both $C_{\gamma Z}$ and $C_{\gamma\gamma}$ are free parameters, sensitivity reaches with $m_a = 1$ GeV in the $C_{\gamma\gamma}/\Lambda$ vs. $C_{\gamma Z}/\Lambda$ plane with $\mathcal{L}_Z = 150$ ab^{-1}. Taken from Ref. [258, 259].

Refs. [258, 259] are follow-up works of Ref. [88]. Ref. [259] considers the eight designs of FDs with different locations, volume, and geometries proposed in Ref. [88], while Ref. [258] considers another far detector design, the LAYCAST. They investigate the potential of different far detector designs for discovering long-lived axion-like particles (ALPs) via the process $e^-e^+ \to \gamma\, a, a \to \gamma\gamma$ at future e^-e^+ colliders running at the CM energy of 91.2 GeV and integrated luminosities of 16, 150, and 750 ab^{-1}. Sensitivities to the model parameters in terms of the effective ALP-photon-photon coupling $C_{\gamma\gamma}/\Lambda$ (Λ is the effective cutoff scale), the effective ALP-photon-Z coupling $C_{\gamma Z}/\Lambda$, and the ALP mass m_a, are presented for three physics scenarios: $C_{\gamma Z} = 0$, $C_{\gamma Z} = C_{\gamma\gamma}$, and both $C_{\gamma Z}$ and $C_{\gamma\gamma}$ are independent parameters. Sensitivity results in terms of 3-signal-event contour curves are presented, corresponding to 95% C.L. limits with vanishing background. Besides, sensitivity results in terms of 20-signal-event contour curves for LAYCAST are also presented, corresponding to 95% C.L. limits with about 100 background events, to estimate the effect of non-zero background. Fig. 52 is from Refs. [258, 259] and two plots compare the performances of the representative far detectors FD1, FD3, FD6, LAYCAST and the CEPC/FCC-ee's main detector (MD). Sensitivity results for the case that $C_{\gamma Z} = C_{\gamma\gamma}$ are also given in these studies.

Ref. [298] explores the discovery potential of FDs for long-lived ALPs at future e^-e^+ colliders, such as the ILC. Three possible setups of FDs are proposed, and could be installed in planned underground cavities around the ILC detector hall or on the ground. The authors consider cuboid for the shape of the FDs. The first type "Shaft (S)" is located in the vertical shaft above the collision point, which will be used to lower the main ILD and SiD detectors into the detector hall. Its position is centered around the coordinate $(x, y, z) = (0, 45, 0)$ m, and the geometry is 18 m $\times$ 30 m $\times$ 18 m. The second type "Tunnel (T)" is located inside the access tunnel that surrounds the detector hall. Its position is centered around the coordinate (0, -5, -35) m, and the geometry is 140 m $\times$ 10 m $\times$ 18 m. The third type "Ground (G)" is a large detector placed on the ground above the detector hall. Its position is centered around the coordinate (0, 75, 0) m, and the geometry is 1000 m $\times$ 10 m $\times$ 1000 m.

This study considers sub-GeV long-lived ALPs produced via $e^-e^+ \to \gamma\, a$ or $e^-e^+ \to \gamma\, Z \to \gamma\, (\gamma a)$ process and decaying into pairs of charged leptons at the ILC with $\sqrt{s} = 250$ GeV. The background is assumed to be negligible, and sensitivity reaches are shown in terms of three-signal-event contour curves. We extract Fig. 53 from Ref. [298], which shows the

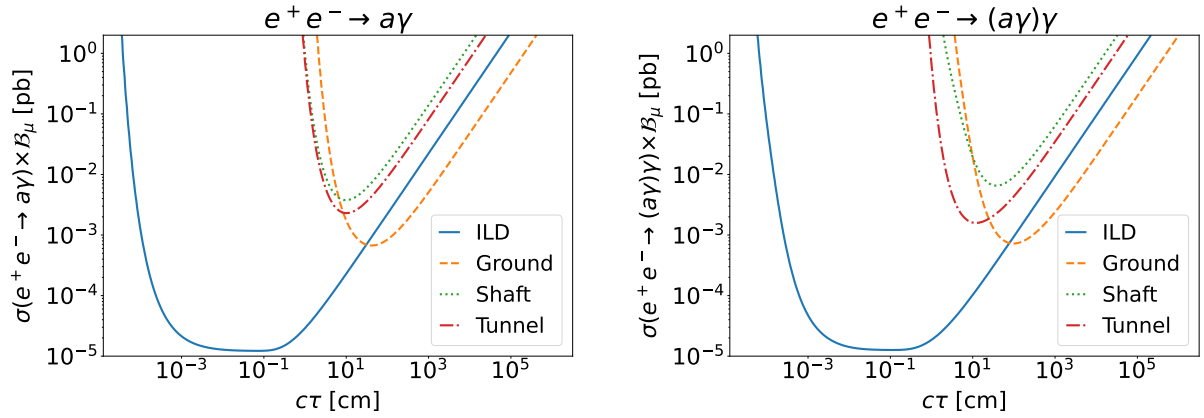

FIG. 53: Contours of $N_a = 3$ ALPs with $m_a = 300$ MeV decaying within various ILC detectors, as a function of the production cross section, σ, and the proper lifetime, $c\tau_a$. Shown are the production channels $e^+e^- \to a\gamma$ (left) and $e^+e^- \to Z\gamma \to (a\gamma)\gamma$ (right) at $\sqrt{s} = 250$ GeV and with $\mathcal{L} = 250$ fb^{-1}. Predictions are made for the ILD (blue, plain) and far detectors placed in the Shaft (green, dotted), in the Tunnel (red, dot-dashed) and on the Ground (orange, dotted). The branching ratio of the ALP into muons is indicated by $\mathcal{B}_\mu$. Taken from Ref. [298].

sensitivity reach of the ILD main detector and the three FD designs to the production cross sections of ALPs with mass $m_a = 300$ MeV. In this study, the results are also compared with searches for long-lived ALPs produced from meson decays at Belle II.

E. Studies with beam dumps

Future e^-e^+ colliders employ high-energy electron and positron beams. The beam dump can result in copious production of LLPs. There exist multiple studies considering a beam-dump experiment to search for LLPs at, e.g. the ILC. It is easily conceivable that similar experimental setups can also be instrumented at other e^-e^+ colliders such as the CEPC, FCC-ee, and CLIC, despite the different beam energies. In particular, Ref. [299] shows Fig. 54 illustrating a sample setup of a beam-dump experiment at the ILC, which consists of four parts: the main beam dump, a muon shield, a decay volume, and a detector. Water is planned as the absorber in the main beam dump of the ILC [300]. The length of water cylinder along the beam axis is $l_{\text{dump}} = 11$ m. Inside the main beam dump, electromagnetic

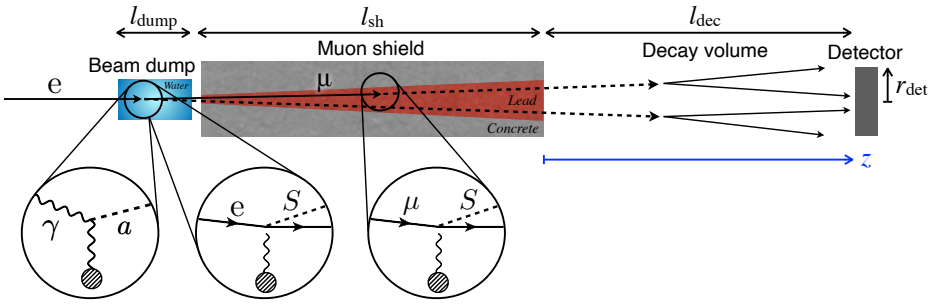

FIG. 54: The setup of the beam-dump experiment at the ILC consists of four parts: the main beam dump, a muon shield, a decay volume, and a detector. The figure depicts LLP signals including ALP (a) emissions via the photon interaction and light scalar particle (S) emissions via the electron and muon interactions. Taken from Ref. [299].

shower produces electrons, positrons, and photons. The muon shield length and the decay volume length are $l_{\rm sh} = 70$ m and $l_{\rm dec} = 50$ m, respectively. The muon shield could consist of the lead shield and the active shield. The shape of the detector is assumed as a cylinder, and its axis should be aligned with the beam axis. The radius of the detector $r_{\rm det}$ is set to be 2 to 3 meters.

Recent LLP studies with beam dump experiments are summarized as follows. Sensitivity results for long-lived heavy neutral leptons are presented in Sec. **??**.

1. ALPs and new scalar particles

The authors of Ref. [299] investigate the sensitivities of a beam-dump experiment at the ILC to a long-lived ALP and a light scalar particle coupled to charged leptons. In their analysis, the lengths of the beam dump region $l_{\rm dump}$, the muon shield $l_{\rm sh}$, and the decay volume $l_{\rm dec}$ are set to be 11 m, 70 m and 50 m, respectively. The radius of the detector $r_{\rm det}$ is set to 2 m and the detection efficiency is assumed to be 100%. The authors consider the case of ILC-250 GeV with the beam energy $E_{\rm beam} = 125$ GeV. The number of incident electrons into the beam dump is assumed to be $N_{\rm EOT} = 4 \times 10^{21}$ per year.

The signal production process is illustrated in Fig. 54. The ALPs are emitted by the photons in the beam dump, pass through the muon shield, and decay in the decay volume into photon pairs, which reach the detector at the end recording a signal event. New scalar

particles are emitted via electron interactions with the oxygen nuclei in the beam dump and via muon interaction with the lead nuclei in the muon shield. The generated scalar particle decays into photons, electron-positron, and muon pair in the decay volume, which reach the detector and are observed as signal events.

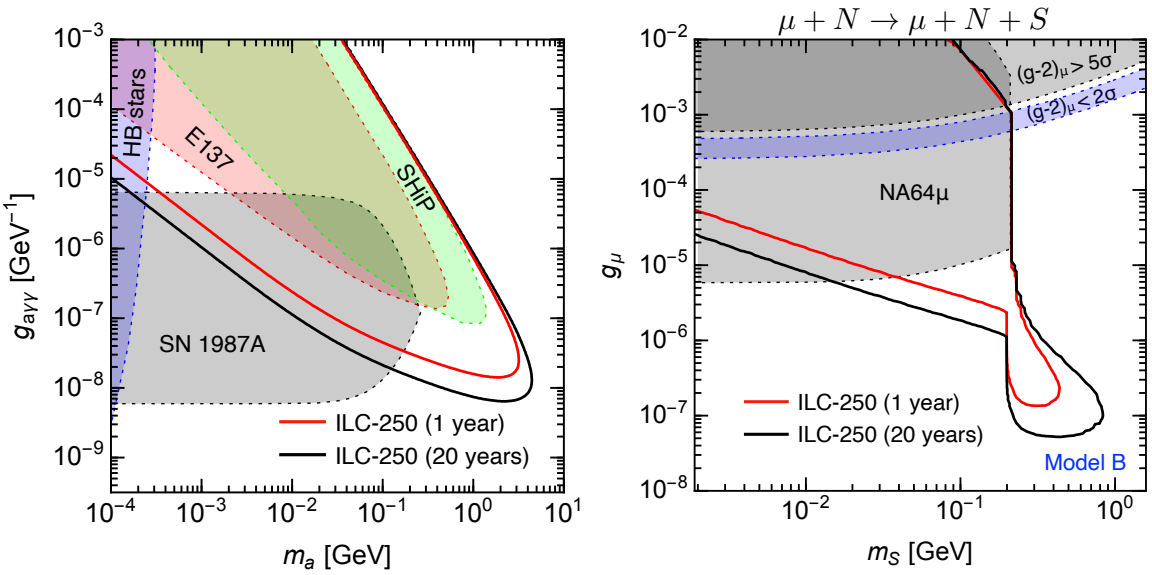

FIG. 55: Both plots are extracted from Ref. [299] and show discovery sensitivities of the beam-dump experiment at the ILC to the ALPs and new scalar particles. Left: sensitivities in the ALP-photon-photon coupling $g_{a\gamma\gamma}$ vs. ALP mass m_a plane, where red and black curves correspond to the bounds of sensitivity for ILC-250 GeV at 95% C.L. with 1- and 20-year statistics; the shaded regions are constraints for E137 from Ref. [301], SN 1987A from Ref. [301, 302], HB stars from Ref. [303], and SHiP from Ref. [301, 304, 305]. Right: sensitivities in the g_μ vs. m_S plane for Model B (S couples to muons only, i.e. $g_\mu \neq 0,\ g_e = g_\tau = 0$), where the signal process contains a muon in the initial state (i.e. $\mu + N \to \mu + N + S$); the gray shaded regions are constraints from NA64μ and muon $g-2$ from Ref. [306]; note that, although the results for $m_S > 2m_\mu$ are absent for NA64μ, it would also have a sensitivity in that region generally.

Background events are assumed to be removed with veto counters located behind the shield and in front of and around the detector. Fig 55 is extracted from Ref. [299]. The left plot shows discovery sensitivities of the beam-dump experiment at the ILC to the ALPs coupling to photons, where the red and black curves correspond to ILC-250 GeV at 95%

C.L. with 1- and 20- year statistics, respectively. The right panel is for the sensitivity reach muon-coupled light scalar particle.

2. *New neutral gauge bosons*

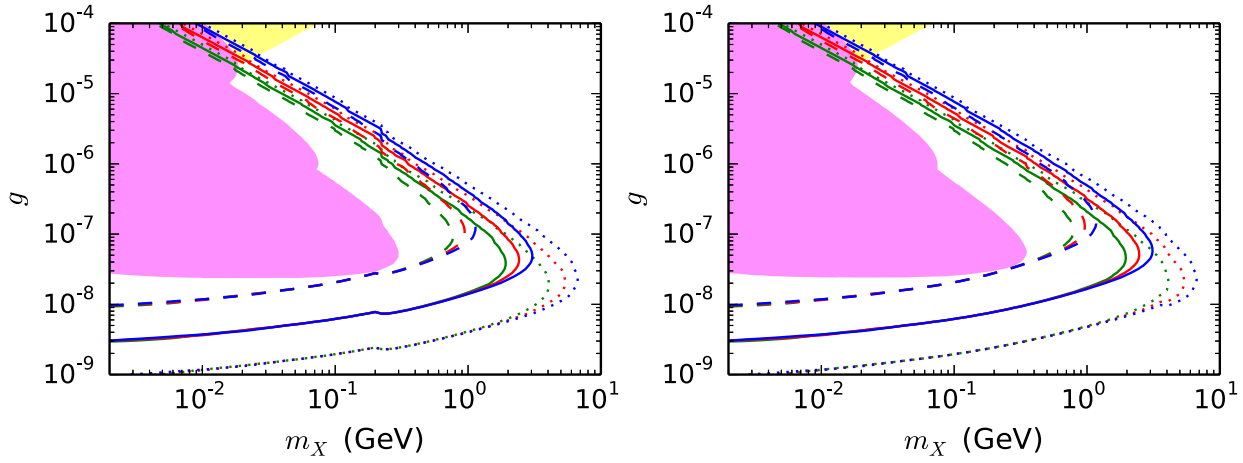

FIG. 56: Left: contours of expected number of signal events for the $U(1)_{e-\mu}$ model; the beam energy is taken to be $E_{\rm beam} = 125$ (green), 250 (red), and 500 GeV (blue); the dotted, solid, and dashed lines are for $N_{\rm sig} = 10^{-2}$, 1, and 10^2, respectively, taking $N_e = 4 \times 10^{21}$; the mixing parameter is taken to be $\kappa_\epsilon = 1$; the pink and yellow shaded regions are excluded by beam-dump and neutrino-electron scattering experiments, respectively. Right: same as the left plot, but for the $U(1)_{e-\tau}$ model. Taken from Ref. [307].

Ref. [307] studies the prospects of searching for light and long-lived leptophilic gauge bosons (LGBs) in the beam-dump experiment using $e^\mp$ beams at the ILC. The experimental setup is similar to that shown in Fig. 54. The authors consider LGBs coupled to leptons e, μ, τ with charges Q_e, Q_μ, Q_τ, respectively. Three cases of $(Q_e, Q_\mu, Q_\tau) =$ (1, -1, 0), (1, 0, -1), or (0, 1, -1) are taken into account, corresponding to U(1)$_{e-\mu}$, U(1)$_{e-\tau}$, and U(1)$_{\mu-\tau}$ models, respectively. With one-year operation, about 4×10^{21} electrons and positrons are injected into the dump. With the injection of the electron (or position) beam into the dump, the LGB (denoted as X) can be produced by the scattering process $e^\pm N \to e^\pm N' X$ (with N and N' being nuclei). SM background is assumed to be negligible.

We extract Fig. 56 from Ref. [307] which shows the expected number of signal events $N_{\rm sig}$ for the cases of U(1)$_{e-\mu}$ and U(1)$_{e-\tau}$ models in the g vs. m_X plane, where g and m_X denote

the X coupling to the charged leptons and the mass of X, respectively. The dotted, solid, and dashed lines correspond to $N_{\rm sig} = 10^{-2}$, 1 and 10^2, respectively, for the beam energy taken to be $E_{\rm beam} = 125$ (green), 250 (red), and 500 GeV (blue). Results for the $U(1)_{\mu-\tau}$ case are also given in Ref. [307].

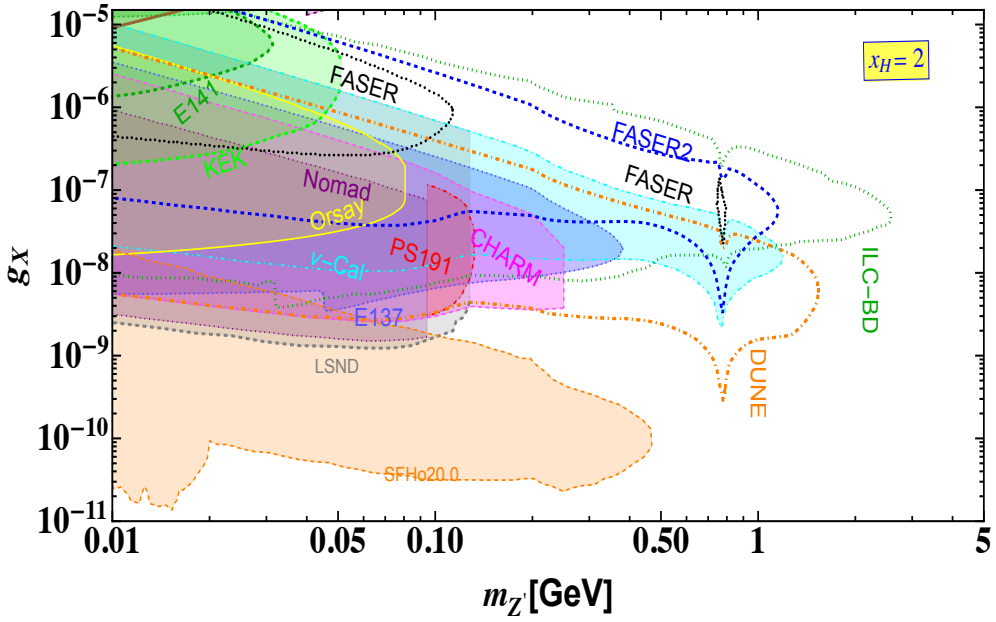

FIG. 57: Limits in the $m_{Z'} - g_X$ plane for $x_H > 0$ and $x_\Phi = 1$ considering 10 MeV $\leq m_{Z'} \leq 5$ GeV, showing the regions that could be probed by FASER, FASER2, ILC-Beam dump, and DUNE. The parameter space is compared with existing bounds from different beam-dump experiments and a cosmological observation of supernova SN1987A (SFH020.0), respectively. Taken from Ref. [308].

Ref. [308] obtains bounds and sensitivities on the chiral Z' gauge boson in the electron-positron beam-dump experiment at the ILC, in the proton beam-dump experiment of DUNE, and the experiments of FASER(2). It assumes 10-year running for the calculations of the future beam-dump experiments, and 150 fb^{-1} (3 ab^{-1}) for LHC Run 3 (high-luminosity LHC). The Z' particle, being lighter than 5 GeV, is considered to be produced in rare meson decay and bremsstrahlung processes for all kinds of beam-dump experiments and additionally pair annihilation process for electron and positron beam-dump experiments. Sensitivities in the parameter space projected for FASER, FASER2, DUNE, and ILC beam dumps are obtained and compared with the existing bounds from Orsay, Nomad, PS191,

KEK, LSND, CHARM, and SN1987A. Fig. 57 is taken from Ref. [308], showing the limits in the $m_{Z'} - g_X$ plane for the case with $x_H = 2$ and $x_\Phi = 1$, where x_H and x_Φ are $U(1)_X$ charge parameters and g_X is the $U(1)_X$ coupling. Further results with different x_H values of 1 and 0.5 are also provided in Ref. [308].

F. Summary and Discussion

The LHC has entered the Run 3 phase, and is slated to continue operation until around 2035. Since decades ago intensive discussion has been going on concerning high-energy lepton colliders to be running during the post-LHC era. Electron-positron colliders operated at selected CM energies can produce large numbers of Z-, Higgs, W-bosons, and heavier particles in a relatively clean environment (with little QCD background), allowing for precision measurements on the properties of these particles including their interactions with other particles. This is especially important for the SM Higgs boson after its discovery at the LHC in 2012, which is naturally a good candidate for connecting new physics with the SM. Beyond precision measurements, these future experiments can also probe BSM physics in terms of light new physics, by searching for light, exotic states. In particular, light new physics is predicted in many BSM theories to manifest itself as LLPs leading to striking collider signatures different from the conventional ones. Such LLPs have a relatively long lifetime for various reasons including feeble couplings to other particles and suppressed phase space, and have been proposed for solving multiple issues present in the SM such as the non-vanishing neutrino masses and the dark matter.

Compared to hadron colliders such as the LHC, e^-e^+ colliders have unique characteristics; higher luminosity is expected, the collider environment is cleaner, the trigger requirement is typically looser, the absence of parton distribution in the electrons fixes the parton-level collision energy, etc. These features are appealing for collider searches for BSM physics especially LLPs. Indeed, various phenomenological analyses have been performed for LLP searches at future e^-e^+ colliders, and thus, as these experiments are currently in the stage of designing and planning, we find it timely to summarize the current status of these phenomenological studies and provide an outlook. In Figure **??**, we show the sensitivity reach for the Higgs decay to a pair of long-lived particle X with subsequent decay $X \to \bar{b}b, \bar{\nu}\nu$ and a pair of long-lived dark photon γ_D with subsequent decay $\gamma_D \to \bar{q}q, \bar{\ell}\ell$ for CEPC and

HL-LHC projections [62, 309], where CEPC is about two orders of magnitude better than HL-LHC.

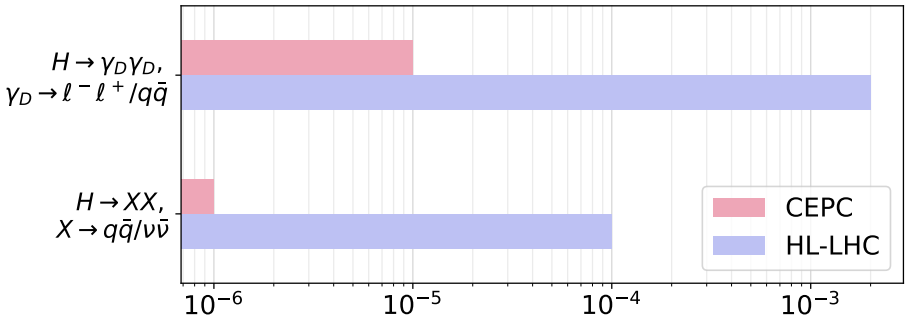

FIG. 58: The sensitivity reach for the Higgs decay to a pair of long-lived particle X with subsequent decay $X \to \bar{b}b, \bar{\nu}\nu$ and a pair of long-lived dark photon γ_D with subsequent decay $\gamma_D \to \bar{q}q, \bar{\ell}\ell$ for CEPC and HL-LHC projections.

We start with a detailed explanation of the typical computation procedure for the number of LLP signal events inside the fiducial volume of a detector. This approach has been widely applied in the literature. We then have reviewed the existing LLP phenomenological studies at future e^-e^+ colliders according to the associated detector type separately. Mainly three types of experimental setups have been under discussion for LLP searches at future electron-positron colliders, namely main detector, far detector, and beam-dump experiment. The main detector (near detector, abbreviated as ND) refers to the default local detector enclosing the IP, the far detector is an external, auxiliary detector with a macroscopic distance from the IP, and the beam-dump experiment puts a detector tens of meters behind the beam dump. For the MD experiments, we have reviewed existing works considering mainly LLPs from rare Higgs and Z-bosons' decays, including new light scalar particles, dark photons, lightest neutralino in the RPV-SUSY, and ALPs. HNLs have also been studied, produced either via direct collision or rare Z-boson decays. Further studies include a long-lived stau in the SUSY, and a vector-like lepton with a long-lived accompanying scalar. Then, FDs with various geometrical configurations have been investigated for their sensitivity reach to a new scalar particle mixed with the SM Higgs boson, HNLs or light neutralinos in the RPV-SUSY from Z-boson decays, as well as ALPs coupled to the SM photon or the Z-boson. In general, we expect a modest improvement on the sensitivity

reaches compared to the case with the default MD only. Finally, a beam-dump experiment has been proposed mainly for electron-positron colliders with a CM energy between 250 GeV and 3 TeV. Various theoretical scenarios including the HNLs, ALPs, new scalar particles, and new neutral gauge bosons have been extensively studied, showing excellent sensitivity reach compared to other existing or proposed experiments.

The MD usually has the best acceptance rates for the LLP signal events; however, its sensitivity reach often still suffers from certain background sources to various extent despite the relatively clean environment. The proposed FDs, have a lower acceptance rate, because they usually cannot have an almost 4π solid-angle coverage; however, with a large distance between the FD and the IP, shielding such as lead and concrete can be instrumented in the space in between, effectively removing the background events. For the FDs, in general we observe sensitivity reach to certain parts of the models' parameter space mildly beyond the region that could be probed by the MD. The beam-dump experiments, set up at e.g. the ILC, have been shown to be able to probe large parts of the parameter space where the other existing and proposed experiments are insensitive.

Before ending this section, we briefly discuss the requirements for program tools, civil engineering and detector technology to promote the LLP studies at high-energy electron-positron colliders.

Requirements for the program tools: performing such phenomenological studies often requires MC simulation. Currently the tools publicly available and specifically for computing LLP signal-event rates, such as `FORESEE` [310], `DDC` [311], and `SensCalc` [312], do not include detector-level effects such as smearing and detector efficiencies. In order to perform realistic estimates for LLP sensitivity reach with fast-simulation tools, these effects should be included within a sophisticated framework.

Requirements for the civil engineering: the FD and beam dump experiments require large spaces for installing the experimental facilities. Depending on the available space, the FD can be placed in a cavern inside or in the vicinity of the experimental hall, in the transverse direction with respect to the IP. It is important that designing and planning of such experiments should already proceed before the construction of the main experiment starts. The same conclusion applies for beam-dump experiment proposals, too.

Requirements for the detector technology: The detector technologies need also further development. For reconstructing a displaced vertex, the trackers should be equipped with

better tracking resolution, and the relevant analysis algorithms should be further developed as well. In order for the FDs to have good sensitivities, a large solid-angle coverage is required; given the macroscopic distance to the IP, the FD should have a large volume. If displaced signatures arise pointing to new physics, it would be important to determine the properties of the observed LLP such as its mass and to identify the LLP decay products. For these purposes, installing magnetic fields and implementing PID (Particle IDentification) strategies and methods such as ionization measurement and Cherenkov imaging would be helpful. Moreover, if timing detectors with a timing resolution in the picosecond regime can be installed, multiple purposes can be fulfilled, such as providing timing information for the LLPs, realizing event correlation between the MD and FD, and removing potential background events from the cosmic rays. See, for example, Refs. [284, 292, 296] for similar discussion on precision timing at the LHC FDs. We further emphasize the importance of shielding that should be instrumented for FDs and the beam-dump experiments; it can consist of concrete, lead, metal, or magnetic field, and sufficiently remove background events. Finally, the associated cost should be contained to an acceptable level.

In this section, we clearly observe the mutual complementarity between the various experimental setups at future high-energy e^-e^+ colliders, for LLP searches. In the future, beyond the usual cut-based studies, machine-learning techniques can also be applied to further improve the discovery potential of these experiments; see, e.g. Ref. [82] for a relevant discussion. Moreover, additional collider experiments with other beam-type setups, can be considered for LLP searches as well, including $\mu^+\mu^-$ [313–317], electron-muon [318, 319], electron-proton [252, 253, 320–322], and muon-proton [323–325] collisions. We expect them to be sensitive to parameter space inaccessible by hadron or e^-e^+ colliders.

VII. SUPERSYMMETRY (TIANJUN, LEI, XUAI, DA)

A. Introduction

Supersymmetry (SUSY) provides an intriguing candidate to solve the gauge hierarchy problem in the Standard Model (SM). The Supersymmetric SMs (SSMs) have many appealing features, including gauge coupling unification, and dynamical electroweak symmetry breaking. In addition, the Lightest Supersymmetric Particle (LSP) such as neutralino

can serve as a viable dark matter (DM) candidate with R-parity conservation. The SUSY searches at the LHC have already set strong constraints on the SSMs [326–329]. The CEPC will run at much lower energies. At the same time, it can be complementary in covering parameter spaces that are difficult for the LHC to reach. This is particularly important for the search for some of the uncolored new physics particles [330–345]. In addition, the precision measurements at the CEPC can probe SUSY even without direct production of the new particles [215, 346–350].

In this section, we will focus the recent studies of the reaches of the CEPC on several scenarios with light electroweakino and sleptons. These scenarios can have various physics motivations (for some examples, see Refs. [330, 351–354]). For both electroweakino and slepton searches, the discovery potential can reach up to the kinematic limit of the detector $\sqrt{s}/2$, and cover interesting parameter regions. It is shown that CEPC can have its role to play in the searches for SUSY. The examples shown here have a minor dependence on the reconstruction model and detector geometry. Moreover, these results can be considered as a reference and benchmark for similar searches at other proposed electron-positron colliders, such as the Future Circular Collider ee (FCC-ee) or the International Linear Collider (ILC), given the similar nature of the facilities, detectors, center-of-mass energies, and target luminosities. Recently prospective studies on electroweakino in the Physics Briefing Book submitted as input for the European Strategy for Particle Physics Update 2020 [355] are also presented. The dark-matter relevant SUSY searches are discussed in Sec. V. A list of long-lived SUSY searches are discussed in Sec. VI.

B. Light electroweakino searches

The light Higgsino particles, well-motivated by naturalness conditions, tend to have small mass splitting among the chargino and neutralino [330]. Therefore, they are quite challenge to be probed in the LHC experiments due to the very soft decay products. The sensitivity studies for chargino pair production by considering scenarios for both a Bino-like and a Higgsino-like neutralino as the LSP have been performed and published at [356]. With a cleaner collision environment and better low-energy particle reconstruction, the CEPC has shown the capability of probing the very compressed region, as shown in Fig. 59.

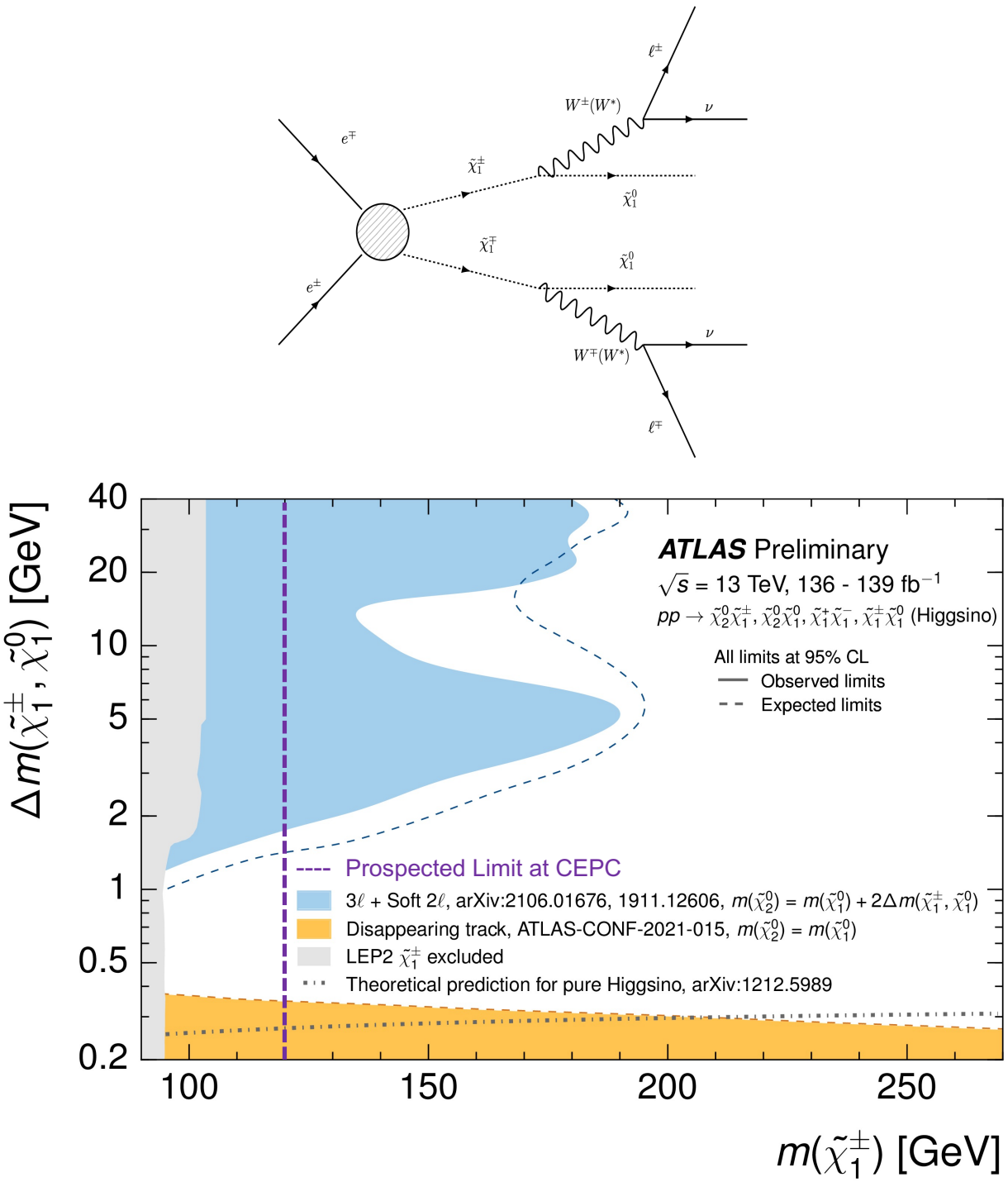

FIG. 59: *Top*: Representative diagram illustrating the pair production of charginos and subsequent decay into a two-lepton final state via W bosons. *Bottom*: The observed and expected exclusion limits on simplified SUSY models for chargino-pair production with Higgsino-like LSP obtained by the ATLAS. The observed limits obtained by the LEP are shown in light grey. The prospected limits at the CEPC are also shown in the dotted purple line for rough comparison.

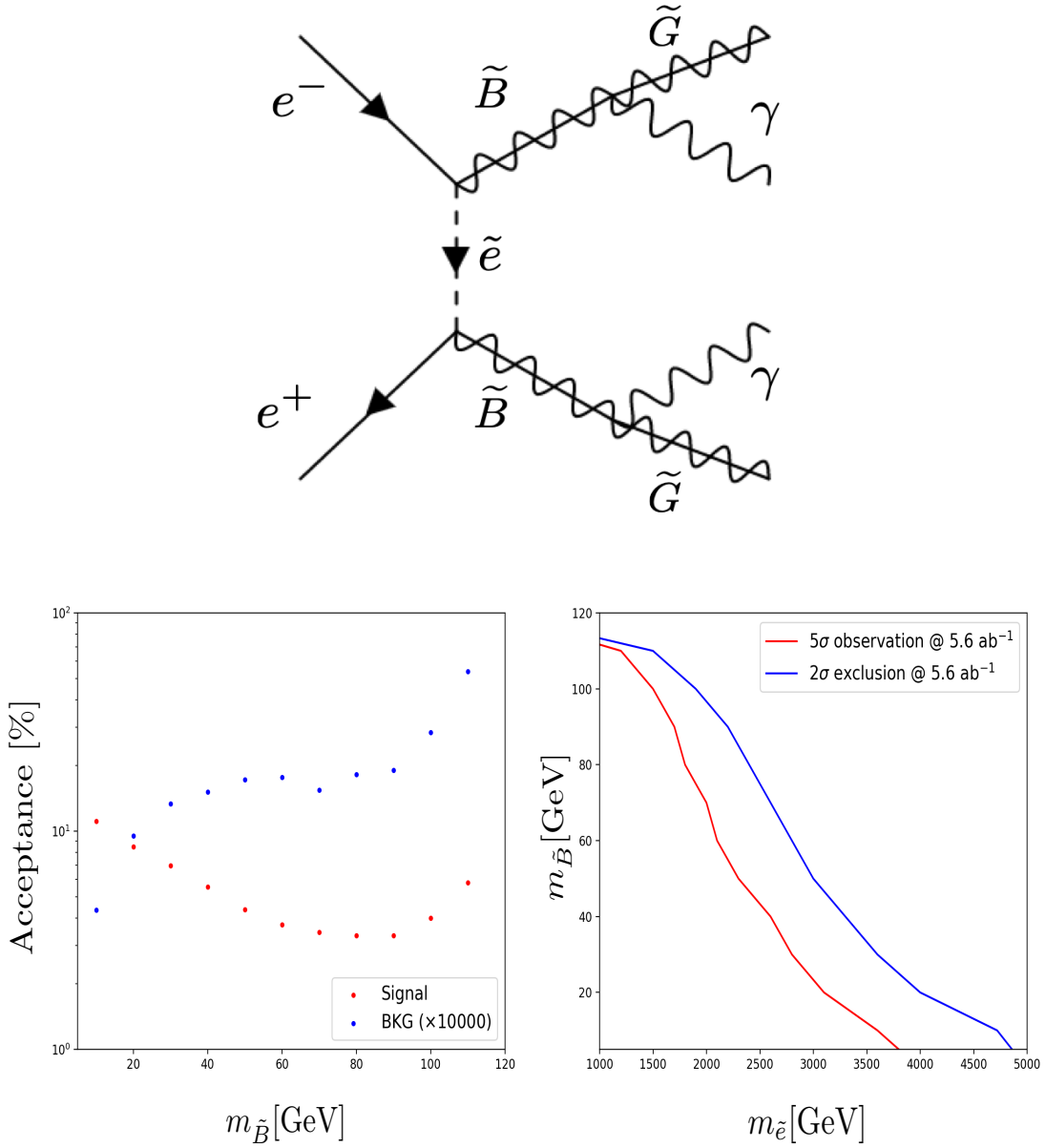

FIG. 60: *Top*: representative diagram illustrating light bino production. *Bottom left*: acceptance of signal and background processes as functions of $m_{\tilde{B}}$. Here the acceptance of the background process has been multiplied by 10,000. *Bottom right*: 2σ exclusion and 5σ observation limits on the $m_{\tilde{e}} - m_{\tilde{B}}$ plane at a future lepton collider running with an integral luminosity 5.6 ab^{-1} and center-of-mass energy 240 GeV. Regions below the red (blue) curves are observable (excluded).

Light bino ($\tilde{B}$, $\mathcal{O}(10)$ GeV scale) scenario is motivated by Gauge-Mediated SUSY Breaking [357]. Such search has been performed [358] at the CEPC, where bino is the next-to-lightest supersymmetric particle (NLSP), while the lightest supersymmetric particle (LSP)

and dark matter candidate is the sub-GeV gravitino ($\tilde{G}$). The process of bino pair production via a t-channel selectron ($\tilde{e}$), where bino subsequently decays to gravitino and a photon, has been considered, namely $e^+e^- \to \tilde{B}\tilde{B} \to \gamma\gamma\tilde{G}\tilde{G}$. The corresponding dominant background process is $e^+e^- \to \gamma\gamma\nu\bar{\nu}$ (via Z boson invisible decay), which has been suppressed by a dedicated cut-flow using a list of kinematic variables with good signal and background separation power. The study shows that the CEPC can exclude selectron lighter than 4.5 TeV (2 TeV) with bino mass around 10 GeV (100 GeV), as shown in Fig. 60. This is much larger than the current LHC bound which excludes selectron mass only up to several hundred GeV.

C. Light slepton searches

Light smuon and stau particles are interesting to search for in their own right, and they are also favored by the latest muon g-2 excess. At the same time, it is challenging to search for them at the LHC, especially in the region where their masses are close to that of the LSP. In addition, such regions are favored by dark matter relic density requirements, and have been explored with the CEPC detector [359]. Assuming a flat 5% systematic uncertainty, the discovery sensitivity can reach up to 119 (118) GeV for smuon (stau) mass via direct smuon (stau) production, as shown in Fig. 61 (left). The above results can fill a significant region in the gap in the LHC search.

The center-of-mass energy of the CEPC could be upgraded to 360 GeV after its ten-year running at 240 GeV as a Higgs factory which can provide more opportunities for new physics searches besides the SM precision measurements. A dedicated sensitivity study is performed on the direct stau and smuon pair production at the CEPC with $\sqrt{s} = 360$ GeV. With 1.0 ab^{-1} integrated luminosity and the assumption of flat 5% systematic uncertainty, the CEPC at 360 GeV has the potential to discover the production of combined left-handed and right-handed stau up to 168.5 GeV if exists; the discovery potential of direct smuon reaches up to 175 GeV with the same assumption, as shown in Fig. 61 (right). This result also gives a strong motivation to raise the center-of-mass energy of CEPC from 240 GeV to 360 GeV.

Somewhat heavier selectrons, above the kinematic limit for direct production, can also be searched for in the process [360]: $e_R^+e_R^- \to \tilde{\chi}_1^0(\text{bino}) + \tilde{\chi}_1^0(\text{bino}) + \gamma$, as shown in Fig. 62. The

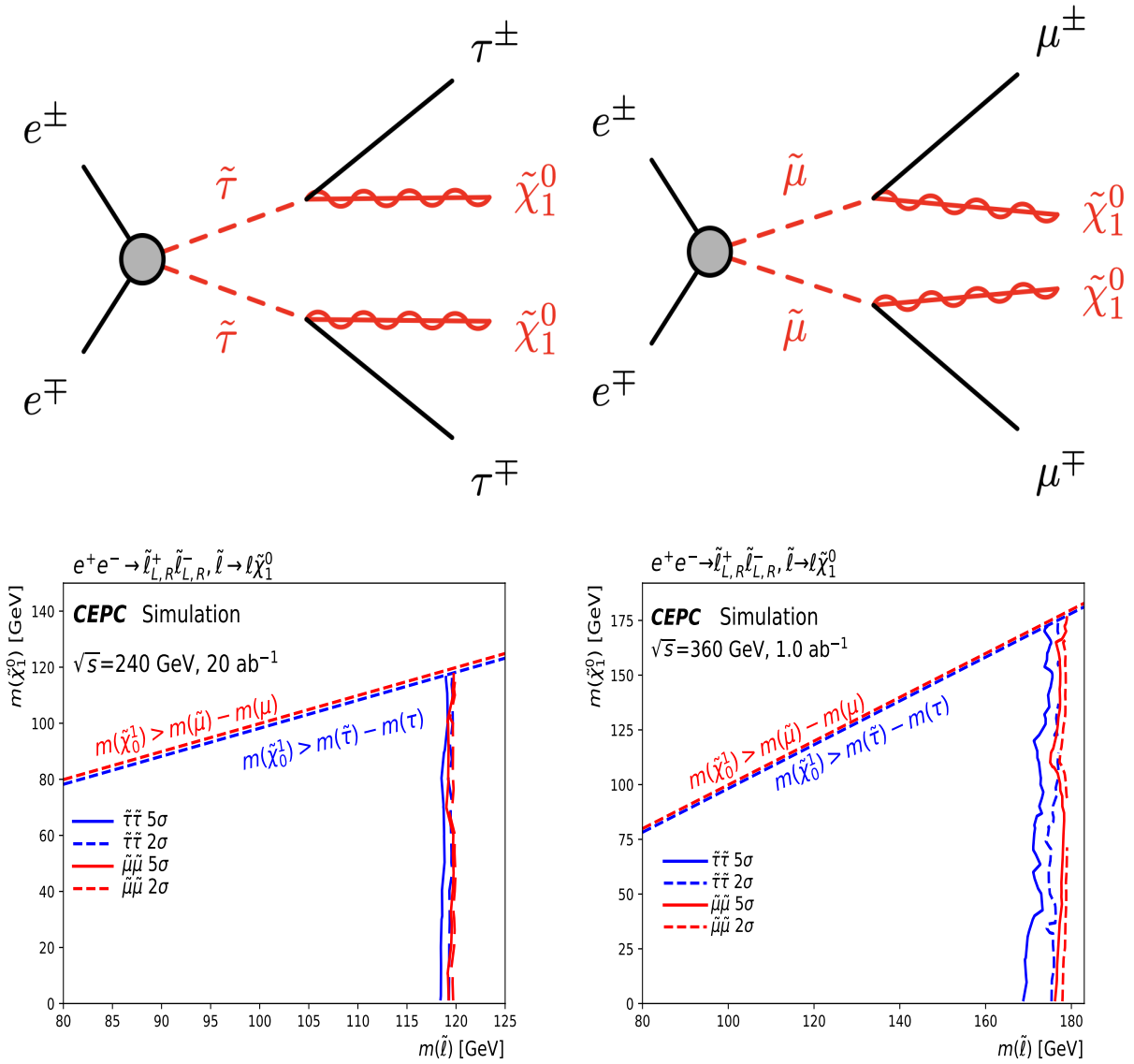

FIG. 61: *Top*: representative diagram illustrating the pair production of charged staus (smuons) and subsequent decay into a two-tau (two-muon) final state. *Bottom*: The 5σ discovery contour (solid line) and 2σ exclusion contour (dashed line) for the direct stau production and direct smuon production with 5% flat systematic uncertainty. Left (Right) plot presents the center-of-mass energy of 240 (360) GeV.

reach depends on the model assumptions. For example, if the relic abundance requirement is satisfied by the LSP annihilating through the Z-pole, the right-handed selectron can be excluded up to 180 (210) GeV respectively at 3(2)σ. On the other hand, if the annihilation through the Higgs pole dominates, right-handed selectron will be excluded up to 140 (180)

GeV at $3(2)\sigma$.

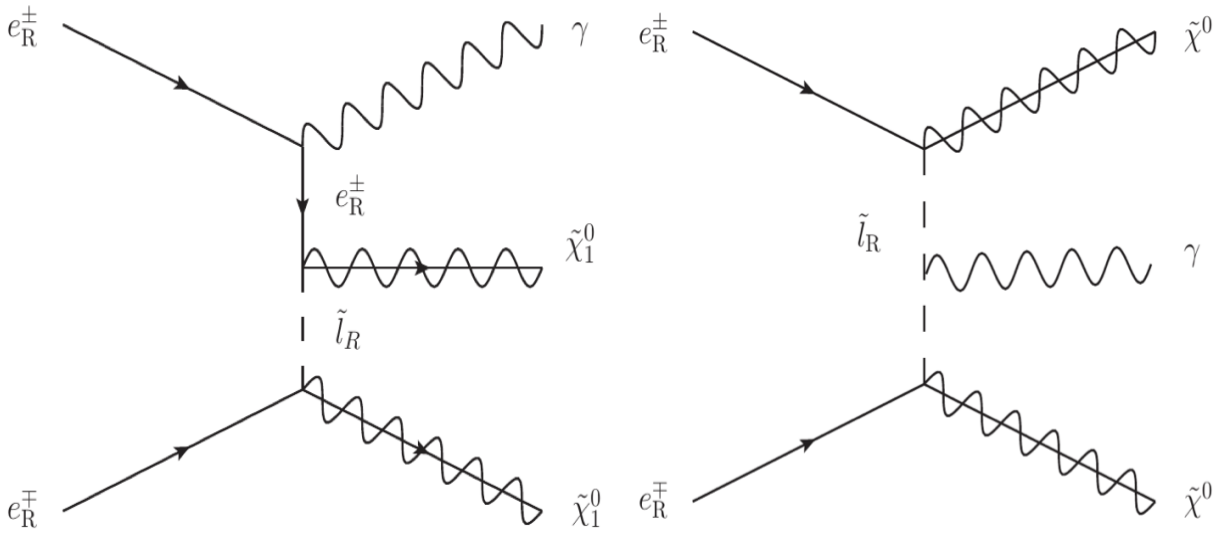

FIG. 62: Representative diagram illustrating heavier selectron production.

Another in-depth exploration is performed in the off-shell sparticle pair production at the CEPC [361]. Assuming a flat 5% systematic uncertainty, the detection (discovery) sensitivity can reach up to 126 GeV (122 GeV) for the smuon mass, shown in Fig. 63. It demonstrates that the combination of the lepton collider advantages and its high-precision detectors can break through the limits of the on-shell kinematic limit of $\sqrt{s}/2$ and enter the off-shell region in detecting new physical processes.

A recent paper [362] considers $\mathcal{F}$-$SU(5)$, *i.e.*, the flipped $SU(5)\times U(1)_X$ GUT model [363] with extra TeV-scale vector-like particles [364] that have been constructed systematically in local F-theory model building [365, 366]. Alternatively, these models can also be realized in free fermionic string constructions [367]. Super-Natural SUSY via No-Scale SUGRA is a natural resolution to the SUSY EWFT problem, but cannot realize the specific scenario with a light Bino LSP due to a correlation of the Bino mass with the Wino and gluino masses. Therefore, the Generalized No-Scale SUGRA is proposed, where Effective Super-Natural SUSY can be realized. To uncover the bulk region for dark matter, only light right-handed sleptons can be considered given that the LHC SUSY searches indicate that all other sfermions must be heavy. First, a determination must be carried out as to whether an interaction between sfermions and the LSP is coannihilation or annihilation. Rendering a judgment involves inspecting the mass difference between the light right-handed sfermions

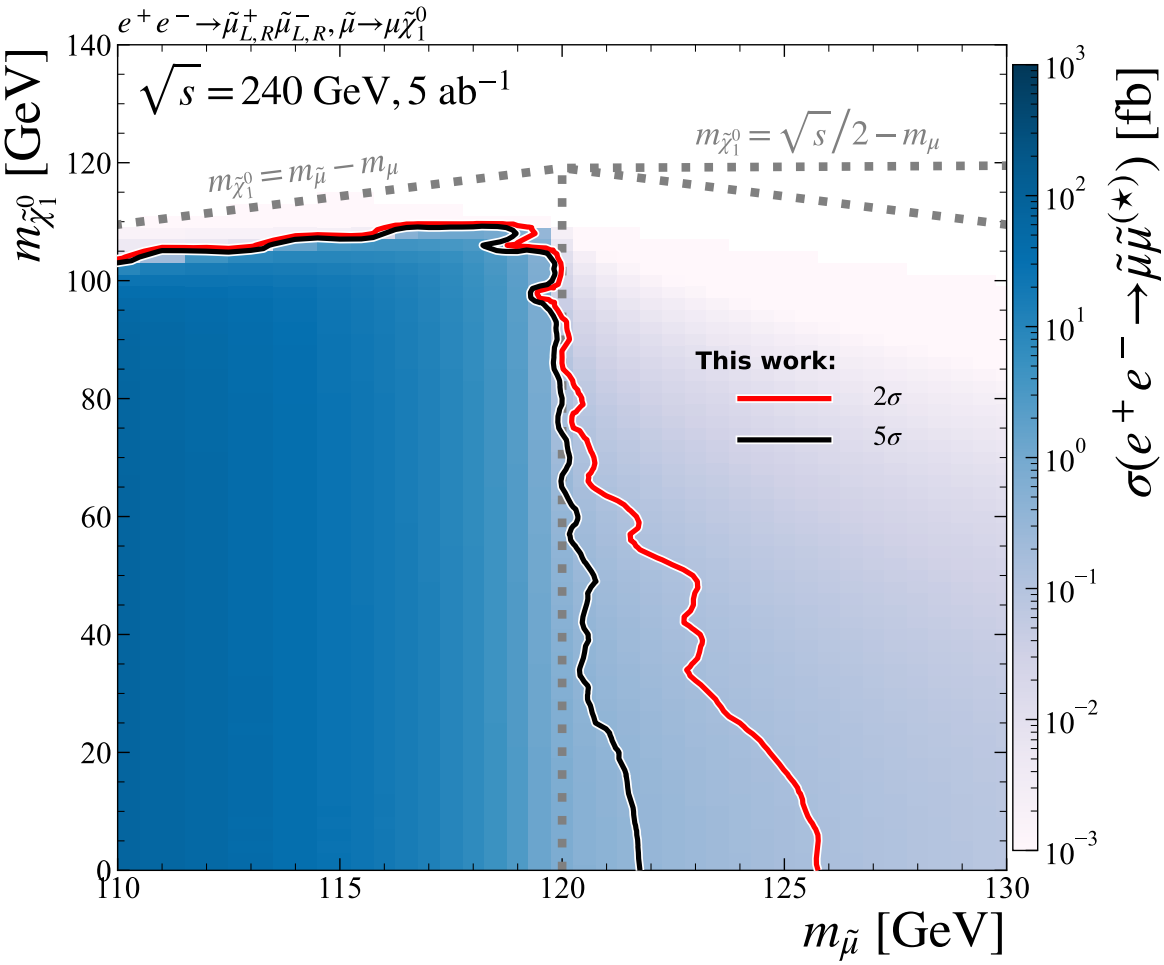

FIG. 63: The prospected exclusion contour and discovery contour at CEPC for the direct smuon production with 5% flat systematic uncertainty.

and LSP, though the ratio of the mass difference $\mathcal{R}_\phi \equiv (m_\phi - m_{\tilde{\chi}^0_1})/m_{\tilde{\chi}^0_1}$ is more important than the absolute mass difference, where ϕ is $\tilde{\tau}_1$ (light stau) or $\tilde{e}_R$ (light selectron). Comprehensive numerical studies in this work show that $\mathcal{R}_\phi \gtrsim 10\%$ is a conservative criterion to formulate the bulk region, *i.e.*, the observed dark matter density is obtained via traditional annihilations, not from coannihilations or resonances, etc. The bulk region in Generalized No-Scale $\mathcal{F}$-$SU(5)$ is illustrated in the left plot of FIG. 64, where $\mathcal{R}_{\tilde{\tau}_1}$ plots as a function of the Bino-like neutralino $m_{\tilde{\chi}^0_1}$. The mass hierarchy in $\mathcal{F}$-$SU(5)$ is $m_{\tilde{\chi}^0_1} < m_{\tilde{\tau}_1} < m_{\tilde{e}_R} = m_{\tilde{\mu}_R}$, hence, $\mathcal{R}_{\tilde{e}_R}$ always exceeds $\mathcal{R}_{\tilde{\tau}_1}$. All points in this plot satisfy all the current experimental constraints. If the Bino contributes all the DM abundance, the ratio $\mathcal{R}_{\tilde{\tau}_1} \gtrsim 10\%$ implies $m_{\tilde{\chi}^0_1} \leq 103.0$ GeV. We present the light right-handed slepton masses in this bulk region in the

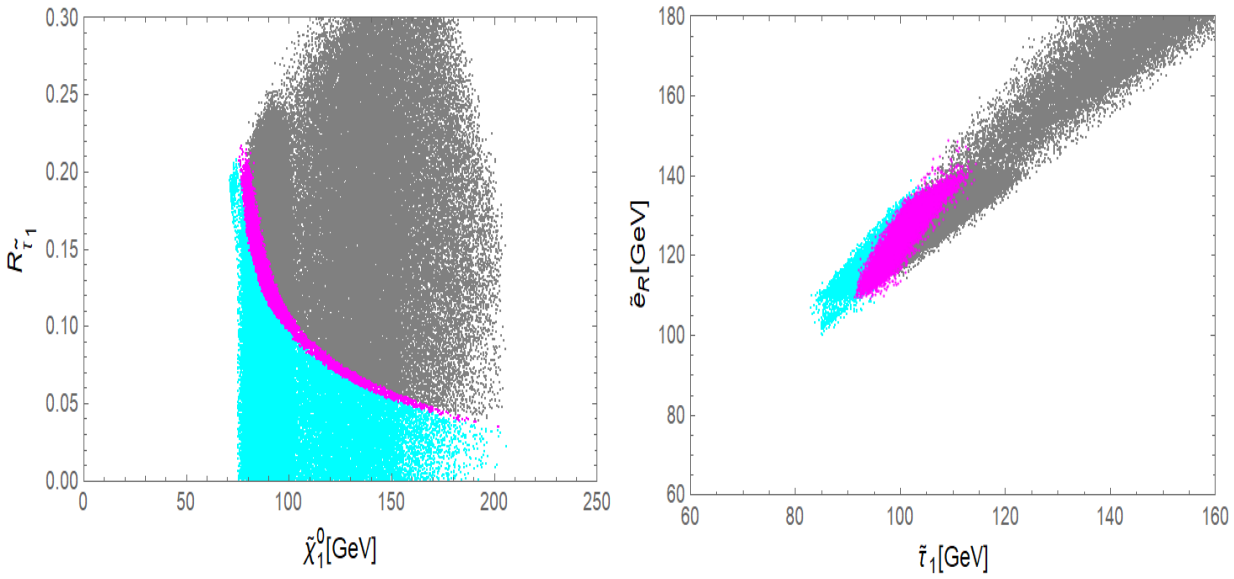

FIG. 64: Left: Bulk region in Generalized No-Scale $\mathcal{F}$-$SU(5)$. Right: Light right-handed slepton masses in this bulk region. Cyan, magenta, and gray points correspond to under-saturated, saturated, and over-saturated DM relic density.

right plot of FIG. 64. It shows the upper limits on the $\tilde{\tau}_1$ and $\tilde{e}_R$ masses are around 115 GeV and 150 GeV, respectively. Recognize that these right-handed sleptons and Bino LSP are *naturally* light, thus, the LSP has not been fine-tuned to fortuitously conform to the Planck satellite 5σ relic density observations. These light sleptons could conceivably be observed at the Future Circular Collider (FCC-ee) [4, 252] at CERN and the Circular Electron-Positron Collider (CEPC) [11] with its sensitivity specified in Ref. [368]. In addition, FIG. 65 shows the compelling expected sensitivity of the 1000-day LUX-ZEPLIN experiment [369], the constraints from the XENONnT [370] and LUX-ZEPLIN [369, 371] experiments, and broad coverage of the No-Scale $\mathcal{F}$-$SU(5)$ bulk region. Thus, the light Bino LSP of such bulk region could be fully probed within the next few years. Likewise, the proton lifetime via dimension-six proton decay is near $3 - 4 \times 10^{34}$ years, so this "fast" dimension-six proton decay is within reach of the future Hyper-Kamiokande experiment [372]. Furthermore, it is investigated outside the tight $\mathcal{F}$-$SU(5)$ constraints by evaluating the phenomenological Minimal Supersymmetric Standard Model (pMSSM).

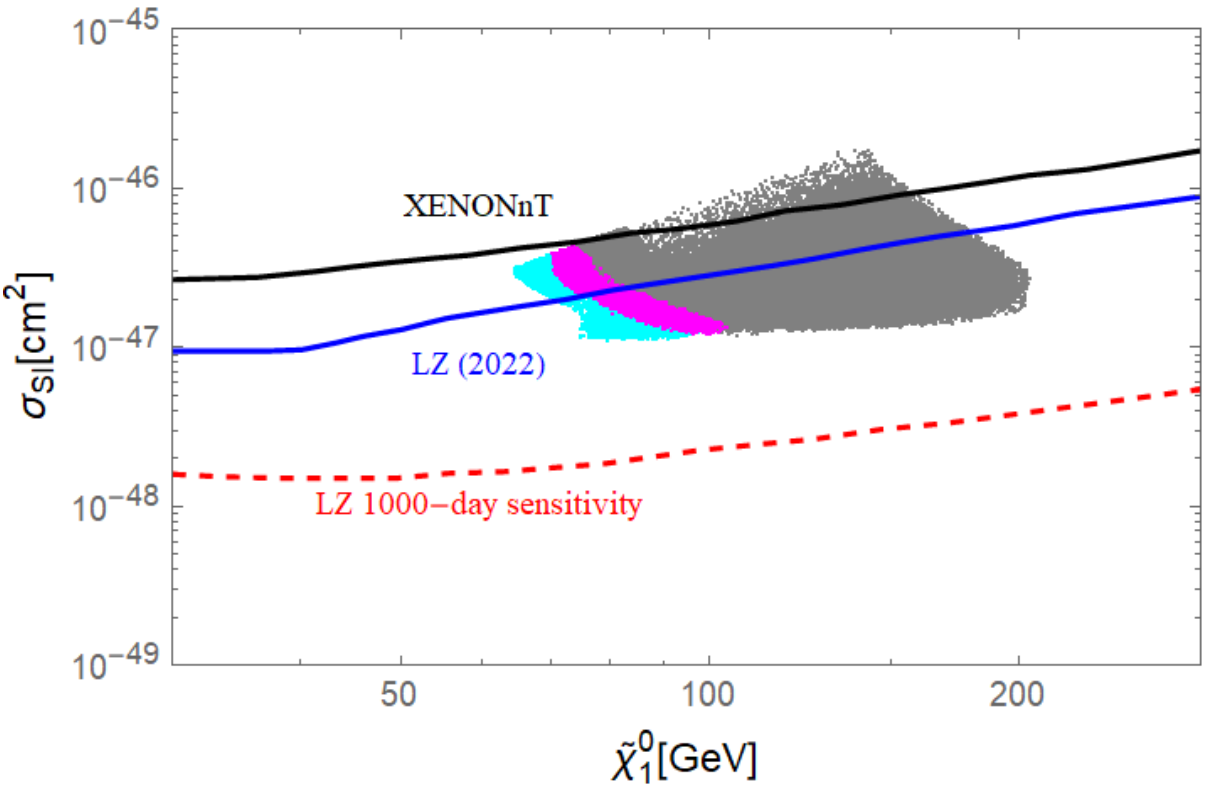

FIG. 65: The spin-independent DM-nuclei cross sections vs the LSP mass in the Generalized No-Scale $\mathcal{F}$-$SU(5)$ bulk region. We present the constraints from the XENONnT [370] and LUX-ZEPLIN [369, 371] experiments. We underscore the significance of the 1000-day LUX-ZEPLIN run that should fully probe the $\mathcal{F}$-$SU(5)$ bulk and about 50% of the pMSSM bulk (not shown here). The color code is the same as in FIG. 64.

D. Input from the European Strategy

In the recently published Physics Briefing Book submitted as input for the European Strategy for Particle Physics Update 2020 [355], the summarized figures are provided for the exclusion reaches for the wino-like and Higgsino-like chargino and neutralino particles as shown in Fig. 66 and 67.

In the compressed scenario, lepton colliders analyses are competitive to hadron colliders: sensitivity up to electroweakino masses equal to $\sqrt{s}/2$ are possible even for $\Delta m(\tilde{\chi}_1^{\pm},\tilde{\chi}_1^0)$ as low as 1 GeV, with no loss in acceptance (The ILC [373] and CLIC [374].).

For the Higgsino case, the sensitivity of lepton colliders depends only weakly on the nature of the LSP: the ILC500 and ILC1000 [373] can cover the full mass range up to $\sqrt{s}/2$

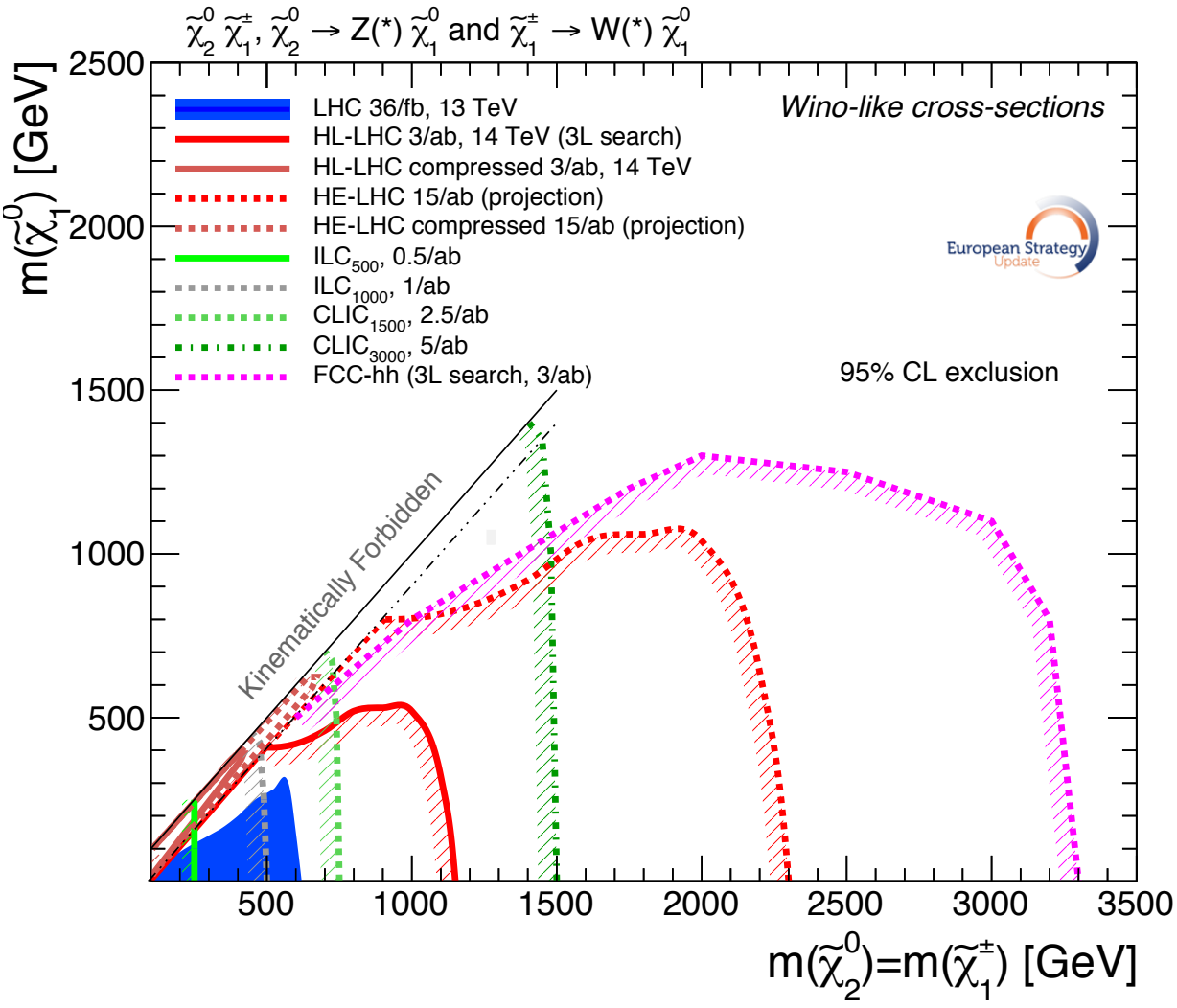

FIG. 66: The exclusion reaches for the Wino-like lightest chargino and next-to-lightest neutralino from the hadron and lepton colliders.

for Δm as low as 0.5 GeV, while the CLIC1500 and CLIC3000 allow a reach up to 650 GeV and 1.3 TeV, respectively [375].

Moreover, lepton colliders could again provide complementary sensitivity to $\tilde{\tau}$ especially in compressed scenarios: the ILC500 [373] would allow discovery of $\tilde{\tau}$ up to 230 GeV even with small datasets, whilst the CLIC3000 would allow reach up to m$\tilde{\tau}$ = 1.25 TeV and Δm($\tilde{\tau}$, $\tilde{\chi}_1^0$) = 50 GeV [375].

In summary, among all the searches discussed in this chapter, which summarized in table X, it is observed that the discovery potential is primarily constrained by the detector kinematics for s-channel SUSY production. However, when a supersymmetric particle can

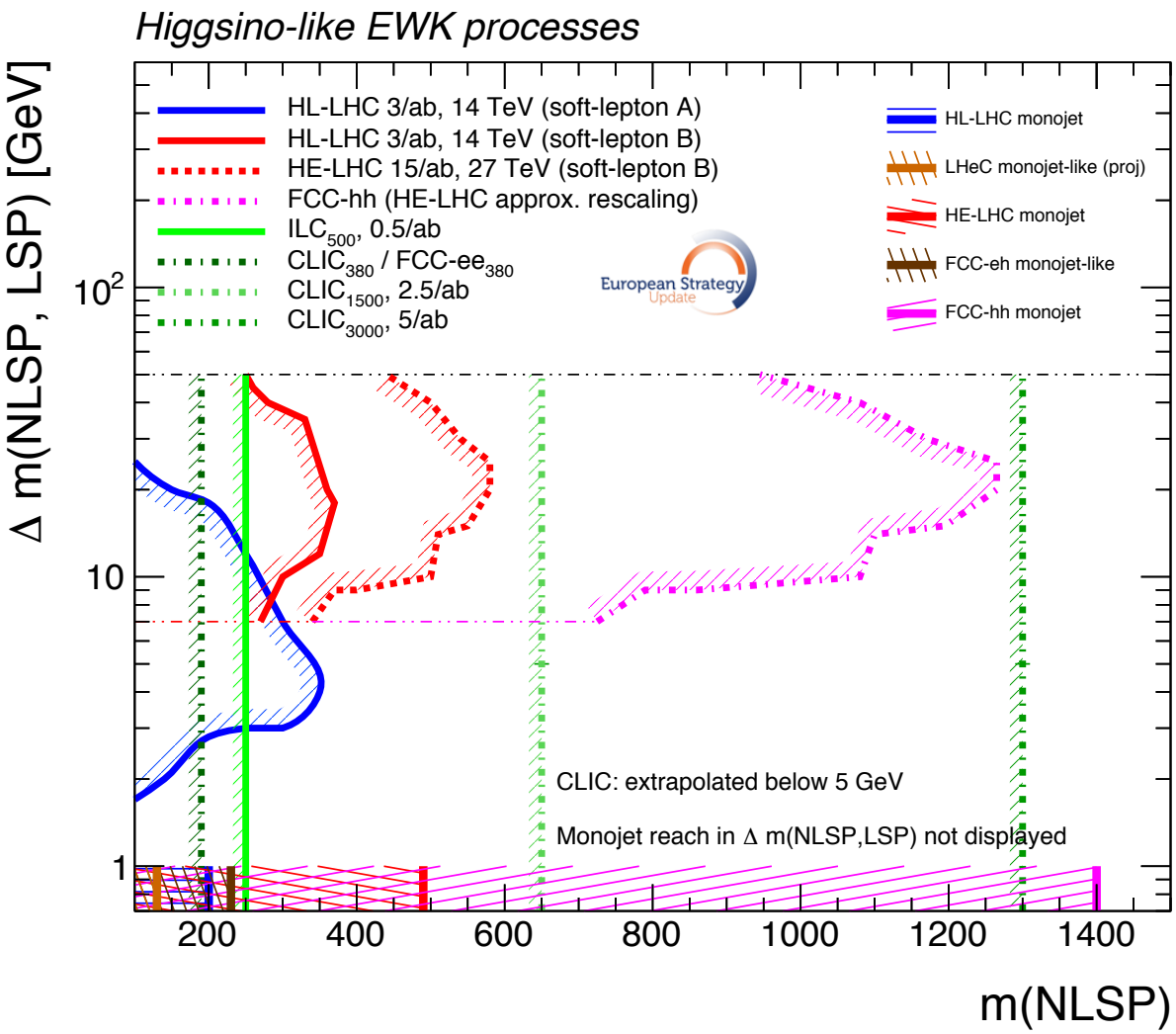

FIG. 67: The exclusion reaches for the Higgsino-like charginos and next-to-lightest neutralinos with equal mass m (NLSP), as a function of the mass difference Dm between NLSP and LSP. Exclusion reaches using monojet searches at the pp and ep colliders are also superimposed.

be produced via the t-channel or when an off-shell supersymmetric particle is produced via the s-channel, it is possible to break through the collision energy limits and probe heavier supersymmetric particles. Furthermore, for most of the studies presented below, the results are based on a center-of-mass energy of 240 GeV. A dedicated search for light smuons and staus extended this study to 360 GeV, reflecting an increase in sensitivity. A similar conclusion of enhanced sensitivity is expected for other searches when the center-of-mass energy reaches 360 GeV.

Search	Production	$\sqrt{s}$ [GeV]	$\mathcal{L}[ab^{-1}]$	Sensitivity	Figs.	Ref.
Light electroweakino	chargino pair	240	5.05	chargino excluded up to 120 GeV	59	[356]
	$e^+e^- \to \tilde{B}\tilde{B} \to \gamma\gamma\tilde{G}\tilde{G}$.	240	5.6	selectron excluded up to 4.5 TeV	60	[358]
Light slepton	smuon pair	240	20	smuon excluded up 119 GeV	61	[359]
	stau pair	240	20	stau excluded up 119 GeV	61	[359]
	smuon pair	360	1	smuon excluded up 177 GeV	61	[]
	stau pair	360	1	stau excluded up 176 GeV	61	[]
	off-shell smuon pair	240	5	smuon excluded up 126 GeV	63	[361]
	$e_R^+e_R^- \to \tilde{\chi}_1^0(\text{bino}) + \tilde{\chi}_1^0(\text{bino}) + \gamma$	240	3	right-handed selectron excluded up to 210 GeV	62	[360]
	$\mathcal{F}$-$SU(5)$	-	-	upper limits on $\tilde{\tau}_1$ up to 115 GeV	64	[362]
	$\mathcal{F}$-$SU(5)$	-	-	upper limits on $\tilde{e}_R$ up to 150 GeV	64	[362]

TABLE X: Recent results from the CEPC study on SUSY. The first column lists the signal signatures, the second column presents the corresponding production modes, the third and fourth columns provide the center-of-mass energy and the integrated luminosity, the fifth column shows the sensitivity to the coupling, suppression scale, or branching ratios, and the last column provides the references.

Compared with LHC, CEPC has significant advantage at compressed scenarios with small mass splitting between NLSP and LSP, as shown in Figure 68. CEPC has excellent search potential up to the kinematic limits in almost all SUSY scenarios.

VIII. FLAVOR PORTAL NEW PHYSICS (LINGFENG, XINQIANG)

The CEPC, when running at the Z pole, allows us to probe the flavour structures of Z couplings to matter fields with extreme precision. This also allows us to get very large samples of all b hadrons, c hadrons, τ leptons, with large boost in a very clean environment. These features make the CEPC also a flavour factory, which has a unique sensitivity to a large number of flavour processes that are generally not accessible at the current LHCb and Belle II experiments [244]. It is also stated in many dedicated studies that the CEPC's higher energy (operating at Z pole or higher), clean lepton collision environment and advanced detector system provide many powerful, sometimes unique, flavor physics probes (see also [32, 376–388] for examples at CEPC or parallel proposals).

CEPC holds significant potential in the realm of flavor physics that enables the imposition of various indirect constraints on BSM. A crucial aspect to consider is the role of the Cabibbo–Kobayashi–Maskawa (CKM) matrix, which, in the SM, is defined and primar-

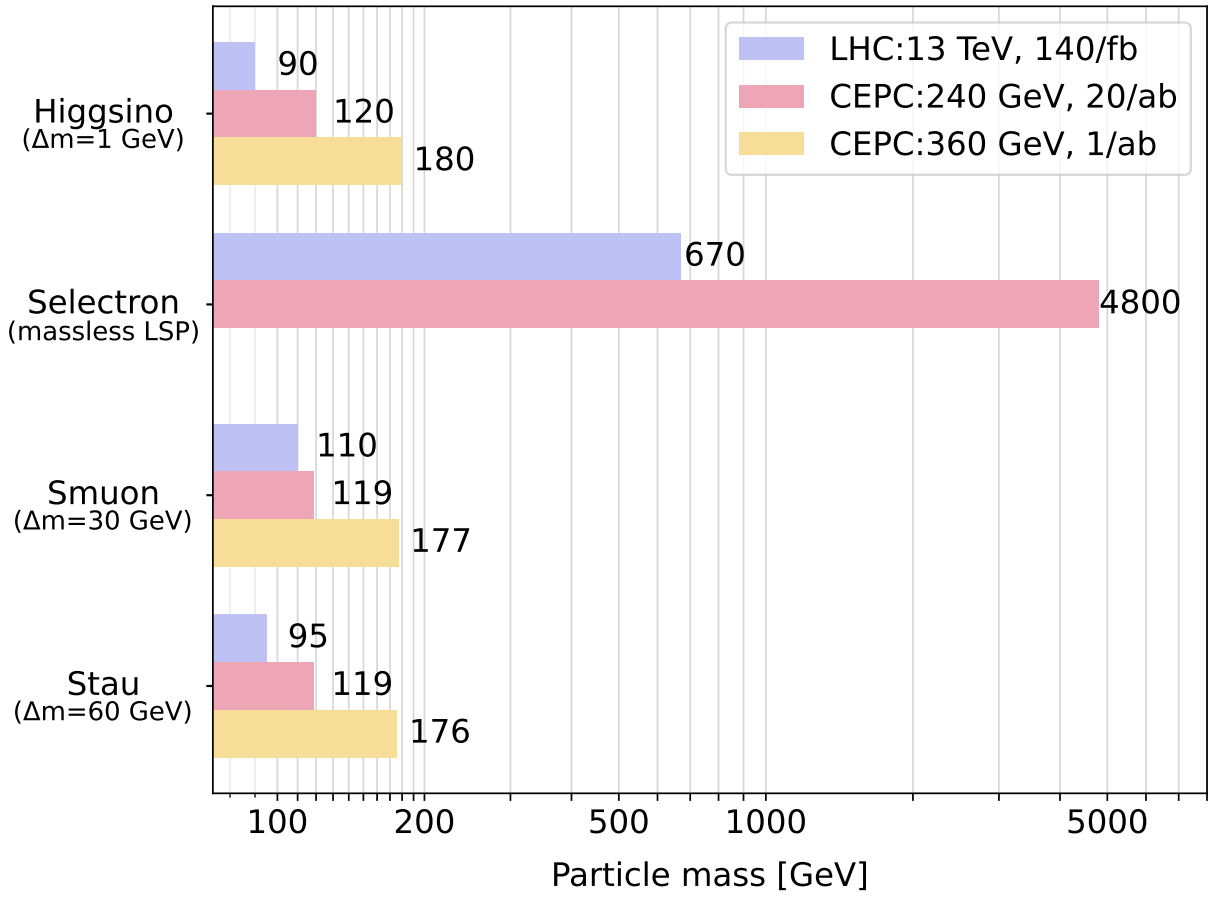

FIG. 68: The exclusion reaches for higgsino and slepton at CEPC and LHC. The compressed SUSY particles are picked for the comparison except for selectron.

ily measured via charged current couplings at the electroweak scale or lower. This matrix is particularly sensitive to general couplings in new physics, especially since many high-precision or highly sensitive flavor processes are not charged current in nature. Governed by electroweak gauge coupling and unitarity, the CKM matrix imposes stringent restrictions on BSM couplings to quarks. Therefore, unless BSM physics introduces couplings to SM quarks that adhere to the specific patterns of the CKM matrix, rather than arbitrary flavor structures, the scale of new physics will be significantly elevated, extending well beyond the TeV range.

The sensitivity of the flavor sector to new physics is underscored by several factors. Firstly, the suppression of FCNC by the Glashow–Iliopoulos–Maiani (GIM) mechanism [389] in the SM is a key aspect. The FCNC prevalent in the SM, notably influencing analyses such

as flavored meson mixing. Secondly, cLFV represents a special case of FCNC, exhibiting even greater suppression due to the light neutrino masses, making any observable cLFV a distinct sign of BSM physics. Thirdly, the flavor sector in the SM is characterized by several (approximate) symmetries. This includes an approximate, accidental symmetry among the three generations, leading to lepton flavor universality (LFU) which is only slightly violated by lepton Yukawa couplings. Other examples are the conservation of lepton and baryon numbers in collider environments. Violations of these symmetries are therefore indicative of BSM physics. Lastly, the decays of heavy flavored states in the SM are markedly suppressed, both by the small off-diagonal elements of the CKM matrix and the hierarchy between fermion masses and the electroweak scale. This results in narrow decay widths ($\lesssim 10^{-12}$ GeV) for many flavored particles, rendering them long-lived. Consequently, the small SM widths significantly amplify the impact of any new physics amplitudes. To better demonstrate the reach of new physics from the flavor sector, one can write the reach of the BSM scale $\Lambda_{\rm NP}$ from dim-6 operators via charged current $b \to c$ transitions as:

$$\Lambda_{\rm NP} \sim (G_F |V_{cb}| \delta_{\rm exp})^{-\frac{1}{2}} \sim (1.5 \text{ TeV}) \times \delta_{\rm exp}^{-\frac{1}{2}} \, . \tag{13}$$

where $\delta_{\rm exp}$ is the relative precision reached in the experiment. Similarily, from FCNC $b \to s$ transitions one may obtain

$$\Lambda_{\rm NP} \sim \left(\frac{\alpha}{4\pi} \frac{m_t^2}{m_W^2} G_F |V_{tb} V_{ts}^*| \delta_{\rm exp} \right)^{-\frac{1}{2}} \sim (30 \text{ TeV}) \times \delta_{\rm exp}^{-\frac{1}{2}} \, . \tag{14}$$

In both cases the interpretation are model-dependent, which are common in indirect searches.

The aforementioned arguments are pertinent to both direct and indirect search methodologies. Indirect probes, particularly abundant in the flavor sector, effectively transform all flavor physics studies into potential avenues for BSM investigation. This is due to the fact that certain processes are more germane to new physics searches for a variety of reasons. Conversely, light BSM degrees of freedom may be produced through their interactions with flavored fermions within the SM. This possibility is imminent since these states' SM gauge interactions must be sufficiently suppressed to align with existing data. The following highlights are some of the most prominent examples of BSM searches at CEPC interfacing with flavor physics, with key numbers summarized in Table. XI. For a more thorough review on the potential and phenomenology of flavor physics at CEPC, see [390].

Measurement	Current Limit	CEPC [390]
BR($Z \to \tau\mu$)	$< 6.5 \times 10^{-6}$	$\mathcal{O}(10^{-9})$
BR($Z \to \tau e$)	$< 5.0 \times 10^{-6}$	$\mathcal{O}(10^{-9})$
BR($Z \to \mu e$)	$< 7.5 \times 10^{-7}$	$10^{-8} - 10^{-10}$
BR($\tau \to \mu\mu\mu$)	$< 2.1 \times 10^{-8}$	$\mathcal{O}(10^{-10})$
BR($\tau \to eee$)	$< 2.7 \times 10^{-8}$	$\mathcal{O}(10^{-10})$
BR($\tau \to e\mu\mu$)	$< 2.7 \times 10^{-8}$	$\mathcal{O}(10^{-10})$
BR($\tau \to \mu ee$)	$< 1.8 \times 10^{-8}$	$\mathcal{O}(10^{-10})$
BR($\tau \to \mu\gamma$)	$< 4.4 \times 10^{-8}$	$\mathcal{O}(10^{-10})$
BR($\tau \to e\gamma$)	$< 3.3 \times 10^{-8}$	$\mathcal{O}(10^{-10})$
BR($B_s \to \phi\nu\bar{\nu}$)	$< 5.4 \times 10^{-3}$	$\lesssim 1\%$ (relative)
BR($B^0 \to K^{*0}\tau^+\tau^-$)	-	$\lesssim \mathcal{O}(10^{-6})$
BR($B_s \to \phi\tau^+\tau^-$)	-	$\lesssim \mathcal{O}(10^{-6})$
BR($B^+ \to K^+\tau^+\tau^-$)	$< 2.25 \times 10^{-3}$	$\lesssim \mathcal{O}(10^{-6})$
BR($B_s \to \tau^+\tau^-$)	$< 6.8 \times 10^{-3}$	$\lesssim \mathcal{O}(10^{-5})$
BR($B^0 \to 2\pi^0$)	$\pm 16\%$ (relative)	$\pm 0.25\%$ (relative)
$C_{CP}(B^0 \to 2\pi^0)$	± 0.22 (relative)	± 0.01 (relative)
BR($B_c \to \tau\nu$)	$\lesssim 30\%$	$\pm$ 0.5% (relative)
BR($B_c \to J/\psi\tau\nu$)/BR($B_c \to J/\psi\mu\nu$)	$\pm$ 0.17 $\pm$ 0.18	$\pm 2.5\%$ (relative)
BR($B_s \to D_s^{(*)}\tau\nu$)/BR($B_s \to D_s^{(*)}\mu\nu$)	-	$\pm 0.2\%$ (relative)
BR($\Lambda_b \to \Lambda_c\tau\nu$)/BR($B_c \to \Lambda_c\mu\nu$)	$\pm$ 0.076	$\pm 0.05\%$ (relative)
BR($\tau \to \mu X_{\text{inv.}}$)	7×10^{-4}	(3-5)$\times 10^{-6}$
BR($B \to \mu X_{\text{LLP}}(\to \mu\mu)$)	-	$\mathcal{O}(10^{-10})$ (optimal)

TABLE XI: Preliminary sensitivities of BSM flavor physics probes at CEPC, adapted from Ref. [390]. The notation X_{inv} stands for an invisible narrow resonance and X_{LLP} represents a long-lived BSM particle. The limit for the LLP particle is obtained when its lifetime is optimal, as shown in the right panel of Fig. 69. For some channels with extremely high precision expected, the actual sensitivities will be mostly determined by systematic effects, which cannot be precisely evaluated at the current stage. Consequently, only the rough sensitivity levels are reported. See [390] for more details.

A. cLFV processes

Reflecting on cLFV searches at CEPC, the facility's significant integrated luminosity in the Z-factory mode notably enhances its capacity to explore cLFV directly from Z and τ

decays. These two modes benefit immensely from the CEPC's design and energy range, making it an ideal platform for such investigations.

cLFV in Z decays is a primary focus, particularly in modes such as $Z \to \mu e$, $Z \to \tau\mu$, and $Z \to \tau e$. Each of these decay processes provides a unique window into potential BSM physics. When searching $Z \to \mu e$ decays, the bottleneck of detection comes from the small but non-negligible lepton misidentification rate. Conversely, in modes involving τ, the extra neutrino from τ decays, puts the detector's momentum/energy resolution in a more significant position. In general, the expected limits at CEPC will exceed the current best by more than two orders of magnitude. Note that testing cLFV new physics at higher scales is also possible at CEPC. One of the most prominent examples would be the cLFV Higgs decays. The phenomenology of these modes, while analogous, is slightly more intricate due to the additional production of Z in the $e^+e^- \to HZ$ process. Although the absolute sensitivity in these Higgs decay modes might be limited by smaller statistics, their higher energy scales, and couplings could provide valuable complementary for new physics.

In terms of τ decays, the CEPC flavor physics project is proposed to investigate a wide array of cLFV processes. The decay modes like $\tau \to 3\mu$, $\tau \to \mu\gamma$, and $\tau \to e\gamma$ are of significant interest as direct resonance peaks can be reconstructed in their final states. Due to the clarity of their phenomenology, they were chosen as benchmark channels. Besides, the τ lepton's heavy mass compared to other leptons renders its collider behavior more akin to flavored hadrons, fitting well with the energy range and detector design of the CEPC. This aspect of τ decays offers an array of valuable channels for cLFV studies, further underscoring the CEPC's discovery potential.

B. Decays of b and c hadrons

Rare b and c hadron decays induced by FCNC processes are inherently one-loop suppressed in the SM, rendering them highly sensitive to potential contributions from new physics. These FCNC processes are intrinsically fascinating in the context of flavor physics. Within the SM, they provide insights into hadronic properties and offer a means to constrain critical parameters like the CKM matrix elements. Meanwhile, some of the charged-current-induced decays of these hadrons, especially for the (semi)leptonic decays involving the τ lepton. In the past years, evidences from a several experiments suggest that LFU is violated

in the tau sector. The magnitude of such violation, if fully confirmed, is a clear indicator of BSM physics. Investigating such possibilities with highest precision are then a great opportunity to investigate the nature of leptons. At CEPC, a systematic proposal for studying these processes is in place, with several results already available.

As a powerful facility for flavor physics, CEPC also presents unique opportunities for studying these rare decays, which may be challenging to probe at other facilities. Such modes often involve final state particles that demand exceptional energy/momentum resolution for precise reconstruction. Additionally, the inherently rare nature of these decays necessitates a very low background level for effective study, conditions that are readily met by the capabilities of CEPC. Importantly, many FCNC processes in the SM exhibit non-trivial CP-violating properties, playing a pivotal role in flavor physics. Measuring these CP properties not only furthers our understanding of flavor physics but also serves as a powerful tool for identifying new sources of CP-violation beyond the SM CKM matrix. Prominent examples of such processes include $b \to s\tau\tau$ transitions, which involve multiple neutrinos in the final state, and $B_{(s)} \to \pi^0\pi^0 \to 4\gamma$ decays. The study of these processes at CEPC could provide crucial insights into the intricacies of flavor physics and CP-violation, shedding light on phenomena that lie beyond the current understanding of the SM.

In parallel with the phenomenology studies for FCNC transitions, the charged-current-induced transitions of b-hadrons at CEPC, especially $b \to c\ell(\tau)\nu$ processes, are being studied. Some of the most prominent examples include the $B_c \to \tau\nu$ and $B_c \to \ell\nu$ decays, which are challenging to measure precisely at other facilities. This is due to the rareness of B_c meson and the elusive nature of $\ell(\tau) + \nu$ final states. To better constrain the form of new physics, other relevant modes with distinct hadron dynamics such as $B_s \to D_s^{(*)}\ell(\tau)\nu$, $B_c \to J/\psi\ell(\tau)\nu$, and $\Lambda_b \to \Lambda_c\ell(\tau)\nu$ are also studied. The characteristic relative sensitivity to these decays achieved at CEPC is of $\mathcal{O}(10^{-2})$ or less, which can also be interpreted to EFT operators with a scale of multi-TeV according to 13.

C. Light BSM degrees of freedom from flavor transitions

In the ongoing research at CEPC, two benchmark cases are currently in the preliminary stage, focusing on detecting BSM states emerging from either cLFV or quark FCNC processes. These benchmarks are distinguished by the nature of the BSM state involved: one

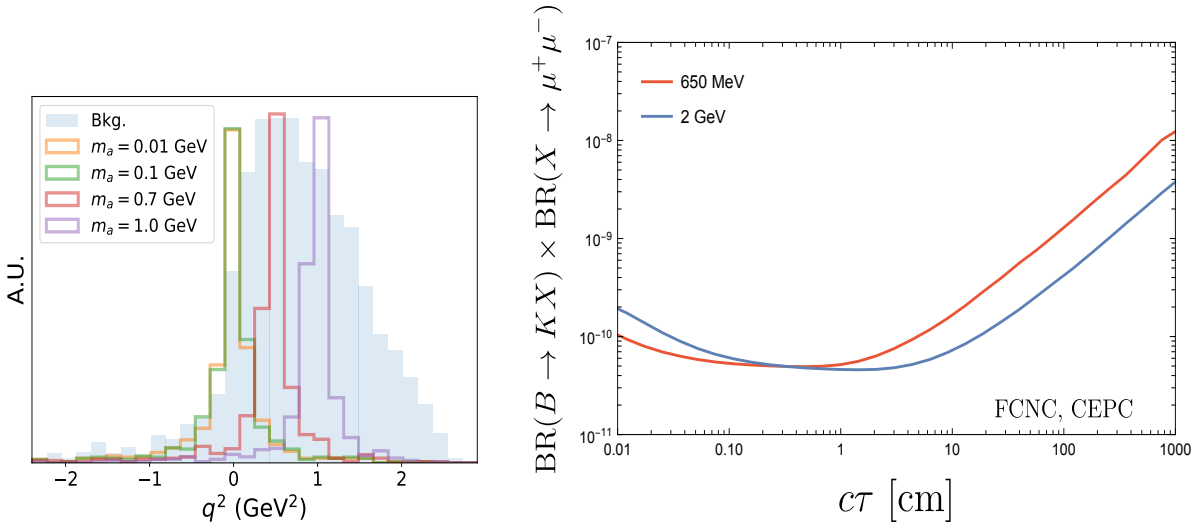

FIG. 69: Left: Reconstruction of invisible particle mass squared from τ decays to μ and an invisible BSM particle, which is also noted as $q^2 \equiv (p_\tau - p_\mu)^2$. Right: the projected sensitivity on FCNC $B \to K X_{\rm LLP}(\to \mu^+\mu^-)$ as a function of $X_{\rm LLP}$ lifetime. Two mass benchmarks are shown as blue and red curves, respectively. Both plots are taken from [390].

involves an invisible BSM state, while the other involves a LLP in the final state.

For the scenario involving invisible new particles, the reconstruction process presents a significant challenge, particularly in the preliminary studies that utilize fast detector simulation instead of a full simulation. The crux of reconstructing such final states lies in relying on the global energy-momentum conservation within the detector system. Supplementary information, such as track impact parameters, is also crucial as it provides additional constraints for the reconstruction process. Given the potential complexity of the reconstruction algorithms required, current studies at CEPC are focusing on inclusive $Z \to \tau\tau + X_{\rm inv.}$ processes, where $X_{\rm inv.}$ is the invisible new particle. In these processes, the extra particle X is either generated via cLFV decays of the form $\tau \to \ell X$ or emerges from final state radiations. This particle could be an ALP or a dark photon, characterized by suppressed or invisible decays.

While other neutrinoless processes are also relevant, they necessitate different reconstruction procedures. By integrating detailed information about the collision point, track momenta and impact parameters, along with global energy data, the current study demonstrates the feasibility of completely reconstructing a light invisible state emanating from

tau decay, provided all these data elements are properly integrated. This achievement is illustrated in the left panel of Fig. 69, showcasing the capability of CEPC in detecting and analyzing such elusive BSM states. Depending on the new particle's mass, the expected sensitivity on BR($\tau \to X_{\text{inv.}}$) may reach $\mathcal{O}(10^{-6})$ level or less.

Following the first benchmark study at CEPC focusing on invisible light BSM states, the second benchmark study shifts attention to light LLPs emerging from heavy quark FCNC transitions. These light LLPs could be exemplified by Axion-Like Particles ALP, dark photons, or other new physics models. A key aspect of this study is the model-independent nature of the search, with the LLPs being describable by a few effective parameters, such as their mass and decay length. In this context, the underlying UV physics does not significantly alter the search strategy. The most distinctive signal feature in this study is a clearly constructed displaced decay vertex. This is vital for identifying the presence of the LLP. However, due to the extremely low target rate - with current constraints on exotic branching ratios producing LLPs from B mesons typically below 10^{-5} - it is unlikely that more than one displaced vertex will be observed in a given event.

The current analysis primarily focuses on the decay mode $X_{\text{LLP}} \to \mu^+\mu^-$, where the phenomenology at CEPC is expected to be straightforward, characterized by a low background level and a high signal efficiency. The production of the LLP is hypothesized to occur via the exclusive decay $B \to K^{(*)} + X_{\text{LLP}}$. Notably, such processes can be generated even in the absence of flavor-violating interactions in the new physics model. The preliminary results of this study are concisely summarized in the right panel of Fig. 69. Since at CEPC the light LLPs could also be produced from Higgs, or more importantly, Z exotic decays [391, 392]. The flavor portal production then serves as a complementary of LLP searches.

Crucially, the sensitivity of this search to the LLP signal is closely tied to the particle's proper decay length. This sensitivity varies depending on the distance the LLP travels before decaying and is found to peak around the centimeter scale. This dependency highlights the intricate interplay between the LLP's decay length and the detector's capability to effectively search for and analyze these rare events at CEPC.

D. Summary

The Z-pole operation of CEPC also serves as a flavor factory, generating and measuring flavored hadrons and leptons with high statistics and resolution. It will become the leading flavor physics experiment, refreshing our knowledge of flavor physics. We present a few benchmarks for investigating feeble BSM effects with flavor physics probes above. In these cases, the SM amplitudes are generically suppressed due to various reasons. Consequently, the relative importance of new physics is enhanced, and a high signal-to-noise ratio may be reached at CEPC. Examples include cLFV transition processes, rare FCNC decay processes, and light BSM particle production from its interaction with the SM flavor sector.

While Table. XI lists several channels where CEPC potentially contributes to BSM physics. However, the interpretation of new physics is highly model-dependent since the BSM impacts are indirect. In Fig. **??**, we illustrate the target precision at CEPC in a model-independent way, together with the current best limits. We present the conservative upper limits for many processes, however the systematic uncertainties cannot be precisely determined at the current stage.

IX. ELECTROWEAK PHASE TRANSITION AND GRAVITATIONAL WAVES (KE-PAN XIE, FA PENG HUANG, SAI WANG, MICHAEL RAMSEY MUSOLF, BRUCE)

A. Introduction

The nonzero vacuum expectation value (VEV) of the Higgs field spontaneously breaks the electroweak gauge group $SU(2)_L \times U(1)_Y$, thereby giving mass to the $W^\pm$ and Z gauge bosons as well as the fermions in the Standard Model (SM). At sufficiently high temperatures, however, thermal quantum corrections involving the particles in the early universe plasma change the shape of the Higgs potential such that – in a purely Standard Model universe – the minimum of energy lies at the origin with $\langle h \rangle = 0$ and EW symmetry restored[393]. ~~However, in the high temperature and dense plasma of the early Universe, the Higgs potential was influenced by thermal corrections, leading to a different VEV from its present state. Generally, at high temperatures, the Higgs VEV becomes $\langle h \rangle = 0$, resulting in the restoration of the electroweak symmetry [393].~~ The thermal history of the Higgs VEV evolution from the

early Universe value to today's $\langle h \rangle = v_{\rm EW} = 246$ GeV, and the associated EW symmetry-breaking transition[394], ~~or say, the nature of the electroweak phase transition,~~ is not only of considerable interest but also of utmost importance. In particular, the occurrence of a first order electroweak phase transition (FOEWPT), if sufficiently strong, can provide the necessary preconditions for generating the cosmic matter-antimatter asymmetry via electroweak baryogenesis and a source of potentially observable gravitational waves. A FOEWPT may also impact the nature and dynamics of the dark matter.

~~It deeply impacts the thermal history of the Universe, and is closely linked to long-standing puzzles in particle physics and cosmology, such as dark matter and matter-antimatter asymmetry.~~

In the SM, the Higgs VEV $\langle h \rangle$ smoothly transitions from zero to $v_{\rm EW}$ as the Universe cools down. Lattice simulations indicate that for $m_h \gtrsim 70$ GeV, this transition is a smooth crossover [395–397]. However, in the presence of new physics beyond the SM (BSM), $\langle h \rangle$ can undergo a discontinuous jump known as a first-order electroweak phase transition (FOEWPT) [398]. During this process, bubbles containing the $\langle h \rangle \neq 0$ vacuum form and expand within the background of the old vacuum where $\langle h \rangle = 0$. These bubbles eventually fill the entire space, converting the Universe from the old false vacuum to the new true vacuum. **[MRM: The following is simply incorrect. The top panel could be a second order transition, whereas the bottom is first order. There is no potential picture or perturbative description that one can use for a smooth crossover.]** The two different patterns of electroweak phase transition are illustrated in Fig. **??**, where the top panel sketches the SM crossover, while the bottom panel sketches the FOEWPT in new physics beyond the SM. The underlying reason for a FOEWPT is the existence of a potential barrier that forbids a smooth transition. One should keep in mind, however, that the presence of a barrier in the potential is a necessary but not sufficient condition for a FOEWPT. For m_h in the vicinity of the "critical Higgs mass" ~ 70 GeV, infrared contributions to thermal loops render the aforementioned perturbative description of EW symmetry-breaking invalid. The latter may occur via a smooth crossover even in the presence of a perturbative thermal barrier in the potential. Below, we highlight recent developments in non-perturbative studies of the EWPT in BSM scenarios and their relevance to future CEPC measurements.

The FOEWPT holds greater scientific interest compared to the SM crossover due to its

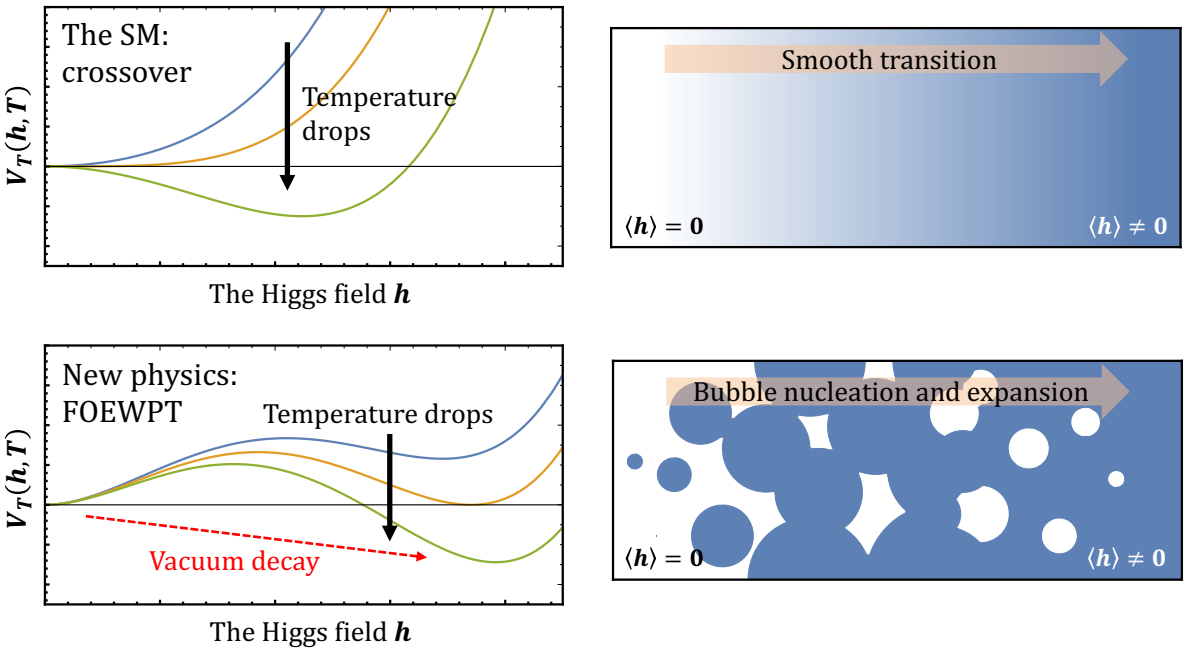

FIG. 70: Illustration of electroweak phase transition patterns. Top: in the SM, the transition is a smooth crossover. Bottom: in many new physics models, the scalar potential exhibits a barrier, allowing for a FOEWPT with bubble nucleation and expansion.

profound cosmological implications. It can drive the Universe out of equilibrium facilitating electroweak baryogenesis to generate the matter-antimatter asymmetry (see Ref. [399] for a review). During this process, fermions engage in CP-violating scatterings with the bubble wall, resulting in the creation of a chiral asymmetry, which is then converted into a net baryon number by electroweak sphalerons. The baryon asymmetry is then swept into the true vacuum through bubble expansion, and stored until today [399–410]. This mechanism has been the primary motivation for studying FOEWPT in the past several decades.

Furthermore, first-order phase transitions generally generate stochastic gravitational wave (GW) backgrounds through bubble collisions, sound wave motion, and turbulence in the plasma [411–415]. A FOEWPT, which typically occurs at $T \sim 100$ GeV, sources GWs that peak at frequencies of $\mathcal{O}$(mHz) today [416–418]. These frequencies fall within the sensitivity range of several near-future space-based detectors, such as LISA [419], TianQin [420, 421], and Taiji [422, 423], and hence will be efficiently probed in the next decade. As we discuss below, the EWPT constitute an ideal "laboratory" for studying FOPT-catalyzed GWs as collider studies provide a complementary probe of the underlying particle physics. Such

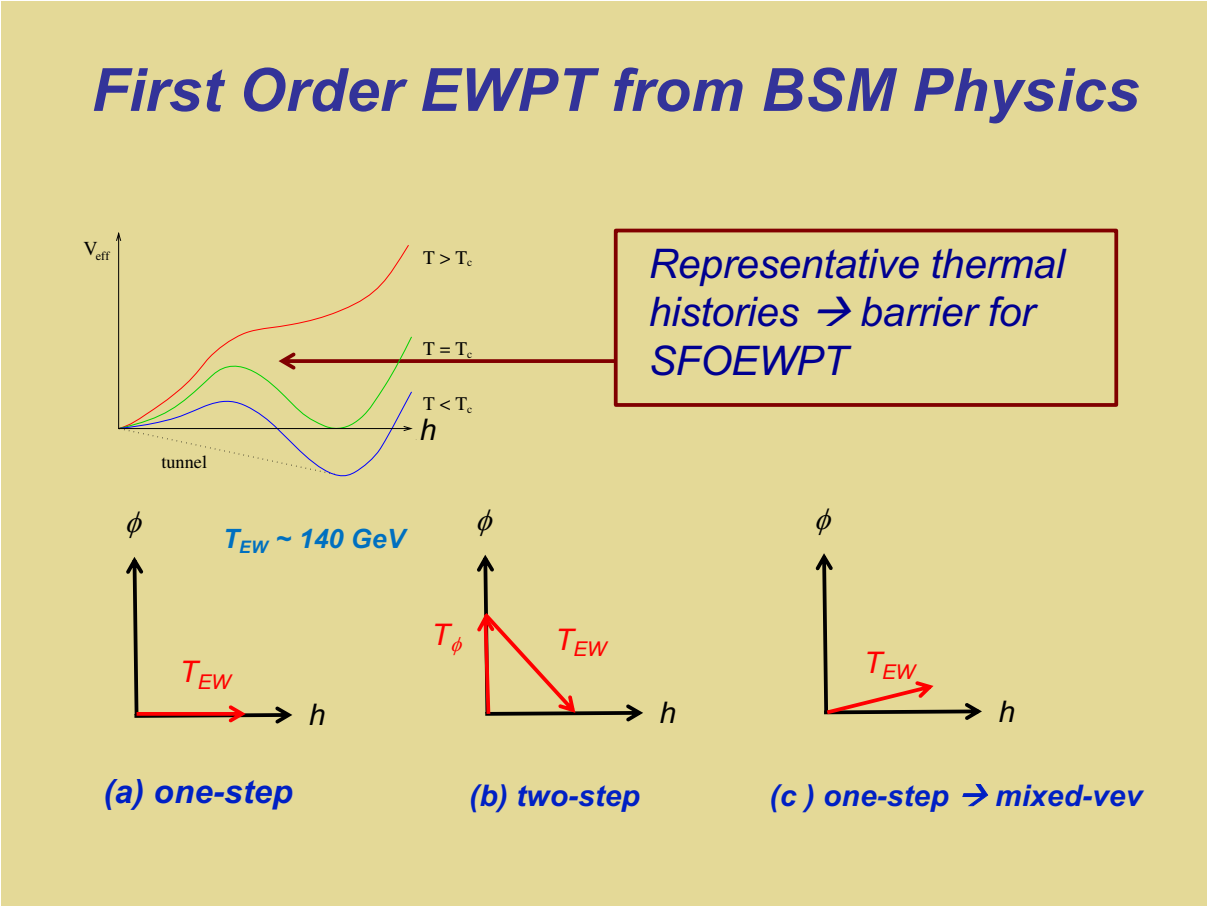

FIG. 71: Thermal history caption goes here.

complementarity may not be available for GWs associated with other scales, such as those detectable in pulsar timing arrays.

Additionally, recent studies suggest that first-order cosmic phase transitions, including FOEWPT, could be crucial in the generation of dark matter and matter-antimatter asymmetry through various processes as follows.

1. It could impact the dark matter production, decay and annihilation via the sudden change of particle mass before and after the phase transition [424–427].

2. The interaction between the bubble wall and particles in the plasma can produce superheavy particles to be dark matter or generate the matter-antimatter asymmetry [428–433].

3. Due to the mass gap between the two sides of the bubble walls, phase transitions can

filter particles to form superheavy dark matter [434–437], or trap particles to form solitons or even primordial black holes (PBHs) [438–450].

4. The bubble collision or over-densities arise from the randomness of bubble nucleation can collapse to PBHs [450–461].

As mentioned above and illustrated in Fig. **??**, from a particle physics perspective, a FOEWPT may occur when there is a barrier separating the two local minima (vacua) of the finite temperature Higgs potential, denoted as $V_T(h, T)$, which originates from physics beyond the SM. This barrier may prevent a smooth transition from the false vacuum to the true vacuum, necessitating a thermal tunneling process known as FOEWPT. The probability of this tunneling is determined by the vacuum decay rate [462]. Once the decay rate exceeds a certain threshold, bubbles begin to form, leading to FOEWPT.

It is useful to characterize the possibility of a FOEWPT in terms of both the thermal history of EW symmetry breaking and the underlying particle physics. In terms of the former, Fig. 71 displays three generic thermal histories in the presence of a new scalar filed ϕ. The latter may either by charged under SM gauge symmetries or a gauge singlet. Fig. 71(a) indicates a one-step transition from the symmetric phase to the present Higgs phase. Fig 71(b) gives a two-step transition history, wherein the universe first goes to a phase associated with a non-zero VEV for ϕ followed by a subsequent transition to the Higgs phase. Fig. 71(c) indicates a one-step transition to a mixed-VEV phase.

The particle physics driving the FOEWPT in these scenarioscan be categorized into four types based on the source of the potential barrier [463]: I) thermally driven, IIA) tree-level with renormalizable operators, IIB) tree-level with high-dimensional operators, and III) zero-temperature loop-driven. Each type encompasses numerous new physics models with diverse cosmological implications and phenomenological signals. Types I, IIB, and III are particularly relevant to the one-step transitions of Fig. 71(a), while type IIA is more germane to the thermal histories of Figs. 71(b,c). As we will see in the following subsections, the CEPC can efficiently probe type-IIB via Higgs precision measurements, and type-I, type-IIA via both precision Higgs measurements and Higgs exotic decay.

~~Particle~~ Collider experiments provide an efficient approach to probe the underlying physics of the barrier and test the nature of the electroweak phase transition and also the associated new physics mechanisms with baryogenesis and/or dark matter. The typical phe-

nomenology of FOEWPT includes the on-shell production of new particles or deviations in the properties of the Higgs boson [464]. Importantly, the globally envisioned future collider program, including the high luminosity LHC as well as future lepton and hadron colliders, is capable of providing a (nearly) definitive test of BSM-induced FOEWPT scenarios. The fundamental reason is that EW symmetry breaking in the Standard Model occurs at the "electroweak temperature" $T_{\rm EW} \sim 140$ GeV. Any BSM physics that changes the transition from a smooth crossover into a FOEWPT cannot be too heavy with respect to $T_{\rm EW}$ and cannot couple too feebly to the Higgs boson. Generic arguments imply that the mass of the new particles responsible for a FOEWPT should be $\lesssim 700$ GeV and that the magnitude of associated changes in Higgs boson properties larger than $\mathcal{O}(1\%)$[464]. While exceptions occur, the vast majority of model-specific studies bear out these generic expectations.

One example is the gauge singlet scalar extension of the Standard Model (referred to as the xSM, falling into type-IIA barrier). For seminal studies, see Refs. NNN and Ref. [464] for a comprehensive set of references. The xSM exhibits a rich collider phenomenology as well as ~~which exhibits~~ correlations and complementarity between high-energy collider searches for di-Higgs/di-boson processes and GW measurements [465–469]. Similar analyses have been conducted for other models, such as the Georgi-Machacek model [470, 471], the inert doublet model (IDM) [472, 473], the dark gauged sector [474], etc. Below we highlight recent xSM studies particularly relevant to the CEPC.

The LHC can investigate new particles associated with the physics of FOEWPT up to the TeV scale due to its exceptionally high collision energy. While the 240 GeV CEPC cannot directly probe heavy degrees of freedom, it presents an opportunity for precise measurements. CEPC can accurately determine the properties of the Higgs boson, indirectly providing insights into FOEWPT. Notably, deviation in the couplings involving the Higgs boson (hWW, hZZ, and h^3) may indicate potential dynamics associated with FOEWPT [465, 469–471, 475–480] [**MRM: update refs**]. Furthermore, under certain circumstances, the CEPC can effectively explore scenarios involving light new degrees of freedom, potentially leading to their discovery. Subsequent subsections will delve into different FOEWPT scenarios, with a particular emphasis on their interplay with the CEPC.

B. Higgs precision measurements

The Higgs couplings can be influenced by new physics associated with the FOEWPT barrier. ~~A comprehensive study demonstrates~~ Recent studies demonstrate that Higgs factories can effectively investigate FOEWPTs in various scenarios [464, 476], including the general and $\mathbb{Z}_2$-symmetric xSMs (type-IIA barrier), the real triplet scalar extension (type I and type-IIA), stop-like scalar and heavy fermion extensions of the SM (type-I barrier). The correlation and complementarity between precise measurements of Higgs properties like the hZZ and h^3 couplings, as well as GW signals, enable this probing. Remarkably, CEPC/ILC/FCC-ee can detect a significant portion of the FOEWPT parameter space by observing deviations in the hZZ coupling. Additionally, the deviation of the h^3 coupling, ~~typically of the order $\mathcal{O}(1)$,~~ can also be investigated.

Here, we illustrate the precision Higgs measurement probes of the FOEWPT using two explicit models as well as the SM effective field theory (EFT). Starting with the xSM, a combination of thermal effective field theory (EFT) and lattice studies have refined the confrontation of theory and experiment. A key quantity that connects the phase transition and collider phenomenology is the singlet-doublet mixing angle, θ. Fig. 72 shows the discontinuity in the order parameter $\langle\phi^\dagger\phi\rangle$ as a function of the $\sin\theta$. The solid lines show the relationship as derived from perturbation theory, while the dots give the results of lattice simulations. The latter indicate for sufficiently small $|\sin\theta|$, the transition is a smooth crossover, whereas perturbation theory always implies the presence of a FOEWPT. The vertical lines show the $\sin\theta$ sensitivities of the HL LHC and CEPC, with the latter dominated by measurements of the associated production $e^+e^- \to ZH$ cross section. Importantly, the perturbative computations imply that there would always be a significant portion of FOEWPT-viable parameter space inaccessible to the CEPC, whereas the lattice results indicate otherwise. For larger (smaller) values of the Higgs portal coupling, the value of $|sin\theta|$ at the crossover-FOEWPT boundary decreases (increases). In short, the state-of-the-art theory suggests that for the singlet-like scalar being relatively heavy, precision Higgs studies at the CEPC will provide a powerful test of the xSM FOEWPT when the latter is connected to non-vanishing singlet-doublet mixing.

The interplay with the HL LHC and future GW probes is illustrated in Fig. 73, which shows the xSM phase diagram in the $\sin\theta$-portal coupling (a_2) plane. The pink region gives

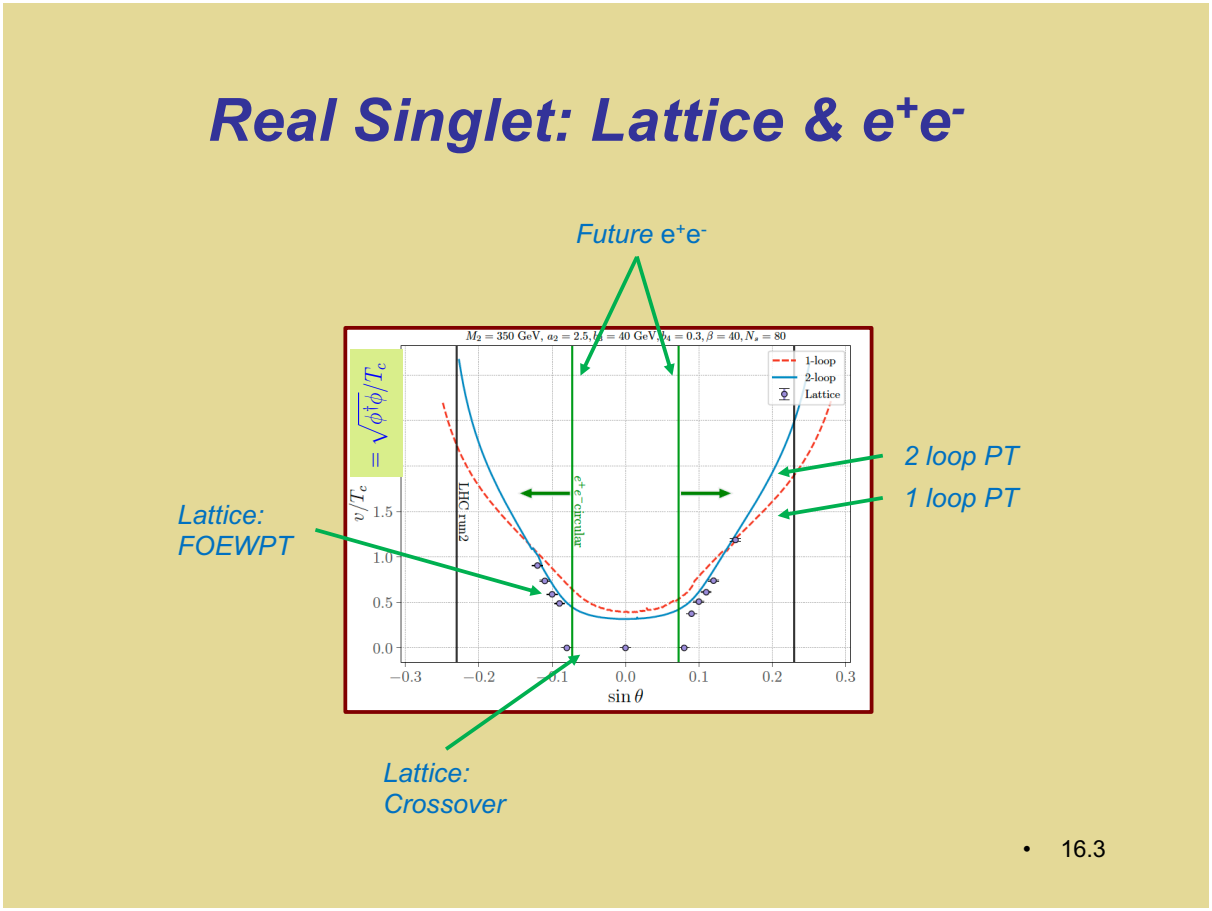

FIG. 72: Lattice-EFT-CEPC caption goes here.

the two-step EWPT viable region, while the purple band indicates the LISA sensitivity for a signal-to-noise ratio ≥ 5 level. The various dashed curves show the discovery reach for resonant di-Higgs production at the HL-LHC in the $b\bar{b}\gamma\gamma$ and $b\bar{b}\tau^+\tau^-$ channels. The vertical line indicates the CEPC sensitivity to $\sin\theta$, which significantly extends the reach as compared to the HL-LHC. In the event of a GW observation, and assuming the xSM is realized in nature, one could either anticipate a CEPC discovery of a significant singlet-doublet mixing or identify the narrow region of xSM parameter space consistent with both sets of experiments.

Lattice studies have also been recently carried out for the real triplet scalar extension, or ΣSM. A SFOEWPT may arise via either thermal effects in the one-step case or tree-level barrier in the two-step case [Fig. 71(b)]. The σSM can also modify Higgs boson properties via loop effects in both the $h \to \gamma\gamma$ and $e^+e^- \to Zh$ processes. The relevant

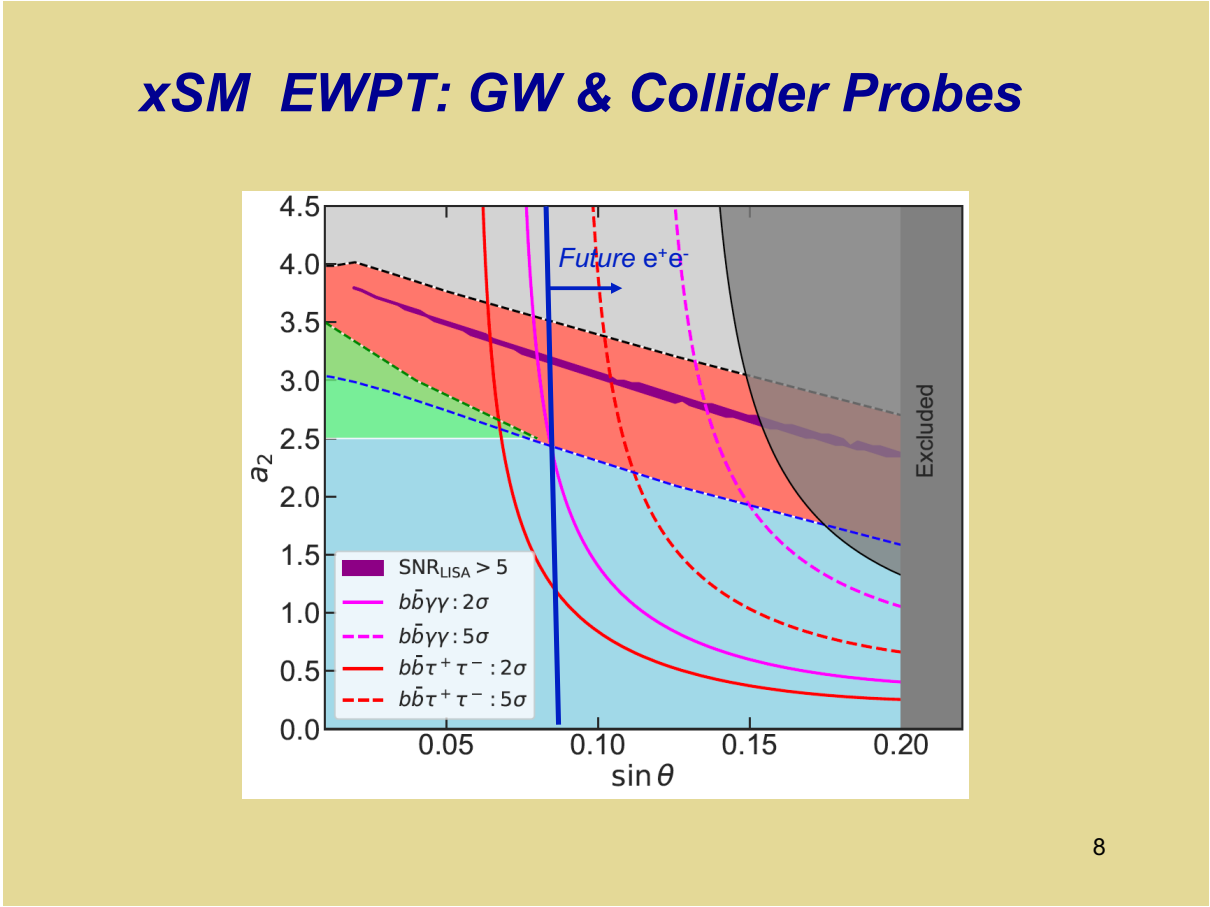

FIG. 73: GW-Collider caption goes here.

parameters are the triplet scalar mass, M_σ, and portal coupling λ_3. As indicated in Fig. 74, the associated production process $e^+e^- \to Zh$ provides a particularly powerful probe of the one-step FOEWPT region, indicated in red. Assuming a 0.5% determination of the cross section, the CEPC could probe nearly all of the one-step FOEWPT-viable parameter space.

Below, we also use the SM effective field theory (EFT) as a representative example of the type-IIB barrier to show the correlation between the Higgs trilinear coupling and the FOEWPT.

If new physics degrees of freedom are significantly heavier than the electroweak scale, they can be integrated out, allowing for an SM EFT description. In the scalar sector, a generic Higgs potential can be derived from the dimension-6 SM EFT framework, as indicated in

$$V(h) = \frac{1}{2}\mu^2 h^2 - \frac{\lambda}{4}h^4 + \frac{1}{8\Lambda^2}h^6. \tag{15}$$

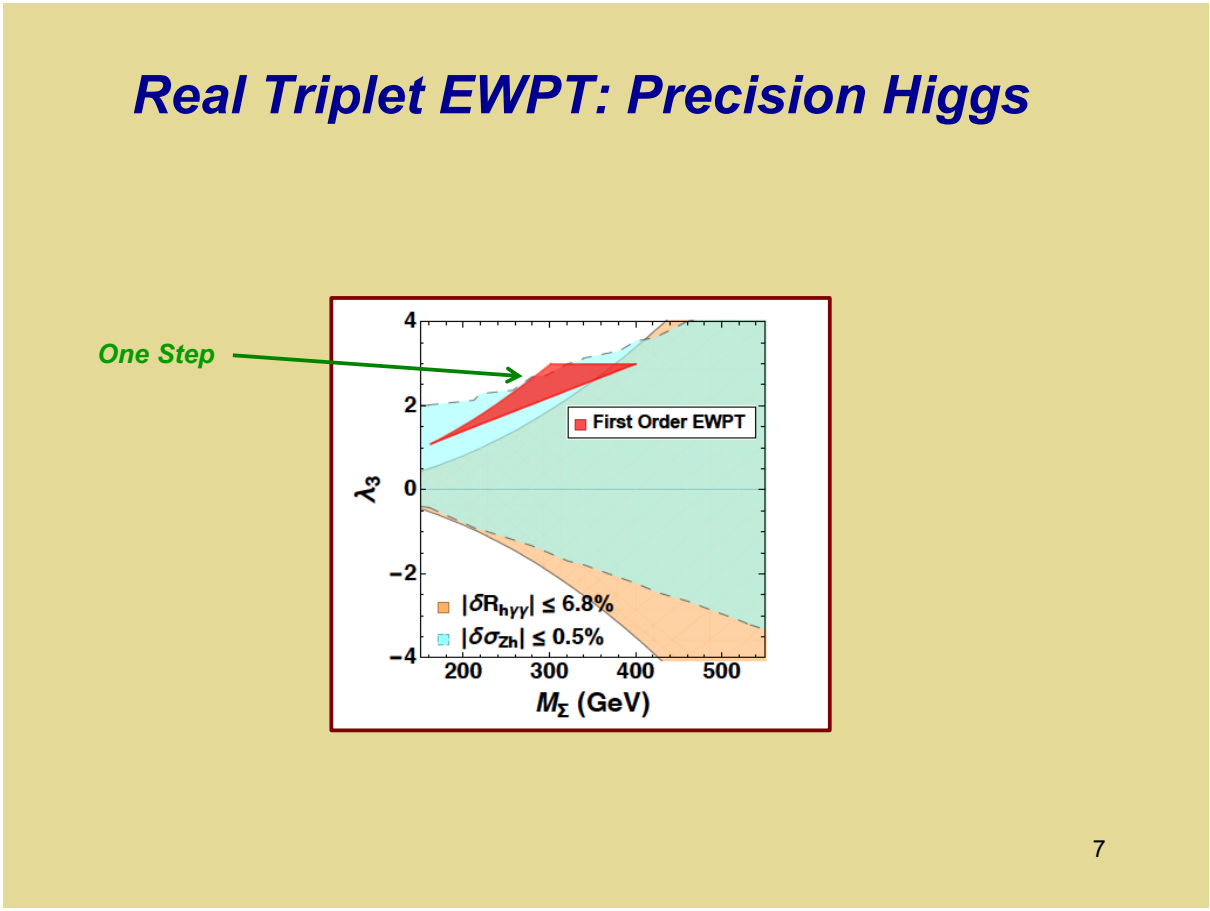

FIG. 74: Real triplet caption goes here.

This potential, involving terms up to order six in the Higgs background field h, has been associated with various new physics models such as inert singlet, doublet, triplet, or composite Higgs models. The parameters in this potential, namely μ^2, λ, and the new physics scale Λ, can be adjusted to yield an SM-like Higgs boson consistent with experimental observations and simultaneously generate a FOEWPT in the early Universe. Notably, the FOEWPT predicts a discernible deviation of the tri-linear Higgs coupling compared to the prediction of the SM, which can be tested at CEPC. At the one-loop level, the deviation of the tri-linear Higgs coupling could be obtained

$$\mathcal{L}_{hhh} = -\frac{1}{3!}\left(1+\delta_h\right) A_h h^3 \quad \text{with } \boldsymbol{\delta_h} \in (\mathbf{0.6}, \mathbf{1.5}), \tag{16}$$

which could be tested by the precise measurements of the cross section of $e^+e^- \to hZ$ at future lepton colliders, such as CEPC [475, 477, 481]. Another important prediction

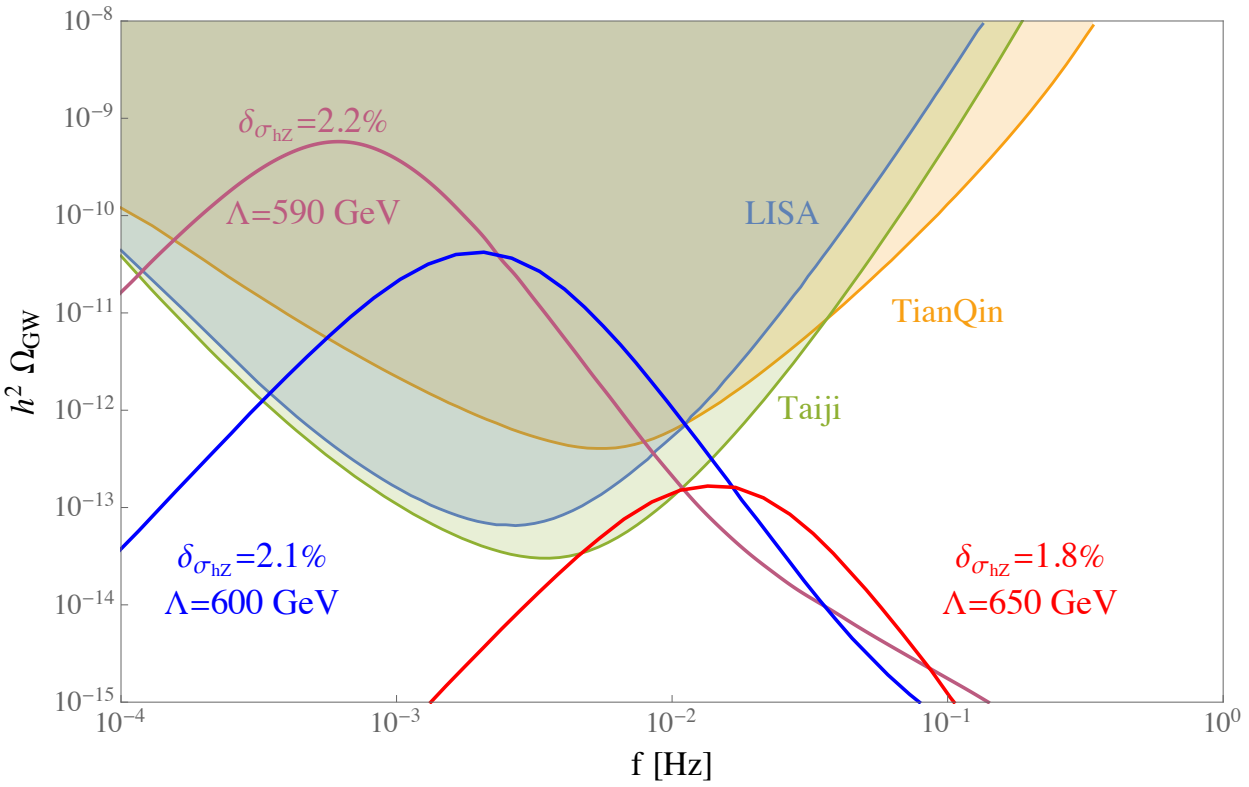

Fig. 75: General prediction of hZ cross section deviation to SM and its corresponding GW signals in the SMEFT under the condition of FOEWPT [475, 481].

of this type of new Higgs potential is the detectable phase transition GWs in near-future space-based interferometers, such as LISA, TianQin, and Taiji. As shown in Fig. 75, the collider in synergy with the GW experiments could make complementary tests on the generic Higgs potential from generic new physics models, which is also directly connected with the electroweak baryogenesis [475, 477, 481].

More precisely, one way to test the FOEWPT scenario at future lepton colliders is through the Z-boson and Higgs boson associated production (the hZ channel). The cross section of the hZ channel σ_{hZ} could be measured with an accuracy of $\mathcal{O}(0.1\%) \sim \mathcal{O}(1\%)$ at future lepton colliders. For example, an accuracy of 0.5% for σ_{hZ} measurement could be achieved at the CEPC with an integrated luminosity of 5ab^{-1}, while the ILC and FCC-ee have similar sensitivities. The operator $\mathcal{O}_6 = |H|^6$ contributes to the hZ cross section through loop corrections. Other dim-6 operators, e.g. $\mathcal{O}_H = \frac{1}{2}\left(\partial_\mu |H|^2\right)^2$ and $\mathcal{O}_T = \frac{1}{2}\left(H^\dagger \overleftrightarrow{D}_\mu H\right)^2$, contribute to the hZ production at tree-level. We define the deviation of cross section of

the hZ production, normalized to the SM cross section, as follows:

$$\delta_{\sigma_{hZ}} \equiv \frac{\sigma_{hZ}}{\sigma_{hZ}^{\rm SM}} - 1.$$

As the golden channel of Higgs factory, the hZ production rate has been calculated very precisely, including one-loop and two-loop quantum corrections. Here, we refer $\sigma_{hZ}^{\rm SM}$ to the most state-of-the-art calculation of hZ production in the SM [482, 483]. At a lepton collider with a center of mass energy $\sqrt{s} = 250$ GeV, the high dimension operators' contribution to the hZ production is approximately given by

$$\begin{aligned}\delta_{\sigma_{hZ}} \simeq (&0.26c_{WW} + 0.01c_{BB} + 0.04c_{WB} - 0.06c_H - 0.04c_T \\ &+0.74c_L^{(3)\ell} + 0.28c_{LL}^{(3)\ell} + 1.03c_L^{\ell} - 0.76c_R^{e}\Big) \times \text{TeV}^2 + 0.016\delta_h, \quad (17)\end{aligned}$$

where δ_h is the deviation of the Higgs trilinear coupling. The contribution δ_h in the hZ channel is often neglected due to its loop suppression in operator analyses. However, we argue against ignoring it in our FOEWPT study based on the following reasons. Firstly, the FOEWPT condition necessitates a significant coefficient c_6, leading to a substantial contribution of $0.96\% - 2.4\%$ to $\delta\sigma_{hZ}$. Importantly, the current experimental constraints on c_6 are practically non-existent. Secondly, compared to other dim-6 operators, the coefficients of which face stricter constraints, c_6 stands out as being less constrained. As such, the contribution δ_h cannot be disregarded.

The above study demonstrates that the possibility of FOEWPT induced by the $|H|^6$ operator remains viable and consistent with current experimental data. Our investigation into the dim-6 operators generated in three scalar extension models can be applied to a wide range of new physics models. Typically, a FOEWPT requires an Higgs portal coupling on the order of unity, and a large Higgs portal coupling may suggest a composite nature for the Higgs boson. If the Higgs boson is a pseudo-Goldstone boson originating from strong dynamics, the coefficients of dim-6 operators can be estimated using naive dimensional analysis. The estimated coefficients of dominant CP-conserving operators are presented below:

$$c_{WW} \sim c_{BB} \sim c_{WB} \sim \frac{1}{\Lambda^2} \sim \frac{1}{(4\pi f)^2}, \quad c_H \sim c_T \sim \frac{1}{f^2}, \quad c_6 \sim -\frac{\Lambda^2}{f^4} = -\frac{1}{(f/4\pi)^2}.$$

If the EW phase transition is a FOEWPT, then one needs

$$\frac{1}{(0.89\ \text{TeV})^2} < -c_6 < \frac{1}{(0.55\text{TeV})^2}, \text{ or equivalently } 6.91\ \text{TeV} < f < 11.18\ \text{TeV}.$$

The coefficients $c_{WW,BB,WB,H,T}$ are consistent with current experiments if the scale f is within the above range. Using Eq. (17), we find $\delta_{\sigma_{hZ}} \sim 0.1\%$ without the δ_h term. The FOEWPT condition requires $0.6 < \delta_h < 1.5$. Therefore, including the δ_h contribution yields $\delta_{\sigma_{hZ}}$ in the range of $(0.96 - 2.4)\%$, which could be probed at future lepton colliders, such as the CEPC.

C. Higgs exotic decay

It has been proposed that studying the exotic decay of the Higgs boson can effectively probe the FOEWPT, for two main reasons. Firstly, the Higgs boson has a very narrow width ($\Gamma_h \approx 4.07$ MeV), which makes it highly sensitive to the BSM physics. Secondly, the FOEWPT requires significant interaction between the Higgs boson and the new physics sector. Consequently, if kinematically allowed, the Higgs boson can have a large decay branching ratio to the new physics particles. Therefore, accurately determining the decay properties of the Higgs boson at the CEPC would greatly assist in testing relevant models and studying the characteristics of the electroweak phase transition. See Section IV for more new physics implications from the Higgs exotic decay, while in this subsection we focus on the relation to the FOEWPT.

This concept has been explored in research on the xSM (i.e. real singlet expansion of the SM), where the potential barrier can be thermally driven (type-I) or tree-level driven with renormalizable operators (type-IIA) [65, 484, 485]. In this scenario, when the singlet s has a $\mathbb{Z}_2$ symmetry, or has a small mixing angle θ with the Higgs boson h, the exotic decay $h \to ss$ partial width can be expressed as

$$\Gamma(h \to ss) \approx \frac{a_2^2 v_{\rm EW}^2}{32\pi m_h} \sqrt{1 - \frac{4m_s^2}{m_h^2}}, \tag{18}$$

where $m_h = 125$ GeV is the Higgs mass, m_s is the singlet mass, and a_2 is the Higgs-portal coupling of $\mathcal{L} \supset -a_2 h^2 s^2/4$. On the other hand, the necessary condition for FOPEWPT requires [485]

$$a_2 > \begin{cases} \dfrac{2m_s^2}{v_{\rm EW}^2}, & \mathbb{Z}_2\text{-odd } s; \\ \dfrac{m_s^2}{4v_{\rm EW}^2} \dfrac{\Delta}{1-\Delta}, & \text{small mixing } s, \text{ with } \Delta \gtrsim 0.6 - 0.8. \end{cases} \tag{19}$$

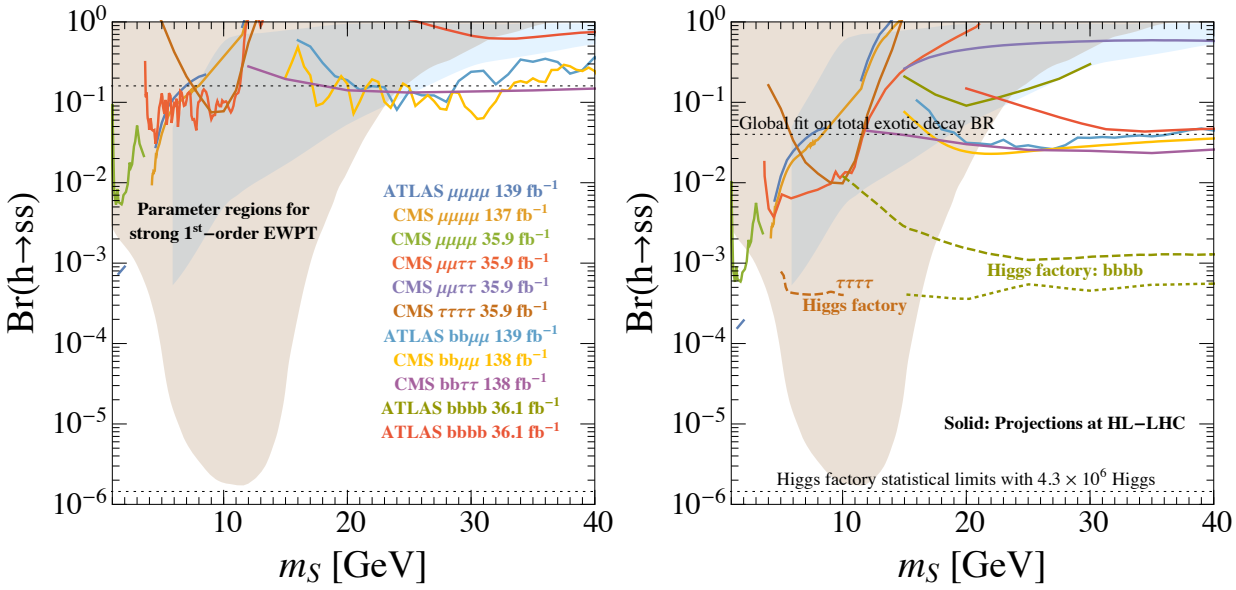

FIG. 76: Updated version of figure from Ref. [65], the Higgs exotic decay $h \to ss \to XXYY$ as a probe for the FOEWPT, where X and Y denote the SM particles. Left: the current bounds; Right: the future projections. The $s \to$ SM decays are assumed to be mediated by h-s mixing [486]. The expected HL-LHC reach for exotic decay branching ratio (4% [487]) and the statistical limit of 4.3×10^6 Higgs at future lepton colliders are shown as upper and lower horizontal dotted lines, respectively. The FOEWPT parameter space is shown in brown and light blue shadowed regions for various benchmarks [484, 485]. Dashed lines are the projected reach of future lepton colliders. See the text for the details.

This clearly shows the relation between FOEWPT and Higgs exotic decay.

For a $\mathbb{Z}_2$-odd s, the $h \to ss$ process leads to the Higgs invisible decay. If s mixes with h, then the decay chain would be $h \to ss \to XXYY$, where X and Y denote SM particles. Recent research, summarized in the left panel of Fig. 76 from Ref. [65], has constrained the FOEWPT parameter space using data from LHC searches targeting specific final states, namely $XXYY = \mu^+\mu^-\mu^+\mu^-$, $\mu^+\mu^-\tau^+\tau^-$, $\tau^+\tau^-\tau^+\tau^-$, $b\bar{b}\mu^+\mu^-$, $b\bar{b}\tau^+\tau^-$, and $b\bar{b}b\bar{b}$. The parameter space corresponds to both the spontaneous $\mathbb{Z}_2$-breaking model (brown region) and the general xSM with a mixing angle $\sin\theta = 0.01$ between the s and h scalar bosons (blue region). These bounds assume that the decays $s \to XX$ and $s \to YY$ are mediated by the mixing between the Higgs boson h and the new scalar boson s, with branching ratios obtained from Ref. [486].

Projections for the HL-LHC are presented in the right panel of Fig. 76. Although the dominant decay channel for s is $s \to b\bar{b}$ when $m_s \gtrsim 10$ GeV, the reach of the b-relevant channels is constrained due to the large multi-jet background at the LHC. However, lepton colliders like CEPC can effectively measure this channel because of the clean collision environment. For example, CEPC operating at $\sqrt{s} = 240$ GeV with an integrated luminosity of 5 ab^{-1} enables probing of the $b\bar{b}b\bar{b}$ channel through associated production $e^+e^- \to hZ$, achieving a branching ratio sensitivity down to 10^{-3}. This coverage extends to a substantial portion of the FOEWPT parameter space, as depicted by the dashed and dotted lines in the right panel of Fig. 76 (from [45] and [488], respectively). A similar sensitivity is found in an ILC-related research [489]. Additionally, CEPC exhibits improved sensitivity for the $\tau^+\tau^-\tau^+\tau^-$ channel compared to the HL-LHC, particularly for 4 GeV $\lesssim m_s \lesssim$ 10 GeV [49]. This is demonstrated by the orange dashed line in Fig. 76. By combining the $b\bar{b}b\bar{b}$ and $\tau^+\tau^-\tau^+\tau^-$ channels, CEPC has the potential to probe almost the entire FOEWPT parameter space for the general xSM with a mixing angle $\sin\theta = 0.01$.

The above discussions are based on the prompt decays of s. A small mixing angle θ for the singlet s can lead to its detection in long-lived particle (LLP) searches, as suggested in Ref. [490]. The use of LLP detectors at the LHC enables an extension of the sensitivity to FOEWPT, surpassing the coverage achievable through prompt searches for exotic Higgs decays. We expect the LLP search at future Higgs factories can also have significant capability in probing the FOEWPT scenario.

Although the discussions presented here are taking the xSM as an example, they also generally apply to other BSM models. For example, a complex scalar S^+ that is an $SU(2)_L$ singlet but carries unit charge under $U(1)_Y$, which generally exists in lepton-portal dark matter models [58, 491–493], can also induce FOEWPT, and the corresponding parameter space can be probed by the $h \to S^+S^-$ decay [58]. Furthermore, the CEPC precise measurement on the Higgs CP property also helps to identify the BSM CP-violating phase [494–497], which is another necessary condition for electroweak baryogenesis. Recently, it has been shown that the Higgs exotic decay can even probe the MeV-scale phase transition accounting for the nano-Hertz GW excess [498].

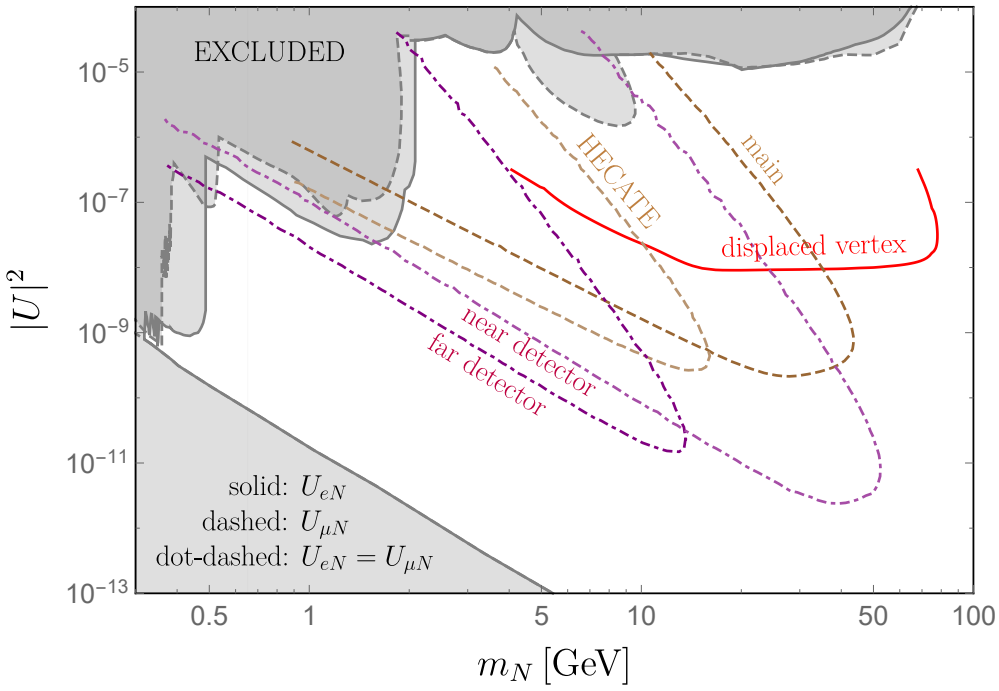

FIG. 77: Summary of prospects of heavy neutrino mass m_N and the heavy-light neutrino mixing $|U|^2$ at the CEPC. The solid lines are for U_{eN}: displaced vertex (red) [499]. The dashed lines are for $U_{\mu N}$: main detector and HECATE (darker and lighter brown) [297]. The dot-dashed lines are for $U_{eN} = U_{\mu N}$: main detector (near detector) and far detectors (lighter and darker purple) [88]. All the shaded regions are excluded by current limits, with solid for U_{eN} and dashed for $U_{\mu N}$ [500].

X. NEUTRINO PHYSICS (BHUPAL, WEI, YONGCHAO)

The observation of neutrino oscillations [501, 502] provides the first (and so far only) laboratory evidence for BSM physics. Within the SM, the neutrinos are exactly massless to all orders in perturbation theory, and even non-perturbative sphaleron effects cannot induce neutrino mass due to the accidental global $B - L$ symmetry. Therefore, studying neutrino mass generation mechanisms could pave the way for the discovery of the underlying BSM physics.

In collider environments, neutrinos simply behave as missing energy and are undetectable by themselves. Nevertheless, the first direct observation of neutrino interactions at a particle collider experiment was recently achieved by the FASER collaboration [503]. However, any nonstandard neutrino interaction effect is yet to be seen. In this section, we will outline

several possible BSM signals associated with the neutrino sector that could potentially be observable at CEPC. We will also discuss their far-reaching implications for other outstanding puzzles of the SM, such as DM and baryogenesis. For reviews of neutrino physics at colliders and complementarity with other observables, see e.g. Refs. [504, 505].

Perhaps the most striking collider signals associated with neutrino mass generation mechanism are the lepton-number violating signals with same-sign charged lepton pairs, e.g. the Keung-Senjanović process $pp \to \ell^\pm\ell^\pm jj$ for hadron colliders [506], which is the high-energy analog of the neutrinoless double beta decay ($0\nu\beta\beta$) process, but now with any lepton flavor. This is generically expected in theories of Majorana neutrinos, when we parametrize the $(B-L)$-breaking effects through an effective dimension-5 Weinberg operator $LLHH/\Lambda$ [507]. A well-known UV-complete example is the type-I seesaw mechanism [508–513] with heavy right-handed neutrinos (RHNs). This can be realized by just adding the Majorana RHNs to the SM particle content, or in more natural ways by extending the SM gauge group to higher gauge groups like $U(1)_{B-L}$ [514–516], $SU(2)_L \times SU(2)_R \times U(1)_{B-L}$ [517–519] or $SO(10)$ [520, 521], where the RHNs are necessary for anomaly cancelation. Thus ensues a very rich collider phenomenology of the RHNs [504], if the seesaw scale happens to be around the electroweak scale. Here we will only cover some aspects of RHN phenomenology directly relevant to CEPC.

Other simple well-motivated tree-level seesaw models include: the type-II seesaw where a left-handed triplet Δ_L is introduced to realize the seesaw framework [513, 522–526]; the type-III seesaw which is similar to the type-I seesaw, with the singlet fermions N replaced by triplet fermions [527, 528]. The tiny neutrino masses can also radiatively generated at loop levels, e.g. in the Zee model [529] and Ma model [136] at 1-loop level and the Zee-Babu model [530, 531] at 2-loop level, where some beyond SM particles, including DM partcles in some models, are introduced to generate the neutrino masses. A comprehensive review of the tree and loop level of neutrino models can be found e.g. in Ref. [532]. The phenomenology of the neutrino models above are closely correlated with the high-precision low-energy physics, e.g. the lepton number violating neutrinoless double-beta decays ($0\nu\beta\beta$) and the parity-violating MOLLER experiment [533–546].

In this section we focus mainly on the prospects of neutrino relevant physics at the CEPC. Subsection X A is on the prospects of heavy neutrino N at the CEPC. The heavy neutrino N can be produced at high-energy lepton colliders via the process $e^+e^- \to \nu N$ through

the heavy-light neutrino mixing $U_{\alpha N}$ with the flavor index $\alpha = e, \mu, \tau$, and tends to be long-lived at the CEPC for its mass m_N below tens of GeV. The prospects of m_N and $|U|^2$ at CEPC are collected in Fig. 77. As clearly seen in this figure, the mixing angle $|U|^2$ can be probed down to $\mathcal{O}(10^{-11})$ at the CEPC. The heavy neutrino can be pair produced from SM Higgs decay, i.e. $h \to NN$. It is found that the corresponding branching fraction can be probed up to $\mathcal{O}(10^{-4})$ at the CEPC at the 2σ C.L. (cf. Fig. 82) [547], and the sensitivity of heavy-light neutrino mixing angle $|U|^2$ can be significantly improved to $\mathcal{O}(10^{-14})$ in this channel (cf. Fig. 83) [548]. In some scenarios, N can also be produced at the lepton colliders via other BSM particles, e.g. the Z' boson in $U(1)$ models or the $SU(2)_R$-breaking scalar in the LRSM (cf. Figs. 84 and 85) [549, 550]. The prospects of non-standard neutrino interactions (NSIs) is presented in Subsection X B. It is found that such interactions can be probed as small as 0.002 (cf. Fig. 86) [551]. The active-sterile neutrino transition magnetic moments can be probed up to $\mathcal{O}(10^{-7}\ \text{GeV}^{-1})$, as shown in Fig. 87 of Section X C [552]. The sensitivities of neutral and doubly-charged scalars in seesaw models is given in Section X D. The Yukawa coupling of neutral scalar H to charged leptons can be probed up to $\mathcal{O}(10^{-4})$ at the CEPC in the on-shell channels (cf. Fig. 88), while the neutral and doubly-charged scalar masses can be probed up to the few-TeV range in the off-shell channels (cf. Figs. 89 and 90) [553, 554]. The connection of neutrino physics to DM and baryon asymmetry in the Universe is investigated in Section X E. It is found that the CEPC can probe wide region of m_N and $|U|^2$ which is consistent with seesaw mechanism and leptogenesis (cf. Fig. 91) [555].

A. Prospects of heavy neutrinos

1. *Heavy neutrinos at the main detector*

In Ref. [499], the authors investigate the sensitivity of future lepton colliders to long-lived heavy (almost sterile) neutrinos N with electroweak scale masses and detectable time of flight, via displaced vertex signatures. The theoretical framework is an explicit low-scale seesaw, the Symmetry Protected Seesaw Scenario (SPSS) model [556]. The signal process is $e^-e^+ \to \nu N$ running at the Z-pole and $\sqrt{s} = 240$ GeV at the CEPC. The ILC's Silicon Detector (SiD) is used as the benchmark detector at future lepton colliders. The background processes are analyzed, and the heavy neutrino N decays with a vertex displacement between

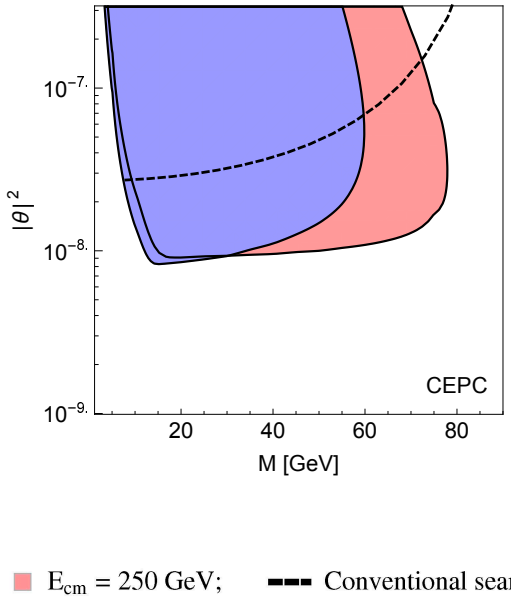

FIG. 78: Sensitivity at the 2σ C.L. for heavy neutrino searches via displaced vertices at the CEPC, assuming 100% signal efficiency. The sensitivities for $E_{\rm cm} \neq m_Z$ are understood for $|\theta|^2 = |\theta_e|^2$ (with θ_μ, $\theta_\tau = 0$). The black dashed lines denote the conventional Z pole searches [556]. Taken from Ref. [499].

10 μm and 249 cm (the outer radius of the HCAL) are considered to be free of backgrounds and detectable by SiD. Sensitivity results of m_N and the squared mixing angle $|\theta|^2$ of heavy neutrino with the active neutrinos at the CEPC are presented in terms of 4-signal-event contour curves in Fig. 78, where the CEPC are assumed to be running with the integrated luminosity of 0.1 ab^{-1} at $\sqrt{s} = 90$ GeV and 5 ab^{-1} at $\sqrt{s} = 240$ GeV, respectively. If the luminosities are as high as the nominal ones, i.e. 100 ab^{-1} at the Z-pole and 20 ab^{-1} at 240 GeV, it is expected that the corresponding sensitivities of $|\theta|^2$ in Fig. 78 will be improved by roughly a factor of $100/0.1 = 10^3$ and $20/5 = 4$, respectively.

There are also some other researches of heavy neutrinos N performing as displaced vertex at future lepton colliders. Here we list some of them. Ref. [557] studies heavy neutrinos N at future lepton colliders in the framework of the neutrino-extended Standard Model Effective Field Theory (νSMEFT). The study focuses on four representative running modes: the FCC-ee with $\sqrt{s} = 90$ and 240 GeV, the CLIC with $\sqrt{s} = 3$ TeV, and a representative muon collider with $\sqrt{s} = 3$ TeV. With dimension-six EFT operators included, additional

production and decay modes for the heavy neutrinos are present besides those arising from the mixing with the active neutrinos. The authors consider single- and pair-production of N via four-fermion operators, and the most relevant additional decay modes are identified to be $N \to \nu\gamma$ when $m_N \lesssim 15$ GeV and $N \to 3f$ for larger masses, where $3f$ denotes various possible three-fermion combinations. Depending on the heavy neutrino mass and the cutoff scale Λ at which the EFT breaks down, the heavy neutrinos N can decay either promptly or with a macroscopic distance, or appears stable at the detector level. For the displaced vertex searches, the decay vertex is required to lie between 1 cm and 100 cm from the primary vertex. The background is assumed to be negligible, and in both the two decay modes $N \to \nu\gamma,\ 3f$, the cutoff scaled can be probed up to roughly 20 TeV at the FCC-ee 240 GeV with an integrated luminosity of 5 ab^{-1}.

Similarly, Ref. [558] focuses on long-lived heavy neutrino via displaced vertex signature at the FCC-ee running at the Z-pole. This study assumes that only one Majorana heavy neutrino N mixing with the electron neutrino. The signal process is $e^-e^+ \to \nu N \to \nu(e^+e^-\nu)$, and the background processes include $Z \to e^+e^-, \tau^+\tau^-, b\bar{b}, c\bar{c}, uds$. For LLPs decaying at a displaced vertex, the transverse impact parameter d_0 of the displaced particles can be used as a complementary variable to the decay length. d_0 is given as the distance from the beam line to the projected back-trace of the displaced tracks in the transverse plane. LLPs' decay products are expected to exhibit larger values of d_0. This study selects long-lived heavy neutrinos by requiring both final-state electrons to have $d_0 > 0.5$ mm. Assuming Z-pole running with an integrated luminosity of 150 ab^{-1}, it is found that the squared mixing $|V_{eN}|^2$ can be probed up to $\mathcal{O}(10^{-8})$ for a heavy neutrino with mass of $\mathcal{O}(10$ GeV$)$.

Ref. [559] investigates methods to observe lepton number violation (LNV) and distinguish Dirac and Majorana heavy neutrinos N at future lepton colliders. These methods include the angular distribution and spectrum of the heavy neutrino's decay products as well as their lifetime. The latter exploits the fact that the total decay width of N differs by a factor of two between the Majorana and Dirac cases, leading to a decay length λ differing in displaced vertex searches at colliders. Therefore, according to Eq. (10), the decay probabilities inside the same detector should be different between the Majorana and Dirac cases as well. This implies different numbers of observed signal events in displaced-vertex searches, and can be used to distinguish Dirac and Majorana heavy neutrinos. The analytic estimates for the number of events and sensitivity regions during the Z-pole run for both Majorana and Dirac

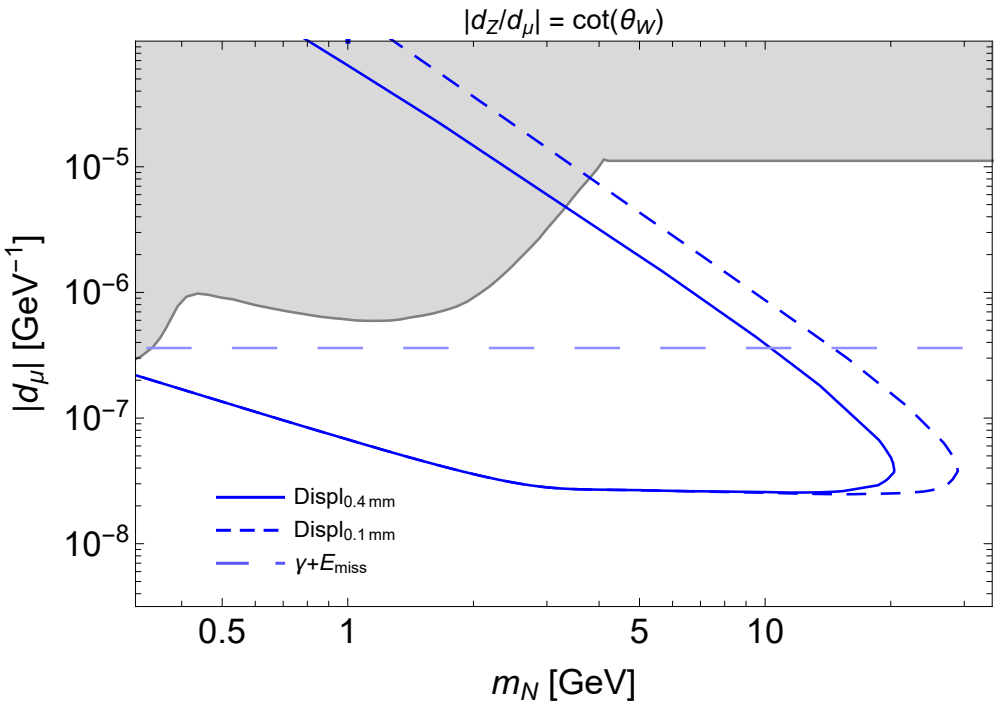

FIG. 79: The potential of FCC-ee to m_N and the dipole coupling $|d_\mu|$ at the 90% C.L. at the Z-pole. The solid and short-dashed blue lines correspond respectively to the vertex transverse displacement of 0.4 mm and 0.1 mm, and the long-dashed light blue line denotes the sensitivity corresponding to the γ+missing energy signature. Taken from Ref. [560].

HNLs are also present in this study.

Ref. [560] studies the potential of future colliders to explore the parameter space of heavy neutrinos through the dipole portal. This work considers various signatures for the HNLs including missing energy and displaced decays, and discusses the complementarity between the hadron and lepton colliders. At lepton colliders, the signal process is $e^-e^+ \to Z \to \nu N, N \to \nu e^- e^+, \nu\gamma$ at $\sqrt{s} = 91.2$ GeV. For the displaced vertex searches, the decay volume is considered to be the Innovative Detector for Electron–positron Accelerators (IDEA), which is a cylinder with radius $r = 4.5$ m and longitudinal size $L = 11$ m [561]. For the e^-e^+ final state, the background processes include $Z \to e^-e^+ +$ inv., $e^-e^+ \to e^-e^+\nu\bar{\nu}$. To reject the background by exploiting the long-lived signature of N, the following two choices of a displacement cut are applied: $r_{\mathrm{displ}} > 0.4$ mm and 0.1 mm, depending on the spatial resolution of the tracker. Here r_{displ} is the vertex transverse displacement from the collision point. Fig. 79 shows the FCC-ee potential to the parameter space of the heavy neutrino mass m_N and the dipole coupling $|d_\mu|$, assuming 5×10^{12} Z-bosons produced in total corresponding

to a luminosity of 150 ab^{-1}. Here the active neutrino flavor has been chosen to be muonic, which applies also to the electron and tauon flavors, as the FCC-ee sensitivity is flavor universal. Sensitivity reaches of the HL-LHC and FCC-hh are also given for comparison purpose in this work.

2. Heavy neutrinos at far detectors

Ref. [88] considers Z boson decays to an active neutrino and a long-lived heavy neutrino N, $Z \to \nu N$, at $\sqrt{s} = 91.2$ GeV. In the analysis, the total number of the Z bosons produced at the CEPC is specified as $N_Z^{\rm CEPC} = 7.0\times10^{11}$ corresponding to a total integrated luminosity of $\mathcal{L}_Z^{\rm CEPC} = 16$ ab^{-1}, while $N_Z^{\rm FCC-ee} = 5.0 \times 10^{12}$ corresponding to $\mathcal{L}_Z^{\rm FCC\text{-}ee} = 150$ ab^{-1}. The background is assumed to be negligible. Sensitivity results at the 95% C.L. in terms of 3-signal-event contour curves are presented in Fig. 80, reproduced from Ref. [88]. The sensitivity reaches of the CEPC/FCC-ee's far detectors FD1, FD3 and FD6 in the plane of m_N and $|V_{\alpha N}|^2$ (with $\alpha = e$ or μ) are shown in the upper panel, in comparison with the current constraints in gray and prospects at the main detector (near detector, abbreviated as ND) and other experiments including the LHC FDs. The luminosity has taken to be 150 ab^{-1}. The sensitivities of the main detector (near detector, abbreviated as ND), FD3 and FD6 with three different luminosities of $\mathcal{L} = 16$, 150 and 750 ab^{-1} are presented in the lower panel. The prospects for the case of heavy neutrino with equal mixings with all three active neutrino generations, i.e. $|V_{eN}|^2 = |V_{\mu N}|^2 = |V_{\tau N}|^2$, are shown as the dashed lines in the lower panel, with $\mathcal{L}_Z = 750$ ab^{-1}. It is clear that the main detector and FD6 at the CEPC or FCC-ee may probe the type-I seesaw limits on $|V_{\alpha N}|^2$, if m_N lies between 10 GeV and 60 GeV.

We note that if high-precision timing information ($\mathcal{O}$(picosecond)) can be obtained, it is possible to correlate the activities at the MD and the FD that stem from the same collision event at the IP. Achieving this event correlation would allow for observing lepton-number-violating (LNV) processes that could arise, e.g. from long-lived HNLs. Ref. [296], for instance, shows its feasibility with the proposed LHC far detectors; if observed, such LNV processes can pin down the Majorana nature of the neutrinos. In principle, similar strategies can also be implemented at high-energy e^+e^- colliders.

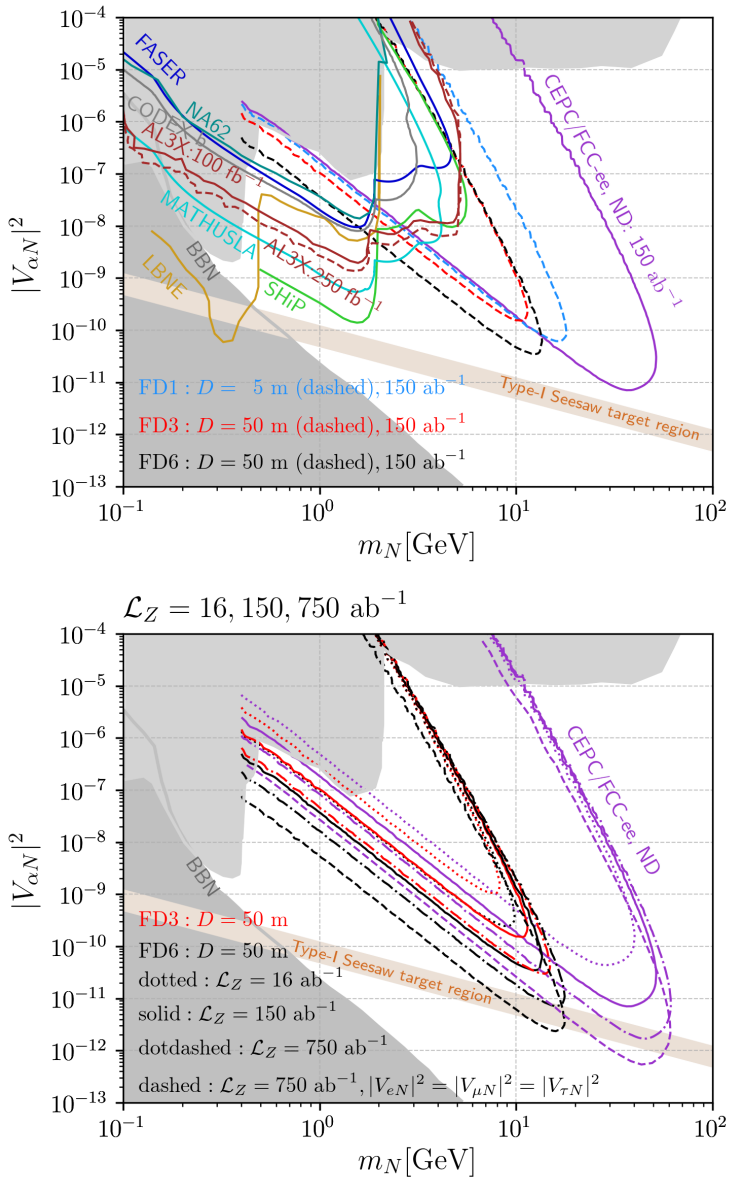

FIG. 80: *Upper panel*: Sensitivity reaches of the CEPC/FCC-ee's far detectors FD1, FD3, FD6, in comparison with prospects at the main detector (near detector, abbreviated as ND) and other experiments. *Lower panel*: Sensitivity reaches of ND, FD3 and FD6 at the CEPC/FCC-ee with three different integrated luminosities $\mathcal{L}_Z = 16$, 150 and 750 fb^{-1}. The gray regions are excluded by current constraints. Taken from Ref. [88].

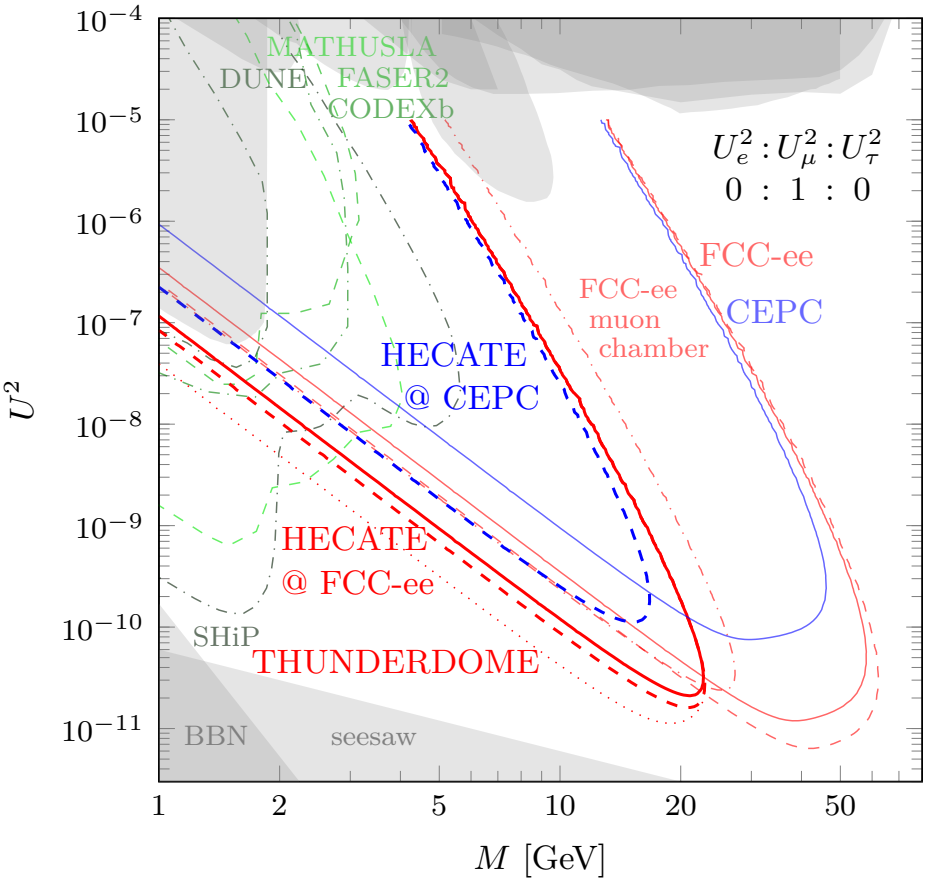

FIG. 81: Sensitivities for nine signal events that can be achieved at FCC-ee (red) and CEPC (blue). The faint and thick curves are the prospects for the main detectors and HECATE, respectively. The shaded regions are excluded by current experiments, and the expected sensitivities of selected other experiments are indicated by the green curves. See the text for more details. Taken from Ref. [297].

Ref. [297] proposes to install a HErmetic CAvern TrackEr (HECATE) at the CEPC and FCC-ee. The HECATE detector would consist of resistive plate chambers (RPCs) or scintillator plates, constructed from extruded scintillating bars, located around the cavern walls and forming a 4π detector. In order to obtain timing information and to distinguish particles from cosmic background, the HECATE detector should have at least two layers of detector material separated by a sizable distance. For reliable tracking, at least four layers, along with a smaller size or optimized geometry of the detector plates, would be required.

This study estimates the HECATE sensitivity for long-lived heavy neutrino produced from Z boson decays $Z \to \nu N$ at $\sqrt{s} = 91.2$ GeV. Similar to Eq. (10), in their analyses, the

decay probability of long-lived heavy neutrino inside the detector's fiducial volume is related to $\exp\{-l_0/\lambda_N\} - \exp\{-l_1/\lambda_N\}$. The total number of Z bosons are taken to be 3.5×10^{11} and 2.5×10^{12} at CEPC and FCC-ee, respectively. We extract Fig. 81 from Ref. [297] which shows the isocurve for nine signal events with the HECATE at CEPC and FCC-ee, which are shown respectively as the blue and red lines. Two setups of HECATE are investigated with $l_0 = 4$ m and $l_1 = 15$ m (solid) or 25 m (dashed). Sensitivities are also compared with multiple other experiments in this study. The faint solid curves show the main detector sensitivity ($l_0 = 5$ mm, $l_1 = 1.22$ m). The faint dash-dotted curve indicates the additional gain if the muon chambers are used at the FCC-ee ($l_0 = 1.22$ m, $l_1 = 4$ m). The thick curves show the sensitivity of HECATE with $l_0 = 4$ m, $l_1 = 15$ m (solid) and $l_0 = 4$ m, $l_1 = 25$ m (dashed), respectively. Finally, the faint dashed red line shows the FCC-ee main detector sensitivity with 5×10^{12} Z bosons, corresponding to the luminosity at two IPs. The difference of the FCC-ee and CEPC sensitivities is mainly due to the larger luminosity at the FCC-ee. For comparison we indicate the expected sensitivity of selected other experiments with the different green curves as indicated in the plot [270, 271, 288, 562, 563]. The gray areas in the upper part of the plot show the region excluded by past experiments [564–572], while the grey areas at the bottom mark the regions that are disfavoured by BBN [573] and neutrino oscillation data in the Neutrino Minimal Standard Model (νMSM, labelled as "seesaw" in the figure) [574, 575].

3. SM Higgs decay $h \to NN$

CEPC can search for heavy N within the reach of its center of mass energy. There have been studies on the weak single N production at CEPC in the process $e^-e^+ \to \nu N$ for center-of-mass energy $\sqrt{s} = 240$ GeV [576], and on high luminosity Z-pole running mode [577, 578]. As N has a large Majorana mass, lepton number violation occurs in N decay. Same-sign, same flavor dileptons, and a reconstructable N mass peak of final state lepton-jet system are the 'smoking gun' signals for heavy N search [579]. CEPC is designed to yield ∼4M Higgs events. The high identification efficiency for soft leptons and low hadronic background at the CEPC offers a clean search opportunity for $h \to NN$. The dominant Higgs production channel at CEPC is $e^+e^- \to Zh$. The associated Z complicates the signal and background analysis, as the Z boson's decay products can be confused with

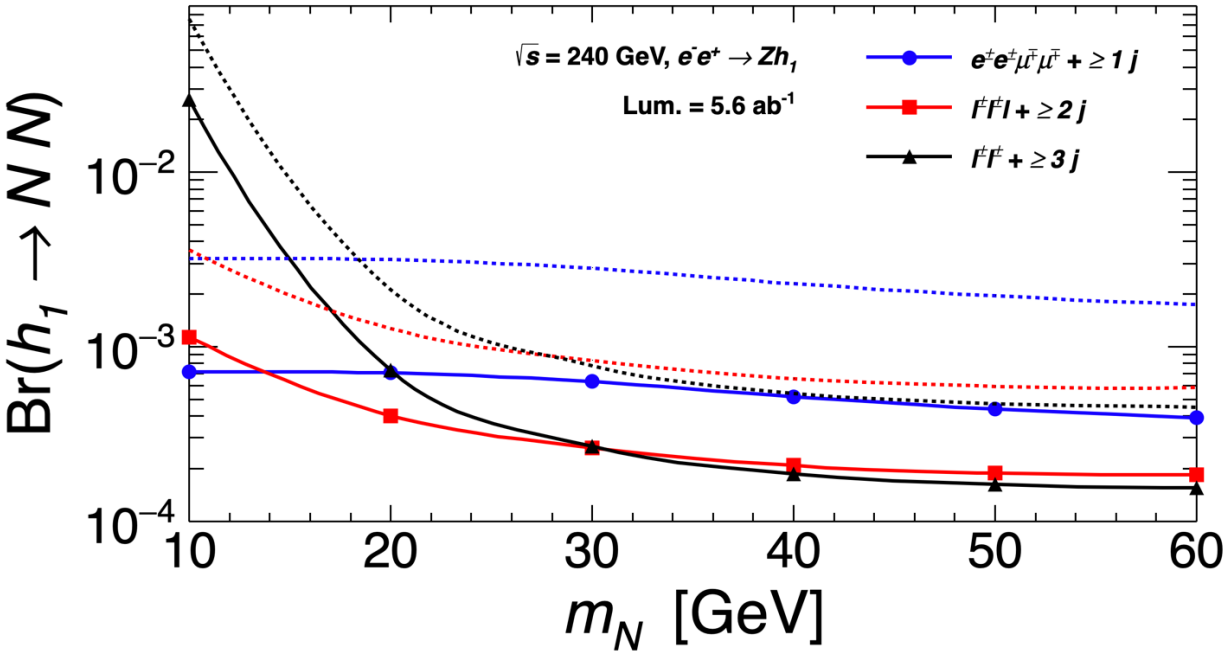

FIG. 82: The projected CEPC sensitivities, 2σ (solid) and 5σ (dashed), to the decay branching ratio of $h \to NN$ for 2-4ℓ channels. Sensitivities at 240 GeV and 5.6 ab^{-1} are comparable to HL-LHC projections [580]. Adapted from Ref. [547].

those from heavy N decay. On the other hand, with an extra Z boson, the SM backgrounds can also be suppressed by requiring one more weak vertex. The leading SM backgrounds are from multi-tau production with one or two associated weak vector bosons ($V = W, Z$), e.g. $4\tau, 4\tau V, 2\tau 2\ell V$, etc., in which non-isolated and missing leptons can lead to same-sign same-flavor lepton pairs.

SM background analysis of the n-lepton ($n \geq 2$) channels with at least one set of same-sign dileptons [547] shows that the semileptonic heavy N decay, requiring only one same-sign lepton pair, gives higher sensitivity than fully leptonic N decay channels. Jet and lepton number counting plays an essential role in removing the SM background contamination. Leptonic decay of the associated Z boson also leads to a same-sign same-flavor trilepton signal. For CEPC 240 GeV @ 5.6 ab^{-1} luminosity, multi-lepton rare decay search for $h \to NN$ will be sensitive to Higgs-BSM scalar mixing angle up to around $|\sin\alpha|^2 \leq 10^{-4}$. The reaches on multi-lepton Higgs rare decay branching ratios are shown in Fig. 82.

In the meantime, $h \to NN$ channel can also be used to test the origin of neutrino masses, i.e. seesaw mechanisms. In Ref. [548], pair-produced long-lived N from Higgs decays is

searched at colliders, including CEPC and ILC, for the $U(1)_{B-L}$ model. At the CEPC, with a center-of-mass energy $\sqrt{s} = 250$ GeV, the dominant Higgs production process is Higgs-Strahlung, $e^+e^- \to Z^* \to Zh$, which cross section is $\sigma \sim 240$ fb for $\sqrt{s} = 250$ GeV, and reduced by the Higgs-BSM mixing angle, $\propto \cos^2\alpha$. Comparing to the LHC, the Higgs production is about 200 times smaller, but CEPC has larger luminosity and clean background. The SM Higgs can decay into a pair of heavy N, with

$$\mathrm{Br}(h \to NN) = \frac{\Gamma(h \to NN)}{\Gamma(h)_{\mathrm{SM}} \cos\alpha^2 + \Gamma(h \to NN)}, \tag{20}$$

where $\Gamma(h)_{\mathrm{SM}} \approx 4.2 \times 10^{-3}$ GeV is the total decay width of the SM Higgs, and $\tilde{x}$ is the VEV of the $B - L$ scalar, and

$$\Gamma(h \to NN) = \frac{2}{3}\sin^2\alpha \frac{M_N^2}{\tilde{x}^2}\frac{m_h}{8\pi}\left(1 - \frac{4M_N^2}{m_h^2}\right)^{3/2}. \tag{21}$$

Hence, the cross section of pair-produced heavy N at the CEPC, from ($e^+e^- \to Z \to Zh \to Z + NN$) dependent both on M_N and $\sin\alpha$, when we fix $\tilde{x} = 3.75$ TeV. It is found that the production cross section peaks where $M_N \approx 40$ GeV, and can reach $\mathcal{O}(0.1)$ fb, when the Higgs-BSM mixing is at the current upper limits, $\sin\alpha \sim 0.3$ [581].

The heavy N, can subsequently decay into SM states, via the active-sterile mixing. Giving our interested parameter space, $M_N \lesssim 60$ GeV, $|V_{\ell N}|^2 \sim m_\nu/M_N \approx 10^{-12}$, and N mainly decays via three-body processes such as $N \to \ell^\pm q\bar{q}$ and $N \to \ell^+\ell^-\nu$. Hence, N can be long-lived, and the resulting decay length for $M_N \lesssim m_Z$ can be expressed as

$$L_N \approx 0.025 \text{ m} \cdot \left(\frac{10^{-12}}{|V_{\ell N}|^2}\right) \cdot \left(\frac{100 \text{ GeV}}{M_N}\right)^5. \tag{22}$$

Therefore, the N can possesses decay length $\mathcal{O}(0.1)$ m, leading to displaced vertex signatures at the CEPC. To estimate the events of displaced vertex signals, we simplify the geometry and detector response of the CEPC detector. In Table XII, we show the size and resolution of the CEPC detector [5], comparing to the ILC [250, 582]. Here, σ_d^t is the resolution of the detector in transverse direction, and d_0 is the transverse distance between the heavy N and lepton in the final states, such as $|d_0| = |xp_y - yp_x|/p_T$, where x and y are the position where the heavy N decayed, and p_x, p_y, p_T are the components of momentum and transverse momentum of the final particles ℓ, and L_{xy} and L_z are the transverse and longitudinal decay lengths of the HNLs, respectively. The Region 1 and 2, are approximated the tracker and muon systems of the corresponding detector. Giving they can detect muons better, for the

Region	Inner Radius	Outer Radius	z-Extent	$\lvert d_0\rvert/\sigma_d^t$	σ_d^t
ILC Region 1	22	120	152	12	0.002
ILC Region 2	120	330	300	4	2
CEPC Region 1	15	180	240	12	0.007
CEPC Region 2	180	440	400	4	2

TABLE XII: Parameters of simplified detector geometries representing future detectors, namely ILC [250, 582], CEPC [5]. All length units are in cm.

later results, we take $\ell = \mu$. For heavy N, if it is decayed either inside the Region 1 or 2, and $|d_0|/\sigma_d^t$ is larger than required, we assume it can be detected by the detector with 100% efficiency.

With such long-lived N, we assume the background can be negligible, so the sensitivity can be estimated by requiring the number of signal events, $N_S \gtrsim 3$, at 95% CL. And the results of CEPC with 20 ab^{-1} integrated luminosity, is shown in Fig. 83. Assuming no observation of a single displaced vertex, the excluded regions in the $(M_N, V_{\mu N})$ parameter space at 95% CL is shown. The grey band indicates the parameter region where a light neutrino mass in the interesting range is generated, 0.01 eV $< m_\nu = |V_{\mu N}|^2 m_N <$ 0.3 eV. From the figure, we find the sensitivity region roughly tracks where decay length $L_N \sim \mathcal{O}(1)$ m. CEPC can reach the parameter space where type-I seesaw predicts, and even below it. Therefore, we have shown that CEPC have potential in revealing the nature of neutrino masses. However, such statement rely on the existence of significant Higgs-BSM mixing angle, which might be excluded by the precision measurement of Higgs signal rates at the CEPC [583].

4. *Prospects of heavy neutrinos in $U(1)$ models*

Under the general $U(1)$ framework, a neutral BSM gauge boson (Z') is evolved. Such a Z' gauge boson can be tested at the high energy experiments. We find that if e^+e^- colliders are built then we can study forward-backward (FB), left-right (LR) and left-right forward-backward (LR-FB) asymmetries at different center of mass energies [584]. The Z' in this scenario can directly interact with the right-handed neutrinos (RHNs). Hence we can study

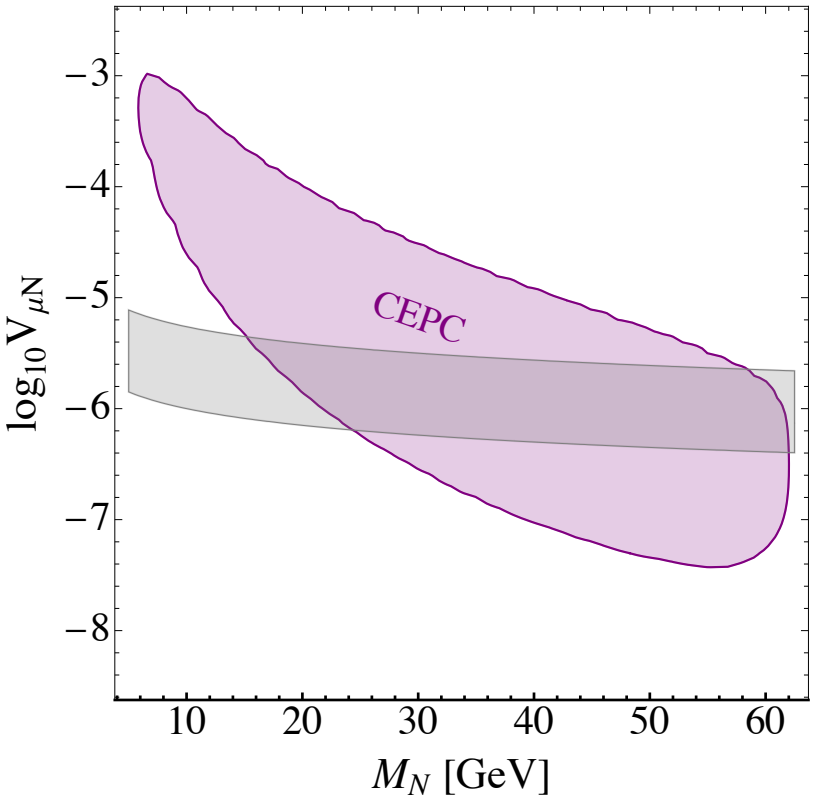

FIG. 83: Excluded regions in the $(M_N, V_{\mu N})$ parameter space at 95% CL assuming no observation of a single displaced vertex for the 20 ab^{-1} CEPC (purple). The grey band indicates the parameter region where a light neutrino mass in the interesting range is generated, 0.01 eV $< m_\nu = |V_{\mu N}|^2 m_N <$ 0.3 eV. We fix the Higgs-BSM mixing $\sin\alpha = 0.3$. Adapted from Ref. [548].

the pair production of RHNs from the Z' at the LHC and other proton-proton colliders at $\sqrt{s} = 27$ TeV and 100 TeV from prompt and displaced scenarios after the decay of RHNs. We find that the RHNs pair production from the Z' can be enhanced at $x_H = -1.2$ which is the general $U(1)$ charge of SM Higgs doublet [549, 585]. We find the branching ratio of Z' into a pair of RHNs (BR($Z' \to 2N$)) is nearly one order of magnitude larger than the branching ratio of Z' into lepton doublets (BR($Z' \to 2\ell$)). We produce the RHNs from Z' at the e^-e^+ collider following

$$\sigma(e^+e^- \to Z'^* \to N_i N_i) \simeq \left(\frac{g'^4}{{M_{Z'}}^4}\right) \frac{s(8 + 12x_H + 5x_H^2)}{192\pi} \left(1 - \frac{4M_N^2}{s}\right)^{3/2}. \tag{23}$$

Studying the signal of same sign dilepton plus four jets and corresponding SM backgrounds, we show the $2-\sigma$ contours on the $M_{Z'} - M_N$ plane in Fig. 84 for $x_H = -2$. The luminosities

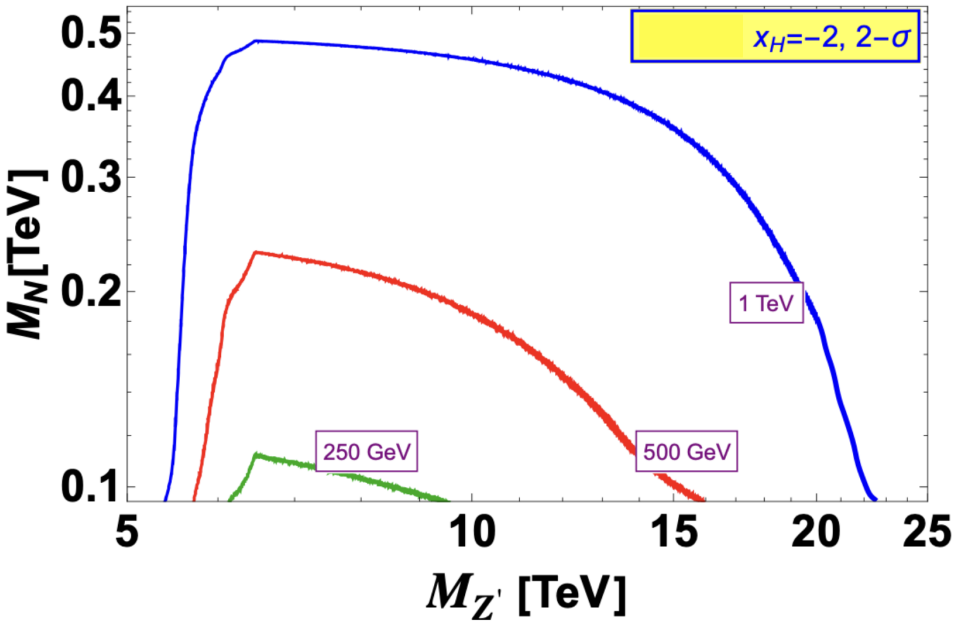

FIG. 84: 2-σ contour of the $M_N - M_{Z'}$ plane at the electron-positron colliders at different center of mass energies studying same-sign dilepton plus four jet final states. Taken from Ref. [549]

are respectively 2 ab^{-1}, 4 ab^{-1} and 8 ab^{-1} for 250 GeV, 500 GeV and 1 TeV. The contours for other values of x_H can be found in Ref. [549].

5. *Prospects of heavy neutrinos in the LRSM*

The production of N in the minimal left-right symmetric model (LRSM) [518, 519, 586] can be sizeable at lepton colliders, even for relatively high W_R mass and small Higgs mixing. In particular, the neutral component Δ_0 of the right-handed triplet Δ_R couples directly with the heavy neutrinos, and could mix with the SM Higgs. One of the resultant physical scalars, Δ, is predominantly from Δ_0. For $\sqrt{s} < \mathcal{O}(100)$ GeV, the dominant production of Δ at e^+e^- colliders occurs in the associated ΔZ production, and the corresponding leading-order cross section is

$$\sigma(e^+e^- \to \Delta Z) = s_\theta^2 \frac{G_F^2 M_Z^4}{96\pi s} \left(\hat{v}_e^2 + \hat{a}_e^2\right) \sqrt{\lambda} \frac{\lambda + 12\left(M_Z^2/s\right)}{1 - \left(M_Z^2/s\right)^2}\,, \tag{24}$$

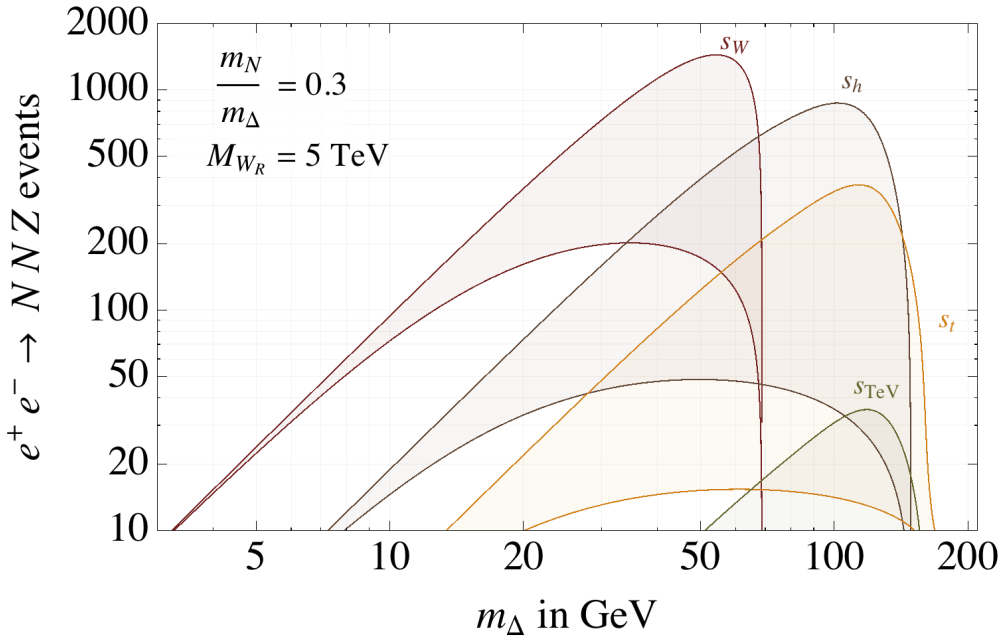

FIG. 85: Signal event rates for $e^+e^- \to ZNN$ productions at lepton colliders for different $\sqrt{s}$, with a universal luminosity of $\mathcal{L} = 1$ ab^{-1} and $m_N = m_\Delta/3$. The shaded regions cover the range of $\sin\theta \in (0.01, 0.1)$. Figure from Ref. [550].

where $\lambda = (1 - m_h^2/s - M_Z^2/s)^2 - 4m_h^2 M_Z^2/s^2$, $\hat{v}_e = -1$, $\hat{a}_e = -1 + 4s_w^2$, and the $\Delta\nu\nu$ one via WW fusion, see e.g. Ref. [587]. The decay $\Delta \to NN$ leads to the NNZ final state with up to four leptons and no missing energy when Z decays leptonically. The total integrated luminosity at LEP was too small to find more than ~ 2 NNZ events from the collected data. On the other hand, the future e^+e^- machines may have sufficient sensitivity to look for heavy neutrinos from Δ decays. Various production c.m. energies are currently under consideration from the Z pole at 90 GeV all the way to a 3 TeV machine, with $\sqrt{s_{W,h,t,\rm TeV}} = \{0.16, 0.24, 0.35, 1\}$ TeV [588]. The backgrounds depend on the c.m. energy and are particularly low below the $t\bar{t}$ threshold. Moreover, they can be reduced with cuts to a small level even above this energy. Conversely, for TeV machines, the W VBF channel takes over and the $NN\nu\overline{\nu}$ final state dominates. The exact capabilities of the detectors are presently unknown, therefore we only show the signal event counts for different $\sqrt{s}$ cases in Fig. 85, as function of the scalar mass m_Δ [550].

B. Non-standard neutrino interactions

The presence of nonstandard neutrino interactions (NSI) has a large effect on the precision measurements at next-generation neutrino oscillation experiments, and other types of experiments can also constrain the NSI parameter space. Ref. [551] considered the monophoton channel at the CEPC. The Lagrangian of neutral current (NC) NSI with electrons can be written as,

$$\mathcal{L}_{\rm NSI}^{\rm NC,e} = -2\sqrt{2}G_F\epsilon_{\alpha\beta}^{eL}(\bar{\nu}_\alpha\gamma^\mu P_L\nu_\beta)(\bar{e}\gamma_\mu P_L e) - 2\sqrt{2}G_F\epsilon_{\alpha\beta}^{eR}(\bar{\nu}_\alpha\gamma^\mu P_L\nu_\beta)(\bar{e}\gamma_\mu P_R e), \quad (25)$$

where α, β label the lepton flavors (e, μ, τ).

With the monophoton searches, Fig. 86 shows the allowed 90% C.L. region for NSI with electrons in the plane of $(\epsilon_{ee}^{eL},\ \epsilon_{ee}^{eR})$ at CEPC with 5.6 ab^{-1} data of $\sqrt{s} = 240$ GeV (Black), with 2.6 ab^{-1} data of $\sqrt{s} = 160$ GeV (Red), and with 16 ab^{-1} data of $\sqrt{s} = 91.2$ GeV (Blue), respectively, from the production of single photon associated with neutrino pair $e^+e^- \to \nu\bar{\nu}\gamma$. From the left side of Fig. 86, one can see that the allowed region for each running mode lies between the two concentric circles, which can be a good complementary with current global analysis in constraining $(\epsilon_{ee}^{eL},\ \epsilon_{ee}^{eR})$. The coordinates of circle center for the contour of $(\epsilon_{ee}^{eL},\ \epsilon_{ee}^{eR})$ are dependent on $\sqrt{s}$. We can find that the direction from the SM point (0,0) to the circle center with $\sqrt{s} = 91.2$ GeV is approximately perpendicular to that with the other two running modes. Thus, by combining the data from the three different running modes, the allowed regions for NSI parameters with electrons can be severely constrained as compared to the global analysis, which is shown on the right side of Fig. 86 with a green curve. Even if both ϵ_{ee}^{eL} and ϵ_{ee}^{eR} are present, the allowed ranges for $|\epsilon_{ee}^{eL}|$ or $|\epsilon_{ee}^{eR}|$ can be constrained to be smaller than 0.002.

C. Active-sterile neutrino transition magnetic moments

The discovery that neutrinos oscillate, and therefore neutrinos have distinct mass and flavor eigenstates, has proven to be one of the most definitive pieces of evidence for physics beyond the Standard Model (BSM) in the last two decades, which can be explained by including the additional heavy neutral leptons N (often referred to sterile neutrinos). Ref. [552] studied the active-sterile neutrino transition magnetic moments. The relevant operators

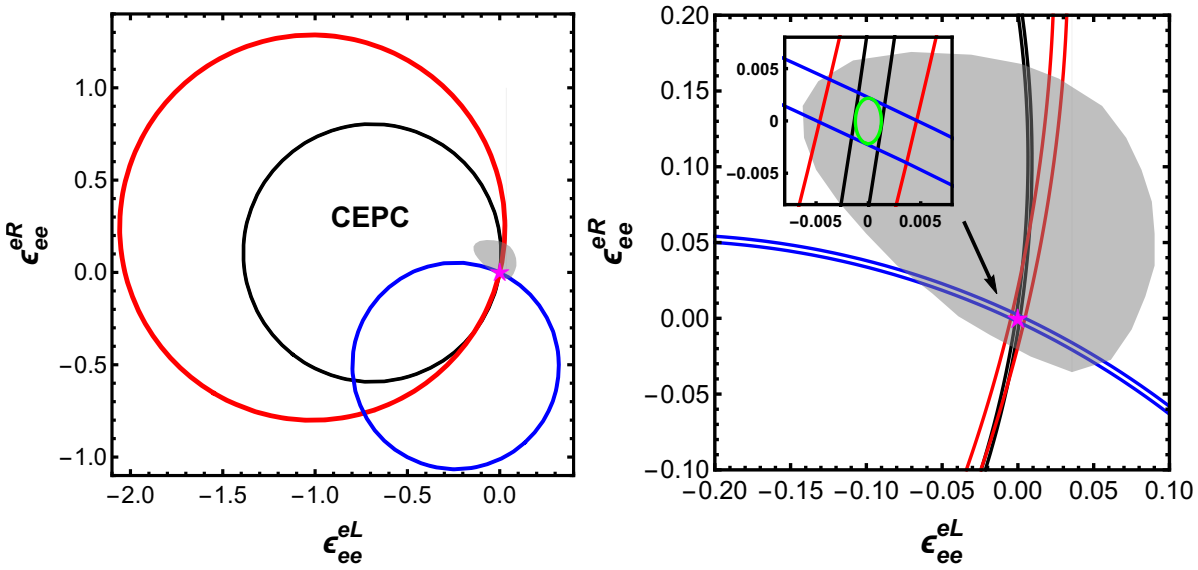

FIG. 86: The allowed 90% C.L. region for electron-type neutrino NSI in the planes of $(\epsilon_{ee}^{eL},\ \epsilon_{ee}^{eR})$ at future CEPC with 5.6 ab^{-1} data of $\sqrt{s} = 240$ GeV (Black), with 2.6 ab^{-1} data of $\sqrt{s} = 160$ GeV (Red), and with 16 ab^{-1} data of $\sqrt{s} = 91.2$ GeV (Blue), respectively. The allowed 90% C.L. regions arising from the global analysis of the LEP, CHARM, LSND, and reactor data [589], are shown in the shaded gray regions. With all the data collected in all three running modes, the combined result (green) is shown in the right panel. Figure from Ref. [551]

respecting the $\mathrm{SU}(2)_L \otimes \mathrm{U}(1)_Y$ gauge symmetry can be written as [590]

$$\mathcal{L} \supset \bar{L}^k (d_{\mathcal{W}}^k \mathcal{W}_{\mu\nu}^a \tau^a + d_B^k B^{\mu\nu}) \tilde{H} \sigma_{\mu\nu} N + \mathrm{H.c.}, \tag{26}$$

where $\tilde{H} = i\sigma_2 H^*$, $\tau^a = \sigma^a/2$ with σ^a being Pauli matrices, $\mathcal{W}_{\mu\nu}^a$ and $B^{\mu\nu}$ denote the $\mathrm{SU}(2)_L$ and $\mathrm{U}(1)_Y$ field strength tensors with $\mathcal{W}_{\mu\nu}^a \equiv \partial_\mu \mathcal{W}_\nu^a - \partial_\nu \mathcal{W}_\mu^a + g\epsilon^{abc} W_\mu^b W_\nu^c$ and $B_{\mu\nu} \equiv \partial_\mu B_\nu - \partial_\nu B_\mu$, and L are the SM lepton doublets. After electroweak symmetry breaking with the Higgs vacuum expectation value v, one obtains

$$\mathcal{L} \supset d_W^k (\bar{\ell}^k W_{\mu\nu}^- \sigma_{\mu\nu} N) + \bar{\nu}_L^k (d_\gamma^k F_{\mu\nu} - d_Z^k Z_{\mu\nu}) \sigma_{\mu\nu} N + \mathrm{H.c.}, \tag{27}$$

which can induce dipole operators to SM photon, the weak boson Z and W, with

$$d_\gamma^k = \frac{v}{\sqrt{2}} \left(d_B^k \cos\theta_w + \frac{d_{\mathcal{W}}^k}{2} \sin\theta_w \right), \quad d_Z^k = \frac{v}{\sqrt{2}} \left(\frac{d_{\mathcal{W}}^k}{2} \cos\theta_w - d_B^k \sin\theta_w \right), \quad d_W^k = \frac{v}{2} d_{\mathcal{W}}^k, \tag{28}$$

where θ_w is the weak mixing angle.

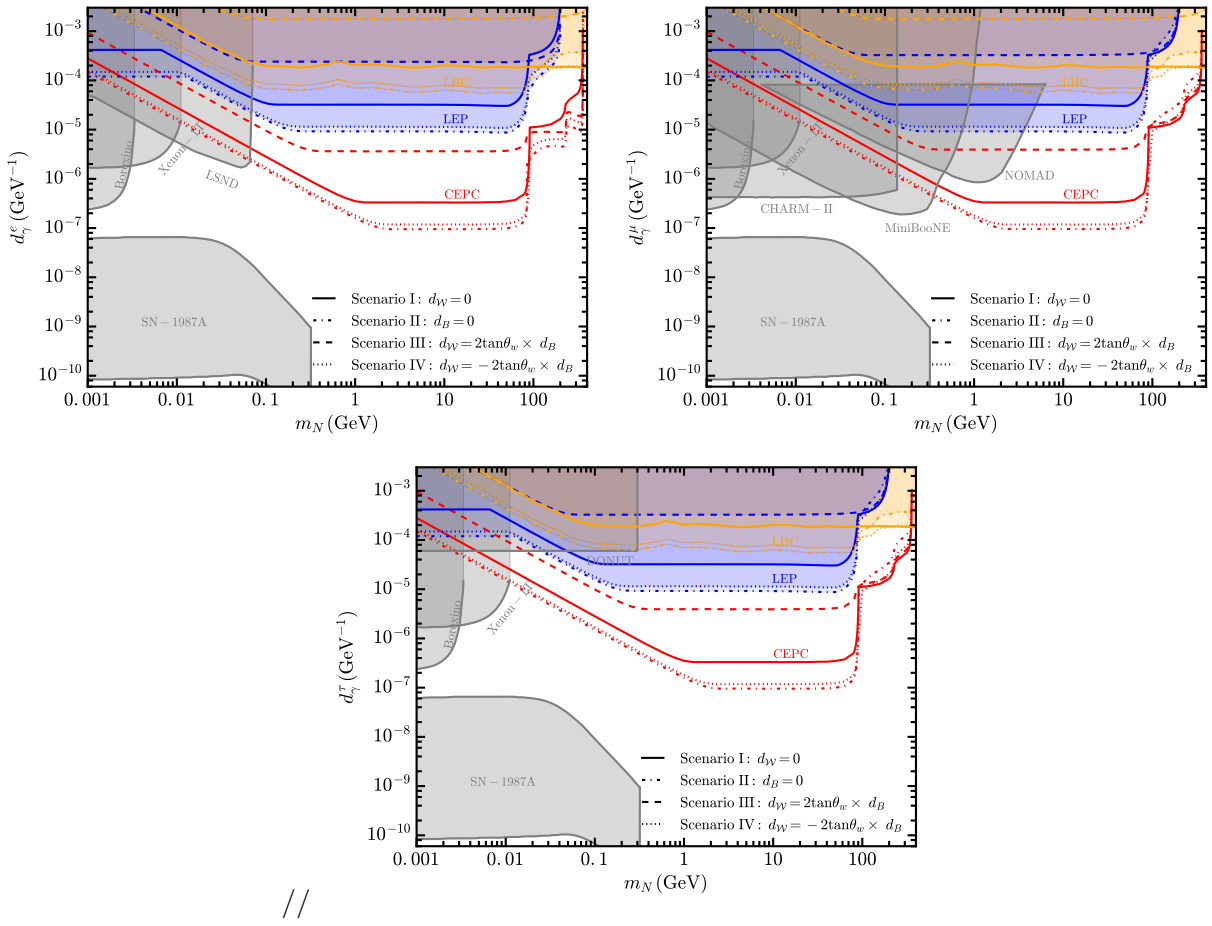

FIG. 87: The expected 95% C.L. exclusion limits on active-sterile neutrino transition magnetic moment d_γ^k in four scenarios at CEPC (red lines), which are the combination of the best constraints from four running modes at CEPC, for the three lepton flavors e (upper), μ (middle) and τ (lower). The landscape of current leading constraints are also shown with shaded regions. Figure from Ref. [552].

At CEPC, the sterile neutrino N production will proceed from the process $e^+e^- \to N\bar{\nu}_k + \mathrm{H.c.}$ via either Z or γ mediator in s-channel depending on dipole portal couplings d_Z^k, d_γ^k with $k = e, \mu, \tau$, or via W mediator in t-channel depending on electron neutrino dipole portal coupling d_W^e in Eq. (27), respectively. With the subsequent decay channel $N \to \nu\gamma$ in the detector, the signature of a single photon final state with missing energy can be searched for at CEPC.

The 95% C.L. upper bounds on the neutrino dipole portal couplings d_γ^k for the three lepton flavors $k = e,\ \mu,\ \tau$ at CEPC are shown in the upper, middle and lower panels of Fig. 87, respectively. And the limits from LEP [169, 591] and LHC [592, 593] are shown

for comparison [594]. The four scenarios with assumptions of $d_{\mathcal{W}} = 0$, $d_B = 0$ and $d_{\mathcal{W}} = \pm 2 \tan\theta_w d_B$ are considered. The combination of the best constraints from four running modes at CEPC with the total luminosity of 20 ab^{-1} data in the Higgs-mode, 6 ab^{-1} in the WW-mode, 100 ab^{-1} in the Z-mode, and 1 ab^{-1} in the $t\bar{t}$-mode is presented. For light sterile neutrino N, the Z-mode has the best sensitivity in all four scenarios. It is expected similar sensitivities could be reached at the FCC-ee. One can see that depending on the the ratio $d_{\mathcal{W}}/d_B$, the constraints on d_γ^k can be fairly different. While the current constraints on d_γ^k from terrestrial experiments such as Borexino, Xenon-1T, CHARM-II, MiniBooNE, LSND, NOMAD, and DONUT, and astrophysics supernovae SN 1987A [590], basically do not dependent on the ratio $d_{\mathcal{W}}/d_B$, since the typical scattering energies are far less than the electroweak scale. The constraints from the monophoton searches at CEPC are in principle different on d_γ^e and on $d_\gamma^{\mu,\tau}$ when $d_{\mathcal{W}} \neq 0$, because there will be additional contributions from W-mediator. In summary, CEPC can explore the previously unconstrained parameter region and will greatly improve the limits on active-sterile neutrino transition magnetic moment d_γ^k compared to current experiments.

D. Neutral and doubly-charged scalars in seesaw models

Future lepton colliders can provide unique insight into the scalar sector of TeV scale models for neutrino masses with local $B - L$ symmetry. Our specific focus is on the TeV scale LRSM [518, 519, 586], which naturally embeds this $B - L$ symmetry. Due to mixing with other scalars, the neutral scalar H_3 from the right-handed triplet scalar Δ_R could acquire sizable flavor violating couplings to the charged leptons. Produced on-shell or off-shell at the planned e^+e^- colliders, it would induce distinct lepton flavor violating (LFV) signals like $e^+e^- \to \ell_\alpha^\pm \ell_\beta^\mp$ $(+H_3)$ $(\alpha,\ \beta = e,\ \mu,\ \tau)$, with the couplings $h_{\alpha\beta}$ probed up to $\sim 10^{-4}$ for a wide range of neutral scalar mass, which is well beyond the reach of current searches for charged LFV [554]. Actually, the LFV signals induced by a neutral scalar are quite general in BSM scenarios [553], e.g. in supersymmetric models with leptonic R-parity violation [595], mirror models [596–598], and two-Higgs doublet models [599, 600], in addition to the LRSM [554, 601].

In the LRSM, the neutral scalar H_3 can be produced at lepton colliders from its scalar coupling with the doubly-charged scalar $H^{\pm\pm}$, Yukawa couplings to the RHNs and charged

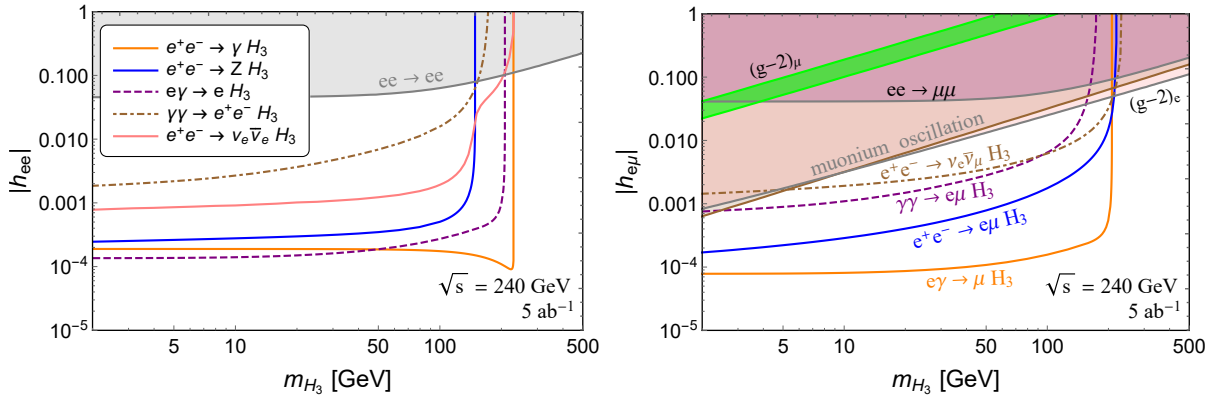

FIG. 88: Prospects of the couplings $|h_{ee}|$ (left) and $|h_{e\mu}|$ (right) from the on-shell production of H_3 at CEPC (240 GeV and 5 ab^{-1}), in the channels of $e^+e^- \to (\gamma/Z)H_3$, $e\gamma \to \ell H_3$, e^+e^-, $\gamma\gamma \to \ell^\pm_\alpha \ell^\mp_\beta H_3$ and $e^+e^- \to \nu\bar{\nu}H_3$. The shaded regions are excluded by current limits, while the yellow band corresponds to the muon $g-2$ discrepancy at 2σ C.L. Figure from Ref. [554].

leptons, the 1-loop coupling to photons, and its mixing with the SM Higgs h [554]. Then one can estimate the prospects of all the independent couplings $h_{\alpha\beta}$ at future lepton colliders. For illustration purpose, the prospects of $|h_{ee}|$ and $|h_{e\mu}|$ at the CEPC 240 GeV with an integrated luminosity of 5 ab^{-1} are shown in the left and right panels of Figure 88, respectively. The sensitivities of other couplings can be found in Ref. [554]. The SM backgrounds are expected to be small, in particular for the LFV processes [553]. For simplicity, we have turned on only one of the couplings $h_{\alpha\beta}$ and set all others irrelevant to be zero. Neglecting the mixing of H_3 with the SM Higgs, the loop decay $H_3 \to \gamma\gamma$ and the decay $H_3 \to \nu\bar{\nu}$ suppressed by the heavy-light neutrino mixing $V^4_{\nu N}$, the neutral scalar H_3 decays predominantly into a pair of leptons, i.e. $H_3 \to \ell^\pm_\alpha \ell^\mp_\beta$. To be concrete, we assume a minimum number of 10 (30) for the signals with (without) LFV, and adopt an efficiency factor of 60% for the tau lepton [602]. In the process $e^+e^- \to ZH_3$, only the visible decay products of Z are taken into account. All the amplitudes for the on-shell production of H_3 depend linearly on the couplings $h_{\alpha\beta}$, thus free of the constraints from the rare LFV decays such as $\mu \to eee$ and $\tau \to e\gamma$ which depend quadratically on the Yukawa couplings $|h^\dagger h|$. The shaded regions are excluded by the muonium oscillation, electron $g-2$, muon $g-2$ (excluded by the theoretical-experimental discrepancy at the 5σ CL) [603] and the LEP $e^+e^- \to \ell^+\ell^-$ data [604]. The yellow band in the right panel can explain the muon $g-2$ anomaly at the 2σ CL.

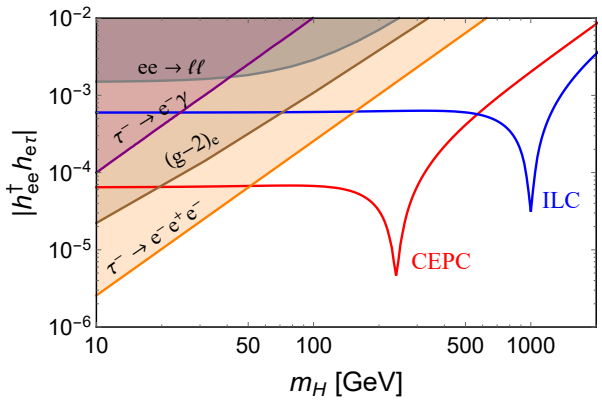

FIG. 89: Prospects of $|h^\dagger_{ee} h_{e\tau}|$ (upper) from searches of $e^+e^- \to e^\pm\tau^\mp$, $\mu^\pm\tau^\mp$ at CEPC (red, $\sqrt{s} = 240$ GeV, $\mathcal{L} = 5$ ab^{-1}) and ILC (blue, 1 TeV and 1 ab^{-1}). The shaded regions are excluded by current limits. Figure from Ref. [553].

The neutral scalar H may also mediate off-shell processes, e.g. $e^+e^- \to \ell^+_\alpha \ell^-_\beta$. For the illustration purpose, the sensitivities of $|h^\dagger_{ee} h_{e\tau}|$ are shown in Fig. 89. The red and blues lines are for the prospects at CEPC 240 GeV with an integrated luminosity of 5 ab^{-1} and ILC 1 TeV with 1 ab^{-1}, respectively. Also shown are the constraints from the rare lepton decays $\tau^- \to e^+e^-e^-$, $\tau^- \to e^-\gamma$, electron $g-2$ [603], and the LEP $e^+e^- \to \ell^+\ell^-$ data [604]. More prospects of the couplings $|h^\dagger h|$ can be found in Refs. [553, 554].

The Yukawa couplings of the doubly-charged scalar $H^{\pm\pm}$ to the charged leptons might also be flavor-violating, which is directly correlated to the heavy RHN masses and mixings in the LRSM. With a combination of the pair, single and off-shell production of $H^{\pm\pm}$ like $e^+e^- \to H^{++}H^{--}$, $H^{\pm\pm}e^\mp\mu^\mp$, $\mu^\pm\tau^\mp$, the Yukawa couplings can be probed up to 10^{-3} at future lepton colliders, which is allowed by current lepton flavor data in a large region of parameter space. As an explicit example, the prospects of $|f^\dagger_{ee} f_{e\tau}|$ in the the doubly-charged scalar induced processes $e^+e^- \to e^\pm\tau^\mp$ and $e^-\gamma \to e^+e^-\tau^- + \tau^+e^-e^-$ are shown in Fig. 90, as function of the doubly-charged scalar mass $M_{\pm\pm}$. The dashed lines are for the CEPC prospects, while the solid ones are the ILC sensitivities. The red and blue lines are for the e^+e^- and $e^-\gamma$ processes, respectively. The shaded regions are excluded by the rare tauon decays $\tau \to e\gamma$, $\tau \to eee$ and the LEP $ee \to \ell\ell$ data [604]. More prospects of other couplings of the doubly-charged scalar can be found in Ref. [554]. As demonstrated in Figs. 89 and 90, for both the neutral and doubly-charged cases, the scalar masses could be probed up to the few-TeV range in the off-shell channel.

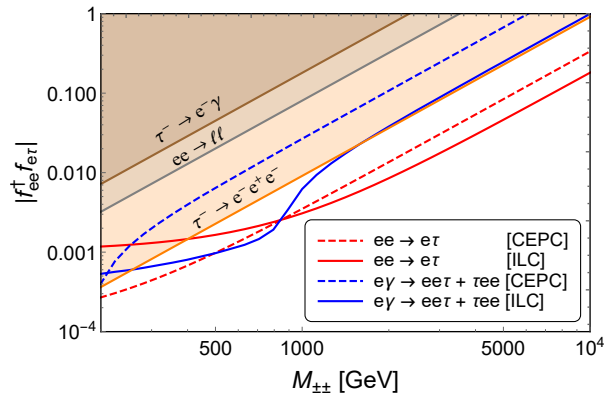

FIG. 90: Prospects of the Yukawa couplings $|f^{\dagger}_{ee} f_{e\tau}|$ for the doubly-charged scalar $H^{\pm\pm}$ production via the $e^+e^- \to e\tau$ (red) and $e^-\gamma \to e^+e^-\tau^- + \tau^+e^-e^-$ (blue) processes, at CEPC with $\sqrt{s} = 240$ GeV and an integrated luminosity of 5 ab^{-1} (dashed) and ILC with $\sqrt{s} = 1$ TeV and 1 ab^{-1} (solid). The shaded regions are excluded by current limits. Figure from Ref. [554].

The type-II seesaw mechanism with an isospin-triplet scalar Δ_L provides one of the most compelling explanations for the observed smallness of neutrino masses [513, 522–526]. The triplet contains a doubly-charged component $H_L^{\pm\pm}$, which decays predominantly to either same-sign dileptons or to a pair of W bosons, depending on the size of the triplet vacuum expectation value. However, there exists a range of Yukawa couplings f_L of the triplet to the charged leptons, wherein a relatively light $H_L^{\pm\pm}$ tends to be long-lived, giving rise to distinct displaced vertex signatures at the high-energy colliders [605–608]. We find that the displaced vertex signals from the leptonic decays $H_L^{\pm\pm} \to \ell_\alpha^\pm \ell_\beta^\pm$ could probe a broad parameter space with $10^{-10} \lesssim |f_L| \lesssim 10^{-6}$ and 45.6 GeV $< M_{H_L^{\pm\pm}} \lesssim 200$ GeV at the high-luminosity LHC. Similar sensitivity can also be achieved at a future 1 TeV e^+e^- collider. The mass reach can be extended to about 500 GeV at a future 100 TeV proton-proton collider. Similar conclusions apply for the right-handed triplet $H_R^{\pm\pm}$ in the TeV-scale left-right symmetric models, which provide a natural embedding of the type-II seesaw. More details can be found in Ref. [608]. However, limited by the relatively low center-of-mass energy, it is expected that the CEPC 240 GeV can only probe much smaller parameter space of the doubly-charged scalar.

E. Connection to Leptogenesis and Dark Matter

Apart from the mysterious neutrino mass problem, there exists other well established evidence beyond the SM, e.g. baryon asymmetry of the universe (BAU), DM, etc. An attractive solution can accommodate the explanations of all three problems in one unified model, the Neutrino Minimal Standard Model (νMSM) [574, 575]. In this model, three generations of RHNs $N_{1,2,3}$, are added to the SM particle contents. These RHNs are all SM singlets, only interacts with the SM components via the active-sterile mixing. Among them, the lightest one N_1 has tiny Yukawa couplings, thus tiny masses, can be the DM candidate [609–613]. The two heavier particles $N_{2,3}$ are responsible for generating the observed active neutrino masses via the aforementioned type-I seesaw mechanism. They also possess very similar masses, closing to the EW scale, which can generate the asymmetry either via CP-violating RHN oscillations, or resonantly enhanced CP asymmetry in RHN decay. Hence, the observed BAU can be explained by leptogenesis via neutrino oscillations [575, 614] and resonant leptogenesis [615–625].

In the νMSM, the BAU is generated by "low scale" leptogenesis, since the mass scale of RHNs is below 10^9 GeV, which is the Davidson-Ibrra bound implied by the 'vanilla' leptogenesis [626]. The "low scale" leptogenesis includes leptogenesis via neutrino oscillations during freeze-in of the RHNs, and resonant leptogenesis during freeze-out [627, 628]. The two mechanisms can be united by a unique set of quantum kinetic equations, as desibed in Refs. [627, 628]. The viable parameter space of the model satisfying both the neutrino masses and BAU problems is thoroughly studied, with the summary shown in Fig. 91 [555, 629]. The two [627, 628] and three [629] RHN scenarios in the case of normal ordering (NO) of neutrino masses, for both vanishing and thermal initial HNL abundances, are included. The shaded region in gray is excluded by past experiments [564–568, 571, 572, 630–633], complemented by the updated BBN bounds in light gray from Refs. [573, 634] and the lower bound from the seesaw mechanism in darker gray. See Refs. [627–629] for details. The various colored lines indicate existing [635–639] and future [230, 257, 292, 562, 563, 640–643] experiments that will be able to probe the low-scale leptogenesis parameter space. As indicated in the figure, the sensitivity of the CEPC, shown in light green, can be sensitive to the parameter space where both seesaw and leptogenesis mechanisms are successful, no matter the number of RHNs and the initial condition.

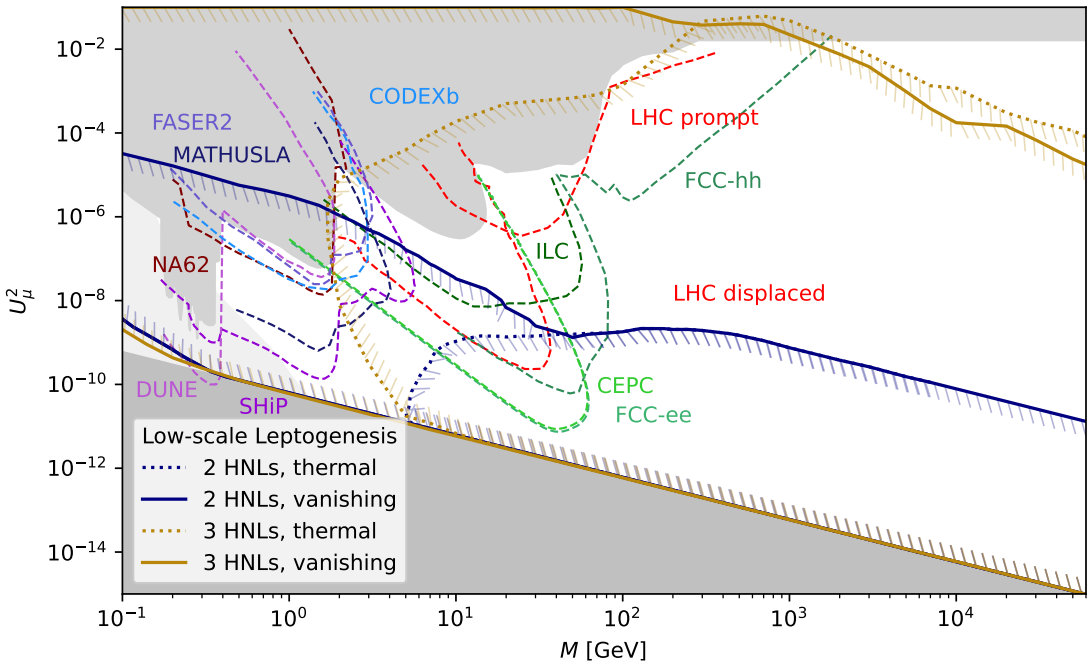

FIG. 91: Comparison of the ranges of the mixing angle U_μ^2 consistent with both the seesaw mechanism and leptogenesis as a function of HNL mass M for leptogenesis with two or three HNL flavours in the case of NO, for both vanishing and thermal initial HNL abundances. The shaded region in gray is excluded by existing limits. complemented by the updated BBN bounds (light gray) and the lower bound from the seesaw mechanism (darker gray) [627–629]. The colored lines indicate prospects at existing and future experiments. Adapted from Ref. [555].

The DM relic density $\Omega_{\rm DM}$ can also be explained by accounting the lightest right-handed neutrinos N_1 as the DM candidate. In the νMSM, $\Omega_{\rm DM}$ is only produced by mixing with active neutrinos [644] [609–613, 645]. Sufficient production is generated if large lepton symmetry is generated at the low temperature of $\mathcal{O}(200)$ MeV [610, 611, 613, 646–650]. To successfully reproduce $\Omega_{\rm DM}$, $M_{N_1} \sim \mathcal{O}(1)$ keV and $M_{N_2} \approx M_{N_3} \gtrsim \mathcal{O}(1)$ GeV [651]. More extended models, e.g. the left-right symmetric model, can also accommodate the origin of BAU and DM [518]. The discussions of the connection between them in such models can be found in Refs. [652, 653]. Such models have already been searched by ℓ+MET signatures at LHC [653], and can be tested at CEPC, for example via $e^+e^- \to NN$ processes medi-

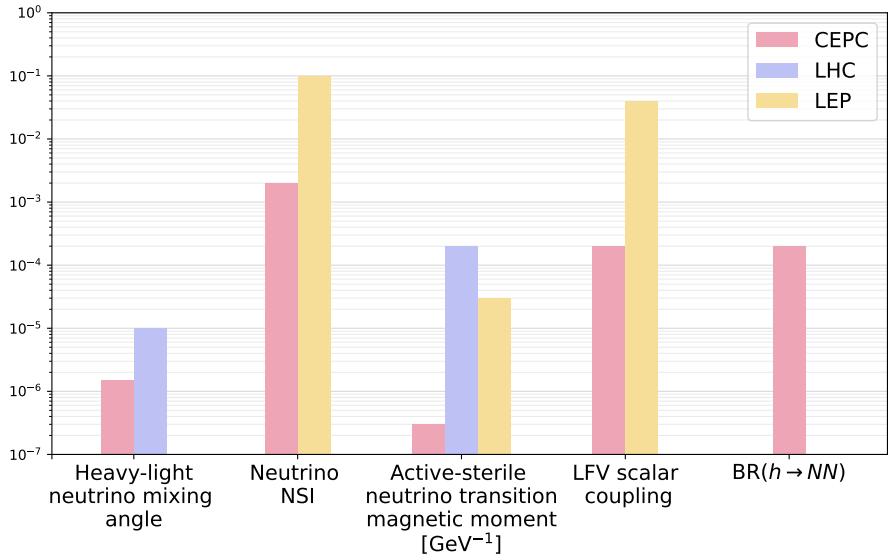

FIG. 92: Prospects of neutrino physics observables at the CEPC, in comparison with the LEP limits and LHC prospects. See text for more details.

ated by the W_R or Z' boson. If $M_N \gtrsim \mathcal{O}(1)$ GeV, same sign dilepton plus multiple jets signatures are studied in Ref. [654], and displaced vertex signatures in Ref. [655], and can be further extended by searching for monophoton signatures if the N is even more stable, when $M_N \sim \mathcal{O}(1)$ keV to explain the DM.

F. Summary

In this sections we have examined the prospects of CEPC to some benchmark scenarios relevant to neutrino physics, in particular for the heavy neutrinos, non-standard neutrino interactions, active-sterile neutrino transition magnetic moments, the neutral and doubly-charged scalars in seesaw models, and the connection to leptogenesis and DM. The CEPC sensitivities of some representative neutrino physics relevant observables are presented in Fig. 92. For illustration purpose we have chosen the heavy-light neutrino mixing angle from Fig. 77, neutrino NSI from Fig. 86, active-sterile neutrino transition magnetic moment (in unit of GeV^{-1}) from Fig. 87, the LFV scalar coupling from Fig. 88, and the branching fraction BR($h \to NN$) from Fig. 82. The comparison of CEPC with the existing LEP limits and the future prospects at the LHC are also shown in this figure; see the subsections above and figures therein for more details. In general, neutrino relevant signals may behave like

rare processes, e.g. the LFV or LNV events or displaced vertices. Benefiting from the high luminosity and clean environment, the neutrino relevant sensitivities can be improved at the CEPC by one or two orders of magnitude, as exemplified in Fig. 92.

XI. MORE EXOTICS (YU, ZUOWEI)

Due to a vast number of new physics scenarios that couple to the SM electroweak and lepton sectors, there is strong interest that exotic searches can benefit from the high luminosity at CEPC's Z-pole and Higgs factory runs. High precision on the Z, h widths and good reconstruction of the decay products offer powerful test of exotic processes, including lepton number/flavor violation, sterile states, axion-like particles and many others. CEPC's low hadronic activity level helps to minimize the contamination from hadronic initial state radiation, hence it enhances the potential to accurately identify signals that involve relatively soft leptons, photons and jets. This section lists several dedicated studies that can benefit from CEPC's. In addition, several recent studies of spin-related kinematical observables, such as transverse spin [656], quantum entanglement [657–659] , etc., provide even more diversified avenues for the CEPC's physics potential.

A. Axion-like particles

As a relaxation solution to the "strong-CP" problem, the Peccei-Quinn mechanism predicts the existence of the QCD axion [660–662], which develops a coupling with gauge bosons at one loop level. The characteristic Chern-Simons term $aF\tilde{F}/f_a$ leads to the generalization toward axion like particles (ALPs), which can rise in many new physics scenarios that contains the breaking of a global U(1) symmetry [663–666]. The prospects for discovering ALPs via a light-by-light scattering at two colliders, the future circular collider (FCC-ee) and circular electron-positron collider (CEPC), have been extensively investigated. At future lepton colliders, promising sensitivities to the effective ALP-photon coupling $g_{a\gamma\gamma}$ can be derived for the parameter $g_{a\gamma\gamma}$ for $m_a \lesssim 10$ GeV [667]. Here we list the projected limits from several recent ALP studies for the Higgs factory and higher-energy runs at the CEPC.

The ALP couplings to gauge boson read as

$$\mathcal{L} = -C_{BB}\frac{a}{f_a}B_{\mu\nu}\tilde{B}^{\mu\nu} - C_{WW}\frac{a}{f_a}W^i_{\mu\nu}\tilde{W}^{\mu\nu,i}. \tag{29}$$

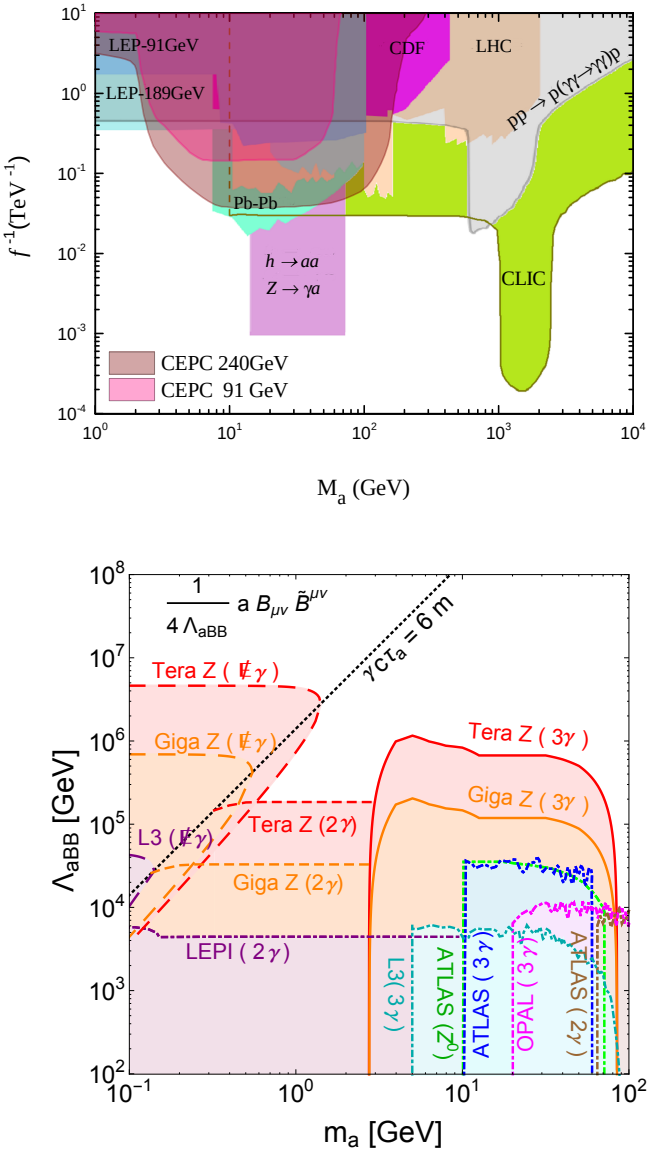

FIG. 93: Top panel: 95 C.L. sensitivity regions on the ALP coupling $g_{a\gamma\gamma}$ as a function of M_a for the process $e^+e^- \to \gamma\gamma e^+e^-$ at the 91 and 240 GeV runs of the CEPC. Bottom panel: sensitivity to the axion's coupling to the SM $U(1)_Y$ hypercharge field at Z-factory [74].

where f_a is the ALP's decay constant. After electroweak symmetry breaking, the neutral B, W^3 fields will be rotated into mass eigenstates γ, Z, and the conventional ALP couplings

to $\gamma\gamma$, WW, ZZ, $Z\gamma$ are given by

$$g_{a\gamma\gamma} = \frac{4}{f_a}(C_{BB}c_w^2 + C_{WW}s_w^2), \qquad g_{aWW} = \frac{4}{f_a}C_{WW}, \tag{30}$$
$$g_{aZZ} = \frac{4}{f_a}(C_{BB}s_w^2 + C_{WW}c_w^2), \qquad g_{aZ\gamma} = \frac{8}{f_a}s_w c_w (C_{WW} - C_{BB})\,.$$

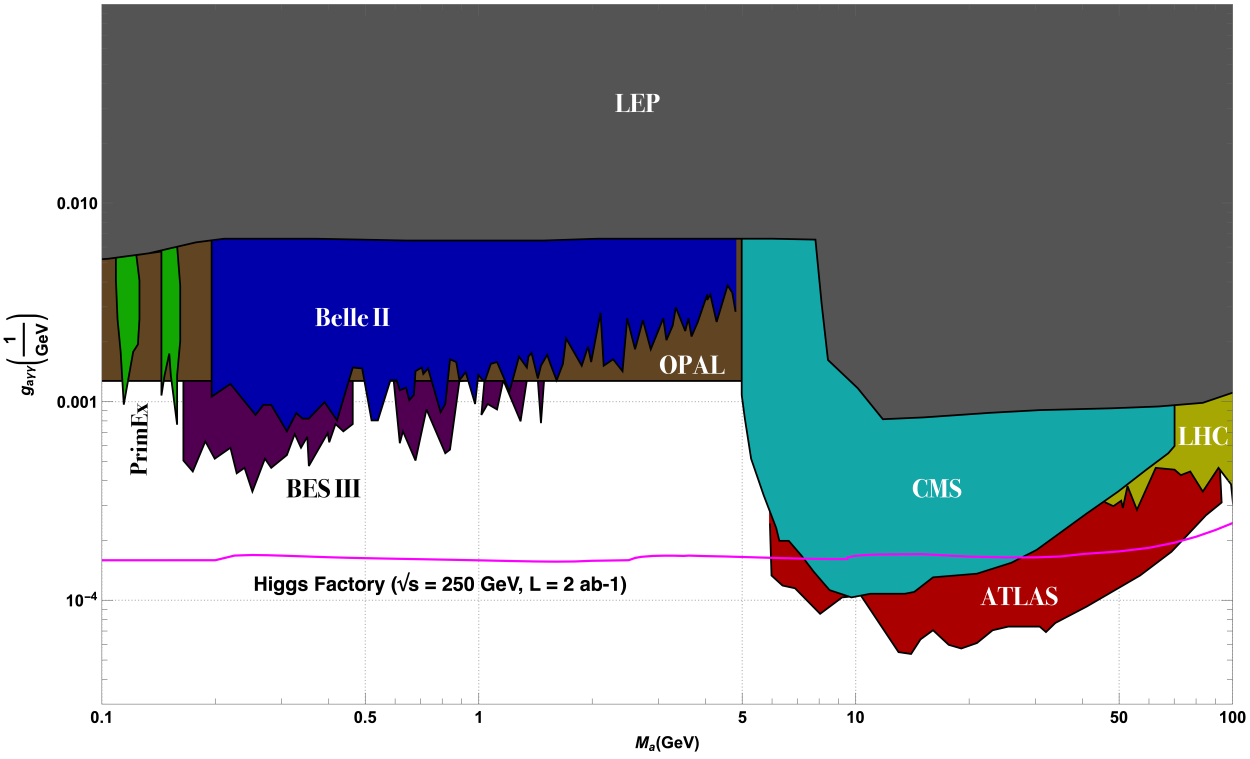

FIG. 94: Summary plot of the sensitivity of $g_{a\gamma\gamma}$ that we can achieve at the Higgs factory $\sqrt{s} = 250$ GeV with an integrated luminosity 2 ab^{-1}. Other existing constraints are shown for comparison.

Ref. [668] investigated the light-by-light scattering $e^+e^- \to \gamma\gamma e^+e^-$ induced by ALP exchange at the CEPC, and derived the production cross-section and expected CEPC sensitivity reach for $\sqrt{s}$ =91/240 GeV runs. The projected limits are shown in the upper panel of Fig. 93. Also at the Z pole, Ref. [74] investigated the axion coupling to the SM $U(1)_Y$ hypercharge field in the process of Z boson decay to $a\gamma$, with the axion subsequently decaying into two photons. The projected sensitivities are labeled as 3γ in the lower panel of Fig. 93.

Ref. [669] employed the processes $e^+e^- \to f^+f^-a$, where $f = e, \mu, \nu$, and devised a set of selection cuts to improve the signal-background ratio. The ALP is emitted by the gauge boson in the internal line of the process. The emitted ALP subsequently decays as $a \to \gamma\gamma$. Fig. 94 illustrates the CEPC sensitivity reach the sensitivity reach for $\sqrt{s} = 250$ GeV with an integrated luminosity of $L = 2\,\text{ab}^{-1}$, and the sensitivity can scale up by the sqrt of luminosity for 20 ab^{-1}. The upcoming Higgs factories can improve the sensitivity from the current constraints down to $2 \times 10^{-4}\,\text{GeV}^{-1}$ for $m_a = 0.1 - 6$ GeV. See Ref. [669] for details of the study.

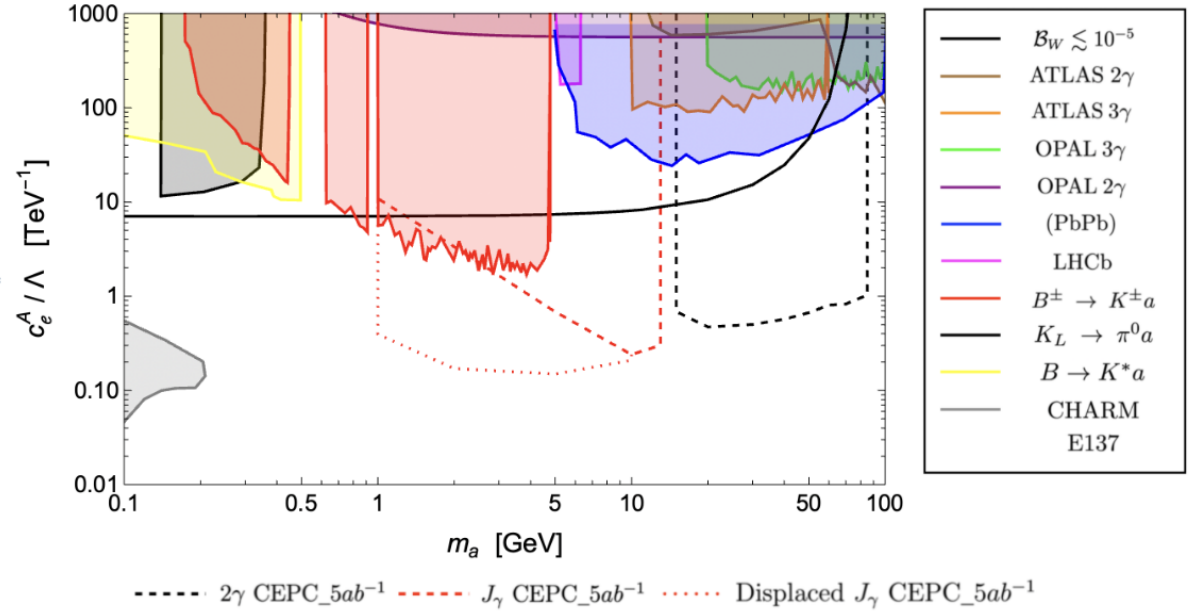

FIG. 95: Future bounds on the coupling c_e^A/Λ of eALPs from CEPC with $\mathcal{L} = 5ab^{-1}$ within 95% confidence level or with a requirement of at least 10 survival events for background-free cases (dashed lines for the eALP prompt decay and dotted lines for the eALP as a long-lived particle) as well as existing bounds (bulk regions). The labels "2γ" and "J_γ" identify two distinct signatures at CEPC. $\mathcal{B}_W \lesssim 10^{-5}$ represents $\mathcal{B}(W^\pm \to \ell^\pm \nu a) < 10^{-5}$ [670] (solid-black line). Other collider bounds are presented for comparison, see Ref. [671] and references therein.

In light of an electroweak-violating scenario, Ref. [670] studied a four-point interaction denoted as W-ℓ-ν-a, a coupling not reliant on the electron mass. This channel provides an opportunity to explore electrophilic ALPs (eALPs) at the GeV scale. In this work,

a novel t-channel process was investigated: $e^+e^- \to \nu_e a\overline{\nu_e}$, which involves the W-ℓ-ν-a four-point interaction with effective coupling ϵ_e^A/Λ. This process exhibits significant energy enhancement behaviors in its cross-sections as collision energy increases [671]. For GeV-scale eALPs, their primary decay mode involves a photon pair, induced by the chiral anomaly, rather than an electron-positron pair. Consequently, the characteristic signal signature for this t-channel process consists of a photon pair accompanied by missing energy. Depending on the mass and decay width of the eALPs, the final state can manifest as either two isolated photons (2γ), a photon-jet (J_γ), or a displaced J_γ. The analysis indicated that the potential future bounds on the coupling c_e^A/Λ can be as stringent as $0.1 - 1.0$ TeV^{-1} for 1 GeV $\leqslant m_a \lesssim M_W$, at CEPC with $\mathcal{L} = 5$ ab^{-1} and $\sqrt{s} = 240$ GeV. These constraints are depicted in Fig. 95.

B. Emergent Hadron Mass

It is common to regard the Higgs boson (HB) as the origin of mass within the Standard Model of particle physics (SM). Certainly, the Higgs (or something like it) is a mechanism that contributes to our understanding of the origin of mass of subatomic particles. Such Higgs couplings into quantum electrodynamics (QED) and quantum chromodynamics (QCD) produce the electron mass, $m_e = 0.511\,\text{MeV}$, and the quark current masses, amongst them the light u (up) and d (down) quarks: $m_u \approx 4m_e \approx 2.2\,\text{MeV}$, $m_d \approx 2m_u$. These particles combine to form the hydrogen atom, the most abundant element in the Universe, whose mass is 939 MeV. Somehow one electron, two u quarks and one d quark, with a total Higgs-generated mass of $\sim 13m_e \approx 6.6\,\text{MeV}$, combine to form an object whose mass is 140-times greater. Plainly, Nature must have another, very effective mass generating mechanism, which is now identified as emergent hadron mass (EHM) [672, 673].

Detailed pictures of the proton and B-meson mass budgets are drawn in Fig. 96. There are striking contrasts between the breakdowns into EHM, EHM+HB, and HB contributions. Modern science must discover and explain the source of these remarkable differences.

Contemporary theory explains EHM as the consequence of the dynamical generation of a gluon mass scale in QCD [674, 675]. This is *mass from nothing*: the SM massless gluon parton becomes a massive quasiparticle owing to self-interactions. The existence of such a mass entails that the QCD running coupling has a stable infrared completion, remaining

finite at all energy scales, from the deep ultraviolet into the far infrared [676, 677]. Together, these phenomena explain the character of mass in the matter sector of strong interactions [672, 673]. Such extraordinary predictions require empirical verification.

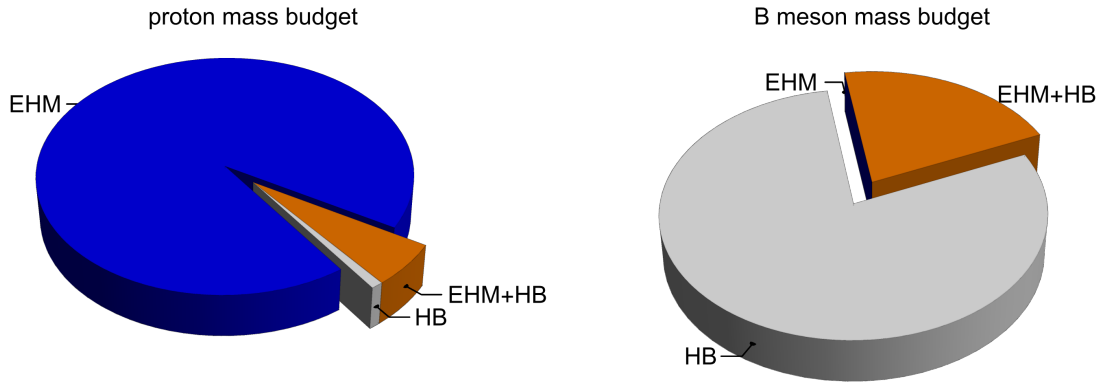

FIG. 96: Poincaré-invariant decompositions of hadron masses: (A) proton; (B) B-meson. Emergent hadron mass (EHM) is the source of 94% of the proton mass; by itself, the Higgs boson (HB) accounts for just 1%; and the remaining 5% is generated by constructive EHM+HB interference. In stark contrast, EHM alone produces none of the B-meson mass. Instead, the Higgs is responsible for 79%; yet, there is a sizeable EHM+HB interference term. (See Refs. [672, 673] for details.)

An open road toward validation is provided by the study of semileptonic weak-interaction transitions between heavy and light hadrons. In fact, heavy pseudoscalar meson to light pseudoscalar meson transitions serve to probe the relative impacts of the strength of EHM+HB interference in the initial and final states, whereas heavy-pseudoscalar to light-vector meson transitions overlap systems in which HB mass is dominant with those whose mass owes almost entirely to EHM. Both classes of transitions, therefore, and analogues involving baryons, present excellent opportunities for exposing the character of EHM and its interference with HB effects in order to identify the source of visible mass and its impact on physical observables. These cases are of heightened interest, of course, because the transitions have long been used to place constraints on the values of the elements of the Cabibbo–Kobayashi–Maskawa (CKM) matrix, which parameterized quark flavour mixing in the SM. Furthermore, confronting measurements of transitions with different leptons in the final state with sound theoretical predictions can shine bright light onto the question of LFU. Searches for violations of CKM matrix unitarity and/or LFU are principal tools in the hunt for physics

beyond the SM. Modern theory is capable of delivering robust predictions for all hadron structure factors necessary for the sound SM prediction of such transitions [678, 679].

Studying the evolution of hadron properties with quark current mass, *i.e.*, the strength of HB couplings into QCD, provides a clear window onto constructive interference between Nature's two sources of mass. This is a new feature of flavour physics, which adds enormously to its role in searching for physics beyond the SM. Here, the circular electron-positron collider (CEPC) can play a decisive role. It will deliver copious numbers of hadrons containing heavy quarks. Exploiting this capacity, the CEPC can play a key role in exposing the origin and character of mass.

C. Lepton form factors

The e^+e^- collisions at CEPC offer high luminosity in photon-mediated processes, hence provides a unique opportunity to measure photon-lepton interactions. Leptons' effective electromagnetic vertices have long been a popular topic with high-energy lepton collisions, as measurements of the lepton-photon coupling above pair-production threshold or at the weak scale can be interpreted into probes of BSM theory that can modify such form factors.

1. General remarks on μ/e g-2

Muon/electron $g-2$ measurements can serve as important probes for new physics beyond the SM. It has been known for a long time that the theoretical prediction of the muon anomalous magnetic moment $a_\mu \equiv (g-2)_\mu/2$ for SM has subtle deviations from the experimental values. Combining the recent reported FNAL muon $g-2$ measurement with the previous BNL+FNAL results, the updated world average experimental value of a_μ has a 5.1σ deviation from the SM predictions by comparing to the latest experimental result with prediction from the theory white paper [680]. Besides, the SM prediction on electron $g-2$ also has a $2.4\sigma/1.6\sigma$ deviation using $^{133}Cs/^{87}Rb$ [681, 682] atoms experimental data with negative/positive central value. However this picture is complicated by recent lattice results for the hadronic vacuum polarisation (HVP) contributions to the anomalous moment. The only lattice result with a comparable uncertainty comes from the Budapest-Marseille-Wuppertal (BMW) collaboration [683] and it disagrees significantly with the data-driven

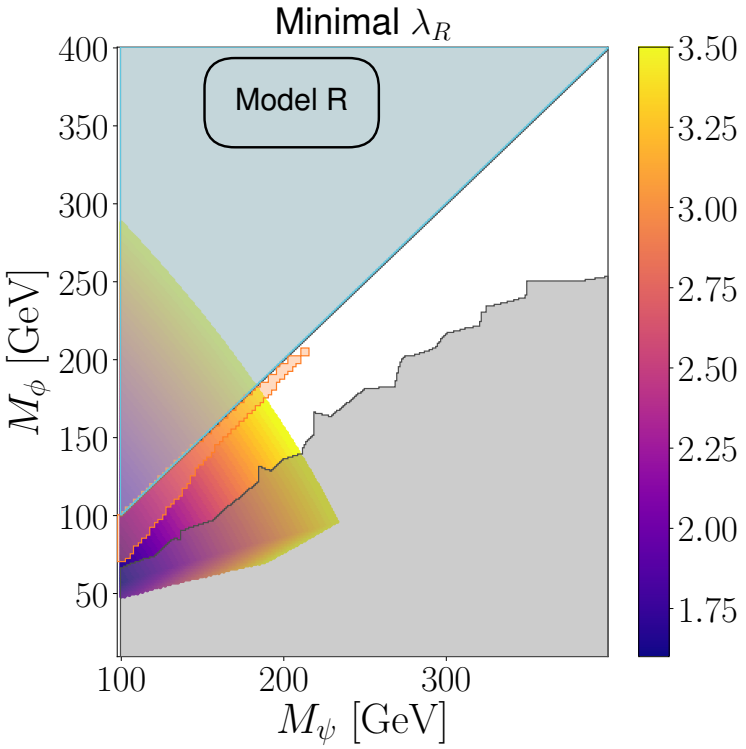

FIG. 97: A simple model with a new scalar and a new fermion. The color-coding shows the minimal value of the coupling to right-handed muons to explain muon g-2. Outside of this colored region, muon g-2 cannot be explained within 1σ. The shaded grey region shows LHC exclusions and the shaded orange region is excluded by compressed spectra. The shaded blue region (top left) is excluded due to a charged stable particle.

estimate. Using the lattice value instead would reduce the deviation to about 1.7σ. This result is also supported by recent lattice comparing to the BMW result [684]. A comparison of different lattice results and the data-driven approach [685] gives a 3.8σ tension between the data-driven estimate and the lattice QCD estimates. As a result, the discrepancy between the data-driven estimates and the lattice QCD calculations still needs to be settled before unambiguously calling out for new physics. However new physics explanations of the deviation between the theory white paper prediction and the measured value [686] also make predictions that can be tested at the future colliders, such as the CEPC.

The generic new physics contributions to muon g-2 is expected to scale as

$$\Delta a_\mu^{\rm BSM} \approx C_{\rm BSM} \frac{m_\mu^2}{M_{\rm BSM}^2}, \tag{31}$$

where $M_{\rm BSM}$ is the mass of the new physics particles in the loop and $C_{\rm BSM}$ is a loop suppressed

coefficient. This means that without some special enhancement the mass scale of the new physics should be $\lesssim 200 - 300$ GeV for perturbative new physics explanations. This is illustrated for simple model with a new scalar and a new fermion in Fig. 97, where the colour contours show the minimum value of the coupling to right handed muons required to explain muon $g-2$, and anything outside that region cannot explain muon $g-2$ within 1σ.

LHC has already excluded many such scenarios. However, there can be gaps in the exclusion from compressed spectra (as shown in 97) and it has been shown, for example, that constraints on light new electroweakinos are not very robust [687]. Therefore, it still opens up the possibility of directly producing the states at future colliders. On the other hand, an elegant solution to the tension between the LHC and muon g-2 comes in the form of a chirality flipping enhancement, see Ref. [686] for a recent review. In Eq. 31, one factor of m_μ appears because of the dipole operator flips the fermion chirality, thus a muon mass insertion exist on one of the external legs. If this chirality flip can instead be done inside the new loop diagram from new physics, then the muon mass will be replaced with a mass or parameter from the new physics that can be much larger. This chirality flipping enhancement is automatically present in supersymmetric extensions, as well as in non-SUSY models such as scalar leptoquarks and vector-leptoquarks, which alleviates this tension also makes it easier to construct simultaneous explanations of dark matter and muon g-2. New physics contribution to muon g-2 typically also implies large corrections to the self energy of the muon. This leads to a fine tuning in the muon mass if the masses much heavier than $\mathcal{O}(1\text{TeV})$ [686]. Furthermore, this also implies an enhanced Yukawa coupling which means that precision measurements of $h \to \mu^+\mu^-$ at the future colliders such as the CEPC could either exclude these explanations or give rise to a discovery level deviation from the standard model [688].

2. μ/e dipole moments in SUSY

As a popular BSM scenario, SUSY contributes to muon $g-2$ mostly via the chargino-sneutrino and the neutralino-smuon loops, which always need light electroweakinos and sleptons to explain the anomaly. However, such requirements potentially have tensions with the observed 125 GeV Higgs mass and LHC exclusion bounds, which in general prefer heavy colored sparticles. Weak scale phenomenological MSSM needs intricate parameter regions

to survive the current LHC, dark matter and Higgs mass bounds, and can give a sizable contribution to muon/electron $g-2$ and at the same time.

Studies of the gluino-SUGRA, the anomaly mediated SUSY breaking (AMSB) models [689–691] and the gauge/Yukawa mediated SUSY breaking models [692] indicate that it is challenging yet possible to explain both e and μ anomalies in a unified SUSY framework. This is because without any flavor violation in the lepton sector, new physics contributions to the lepton $g-2$ are in general scaled with the corresponding lepton mass-square. Such a scaling relation can still explain the electron $g-2$ anomaly in 2σ range for positive central value electron $g-2$ experimental data when the muon $g-2$ anomaly is explained in 1σ range.

Generalized gravity mediation models always adopt various universal boundary conditions at the GUT scale. Given the stringent constraints on the first two generation squarks by LHC and the stop masses by the 125 GeV Higgs, the mSUGRA slepton masses can not be light at the EW scale with universal sfermion mass inputs at the GUT scale. Thus, it is challenging to explain the muon $g-2$ anomaly within the frame work of GUT-scale constrained SUSY, especially the mSUGRA [342].

Gluino-SUGRA ($\tilde{g}$SUGRA) [693] is an economical extension of mSUGRA , and it is a special case of non-universal gaugino mass realization at GUT scale. In $\tilde{g}$SUGRA the gluino mass can be much heavier than other gauginos and sfermions at the unification scale, hence the gaugino masses ratios at the EW scale will no longer constrain the electroweakino masses for a heavy gluino mass. The sleptons, which carry no color charge, will stay light. So, the RGE evolution will split the squark masses from slepton masses at the electroweak scale, which is needed for the muon $g-2$. Ref. [694] showed that with $M_1 = M_2$ at the GUT scale and a viable bino-like dark matter, $\tilde{g}$SUGRA can explain the muon $g-2$ anomaly at 1σ level and be consistent with the updated LHC constraints. In this case, a light stau is needed for co-annihilation, and it is possible that the mild mass splittings between the first two generations of sleptons and $\tilde{\chi}_1^0$ will lead to energetic lepton final states so that they can be tested at CEPC. It is also possible to connect the $g-2$ explanation to neutrino masses [695].

3. τ weak-electric dipole moments

Electric dipole moments (EDM) and weak electric dipole moments (WDM) of fundamental fermions are important targets of experimental search for new physics, in particular for CP-violation beyond the Kobayashi-Maskawa mechanism. Any experimental observation of a nonzero value of an EDM (d) and/or WDM (d^w) for a lepton would be a smoking-gun evidence of non-SM sources of CP-violation, because the (loop-induced) SM contributions to these quantities for leptons are extremely small[696–698]. While d_τ can probed via $e^+e^- \to \tau^+\tau^-$ at energies much lower than the Z-boson mass, such as at $\Upsilon(4S)$ in BELLE [699, 700], the optimal measurement of d_τ^w should be the τ-pair production at the Z resonance.

To date, the best results are from LEP by measuring the transverse and normal τ-lepton polarizations [701, 702], which gave the limits on the real and imaginary parts [703–705]:

$$\begin{aligned} \mathrm{Re}[d_\tau^w] &= (-0.65 \pm 1.49) \times 10^{-18}\, e\,\mathrm{cm}, \\ \mathrm{Im}[d_\tau^w] &= (0.04 \pm 0.38) \times 10^{-17}\, e\,\mathrm{cm}. \end{aligned} \tag{32}$$

The large amount of $\tau^+\tau^-$ pairs during the planned Tera-Z mode of CEPC, along with an improved τ-reconstruction efficiency, will be able to test d_τ^w to a precision significantly higher than existing bounds.

Ref. [706] performed an exploratory study of the potential of CEPC for the measurements of d_τ^w, using both simple and optimal CP-violation observables[707–709], albeit with a particular emphasis on the latter due to its clear advantage over the former. In this work, $e^+e^- \to \tau^+\tau^-$ is considered exactly at the Z-resonance with the leading order SM couplings. d_τ^w is included through an effective $Z\tau\tau$-vertex followed by τ-decays, taking into account all spin-correlation effects. Assuming 1.38×10^{11} τ-pairs collected at the Z-resonance, we obtain the 1 s.d. statistical uncertainties in $\delta\mathrm{Re}[d_\tau^w]$ and $\delta\mathrm{Im}[d_\tau^w]$ are obtained, using both the simple observables T_{33}, $\hat{T}_{33}$, Q_{33}, $\hat{Q}_{33}$ where only one-prong decays of $\tau^\pm$ are included, and the optimal observables O_R, O_I that use the purely semi-hadronic decays of $\tau^\pm$. The analysis results are as given in Table XIII (see Ref. [706] for more details).

These numbers show that the CEPC sensitivity on d_τ^w can reach the level of $10^{-21}\, e\,\mathrm{cm}$ using O_R and O_I, far better than the current best bounds [703, 705] quoted above. Note e cm$= 5 \times 10^{13}$ e GeV^{-1} in natural units, a sensitivity to $10^{-21}\, e$ cm is equivalent to the

TABLE XIII: Ideal 1 s.d. statistical errors on $\mathrm{Re}[d_\tau^w]$ and $\mathrm{Im}[d_\tau^w]$.

$\delta\mathrm{Re}[d_\tau^w]$ [e cm]			$\delta\mathrm{Im}[d_\tau^w]$ [e cm]		
$\langle T_{33}\rangle$	$\langle\hat{T}_{33}\rangle$	$\langle O_R\rangle$	$\langle Q_{33}\rangle$	$\langle\hat{Q}_{33}\rangle$	$\langle O_I\rangle$
3.4×10^{-21}	3.4×10^{-21}	1.4×10^{-21}	3.2×10^{-19}	4.0×10^{-20}	2.1×10^{-21}

effective dipole moment $d\sim6\times10^{-6}$ GeV^{-1}. This is sufficient to be sensitive to certain beyond-SM models that predict values for d_τ^w of the order $10^{-19}\,e$ cm (see, e.g. [710, 711]). In particular, the sensitivity to $\mathrm{Re}[d_\tau^w]$ is improved by more than a factor two with O_R as compared to using the simple ones, whereas the sensitivity to $\mathrm{Im}[d_\tau^w]$ is improved by more than a factor ten, despite the restriction to purely semi-hadronic $\tau^\pm$ decay channels. In perspective, a more refined analysis will take SM radiative corrections into account, such as $Z\gamma$-interference etc., on top of the exploratory study above.

D. Spin entanglement

Recently, studies on quantum entanglement in the high energy regime have gained significant momentum. At colliders, reconstruction of the final-state particle helicity state offers an observation window on spin entanglement at energies much higher than that in optics laboratories. As a benchmark of spin entanglement, the test of the Bell inequality is of primary interest. It delivers a direct justification if Quantum Mechanics (QM) is a complete local theory and shows the contradiction of the local hidden variable theory (LHVT) with QM [712–714].

As the Higgs boson is the only spin-0 elementary particle in the Standard Model (SM), it offers a natural spin singlet state to test LHVT. The decay of the Higgs boson into two spin-1/2 particles provides an ideal system to reveal quantum entanglement and Bell inequality violation at high energies. In Ref. [715], it is proposed to test the Bell inequality through the Higgsstrahlung process $e^+e^-\to Zh$ at the CEPC.Two realistic methods of testing Bell inequality, i.e., Törnqvist's method [716] and the Clauser, Horne, Shimony and Holt (CHSH) inequality [717] are studied in terms of the polarization correlation in decay chain $h\to\tau^+\tau^-\to\pi^+\bar{\nu}_\tau\pi^-\nu_\tau$. We use the method of impact parameters for the reconstruction of τ lepton in our detector-level simulation and consider both the hadronic and leptonic decay

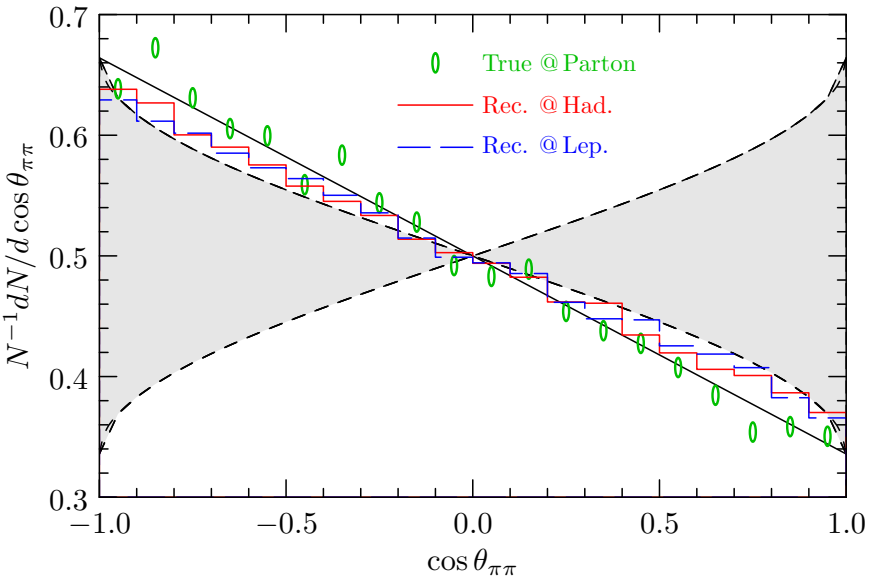

FIG. 98: Reconstructed distributions of $\cos\theta_{\pi\pi}$ for Törnqvist's test of Bell inequality. The gray-fitted region is the phase space consistent with classical prediction. The simulation results after using the method of impact parameters are represented by the red and blue histograms for hadronic and leptonic decay modes of Z boson, respectively.

modes of Z boson.

The experimental sensitivity of CEPC for the Törnqvist's approach is studied by defining the following asymmetric observable

$$\mathcal{A} = \frac{N(\cos\theta_{\pi\pi} < 0) - N(\cos\theta_{\pi\pi} > 0)}{N(\cos\theta_{\pi\pi} < 0) + N(\cos\theta_{\pi\pi} > 0)}, \tag{33}$$

where $\cos\theta_{\pi\pi} = \vec{p}_{\pi^-} \cdot \vec{p}_{\pi^+}/(|\vec{p}_{\pi^-}||\vec{p}_{\pi^+}|)$ in the Higgs rest frame. Fig. 98 shows the distribution of $\cos\theta_{\pi\pi}$ and the LHVT holds between the two dashed lines. The analytical prediction of the observable gives an upper bound $\mathcal{A} = 0.119$ in LHVT. From the simulation results of SM expectation, we obtain $\mathcal{A} = 0.133 \pm 0.269$ for $Z \to \ell\ell$ channel and $\mathcal{A} = 0.137 \pm 0.1$ for $Z \to jj$ channel, respectively, as listed in Table XIV. Smaller uncertainties can be obtained with $\mathcal{A} = 0.133 \pm 0.142$ or $\mathcal{A} = 0.137 \pm 0.053$ for updated luminosity $\mathcal{L} = 20$ ab^{-1}. In the CHSH approach, the LHVT supports the fact that the sum of the two largest eigenvalues (denoted by m_1+m_2) of the matrix $U = C^T C$ with C being the spin correlation matrix is not larger than 1. It turns out that both channels lead to $m_1 + m_2 > 1$, as listed in Table XIV. For both the Törnqvist's and CHSH approaches, the Bell inequality can be tested below 1σ level at the CEPC. It is expected that the sensitivity can be further improved by using

sophisticated jet reconstruction method and enhanced τ-jet identification efficiency.

Channels	Observable	LHVT	CEPC @ 5.6 ab^{-1}	CEPC @ 20 ab^{-1}
$Z \to \ell\ell$	$\mathcal{A}$	≤ 0.119	0.133 ± 0.269	0.133 ± 0.142
	$m_1 + m_2$	≤ 1	1.04 ± 0.921	1.04 ± 0.481
$Z \to jj$	$\mathcal{A}$	≤ 0.119	0.137 ± 0.1	0.137 ± 0.053
	$m_1 + m_2$	≤ 1	1.05 ± 0.355	1.05 ± 0.188

TABLE XIV: The results of observables testing the Bell inequality in Törnqvist's method and the CHSH approach. The experimental predictions are given for the CEPC with colliding energy $\sqrt{s} = 240$ GeV and total luminosities 5.6 ab^{-1} and 20 ab^{-1}.

Ref. [718] has studied quantum entanglement properties of the rare Higgs boson three-body decays into γ and dileptons within the context of the Standard Model, with electroweak 1-loop corrections included. Novel observables for these three-body decay are presented for the analysis of three lepton families ($l = e, \mu, \tau$), with each family analyzed separately since they lead to different experimental channels and the 1-loop contribution dominates different energy regimes in each case. Hence, they offer a unique opportunity to examine quantum correlations, between the spin degrees of freedom of the final state particles, arising at next-to-leading-order in perturbation theory for 3-qubit systems. The Higgs boson is the only spin-0 elementary particle in the SM and its properties will be measured to high precision at the 'Higgs factory' run of the Circular Electron Positron Collider (CEPC). Concretely, the dominant production mode corresponds to $e^- e^+ \to ZH$ and this future collider could improve the measurement accuracy of the spin correlation of the final decay products.

Based on the concurrence and Bell operator definitions for tripartite systems, the goal was to identify regions of the phase-space where the final particles are entangled after the Higgs boson decay and to determine the feasibility of testing non-locality under these kinematical configurations. For the three-body final state, various entanglement measures were computed, including one-to-other and one-to-one concurrences, the conditions for genuine entanglement of 3-qubit systems using the concurrence vector, the area of the concurrence triangle ($\mathcal{F}_3$) and the three-tangle measure. Regarding the Bell non-locality, both Mermin

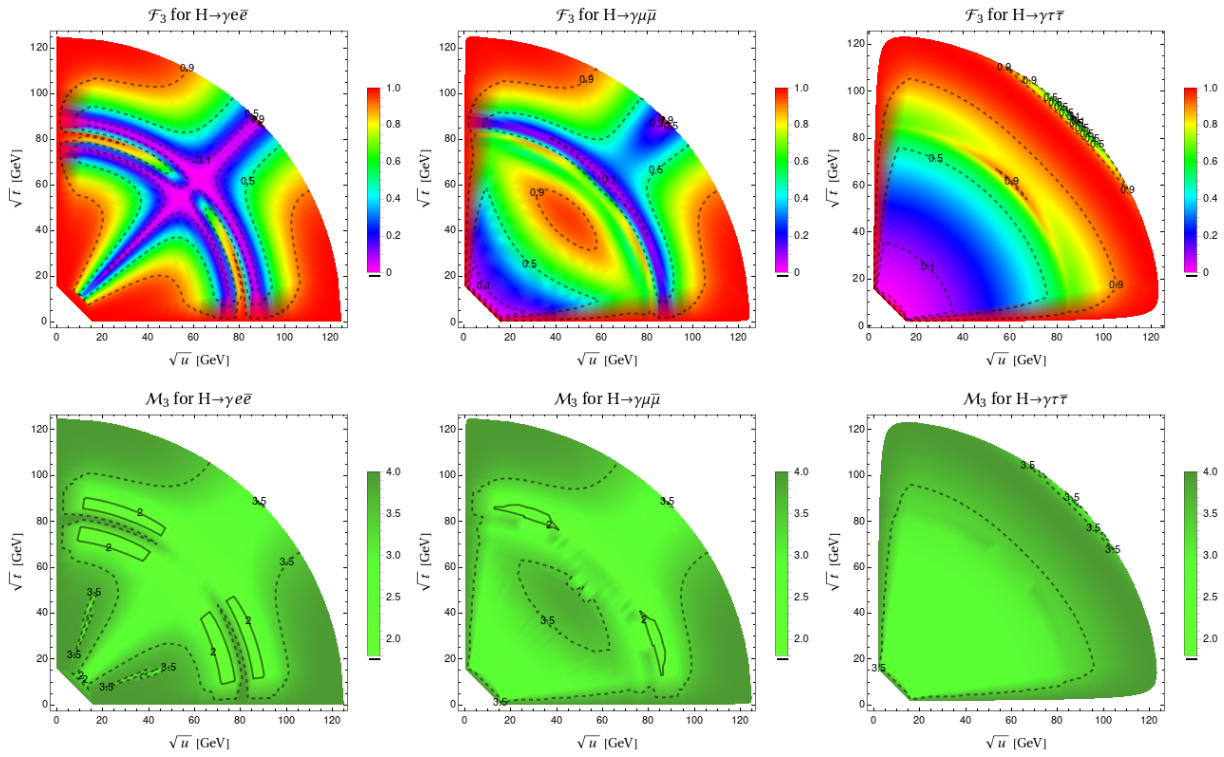

FIG. 99: Dalitz plot representation for genuine multipartite entanglement (first row) and Bell non-locality (second row) quantifiers within the SM for Higgs boson's $h \to l^+l^-\gamma$ decays. $l = e, \mu, \tau$ are shown in the left, middle and right columns, respectively. The Mandelstam variables t and u correspond to the subsystems photon-lepton and photon-anitlepton.

($\mathcal{M}_3$) and Svetlichny operators for 3-qubit systems were computed. Moreover, post-decay entanglement and auto-distillation phenomena for a dilepton invariant mass close to the Z-pole mass were analyzed.

It is found that the final photon, lepton, and antilepton result entangled after the Higgs boson decay since $\mathcal{F}_3$ is non-vanishing, as can be seen from the first row of Fig. 99. This also holds by considering the one-to-one and one-to-other concurrences of the subsystems among them. The amount of entanglement depends on the final state kinematical configuration and maximally entangled subsystems appear in certain regions of the phase-space (red regions where $\mathcal{F}_3 \sim 1$). Concerning the Bell non-locality (second row of Fig. 99), predictions incompatible with local realism ($2 \leq \mathcal{M}_3 \leq 4$) were obtained in the whole phase-space, except for a few particular configurations, suggesting that $H \to \gamma l\bar{l}$ could serve as an ideal

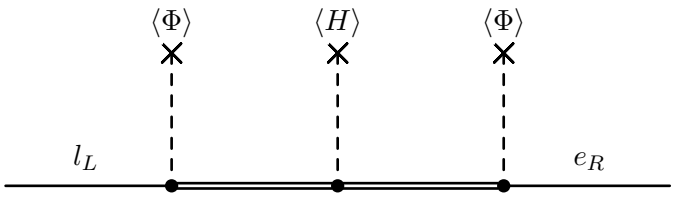

FIG. 100: A Feynman diagram which generates the charged lepton mass matrix. Plain lines represent the Standard Model charged leptons. Double lines represent heavy fermions. Dashed lines represent Higgs tadpoles as labeled.

laboratory for testing Bell inequality. On the other hand, CP-violating interactions in the Yukawa sector are suppressed by lepton masses, thus less powerful for such kind of new physics. Furthermore, a natural multipartite extension is to consider the four-fermion Higgs decays, constituting a 4-qubit system.

E. Exotic lepton mass models

Even more exotic models involving the lepton sector can benefit from the CEPC. For example, to a certain level of precision the SM's charged lepton masses seem to satisfy the curious formula:

$$K = \frac{m_e + m_\mu + m_\tau}{\left(\sqrt{m_e} + \sqrt{m_\mu} + \sqrt{m_\tau}\right)^2} = \frac{2}{3}, \tag{34}$$

proposed by Koide in early 1980's [719–721], it exhibits consistency with experimental data. The character K calculated from the PDG 2022 data of charged lepton masses [722] is $K = (2/3) \times (0.999991 \pm 0.000011)$, within 10^{-5} precision and within one sigma error. On the other hand, taking $K = 2/3$ as an input and using the measured electron and muon masses with high precision, the tau mass is predicted to be $m_\tau = 1776.969027 \pm 0.000036$ MeV/c^2. It agrees with the PDG 2022 data $m_\tau = 1776.86 \pm 0.12$ MeV/c^2 and the Belle II 2023 result [723] $m_\tau = 1777.09 \pm 0.08 \pm 0.11$ MeV/c^2 within one sigma error.

Proposals to explain such flavor mass pattern include the Froggatt-Nielsen model [724], the seesaw-type model [725] and the supersymmetric Yukawaon model [726]. The key idea is to express the charged lepton mass matrix as $M \propto \langle \Phi\Phi \rangle$, where Φ is a Hermitian nonet scalar field in the $\mathbf{3} \otimes \mathbf{3}^* = \mathbf{8} \oplus \mathbf{1}$ representation of the SU(3) flavor symmetry. In the Froggatt-Nielsen model or the seesaw-type model, the charged leptons couple to new fermions with a heavy mass m_F through Yukawa couplings involving Φ. Diagrams similar to Figure 100 generates a seesaw type mass matrix $M \propto \langle H\Phi\Phi \rangle / m_F^2$. In the Yukawaon model, the

Standard Model Yukawa coupling terms for leptons are replaced by dimension-five operators:

$$\mathcal{L}^{(5)} = -\frac{y_0}{\Lambda}\bar{l}_L Y H e_R + \text{h.c.}, \tag{35}$$

where Y is a flavor nonet scalar field called the Yukawaon. In a supersymmetric model with the superpotential

$$W = \mu\,\text{Tr}\,(YA) + \lambda\,\text{Tr}\,(\Phi\Phi A)\,, \tag{36}$$

where A is another flavor nonet scalar field, the F-term equations for A gives $\langle Y\rangle \propto \langle\Phi\Phi\rangle$ and thus $M \propto \langle\Phi\Phi\rangle$ after electroweak symmetry breaking. Any of these models give $K = \text{Tr}\langle\Phi\Phi\rangle/(\text{Tr}\langle\Phi\rangle)^2$. Then a superpotential for Φ is build through symmetry considerations [727, 728], and the F-term equations may set the vacuum expectation value of Φ which leads to $K = 2/3$. Future collider measurement of lepton masses, such as at the CEPC, will further scrutinize on empirical lepton mass patterns. Underlying physical models can be tested in leptonic channels of Higgs decay measurements on future colliders as well as from extra scalar/Higgs searches.

Quantity	Channel	Sensitivity scale (GeV)	CEPC Run
ALP $g_{a\gamma\gamma}^{-1}$	$e^+e^-\gamma\gamma$	6.7×10^3 [668]	Tera-Z
	$e^+e^-\gamma\gamma$	2.2×10^4 [668]	240 GeV
	$\bar{f}fa$	6.5×10^3 [668]	250 GeV
ALP $(g_{aBB}/4)^{-1}$	3γ	10^6 [74]	Tera-Z
	$\not{E}_T\gamma$	4.8×10^6 [74]	Tera-Z
ALP $(\epsilon_e^A/\Lambda)^{-1}$	$W\to\ell^\pm\nu a$	10^3 [670]	240 GeV
Tau $(d_\tau^{weak})^{-1}$	$\tau^+\tau^-$	6×10^6 [706]	Tera-Z
Bell Inequality	$Z,h\to\tau^+\tau^-$	1σ [715]	240 GeV

TABLE XV: Projected energy scale sensitivities via exotic searches at the CEPC.

For a brief summary, this section includes a number of CEPC related exotic physics studies in recent literature. Qualitative results on the projected energy scale sensitivities from dedicated investigation focus on well-motivated topics such as the ALP, τ lepton form factors,

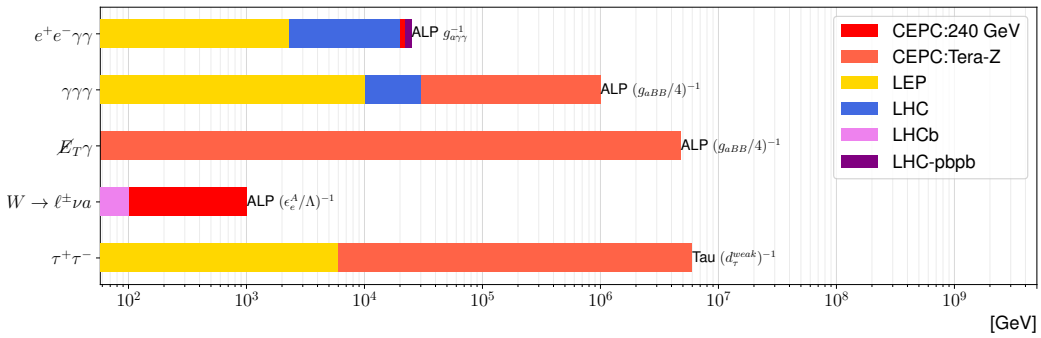

FIG. 101: Energy reach in representative exotic search channels at the CEPC. Note the maximal energy reach may apply to different model parameter regions between experiments.

Bell inequality tests, etc. Quantitative results from these studies are listed in Table XV and illustrated in the bar-chart of Fig. 101.

XII. GLOBAL FITS (JIAYIN, YANG, YONG DU)

Global fits are an essential tool when it comes to obtaining a thorough understanding of a new physics model. They offer a comprehensive analysis by considering a wide range of experimental data. With global fits, we can extract the maximum amount of information possible from these datasets. The primary advantage of global fits is their ability to evaluate and compare the validity of different models. By exploring a variety of model parameters, they can identify the range of values that are most likely or have the highest posterior probability. This, in turn, helps us comprehend the implications and predictions of the models for future searches and experiments.

In this section, we will discuss the latest research findings regarding the impact of the CEPC on the global fit analysis for SMEFT, 2HDMs, and various SUSY models.

A. SMEFT global fits

The SMEFT framework—As has been previously addressed, the null result at the LHC since the Higgs discovery indicates that the SM is possibly a low-energy effective theory of some UV completed theories at a scale $\Lambda \gg \Lambda_{\rm EW}$, with $\Lambda_{\rm EW} = 246\,{\rm GeV}$ the electroweak

scale. This large energy gap then naturally renders the EFT framework ideal for a model-independent study on new physics based on the decoupling theorem [729]. In this section, we focus on the SMEFT framework based on the same $\mathrm{SU}(3)_c \otimes \mathrm{SU}(2)_L \otimes \mathrm{U}(1)_Y$ *local* gauge symmetry as respected by the SM while relaxing the accidental *global* symmetries in the SM. Generically, the SMEFT can be obtained by extending the SM Lagrangian as

$$\mathcal{L} = \mathcal{L}_{\mathrm{SM}} + \sum_{n=5}^{\infty} \sum_{i} \frac{\delta c_i}{\Lambda^{n-4}} \mathcal{O}_i^{(n)}, \tag{37}$$

where $\mathcal{O}^{(n)}$ represents operators with mass dimension n, the index i corresponds to the sum over the operator basis at dimension n, and δc_i is the associated Wilson coefficient. Clearly, contributions from the SMEFT operators will be generically suppressed by powers of p^2/Λ^2, with $p^2 \ll \Lambda^2$ the momentum transfer. Therefore, the dominant contribution will be coming from the dimension-5 operators, which are also known as the Weinberg operators [507]. These operators can induce non-vanishing neutrino masses after the electroweak spontaneous symmetry breaking (EWSSB), but will be otherwise irrelevant for the discussion in this section. With that, we focus on the dimension-6 operators, where a basis, known as the *Warsaw basis*, was provided in[730, 731]. For phenomenological studies, a relatively convenient basis, known as the *Higgs basis*, was proposed in [732] in the broken phase, which is related to the *Warsaw basis* by a linear transformation. The advantage of the *Higgs basis* is that different physics becomes disentangled, thus reducing the number of operators in specific scenarios such as the Higgs, the electroweak, and the four-fermion induced physics as we will discuss in the following.

Methodology—For this global analysis, we will only keep EFT corrections to the SM predictions at $\mathcal{O}(1/\Lambda^2)$, *i.e.*, the interference between the SM and the SMEFT since pure EFT results will be further suppressed by p^2/Λ^2. Then under this approximation, one can generically parameterize

$$O_i = O_i^{\mathrm{SM}} + \delta \vec{c}_i \cdot \vec{O}_{i,\mathrm{SMEFT}}, \tag{38}$$

for any observable O_i, with $\vec{O}_{i,\mathrm{SMEFT}}$ the collection of operator contributions and O_i^{SM} its SM prediction. The global fit is then carried out based on the χ^2 constructed as

$$\chi^2 = \sum_{i,j} \left[O_i - O_i^{\mathrm{exp}}\right] \sigma_{ij}^{-2} \left[O_j - O_j^{\mathrm{exp}}\right], \tag{39}$$

where $O_i^{\rm exp}$ is the experimental measurement of O_i, and $\sigma_{ij}^{-2} = [\delta O_i \rho_{ij} \delta O_j]^{-1}$ with δO_i the experimental uncertainties and ρ_{ij} the experimental correlation between $O_{i,j}$. Note that under the linear SMEFT correction approximation as adopted here, χ^2 is a quadratic function in terms of the δc_i's, thus the global minimum can be analytically obtained from $\partial\chi^2/\partial\vec{\delta c}_i = 0$. On the other hand, this leading order approximation in eq. (38) also makes the optimal observable approach [709] applicable, which utilizes the full information of the process from the differential distributions and can also provide the best statistical reach. For this reason, optimal observables are used for this global analysis when application, $e^+e^- \to W^+W^-$ for instance. It is also worthy of mentioning, from a recent machine learning study in [733], that while this optimal observable approach can lead to satisfying results at the parton level, some bias in data interpretation will be introduced at the the detector level.

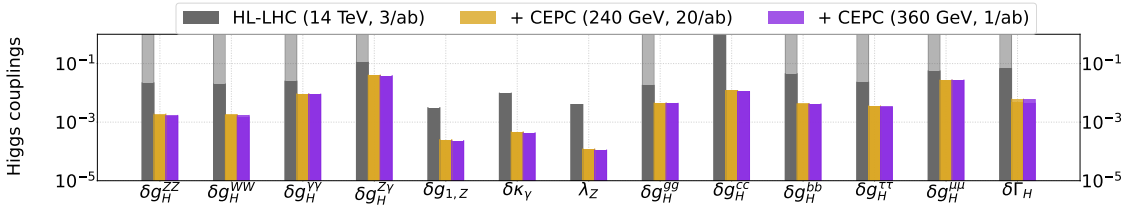

FIG. 102: 1σ relative uncertainties on the SMEFT operators as shown along the horizontal axis from a global analysis of the Higgs couplings. The light bars are obtained by taking the total Higgs decay width Γ_H as a free parameter, and the dark bars those with a constrained Γ_H.

Results—As a Higgs factory, CEPC is expected to improve significantly the SMEFT global analysis due to its high energy and luminosity. Ref. [734] performed a detailed global study on electroweak and Higgs physics, semi-leptonic and pure leptonic 4-fermion operators using the latest CEPC projections. The results are reproduced and shown in figures 102-103 by working in the most general flavor scenario. The central values of the Wilson coefficients in each plot are assumed to be aligned with the SM predictions, and only the 1σ relative uncertainties are shown for the LHC, HL-LHC, and CEPC with the center of mass energy $\sqrt{s} = 240\,(360)\,\text{GeV}$ and the integrated luminosity $\mathcal{L} = 20\,(1)\,\text{ab}^{-1}$. Figure 102 clearly shows that CEPC can improve the Higgs couplings by a factor of a few, or even orders of magnitude as can be seen, for example, for the triple gauge couplings $\delta g_{1,Z}$, $\delta\kappa_\gamma$, and λ_Z.

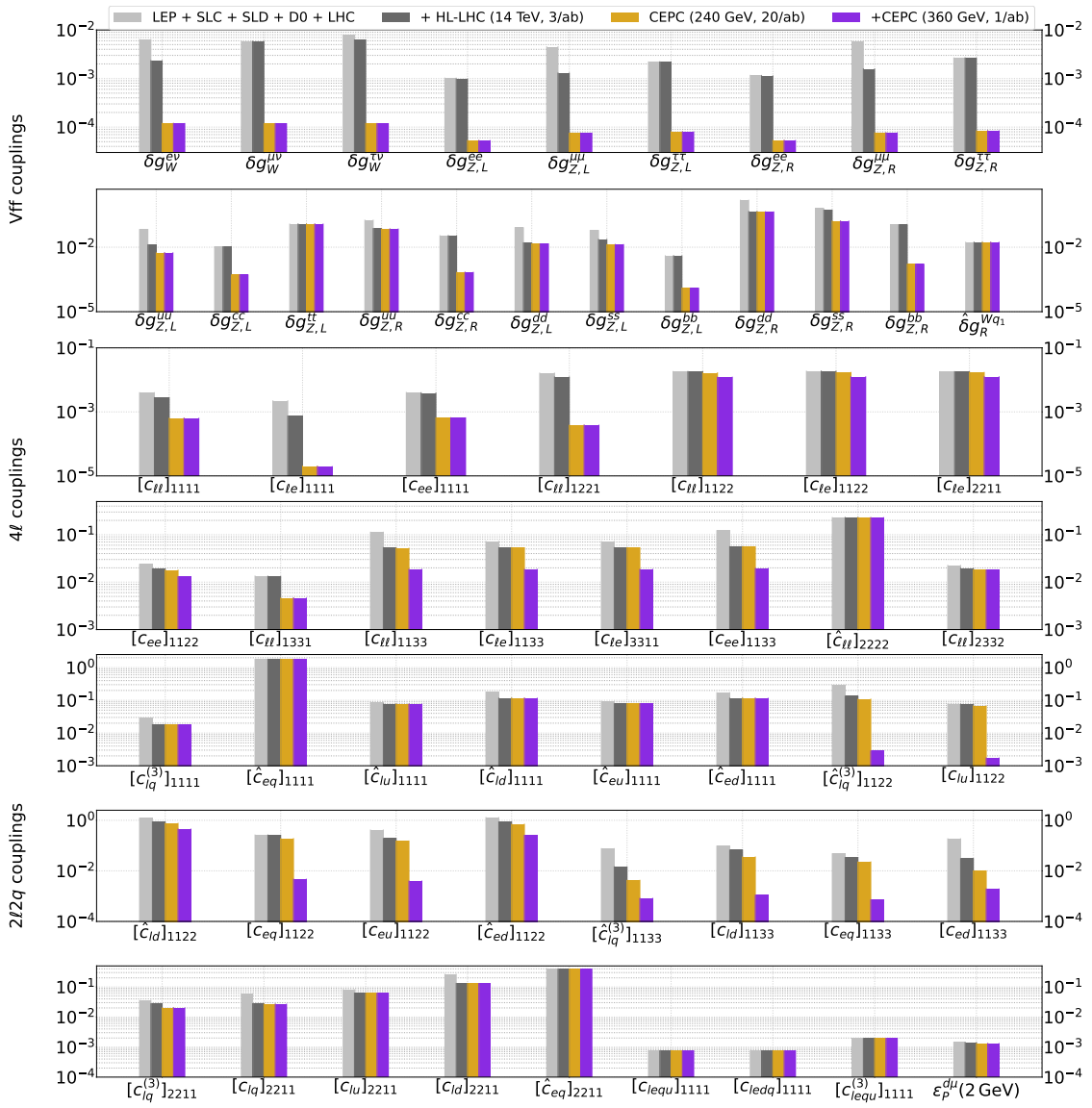

FIG. 103: Same as figure 102 but for the electroweak and 4-fermion operators.

The sensitivity reach of CEPC to leptonic electroweak vertices can be generically reduced down below the unprecedented 10^{-4} level as shown in the first row of figure 103, thanks to the high-luminosity of CEPC and radiative return to the Z pole from initial state radiation. The corresponding sensitivity to the hadronic electroweak vertices can also be improved by a few, or even an order of magnitude better as for $\delta g^{bb}_{Z,L/R}$ for instance. For the 4-fermion operators, CEPC can generically reduce the current uncertainties, as shown explicitly in the last five rows of figures 103. In particular, for the semi-leptonic operators, the global fit results with the inclusion of CEPC can be improved by $\mathcal{O}(10 \sim 10^2)$ for the 2nd and 3rd generation quarks due to tagging efficiencies of heavy quarks at CEPC. These stronger

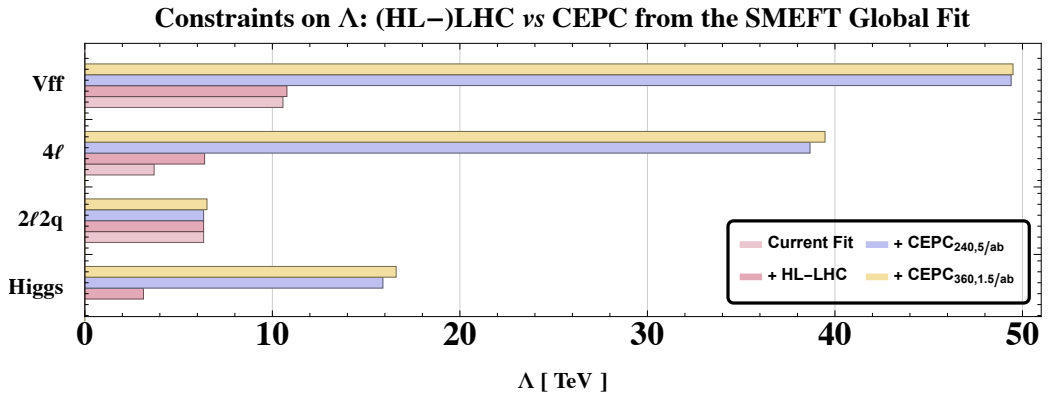

FIG. 104: Sensitivity to the cutoff scale Λ from the SMEFT global fit at the 95% CL. The y axis shows the optimal reach from electroweak physics ("Vff"), pure leptonic four-fermion operator induced physics ("4ℓ"), semileptonic four-fermion operator induced physics ("$2\ell 2q$"), and Higgs physics ("Higgs").

constraints as expected for CEPC will on the other hand also impose new challenges on the theoretical side, for example, theoretical uncertainties on the effective number of relative species during neutrino decoupling in the early Universe [735, 736]. These current theoretical errors will have to be further reduced at the CEPC era to match the precision of CEPC. In summary, CEPC can dramatically increase the sensitivity to Higgs, electroweak, and 4-fermion operators thanks to its high energy and luminosity, and as a result, enhancing its ability in discovering new physics at the 10∼70 TeV scale that could show up in either the Higgs, electroweak, or the 4-fermion sector as seen in the summary plot of figure 104.

B. 2HDM global fits (Tao Han, Shufang Su, Wei Su, Yongcheng Wu)

While all the indications from the current particle physics measurements seem to confirm the validity of the Standard Model (SM) up to the electroweak scale of a few hundreds GeV, and the observed Higgs boson is SM-like, there are compelling arguments, both from theoretical and observational points of view, in favor of the existence of new physics beyond the SM (BSM). As such, searching for new Higgs bosons would be of high priority since they are present in many extensions of theories beyond the SM. One of the most straightforward, but well-motivated extensions is the two Higgs doublet model (2HDM) [599], . There are five massive spin-zero states in the spectrum $(h, H^0, A^0, H^\pm)$ after the electroweak symmetry

breaking.

Complementary to the direct searches, precision measurements of SM parameters and the Higgs properties could lead to relevant insights on new physics. High precision achieved at future Higgs factories with about 10^6 Higgs bosons, and possible Z pole measurements with $10^{10} - 10^{12}$ Z bosons [5, 588, 602, 737] would hopefully shed light on the new physics associated with the electroweak sector. To take advantage of these precisions [583, 738], we make a global fit to explore their abilities of detecting new particles and constraining model parameter space.

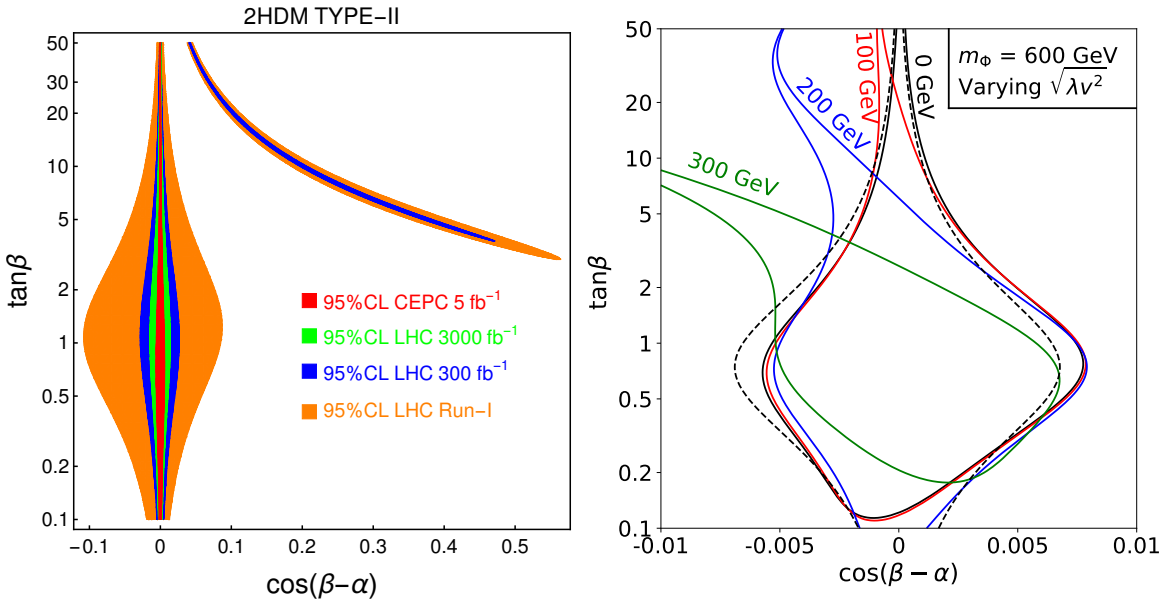

FIG. 105: The allowed region in the plane of $\cos(\beta-\alpha)$-$\tan\beta$ at 95% C.L. for the Type-II of 2HDM, given LHC and CEPC Higgs precision measurements at tree level(left) and loop level under CEPC (right). For the tree-left global fit, the special "arm" regions for the Type-II is the wrong-sign Yukawa region. The right panel shows the parameter space varying the value $\sqrt{\lambda v^2}$ with $m_A = m_H = m_{H^\pm} = m_\Phi = 600$ GeV. The tree-level only global fit results are shown by the dashed black lines for comparison. More details are shown in Ref. [583].

There is a plethora of articles in the literature to study the effects of the heavy Higgs states on the Higgs couplings in Models with extended Higgs sector [583, 599, 738]. In 2HDM, identifying the light CP-even Higgs h to be the experimentally observed 125 GeV Higgs, the couplings of h to the SM fermions and gauge bosons receive two contributions:

tree-level values, which are controlled by the mixing angles α of the CP-even Higgses and $\tan\beta$, ratios of the vacuum expectation values of two Higgses: $\tan\beta = v_2/v_1$, and loop contributions with heavy Higgses running in the loop.

With a global fit to the Higgs rate measurements at the LHC as well as the CEPC, assuming that no deviation to the SM values is observed at future measurements, the 95% C.L. region in the $\cos(\beta-\alpha)$ vs. $\tan\beta$ plane for various types of 2HDM (depending on how the two Higgs doublets are coupled to the quark and lepton sectors) are shown in Figure 105 for tree-level only effects. $\cos(\beta-\alpha)$ in all four types are tightly constrained at both small and large values of $\tan\beta$, except for Type-I (Ref. [583]), in which constraints are relaxed at large $\tan\beta$ due to suppressed Yukawa couplings.

To fully explore the Higgs factory potential in search for new physics beyond the SM, both the tree-level deviation and loop corrections need to be considered. The right panel of Figure 105 shows the 95% C.L. global fit results to all CEPC Higgs rate measurements in the Type-II 2HDM parameter space, including both tree level and loop corrections. Degenerate Heavy Higgs masses $m_A = m_H = m_{H^\pm} = m_\Phi$ are assumed such that Z-pole precision measurements are automatically satisfied. Black, red, blue and green curves are for model parameter $\sqrt{\lambda v^2} = \sqrt{m_\Phi^2 - m_{12}^2/s_\beta c_\beta} = 0$, 100, 200, and 300 GeV, respectively. The tree-level only global fit results are shown by the dashed black lines for comparison. $|\cos(\beta-\alpha)|$ is typically constrained to be less than about 0.008 for $\tan\beta \sim 1$. For smaller and larger values of $\tan\beta$, the allowed range of $\cos(\beta-\alpha)$ is greatly reduced. Loop effects from heavy Higgses tilt the value of $\cos(\beta-\alpha)$ towards negative, especially in the large $\tan\beta$ region.

Going beyond the degenerate mass case, both the Higgs and Z-pole precision variables are sensitive to the mass splittings between the charged Higgs and the neutral ones. Figure 106 shows the 95% C.L. range of $\Delta m_A = m_A - m_H$ vs. $\Delta m_C = m_{H^\pm} - m_H$ plane, for Higgs and Z-pole precision constraints individually in (left panel), and combined constraints (right panel), with $m_H = 600$ GeV and $\sqrt{\lambda v^2} = 300$ GeV. For the Higgs precision fit, the alignment limit (blue curve) leads to both Δm_A and Δm_C around 0 within a few hundred GeV range. Even for small deviation away from the alignment limit, Δm_A is constrained to be positive for $\cos(\beta-\alpha) = 0.007$, and negative for $\cos(\beta-\alpha) = -0.007$. The Z pole precision measurements (shown in region enclosed by blue dashed curves) constrain either $\Delta m_C \sim 0$ or $\Delta m_C \sim \Delta m_A$, equivalent to $m_{H^\pm} \sim m_{H,A}$. Combining both the Higgs and Z pole precisions (right panel), the range of $\Delta m_{A,C}$ are further constrained to a narrower range.

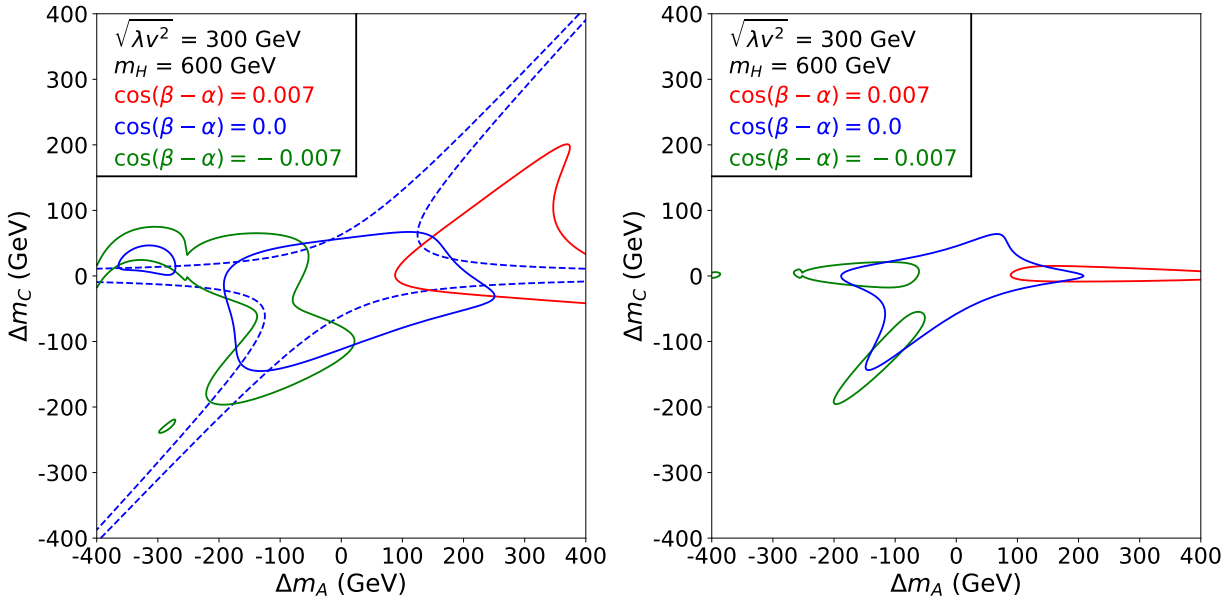

FIG. 106: Three-parameter fitting 95% C.L. range of Δm_A - Δm_C plane, focusing on the $\cos(\beta-\alpha)$ dependence (given by different colored lines), for Higgs and Z-pole precision constraints individually (left panel), and combined constraints (right panel) in the Type-II 2HDM. More details are shown in Ref. [738].

The expected accuracies at the Z-pole and at a Higgs factory are quite complementary in constraining heavy Higgs mass splittings.

In this section, we presented the results for the impactsof the precision measurements of the SM parameters at the proposed Z-factories and Higgs factories on the extended Higgs sector of 2HDM. For the tree-level 2HDM, $|\cos(\beta-\alpha)|$ can be restricted 0.008. When including the loop effects, CEPC precision can give lower bound on non-SM Higgs masses, as well as their splitting. Combining the Higgs and Z-pole precisions, the typical heavy Higgs mass splitting is constrained to be less than about 200 GeV.

C. SUSY global fits

It is shown in Sec. VII that the direct searches for sparticles at electron-positron colliders are restricted by collision energy. However, the high precision measurements of the Higgs and electroweak (EW) sector can significantly affect the global fit of SUSY models. Ref. [739] shown that conducting a global fit solely based on precise Higgs measurements at future

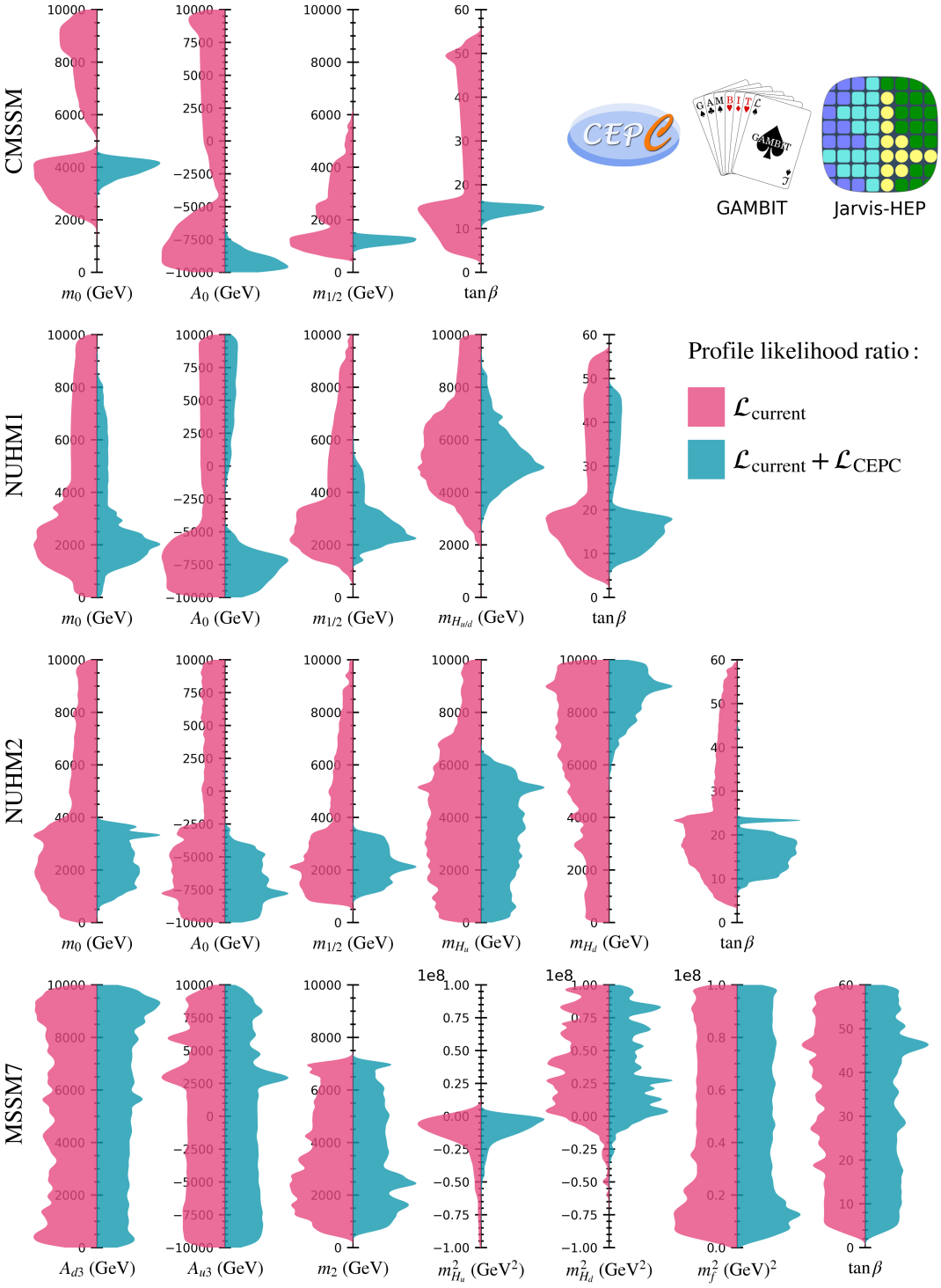

FIG. 107: One-dimensional profiled likelihood ratio for the global fit of the CMSSM, NUHM1, NUHM2, and MSSM7 models, using the present experimental data (left parts) and considering additional CEPC measurements (right parts).

Higgs factories could potentially raise the lower bound of the SUSY scale above TeV, for small values of $\tan\beta$.

Ref [350] performed several comprehensive global fits by combining Higgs measurements at CEPC with existing experimental data, using data provided by the GAMBIT community [740–742], for four supersymmetric models:

- CMSSM (Constrained Minimal Supersymmetric Standard Model). Inspired by scenarios where SUSY breaking is transmitted through supergravity interactions, the soft mass parameters at the Grand Unified Theory (GUT) scale are set to a universal scalar mass m_0, a universal gaugino mass $m_{1/2}$ and a universal trilinear couping A_0. The Higgs sector has two remaining free parameters defined at the scale m_Z: the ratio of the vacuum expectation values of the two Higgs doublets, $\tan\beta = v_u/v_d$ and the sign of μ.

- NUHM1 (Non-Universal Higgs Mass 1). The GUT-scale constraint on the soft scalar Higgs masses is relaxed by introducing an additional free parameter m_H . The soft Higgs masses m_{H_u} and m_{H_d} are not set equal to m_0, but instead obey the relation $m_{H_u} = m_{H_d} = m_H$ at the GUT scale.

- NUHM2 (Non-Universal Higgs Mass 2). The constraint on the soft Higgs masses is further relaxed so that m_{H_u} and m_{H_d} become independent, real, dimension-one parameters at the GUT scale.

- MSSM7 (seven-dimensional phenomenological MSSM). All the input parameters are defined at an energy near the electroweak scale. Inspired by GUT scale gaugino mass universality, the gaugino masses satisfy $3/5\cos^2\theta_W M_1 = \sin^2\theta_W M_2 = \alpha/\alpha_s M_3$. All entries in A_u, A_d and A_e are assumed to be zero except for $(A_u)_{33} = A_{u_3}$ and $(A_d)_{33} = A_{d_3}$. All of the off-diagonal entries in m_Q^2, m_u^2, m_d^2, m_L^2 and m_e^2 to be zero, so as to suppress flavour-changing neutral currents. By setting all remaining mass matrix entries to a universal squared sfermion mass $m_{\tilde{f}}^2$, the final list of free parameters contains M_2, A_{u_3}, A_{d_3}, $m_{\tilde{f}}^2$, $m_{H_u}^2$, $m_{H_d}^2$ and $\tan\beta$ (plus the input scale Q and the sign of μ).

Beside precise Higgs measurements at future Higgs factories, the likelihood functions include a number of direct and indirect dark matter searches, a large collection of electroweak

precision and flavour observables, direct searches for supersymmetry at the LEP and Runs I and II of the LHC, and constraints from Higgs observables.

Fig. 107 shows the profile likelihoods with and without the additional likelihood for the Higgs measurements at CEPC. Here, the central values of measurements at the CEPC are assumed to be the same as those predicted by the best-fit point of each model, because GAMBIT employed advanced sampling methods, resulting in a majority of samples being clustered around the best-fit point. The theoretical uncertainties utilized in the likelihood functions are scaled to be 0.2 times smaller than the current theoretical uncertainties of the SM Higgs. It is evident that a significant portion of the parameter region favored by the current constraints is disallowed when considering the precise Higgs measurements obtained from the CEPC. The preferred regions of the parameter space undergo a noticeable reduction in size, converging closer to the best-fit point. Consequently, the additional measurements from the CEPC hold the potential to differentiate between various dark matter annihilation mechanisms present in the models, as well as provide insights into the signs of the μ parameter. Comparing the results across different models, the constraints placed on the model parameters tend to be weaker in models characterized by a larger number of input parameters, i.e., looser correlations between the model parameters. For 19-parameter phenomenological MSSM, Ref. [743] shows that future the e^+e^- collider can test up to $10\% \sim 12\%$ of the samples obtained from a flat scan that have not been excluded by current LHC direct SUSY searches and flavor physics data.

In conclusion, future Higgs factories equipped with high-precision Higgs coupling measurements have the potential to greatly enhance our comprehension of the parameter space and mass spectrum in the MSSM. They offer valuable complementary information to dark matter searches and EW precision measurements. By providing precise data on Higgs couplings, these Higgs factories can contribute substantially to furthering our understanding of fundamental physics and refining our knowledge of the MSSM.

XIII. CONCLUSION (JIA LIU)

This document describes the beyond the Standard Model physics potential of CEPC. CEPC will run as powerful probes of new physics, through runs on Higgs, Z and W and is capable to upgrade runs above the $\bar{t}t$ threshold. We explore and summarize BSM scenarios

where CEPC can make significant contributions. In this document, we have classified the BSM scenarios following the previous submission for snowmass 2021, including exotic Higgs, W/Z and top decays, the dark matter and dark sector, the long-lived particles, the supersymmetry models, the flavor physics, the electroweak phase transition and gravitational wave physics, the neutrino physic, the exotic models and global fit studies.

Since the major physics goal of CEPC is precision study of the Higgs physics, it is very natural to study the BSM physics connecting to SM physics through the Higgs portal operators and other Higgs related higher dimensional operators. These operators may modify the SM Higgs couplings and lead to the exotic Higgs decays. The CEPC with integrated luminosity of 20 ab^{-1} is able to constrain the BR of various exotic Higgs decay channels, that for the full invisible decay down to 0.24%, semi-invisible decay ranges from [0.03%, 0.2%] and two dark sector particles with further decaying to SM particles ranges from [0.03%, 0.6%]. In the final summary Figure 108, we show the sensitivity comparison for the semi-invisible decay $H \to (jj) + \not{E}$, dark sector particle decays $H \to XX, X \to b\bar{b}$ or $X \to \bar{\tau}\tau$ for CEPC and HL-LHC. Comparing the HL-LHC, the cleaner lepton collider environment leads to better limits on full-visible channels by 2-3 orders of magnitudes, while the ability to fully reconstruct the missing energy helps to provide better constraints for full-invisible and semi-invisible channels by 2-4 orders of magnitudes.

Another important physics goal of CEPC is the precision measurement of the Z gauge boson at the Z-pole, which can significantly increase the precision of the electroweak parameters measured since LEP. The dark sector particles may be effectively charged under the electroweak gauge interactions, therefore leading to various exotic Z decays through off-shell mediation or being the on-shell decay products. The exotic Z decays can also be classified by whether containing invisible particles, light resonance of SM particle pair or non-resonant 3-body decays. In Figure 108, we show the sensitivity comparison for the semi-invisible decays $Z \to \not{E} + \gamma$ and $Z \to (jj) + \not{E}$, dark sector decays $Z \to a + \gamma, a \to \gamma\gamma$ for CEPC and HL-LHC. In general, the Tera-Z setup of CEPC can reach BR limits from $[10^{-7}, 10^{-11}]$ for semi-visible channels and $[10^{-6}, 10^{-9}]$ for full-visible channels. The full-invisible Z decay can place constraints on N_{eff} with relative error of about 10^{-3}, which is also easy to constrain Z coupling to dark matter and sterile neutrinos.

The CEPC is well-suited for probing light dark matter and dark sector particles that couple to the electroweak sector of the Standard Model (SM). Dark matter and dark sector

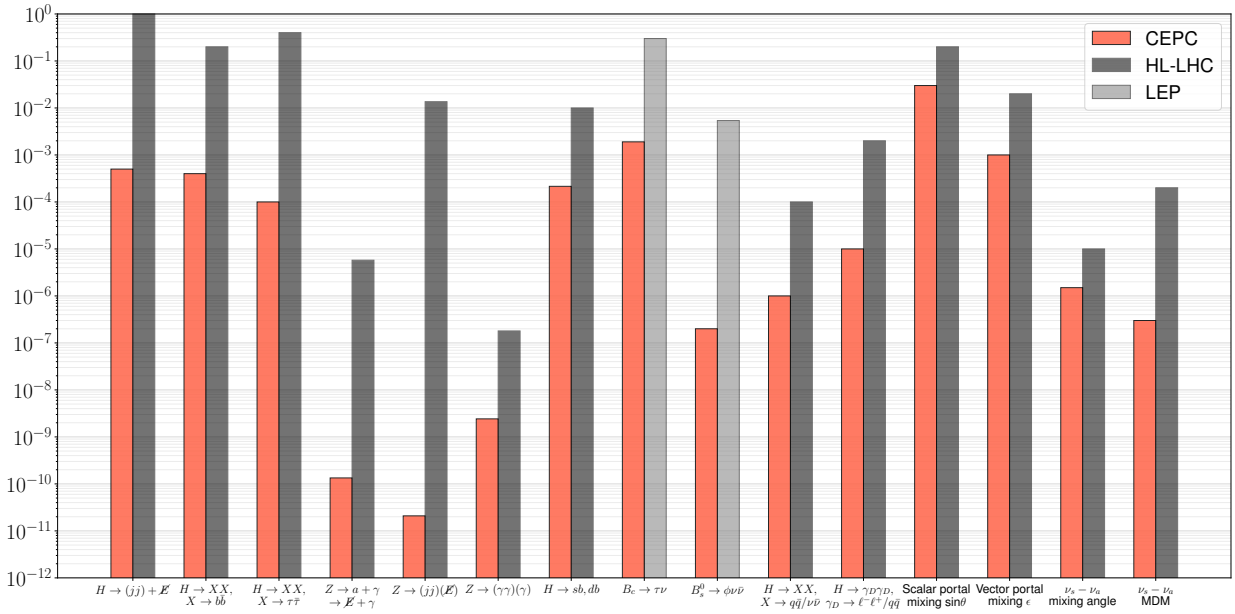

FIG. 108: Projected sensitivities of the CEPC and HL-LHC for various new physics scenarios, including exotic Higgs and Z-boson decays, long-lived particle searches, flavor-violating Higgs and B-meson decays, scalar and vector portal mixing, as well as sterile-active neutrino mixing and magnetic dipole moment interactions. For flavor-violating B-meson decay channels, there are existing constraints from LEP only.

particles can interact with the SM through scalar, fermion, and vector portals. Many of these models can be tested via exotic Higgs and Z decays, as discussed in the previous section. Additionally, CEPC has the potential to directly produce dark sector particles via Drell-Yan processes and dark matter particles through associated production channels. These channels offer up to an order of magnitude improvement in sensitivity to the mixing angle or coupling strength for scalar, fermion, and kinetic portals, as well as the coupling strength for dark matter with electric or magnetic dipole moments. In Figure 108, we show the sensitivity comparison for the scalar portal mixing and the vector portal mixing, where CEPC is better than HL-LHC by about one order. The capability for full final-state reconstruction with missing energy, along with its clean experimental environment, are crucial for CEPC to deliver competitive sensitivity for dark sector models.

BSM particles may be long-lived in collider experiments. The CEPC detectors are well-suited for detecting long-lived particles, and the sensitivities of additional far detectors and beam dump detectors have been discussed. Due to its high integrated luminosity for Z,

Higgs, and W boson production, the CEPC is highly competitive for studying LLP decays from these bosons. In Figure 108, we show the branching ratio sensitivity comparison for the Higgs decay to long-lived dark photon pair, which further decays to quarks or leptons. Furthermore, the CEPC offers a cleaner experimental environment compared to the HL-LHC, enhancing its sensitivity to LLPs decaying into certain final states. For example, this could involve a LLP stau, acting as the NLSP, decaying into a gravitino and a tau lepton. Thus, LLP studies at the CEPC can provide complementary measurements to those at the HL-LHC.

Supersymmetry is a compelling scenario for new physics. While the CEPC has a lower center-of-mass energy compared to the HL-LHC, it can still effectively study light electroweakinos and sleptons, covering masses up to half of its energy. Additionally, if one of the electroweakinos or sleptons in a pair production process is allowed to be off-shell, the mass reach can extend even further. The CEPC also benefits from the low threshold and the clean experimental environment, which enhances its ability to detect soft objects. This is particularly important for improving sensitivity to scenarios with a compressed mass spectrum.

Flavor physics presents significant potential for uncovering new physics, and the CEPC holds great promise in this area due to the high statistics of Z gauge boson events, a cleaner experimental environment, and the ability to fully reconstruct events with missing energy. The high integrated luminosity at the Z pole allows sensitivity improvements of 2-4 orders of magnitude for exotic decays of charged lepton that violate the flavor Z, such as $Z \to \ell\ell'$. Additionally, the CEPC will allow for a highly precise examination of tau lepton cLFV decays, achieving sensitivity improvements of approximately two orders of magnitude. Sensitivity to rare B, B_s, and B_c hadron decays via FCNC processes can also be improved by 2–3 orders of magnitude, particularly in cases where the final state involves a τ lepton. In Figure 108, we show the branching ratio sensitivity comparison for the flavor violating Higgs decay $H \to sb, db$ and B meson decays $B_c \to \tau\nu$ and $B_s^0 \to \phi\bar{\nu}\nu$, where CEPC projected sensitivities are significantly better than HL-LHC and LEP experiments.

The study of electroweak phase transitions and gravitational waves is highly pertinent to the CEPC. BSM physics could induce a first-order electroweak phase transition, significantly altering the Higgs potential, as evidenced by deviations in the Higgs self-coupling (h^3) and its couplings to ZZ bosons. Precision measurements of the hZ cross-section can inform

the Standard Model Effective Field Theory in the context of FOEWPT, complementing gravitational wave observations. Searches for exotic Higgs decays into lighter scalars can effectively constrain the FOEWPT parameter space. CEPC is particularly well-suited for studying the $\tau\tau$ and $b\bar{b}$ decay channels, offering a significant advantage over the HL-LHC.

Neutrino masses and oscillations require BSM physics, and the CEPC can play a significant role in exploring these phenomena. The CEPC can complement existing studies by covering parameter spaces for sterile neutrinos and non-standard neutrino interactions. With its high integrated luminosity at the Z-pole and Higgs associated production, combined with a clean experimental environment, the CEPC can achieve superior sensitivity in detecting displaced sterile neutrinos from Z and Higgs decays, surpassing the capabilities of the HL-LHC. Additionally, with potential main detector setups and far detector or beam dump options, the CEPC could further enhance its reach. The transition dipole operator for sterile neutrinos, particularly for masses above the GeV scale, can be most effectively probed at CEPC, leveraging its full reconstruction capability. In Figure 108, we show the sensitivity reach for the sterile neutrino and active neutrino mixing and magnetic dipole moment interaction.

For general new physics models, the CEPC offers unique capabilities to constrain axion-like particles (ALPs), particularly through their anomalous couplings to Standard Model gauge bosons. The production of ALPs from Higgs and Z bosons at the CEPC provides complementary coverage to that of the HL-LHC and heavy ion colliders, with an advantage in the low-mass region due to the lower production thresholds and cleaner experimental environment of CEPC. Additionally, the precise measurement of the electromagnetic form factor of charged leptons, especially tau leptons, is a crucial test of the Standard Model and a probe for new physics. The CEPC is well-positioned to excel in this area, offering improvements in the measurement of the tau mass, which could be instrumental in testing exotic theories such as the Koide lepton mass formula.

The global fit analysis has been performed for SMEFT, 2HDM, and various SUSY models for CEPC. The CEPC offers a 1-3 order improvement on Higgs coupling SMEFT operators and a 1-2 order improvement on electroweak vector-fermion couplings, especially for leptons and second/third-generation quarks, compared to HL-LHC. For 2HDM, the precision measurement of the Higgs and Z-pole at CEPC can constrain the Higgs parameter $|\cos(\beta-\alpha)|$ to less than 0.008, and the typical mass splitting of heavy Higgs to less than about 200 GeV.

For small $\tan\beta$, the SUSY scale can be raised to above 1 TeV using the precision data of Higgs and electroweak measurements.

In summary, CEPC offers unprecedented high precision Higgs, Z, W boson and top quark measurements. Additionally, CEPC can fully reconstruct missing energy, which is advantageous for searching semi-visible final states compared to hadron colliders. Moreover, CEPC has lower threshold and better tagging efficiency for heavy quarks and leptons, thereby extending the range of search models. Consequently, CEPC serves as a crucial complement to the current HL-LHC for BSM physics related to Higgs and Z gauge bosons, which are generally important for the electroweak sector of the SM and shed light for new physics in a comprehensive manner.

ACKNOWLEDGEMENTS (MANQI?)

SFG and KM would like to thank Ning Zhou, Hai-Jun Yang, and Manqi Ruan for useful discussions. The authors are supported by the National Natural Science Foundation of China (12375101, 12090060, and 12090064) and the SJTU Double First Class start-up fund (WF220442604). SFG is also an affiliate member of Kavli IPMU, University of Tokyo. KM is supported by the Innovation Capability Support Program of Shaanxi (Program No. 2021KJXX-47). XDM is supported by Guangdong Major Project of Basic and Applied Basic Research (No. 2020B0301030008).

GLOSSARY (XUAI)

ATLAS A Toroidal LHC Apparatus

ALP Axion-like Particle

BNL Brookhaven national laboratory

BSM Beyond the Standard Model

CDR Conceptual Design Report

CEPC Circular Electron-Positron Collider

cFLV charged Lepton Flavour Violation

CHARM CERN-Hamburg-Amsterdam-Rome-Moscow collaboration

CHSH Clauser, Horne, Shimony and Holt

CKM Cabibbo–Kobayashi–Maskawa

CMSSM Constrained Minimal Supersymmetric Standard Model

CP Charge Parity

DM Dark Matter

DS Dark Sector

EDM Electric Dipole Moments

EFT Effective Field Theory

EHM Emergent Hadron Mass

EW ElectroWeak

EWKino ElectroWeakino

EWPT ElectroWeak Phase Transition

FCC Future circular collider

FD Far Detector

FNAL Fermi national accelerator laboratory

FOEWPT First Order ElectroWeak Phase Transition

HB Higgs boson

HVP Hadronic vaccum polarisation

GUT Grand Unification Theory

GW Gravitational Waves

LEP Large electron-positron collider

LFU Lepton Flavour Unitarity

LFV Lepton Flavour Violation

LHC Large hadron collider

LHVT Local hidden variable theory

LLP Long-Lived Particle

MC Monte Carlo

MD Main Detector

MSSM Minimal Supersymmetric Standard Model

ND Near Detector

NP New Physics

NSI Non-Standard Interaction

NUHM Non-Universal Higgs Mass

OPAL Omni-Purpose Apparatus at LEP

PDG Particle data group

QED Quantum ElectroDynamics

QCD Quantum ChromoDynamics

QM Quantum Mechanics

SM the Standard Model

SMEFT the Standard Model Effective Field Theory

SUSY Supersymmetry

SUGRA Supersymmetric gravity

2HDM Two-Higgs-Doublet Model

VLL Vector-like Lepton

WDM Weak Dipole Moment

WIMP Weakly Interacting Massive Particle

---

[1] S. Dawson *et al.*, "Report of the Topical Group on Higgs Physics for Snowmass 2021: The Case for Precision Higgs Physics," in *Snowmass 2021*. 9, 2022. arXiv:2209.07510 [hep-ph].

[2] **ILC International Development Team** Collaboration, I. Adachi *et al.*, "The International Linear Collider: Report to Snowmass 2021," arXiv:2203.07622 [physics.acc-ph].

[3] **CLIC** Collaboration, J. de Blas *et al.*, "The CLIC Potential for New Physics," arXiv:1812.02093 [hep-ph].

[4] **FCC** Collaboration, A. Abada *et al.*, "FCC-ee: The Lepton Collider: Future Circular Collider Conceptual Design Report Volume 2," *Eur. Phys. J. ST* **228** (2019) no. 2, 261–623.

[5] M. Ahmad *et al.*, "CEPC-SPPC Preliminary Conceptual Design Report. 1. Physics and Detector," 3, 2015. IHEP-CEPC-DR-2015-01, IHEP-TH-2015-01, IHEP-EP-2015-01.

[6] "CEPC-SPPC Preliminary Conceptual Design Report. 2. Accelerator," 1, 2015. IHEP-CEPC-DR-2015-01, IHEP-AC-2015-01.

[7] J. de Blas, J. Gu, and Z. Liu, "Higgs Precision at a 125 GeV Muon Collider," arXiv:2203.04324 [hep-ph].

[8] M. Bai *et al.*, "C^3: A "Cool" Route to the Higgs Boson and Beyond," in *2022 Snowmass Summer Study*. 10, 2021. arXiv:2110.15800 [hep-ex].

[9] V. N. Litvinenko, N. Bachhawat, M. Chamizo-Llatas, Y. Jing, F. Méot, I. Petrushina, and T. Roser, "The ReLiC: Recycling Linear e^+e^- Collider," arXiv:2203.06476 [hep-ex].

[10] V. N. Litvinenko, N. Bachhawat, M. Chamizo-Llatas, F. Meot, and T. Roser, "CERC - Circular e^+e^- Collider using Energy-Recovery Linac," in *2022 Snowmass Summer Study*. 3, 2022. arXiv:2203.07358 [physics.acc-ph].

[11] **CEPC Study Group** Collaboration, M. Dong *et al.*, "CEPC Conceptual Design Report: Volume 2 - Physics & Detector," arXiv:1811.10545 [hep-ex].

[12] **CEPC Study Group** Collaboration, W. Abdallah *et al.*, "CEPC Technical Design Report: Accelerator," *Radiat. Detect. Technol. Methods* **8** (2024) no. 1, 1–1105, arXiv:2312.14363 [physics.acc-ph].

[13] J. Tang, Y. Zhang, Q. Xu, J. Gao, X. Lou, and Y. Wang, "Snowmass 2021 White Paper AF4 - SPPC," in *2022 Snowmass Summer Study*. 3, 2022. arXiv:2203.07987 [hep-ex].

[14] **CEPC Accelerator Study Group** Collaboration, J. Gao, "Snowmass2021 White Paper AF3-CEPC," arXiv:2203.09451 [physics.acc-ph].

[15] T. Sjöstrand, S. Ask, J. R. Christiansen, R. Corke, N. Desai, P. Ilten, S. Mrenna, S. Prestel, C. O. Rasmussen, and P. Z. Skands, "An introduction to PYTHIA 8.2," *Comput. Phys.*

Commun. **191** (2015) 159–177, arXiv:1410.3012 [hep-ph].

[16] M. Ruan and H. Videau, "Arbor, a new approach of the Particle Flow Algorithm," in *International Conference on Calorimetry for the High Energy Frontier*, pp. 316–324. 2013. arXiv:1403.4784 [physics.ins-det].

[17] J. S. Marshall and M. A. Thomson, "Pandora Particle Flow Algorithm," in *International Conference on Calorimetry for the High Energy Frontier*, pp. 305–315. 2013. arXiv:1308.4537 [physics.ins-det].

[18] Y. Wang, S. Descotes-Genon, O. Deschamps, L. Li, S. Chen, Y. Zhu, and M. Ruan, "Prospects for $B^0_{(s)} \to \pi^0\pi^0$ and $B^0_{(s)} \to \eta\eta$ modes and corresponding CP asymmetries at Tera-Z," *JHEP* **12** (2022) 135, arXiv:2208.08327 [hep-ph].

[19] H. Liang, Y. Zhu, Y. Wang, Y. Che, C. Zhou, H. Qu, and M. Ruan, "Jet origin identification and measurement of rare hadronic decays of Higgs boson at e^+e^- collider," arXiv:2310.03440 [hep-ex].

[20] **LHCb** Collaboration, R. Aaij *et al.*, "Measurement of b-hadron branching fractions for two-body decays into charmless charged hadrons," *JHEP* **10** (2012) 037, arXiv:1206.2794 [hep-ex].

[21] H. Cui, M. Zhao, Y. Wang, H. Liang, and M. Ruan, "Jet charge identification in ee-Z-qq process at Z pole operation," arXiv:2306.14089 [hep-ex].

[22] L. Li, M. Ruan, Y. Wang, and Y. Wang, "Analysis of $B_s \to \phi\nu\nu$ at CEPC," *Phys. Rev. D* **105** (2022) no. 11, 114036, arXiv:2201.07374 [hep-ph].

[23] Y. Zhu, S. Chen, H. Cui, and M. Ruan, "Requirement analysis for dE/dx measurement and PID performance at the CEPC baseline detector," *Nucl. Instrum. Meth. A* **1047** (2023) 167835, arXiv:2209.14486 [physics.ins-det].

[24] F. Cuna, N. De Filippis, F. Grancagnolo, and G. F. Tassielli, "Simulation of particle identification with the cluster counting technique," in *International Workshop on Future Linear Colliders*. 5, 2021. arXiv:2105.07064 [physics.ins-det].

[25] T. S. M. Ho, X.-H. Jiang, T. H. Kwok, L. Li, and T. Liu, "Testing Lepton Flavor Universality at Future Z Factories," arXiv:2212.02433 [hep-ph].

[26] F. Bedeschi, M. Caccia, R. Ferrari, P. Giacomelli, F. Grancagnolo, P. Azzi, and S. Braibant, "IDEA detector Letter of Intent." https://www.snowmass21.org/docs/files/summaries/EF/SNOWMASS21-EF1_EF4-IF3_IF6-096.pdf, 2021.

[27] Y. Che, V. Boudry, H. Videau, M. He, and M. Ruan, "Cluster time measurement with CEPC calorimeter," *Eur. Phys. J. C* **83** (2023) no. 1, 93, arXiv:2209.02932 [physics.ins-det]. [Erratum: Eur.Phys.J.C 83, 470 (2023)].

[28] R. Manqi, "The CEPC simulation and tools: software and performance." http://ias.ust.hk/program/shared_doc/2019/201901hep/conf/20190121_4042_pm_Manqi%20Ruan.pdf, 2019.

[29] Y. Shen, H. Xiao, H. Li, S. Qin, Z. Wang, C. Wang, D. Zhang, and M. Ruan, "Photon Reconstruction Performance at the CEPC baseline detector," arXiv:1908.09062 [physics.ins-det].

[30] P.-Z. Lai, M. Ruan, and C.-M. Kuo, "Jet performance at the circular electron-positron collider," *JINST* **16** (2021) no. 07, P07037, arXiv:2104.05029 [hep-ex].

[31] D. Yu, T. Zheng, and M. Ruan, "Lepton identification performance in Jets at a future electron positron Higgs Z factory," arXiv:2105.01246 [hep-ex].

[32] X. Li, M. Ruan, and M. Zhao, "Prospect for measurement of CP-violation phase ϕ_s study in the $B_s \to J/\Psi\phi$ channel at future Z factory," arXiv:2205.10565 [hep-ex].

[33] T. Zheng, J. Wang, Y. Shen, Y.-K. E. Cheung, and M. Ruan, "Reconstructing K_S^0 and Λ in the CEPC baseline detector," *Eur. Phys. J. Plus* **135** (2020) no. 3, 274.

[34] D. Yu, M. Ruan, V. Boudry, H. Videau, J.-C. Brient, Z. Wu, Q. Ouyang, Y. Xu, and X. Chen, "The measurement of the $H \to \tau\tau$ signal strength in the future e^+e^- Higgs factories," *Eur. Phys. J. C* **80** (2020) no. 1, 7.

[35] **CEPC calorimetry working group** Collaboration, Y. Liu, J. Jiang, and Y. Wang, "High-granularity crystal calorimetry: conceptual designs and first studies," *JINST* **15** (2020) no. 04, C04056.

[36] M. T. Lucchini, L. Pezzotti, G. Polesello, and C. G. Tully, "Particle flow with a hybrid segmented crystal and fiber dual-readout calorimeter," *JINST* **17** (2022) no. 06, P06008, arXiv:2202.01474 [hep-ex].

[37] Z. Xiao and Z. Huaqiao, "Performance study of cross-crystal Fan Ecal for CEPC.." https://indico.ihep.ac.cn/event/16906/contributions/50989/attachments/24588/27822/cross-crystal_fan_Ecal.pptx, 2022.

[38] B. Qi and Y. Liu, "R&D of a Novel High Granularity Crystal Electromagnetic Calorimeter," *Instruments* **6** (2022) no. 3, 40.

[39] A. Ronzhin, S. Los, E. Ramberg, A. Apresyan, S. Xie, M. Spiropulu, and H. Kim, "Study of the timing performance of micro-channel plate photomultiplier for use as an active layer in a shower maximum detector," *Nucl. Instrum. Meth. A* **795** (2015) 288–292.

[40] J. Va'vra, "PID Techniques: Alternatives to RICH Methods," *Nucl. Instrum. Meth. A* **876** (2017) 185–193, arXiv:1611.01713 [physics.ins-det].

[41] X. She *et al.*, "Development of Time Projection Chamber prototype integrated with UV laser tracks for the future circular e^+e^- collider," *JINST* **18** (2023) no. 07, C07015.

[42] H. Qu and L. Gouskos, "ParticleNet: Jet Tagging via Particle Clouds," *Phys. Rev. D* **101** (2020) no. 5, 056019, arXiv:1902.08570 [hep-ph].

[43] G. Li, L. Liao, X. Lou, P. Shen, W. Song, S. Wang, and Z. Zhang, "Classify the higgs decays with the pfn and particlenet at electron–positron colliders*," *Chinese Physics C* **46** (nov, 2022) 113001. https://dx.doi.org/10.1088/1674-1137/ac7f21.

[44] H. Liang, Y. Zhu, Y. Wang, Y. Che, M. Ruan, C. Zhou, and H. Qu, "Jet-origin identification and its application at an electron-positron higgs factory," *Phys. Rev. Lett.* **132** (May, 2024) 221802. https://link.aps.org/doi/10.1103/PhysRevLett.132.221802.

[45] Z. Liu, L.-T. Wang, and H. Zhang, "Exotic decays of the 125 GeV Higgs boson at future e^+e^- lepton colliders," *Chin. Phys. C* **41** (2017) no. 6, 063102, arXiv:1612.09284 [hep-ph].

[46] D. Curtin *et al.*, "Exotic decays of the 125 GeV Higgs boson," *Phys. Rev.* **D90** (2014) no. 7, 075004, arXiv:1312.4992 [hep-ph].

[47] **LHC Higgs Cross Section Working Group** Collaboration, D. de Florian *et al.*, "Handbook of LHC Higgs Cross Sections: 4. Deciphering the Nature of the Higgs Sector," arXiv:1610.07922 [hep-ph].

[48] M. Cepeda, S. Gori, V. M. Outschoorn, and J. Shelton, "Exotic Higgs Decays," arXiv:2111.12751 [hep-ph].

[49] J. Shelton and D. Xu, "Exotic Higgs Decays to Four Taus at Future Electron-Positron Colliders," 10, 2021. arXiv:2110.13225 [hep-ph].

[50] Y. Kato, "Search for higgs decaying to exotic scalers at the ilc." Presentation at the 2021 international workshop on the high energy circular electron-positron collider (cepc), nov. 8-12, 2021, https://indico.ihep.ac.cn/event/14938.

[51] **CMS** Collaboration, "Projection of searches for exotic Higgs boson decays to light pseudoscalars for the High-Luminosity LHC,".

[52] K. Wang and J. Zhu, "A Novel Scenario in the Semi-constrained NMSSM," *JHEP* **06** (2020) 078, arXiv:2002.05554 [hep-ph].

[53] K. Wang and J. Zhu, "Funnel annihilations of light dark matter and the invisible decay of the Higgs boson," *Phys. Rev. D* **101** (2020) no. 9, 095028, arXiv:2003.01662 [hep-ph].

[54] K. Wang, J. Zhu, and Q. Jie, "Higgsino Asymmetry and Direct-Detection Constraints of Light Dark Matter in the NMSSM with Non-Universal Higgs Masses," *Chin. Phys. C* **45** (2021) no. 4, 041003, arXiv:2011.12848 [hep-ph].

[55] S. Ma, K. Wang, and J. Zhu, "Higgs decay to light (pseudo)scalars in the semi-constrained NMSSM," *Chin. Phys. C* **45** (2021) no. 2, 023113, arXiv:2006.03527 [hep-ph].

[56] **CMS** Collaboration, A. M. Sirunyan *et al.*, "Search for invisible decays of a Higgs boson produced through vector boson fusion in proton-proton collisions at $\sqrt{s} = 13$ TeV," *Phys. Lett. B* **793** (2019) 520–551, arXiv:1809.05937 [hep-ex].

[57] Y. Tan *et al.*, "Search for invisible decays of the Higgs boson produced at the CEPC," *Chin. Phys. C* **44** (2020) no. 12, 123001, arXiv:2001.05912 [hep-ex].

[58] J. Liu, X.-P. Wang, and K.-P. Xie, "Searching for lepton portal dark matter with colliders and gravitational waves," *JHEP* **06** (2021) 149, arXiv:2104.06421 [hep-ph].

[59] Z. Chacko, P. J. Fox, R. Harnik, and Z. Liu, "Neutrino Masses from Low Scale Partial Compositeness," arXiv:2012.01443 [hep-ph].

[60] N. Craig, A. Katz, M. Strassler, and R. Sundrum, "Naturalness in the Dark at the LHC," *JHEP* **07** (2015) 105, arXiv:1501.05310 [hep-ph].

[61] D. Curtin and C. B. Verhaaren, "Discovering Uncolored Naturalness in Exotic Higgs Decays," *JHEP* **12** (2015) 072, arXiv:1506.06141 [hep-ph].

[62] J. Liu, Z. Liu, and L.-T. Wang, "Enhancing Long-Lived Particles Searches at the LHC with Precision Timing Information," *Phys. Rev. Lett.* **122** (2019) no. 13, 131801, arXiv:1805.05957 [hep-ph].

[63] S. Alipour-Fard, N. Craig, S. Gori, S. Koren, and D. Redigolo, "The second Higgs at the lifetime frontier," *JHEP* **07** (2020) 029, arXiv:1812.09315 [hep-ph].

[64] J. Liu, Z. Liu, L.-T. Wang, and X.-P. Wang, "Enhancing Sensitivities to Long-lived Particles with High Granularity Calorimeters at the LHC," *JHEP* **11** (2020) 066,

arXiv:2005.10836 [hep-ph].

[65] M. Carena, J. Kozaczuk, Z. Liu, T. Ou, M. J. Ramsey-Musolf, J. Shelton, Y. Wang, and K.-P. Xie, "Probing the Electroweak Phase Transition with Exotic Higgs Decays," in *2022 Snowmass Summer Study*. 3, 2022. arXiv:2203.08206 [hep-ph].

[66] Z. Wang, X. Zhu, E. E. Khoda, S.-C. Hsu, N. Konstantinidis, K. Li, S. Li, M. J. Ramsey-Musolf, Y. Wu, and Y. E. Zhang, "Study of Electroweak Phase Transition in Exotic Higgs Decays at the CEPC," in *2022 Snowmass Summer Study*. 3, 2022. arXiv:2203.10184 [hep-ex].

[67] S. Jung, Z. Liu, L.-T. Wang, and K.-P. Xie, "Probing Higgs exotic decay at the LHC with machine learning," arXiv:2109.03294 [hep-ph].

[68] N. Arkani-Hamed, T. Cohen, R. T. D'Agnolo, A. Hook, H. D. Kim, and D. Pinner, "Solving the Hierarchy Problem at Reheating with a Large Number of Degrees of Freedom," *Phys. Rev. Lett.* **117** (2016) no. 25, 251801, arXiv:1607.06821 [hep-ph].

[69] N. Arkani-Hamed, R. Tito D'agnolo, and H. D. Kim, "The Weak Scale as a Trigger," arXiv:2012.04652 [hep-ph].

[70] P. Meade and H. Ramani, "Unrestored Electroweak Symmetry," *Phys. Rev. Lett.* **122** (2019) no. 4, 041802, arXiv:1807.07578 [hep-ph].

[71] I. Baldes and G. Servant, "High scale electroweak phase transition: baryogenesis and symmetry non-restoration," *JHEP* **10** (2018) 053, arXiv:1807.08770 [hep-ph].

[72] A. Glioti, R. Rattazzi, and L. Vecchi, "Electroweak Baryogenesis above the Electroweak Scale," *JHEP* **04** (2019) 027, arXiv:1811.11740 [hep-ph].

[73] O. Matsedonskyi and G. Servant, "High-Temperature Electroweak Symmetry Non-Restoration from New Fermions and Implications for Baryogenesis," *JHEP* **09** (2020) 012, arXiv:2002.05174 [hep-ph].

[74] J. Liu, L.-T. Wang, X.-P. Wang, and W. Xue, "Exposing the dark sector with future Z factories," *Phys. Rev.* **D97** (2018) no. 9, 095044, arXiv:1712.07237 [hep-ph].

[75] **FCC** Collaboration, A. Abada *et al.*, "FCC Physics Opportunities: Future Circular Collider Conceptual Design Report Volume 1," *Eur. Phys. J. C* **79** (2019) no. 6, 474.

[76] M. Drees, M. M. Nojiri, D. P. Roy, and Y. Yamada, "Light Higgsino dark matter," *Phys. Rev. D* **56** (1997) 276–290, arXiv:hep-ph/9701219. [Erratum: Phys.Rev.D 64, 039901 (2001)].

[77] A. Djouadi, M. Drees, P. Fileviez Perez, and M. Muhlleitner, "Loop induced Higgs and Z boson couplings to neutralinos and implications for collider and dark matter searches," *Phys. Rev. D* **65** (2002) 075016, arXiv:hep-ph/0109283.

[78] H. Eberl, M. Kincel, W. Majerotto, and Y. Yamada, "One loop corrections to neutral Higgs boson decays into neutralinos," *Nucl. Phys. B* **625** (2002) 372–388, arXiv:hep-ph/0111303.

[79] A. Berlin, D. S. Robertson, M. P. Solon, and K. M. Zurek, "Bino variations: Effective field theory methods for dark matter direct detection," *Phys. Rev. D* **93** (2016) no. 9, 095008, arXiv:1511.05964 [hep-ph].

[80] **ATLAS** Collaboration, "Search for invisible Higgs boson decays with vector boson fusion signatures with the ATLAS detector using an integrated luminosity of 139 fb^{-1},".

[81] C. Bernaciak, T. Plehn, P. Schichtel, and J. Tattersall, "Spying an invisible Higgs boson," *Phys. Rev.* **D91** (2015) 035024, arXiv:1411.7699 [hep-ph].

[82] Y. Zhang, C. Mo, X. Chen, B. Li, H. Chen, J. Hu, and L. Li, "Search for Long-lived Particles at Future Lepton Colliders Using Deep Learning Techniques," arXiv:2401.05094 [hep-ex].

[83] S. Alipour-Fard, N. Craig, M. Jiang, and S. Koren, "Long Live the Higgs Factory: Higgs Decays to Long-Lived Particles at Future Lepton Colliders," *Chin. Phys. C* **43** (2019) no. 5, 053101, arXiv:1812.05588 [hep-ph].

[84] K. Cheung and Z. S. Wang, "Probing Long-lived Particles at Higgs Factories," *Phys. Rev. D* **101** (2020) no. 3, 035003, arXiv:1911.08721 [hep-ph].

[85] L. Jeanty, L. Nosler, and C. Potter, "Sensitivity to decays of long-lived dark photons at the ILC," arXiv:2203.08347 [hep-ph].

[86] Z. S. Wang and K. Wang, "Long-lived light neutralinos at future $Z-$factories," *Phys. Rev. D* **101** (2020) no. 11, 115018, arXiv:1904.10661 [hep-ph].

[87] L. Calibbi, Z. Huang, S. Qin, Y. Yang, and X. Yin, "Testing axion couplings to leptons in Z decays at future e+e- colliders," *Phys. Rev. D* **108** (2023) no. 1, 015002, arXiv:2212.02818 [hep-ph].

[88] Z. S. Wang and K. Wang, "Physics with far detectors at future lepton colliders," *Phys. Rev. D* **101** (2020) no. 7, 075046, arXiv:1911.06576 [hep-ph].

[89] **CMS** Collaboration, "Search for a standard model-like Higgs boson in the mass range between 70 and 110 GeV in the diphoton final state in proton-proton collisions at $\sqrt{s} = 13$ TeV,".

[90] **ATLAS** Collaboration, "Search for diphoton resonances in the 66 to 110 GeV mass range using 140 fb^{-1} of 13 TeV pp collisions collected with the ATLAS detector,".

[91] T. Biekötter, S. Heinemeyer, and G. Weiglein, "95.4 GeV diphoton excess at ATLAS and CMS," *Phys. Rev. D* **109** (2024) no. 3, 035005, arXiv:2306.03889 [hep-ph].

[92] **LEP Working Group for Higgs boson searches, ALEPH, DELPHI, L3, OPAL** Collaboration, R. Barate *et al.*, "Search for the standard model Higgs boson at LEP," *Phys. Lett. B* **565** (2003) 61–75, arXiv:hep-ex/0306033.

[93] J. Cao, X. Guo, Y. He, P. Wu, and Y. Zhang, "Diphoton signal of the light Higgs boson in natural NMSSM," *Phys. Rev. D* **95** (2017) no. 11, 116001, arXiv:1612.08522 [hep-ph].

[94] A. Azatov, R. Contino, and J. Galloway, "Model-Independent Bounds on a Light Higgs," *JHEP* **04** (2012) 127, arXiv:1202.3415 [hep-ph]. [Erratum: JHEP 04, 140 (2013)].

[95] T. Biekötter, S. Heinemeyer, and G. Weiglein, "The CMS di-photon excess at 95 GeV in view of the LHC Run 2 results," *Phys. Lett. B* **846** (2023) 138217, arXiv:2303.12018 [hep-ph].

[96] T. Biekötter and M. O. Olea-Romacho, "Reconciling Higgs physics and pseudo-Nambu-Goldstone dark matter in the S2HDM using a genetic algorithm," *JHEP* **10** (2021) 215, arXiv:2108.10864 [hep-ph].

[97] P. Drechsel, G. Moortgat-Pick, and G. Weiglein, "Prospects for direct searches for light Higgs bosons at the ILC with 250 GeV," *Eur. Phys. J. C* **80** (2020) no. 10, 922, arXiv:1801.09662 [hep-ph].

[98] M. Cepeda *et al.*, *Report from Working Group 2: Higgs Physics at the HL-LHC and HE-LHC*, vol. 7, pp. 221–584. 12, 2019. arXiv:1902.00134 [hep-ph].

[99] P. Bambade *et al.*, "The International Linear Collider: A Global Project," arXiv:1903.01629 [hep-ex].

[100] S. Heinemeyer, C. Li, F. Lika, G. Moortgat-Pick, and S. Paasch, "Phenomenology of a 96 GeV Higgs boson in the 2HDM with an additional singlet," *Phys. Rev. D* **106** (2022) no. 7, 075003, arXiv:2112.11958 [hep-ph].

[101] K. Kong, H.-S. Lee, and M. Park, "Dark decay of the top quark," *Phys. Rev. D* **89** (2014) no. 7, 074007, arXiv:1401.5020 [hep-ph].

[102] Z. Li, X. Sun, Y. Fang, G. Li, S. Xin, S. Wang, Y. Wang, Y. Zhang, H. Zhang, and Z. Liang, "Top quark mass measurements at the $t\bar{t}$ threshold with CEPC," *Eur. Phys. J. C* **83** (2023) no. 4, 269, arXiv:2207.12177 [hep-ex]. [Erratum: Eur.Phys.J.C 83, 501 (2023)].

[103] G. Bertone and D. Hooper, "History of dark matter," *Rev. Mod. Phys.* **90** (2018) no. 4, 045002, arXiv:1605.04909 [astro-ph.CO].

[104] L. Roszkowski, E. M. Sessolo, and S. Trojanowski, "WIMP dark matter candidates and searches status and future prospects," *Rept. Prog. Phys.* **81** (2018) no. 6, 066201, arXiv:1707.06277 [hep-ph].

[105] M. Cirelli, A. Strumia, and J. Zupan, "Dark Matter," arXiv:2406.01705 [hep-ph].

[106] A. Boveia and C. Doglioni, "Dark Matter Searches at Colliders," *Ann. Rev. Nucl. Part. Sci.* **68** (2018) 429–459, arXiv:1810.12238 [hep-ex].

[107] M. Pospelov, A. Ritz, and M. B. Voloshin, "Secluded WIMP Dark Matter," *Phys. Lett. B* **662** (2008) 53–61, arXiv:0711.4866 [hep-ph].

[108] **CEPC Physics Study Group** Collaboration, H. Cheng *et al.*, "The Physics potential of the CEPC. Prepared for the US Snowmass Community Planning Exercise (Snowmass 2021)," in *Snowmass 2021*. 5, 2022. arXiv:2205.08553 [hep-ph].

[109] **LHC New Physics Working Group** Collaboration, D. Alves, "Simplified Models for LHC New Physics Searches," *J. Phys. G* **39** (2012) 105005, arXiv:1105.2838 [hep-ph].

[110] J. Liu, X.-P. Wang, and F. Yu, "A Tale of Two Portals: Testing Light, Hidden New Physics at Future e^+e^- Colliders," *JHEP* **06** (2017) 077, arXiv:1704.00730 [hep-ph].

[111] M. Zhang, "Leptophilic composite asymmetric dark matter and its detection," *Phys. Rev. D* **104** (2021) no. 5, 055008, arXiv:2104.06988 [hep-ph].

[112] Q.-H. Cao, J. Guo, J. Liu, Y. Luo, and X.-P. Wang, "Long-lived searches of vectorlike lepton and its accompanying scalar at colliders," *Phys. Rev. D* **110** (2024) no. 1, 015029, arXiv:2311.12934 [hep-ph].

[113] Z. Liu, Y.-H. Xu, and Y. Zhang, "Probing dark matter particles at CEPC," *JHEP* **06** (2019) 009, arXiv:1903.12114 [hep-ph].

[114] Y. Zhang, M. Song, and L. Chen, "Dark states with electromagnetic form factors at electron colliders," *Phys. Rev. D* **107** (2023) no. 5, 055023, arXiv:2208.08142 [hep-ph].

[115] S. Kundu, A. Guha, P. K. Das, and P. S. B. Dev, "A model-independent analysis of leptophilic dark matter at future electron-positron colliders in the mono-photon and mono-Z channels," arXiv:2110.06903 [hep-ph].

[116] S.-F. Ge, K. Ma, X.-D. Ma, and J. Sheng, "Associated Production of Neutrino and Dark Fermion at Future Lepton Colliders," arXiv:2306.00657 [hep-ph].

[117] J. Kumar and D. Marfatia, "Matrix element analyses of dark matter scattering and annihilation," *Phys. Rev. D* **88** (2013) no. 1, 014035, arXiv:1305.1611 [hep-ph].

[118] Y. Bai and J. Berger, "Lepton Portal Dark Matter," *JHEP* **08** (2014) 153, arXiv:1402.6696 [hep-ph].

[119] **Planck** Collaboration, N. Aghanim *et al.*, "Planck 2018 results. I. Overview and the cosmological legacy of Planck," *Astron. Astrophys.* **641** (2020) A1, arXiv:1807.06205 [astro-ph.CO].

[120] **Planck** Collaboration, P. A. R. Ade *et al.*, "Planck 2015 results. XIII. Cosmological parameters," *Astron. Astrophys.* **594** (2016) A13, arXiv:1502.01589 [astro-ph.CO].

[121] D. E. Kaplan, M. A. Luty, and K. M. Zurek, "Asymmetric Dark Matter," *Phys. Rev. D* **79** (2009) 115016, arXiv:0901.4117 [hep-ph].

[122] K. Petraki and R. R. Volkas, "Review of asymmetric dark matter," *Int. J. Mod. Phys. A* **28** (2013) 1330028, arXiv:1305.4939 [hep-ph].

[123] K. M. Zurek, "Asymmetric Dark Matter: Theories, Signatures, and Constraints," *Phys. Rept.* **537** (2014) 91–121, arXiv:1308.0338 [hep-ph].

[124] Y. Bai and P. Schwaller, "Scale of dark QCD," *Phys. Rev. D* **89** (2014) no. 6, 063522, arXiv:1306.4676 [hep-ph].

[125] **ATLAS** Collaboration, "Search for long-lived neutral particles decaying into displaced lepton jets in proton–proton collisions at $\sqrt{s} = 13$ TeV with the ATLAS detector,".

[126] S. Davidson, S. Hannestad, and G. Raffelt, "Updated bounds on millicharged particles," *JHEP* **05** (2000) 003, arXiv:hep-ph/0001179 [hep-ph].

[127] D. E. Soper, M. Spannowsky, C. J. Wallace, and T. M. P. Tait, "Scattering of Dark Particles with Light Mediators," *Phys. Rev.* **D90** (2014) no. 11, 115005, arXiv:1407.2623 [hep-ph].

[128] G. Magill, R. Plestid, M. Pospelov, and Y.-D. Tsai, "Millicharged particles in neutrino experiments," *Phys. Rev. Lett.* **122** (2019) no. 7, 071801, arXiv:1806.03310 [hep-ph].

[129] Z. Liu and Y. Zhang, "Probing millicharge at BESIII via monophoton searches," *Phys. Rev.* **D99** (2019) no. 1, 015004, arXiv:1808.00983 [hep-ph].

[130] X. Chu, J. Pradler, and L. Semmelrock, "Light dark states with electromagnetic form factors," *Phys. Rev. D* **99** (2019) no. 1, 015040, arXiv:1811.04095 [hep-ph].

[131] C. Arina, A. Cheek, K. Mimasu, and L. Pagani, "Light and Darkness: consistently coupling dark matter to photons via effective operators," *Eur. Phys. J. C* **81** (2021) no. 3, 223, arXiv:2005.12789 [hep-ph].

[132] X. Chu, J.-L. Kuo, and J. Pradler, "Dark sector-photon interactions in proton-beam experiments," *Phys. Rev. D* **101** (2020) no. 7, 075035, arXiv:2001.06042 [hep-ph].

[133] X. Chu, J.-L. Kuo, J. Pradler, and L. Semmelrock, "Stellar probes of dark sector-photon interactions," *Phys. Rev. D* **100** (2019) no. 8, 083002, arXiv:1908.00553 [hep-ph].

[134] L. M. Krauss, S. Nasri, and M. Trodden, "A Model for neutrino masses and dark matter," *Phys. Rev. D* **67** (2003) 085002, arXiv:hep-ph/0210389.

[135] E. A. Baltz and L. Bergstrom, "Detection of leptonic dark matter," *Phys. Rev. D* **67** (2003) 043516, arXiv:hep-ph/0211325.

[136] E. Ma, "Verifiable radiative seesaw mechanism of neutrino mass and dark matter," *Phys. Rev. D* **73** (2006) 077301, arXiv:hep-ph/0601225.

[137] T. Hambye, K. Kannike, E. Ma, and M. Raidal, "Emanations of Dark Matter: Muon Anomalous Magnetic Moment, Radiative Neutrino Mass, and Novel Leptogenesis at the TeV Scale," *Phys. Rev. D* **75** (2007) 095003, arXiv:hep-ph/0609228.

[138] R. Bernabei *et al.*, "Investigating electron interacting dark matter," *Phys. Rev. D* **77** (2008) 023506, arXiv:0712.0562 [astro-ph].

[139] M. Cirelli, M. Kadastik, M. Raidal, and A. Strumia, "Model-independent implications of the e+-, anti-proton cosmic ray spectra on properties of Dark Matter," *Nucl. Phys. B* **813** (2009) 1–21, arXiv:0809.2409 [hep-ph]. [Addendum: Nucl.Phys.B 873, 530–533 (2013)].

[140] C.-R. Chen and F. Takahashi, "Cosmic rays from Leptonic Dark Matter," *JCAP* **02** (2009) 004, arXiv:0810.4110 [hep-ph].

[141] X.-J. Bi, P.-H. Gu, T. Li, and X. Zhang, "ATIC and PAMELA Results on Cosmic e+- Excesses and Neutrino Masses," *JHEP* **04** (2009) 103, arXiv:0901.0176 [hep-ph].

[142] A. Ibarra, A. Ringwald, D. Tran, and C. Weniger, "Cosmic Rays from Leptophilic Dark Matter Decay via Kinetic Mixing," *JCAP* **08** (2009) 017, arXiv:0903.3625 [hep-ph].

[143] P. S. B. Dev, D. K. Ghosh, N. Okada, and I. Saha, "Neutrino Mass and Dark Matter in light of recent AMS-02 results," *Phys. Rev. D* **89** (2014) 095001, arXiv:1307.6204 [hep-ph].

[144] S. Chang, R. Edezhath, J. Hutchinson, and M. Luty, "Leptophilic Effective WIMPs," *Phys. Rev. D* **90** (2014) no. 1, 015011, arXiv:1402.7358 [hep-ph].

[145] P. Agrawal, Z. Chacko, and C. B. Verhaaren, "Leptophilic Dark Matter and the Anomalous Magnetic Moment of the Muon," *JHEP* **08** (2014) 147, arXiv:1402.7369 [hep-ph].

[146] N. F. Bell, Y. Cai, R. K. Leane, and A. D. Medina, "Leptophilic dark matter with Z' interactions," *Phys. Rev. D* **90** (2014) no. 3, 035027, arXiv:1407.3001 [hep-ph].

[147] A. Freitas and S. Westhoff, "Leptophilic Dark Matter in Lepton Interactions at LEP and ILC," *JHEP* **10** (2014) 116, arXiv:1408.1959 [hep-ph].

[148] Q.-H. Cao, C.-R. Chen, and T. Gong, "Leptophilic dark matter confronts AMS-02 cosmic-ray positron flux," *Chin. J. Phys.* **55** (2017) 10–15, arXiv:1409.7317 [hep-ph].

[149] B.-Q. Lu and H.-S. Zong, "Leptophilic dark matter in Galactic Center excess," *Phys. Rev. D* **93** (2016) no. 8, 083504. [Addendum: Phys.Rev.D 93, 089910 (2016)].

[150] G. H. Duan, L. Feng, F. Wang, L. Wu, J. M. Yang, and R. Zheng, "Simplified TeV leptophilic dark matter in light of DAMPE data," *JHEP* **02** (2018) 107, arXiv:1711.11012 [hep-ph].

[151] E. Madge and P. Schwaller, "Leptophilic dark matter from gauged lepton number: Phenomenology and gravitational wave signatures," *JHEP* **02** (2019) 048, arXiv:1809.09110 [hep-ph].

[152] S. Junius, L. Lopez-Honorez, and A. Mariotti, "A feeble window on leptophilic dark matter," *JHEP* **07** (2019) 136, arXiv:1904.07513 [hep-ph].

[153] S. Ghosh, A. Dutta Banik, E. J. Chun, and D. Majumdar, "Leptophilic-portal Dark Matter in the Light of AMS-02 positron excess," arXiv:2003.07675 [hep-ph].

[154] S. Chakraborti and R. Islam, "Implications of dark sector mixing on leptophilic scalar dark matter," *JHEP* **03** (2021) 032, arXiv:2007.13719 [hep-ph].

[155] S.-I. Horigome, T. Katayose, S. Matsumoto, and I. Saha, "Leptophilic fermion WIMP: Role of future lepton colliders," *Phys. Rev. D* **104** (2021) no. 5, 055001, arXiv:2102.08645 [hep-ph].

[156] **Muon g-2** Collaboration, B. Abi *et al.*, "Measurement of the Positive Muon Anomalous Magnetic Moment to 0.46 ppm," *Phys. Rev. Lett.* **126** (2021) no. 14, 141801, arXiv:2104.03281 [hep-ex].

[157] **DAMA/LIBRA** Collaboration, R. Bernabei *et al.*, "The DAMA project: Achievements, implications and perspectives," *Prog. Part. Nucl. Phys.* **114** (2020) 103810.

[158] **Fermi-LAT** Collaboration, S. Abdollahi *et al.*, "Cosmic-ray electron-positron spectrum from 7 GeV to 2 TeV with the Fermi Large Area Telescope," *Phys. Rev. D* **95** (2017) no. 8, 082007, arXiv:1704.07195 [astro-ph.HE].

[159] **DAMPE** Collaboration, G. Ambrosi *et al.*, "Direct detection of a break in the teraelectronvolt cosmic-ray spectrum of electrons and positrons," *Nature* **552** (2017) 63–66, arXiv:1711.10981 [astro-ph.HE].

[160] **CALET** Collaboration, O. Adriani *et al.*, "Extended Measurement of the Cosmic-Ray Electron and Positron Spectrum from 11 GeV to 4.8 TeV with the Calorimetric Electron Telescope on the International Space Station," *Phys. Rev. Lett.* **120** (2018) no. 26, 261102, arXiv:1806.09728 [astro-ph.HE].

[161] **AMS** Collaboration, M. Aguilar *et al.*, "The Alpha Magnetic Spectrometer (AMS) on the international space station: Part II — Results from the first seven years," *Phys. Rept.* **894** (2021) 1–116.

[162] **Fermi-LAT** Collaboration, M. Ajello *et al.*, "Fermi-LAT Observations of High-Energy γ-Ray Emission Toward the Galactic Center," *Astrophys. J.* **819** (2016) no. 1, 44, arXiv:1511.02938 [astro-ph.HE].

[163] **XENON** Collaboration, E. Aprile *et al.*, "Excess electronic recoil events in XENON1T," *Phys. Rev. D* **102** (2020) no. 7, 072004, arXiv:2006.09721 [hep-ex].

[164] **XENON100** Collaboration, E. Aprile *et al.*, "Exclusion of Leptophilic Dark Matter Models using XENON100 Electronic Recoil Data," *Science* **349** (2015) no. 6250, 851–854, arXiv:1507.07747 [astro-ph.CO].

[165] **XENON** Collaboration, E. Aprile *et al.*, "Light Dark Matter Search with Ionization Signals in XENON1T," *Phys. Rev. Lett.* **123** (2019) no. 25, 251801, arXiv:1907.11485 [hep-ex].

[166] **LZ** Collaboration, D. S. Akerib *et al.*, "Projected sensitivities of the LUX-ZEPLIN (LZ) experiment to new physics via low-energy electron recoils," arXiv:2102.11740 [hep-ex].

[167] C.-Y. Chen, J. Kozaczuk, and Y.-M. Zhong, "Exploring leptophilic dark matter with NA64-μ," *JHEP* **10** (2018) 154, arXiv:1807.03790 [hep-ph].

[168] L. Marsicano, M. Battaglieri, A. Celentano, R. De Vita, and Y.-M. Zhong, "Probing Leptophilic Dark Sectors at Electron Beam-Dump Facilities," *Phys. Rev. D* **98** (2018) no. 11, 115022, arXiv:1812.03829 [hep-ex].

[169] **DELPHI** Collaboration, J. Abdallah *et al.*, "Photon events with missing energy in e+ e- collisions at s**(1/2) = 130-GeV to 209-GeV," *Eur. Phys. J. C* **38** (2005) 395–411, arXiv:hep-ex/0406019.

[170] A. Birkedal, K. Matchev, and M. Perelstein, "Dark matter at colliders: A Model independent approach," *Phys. Rev. D* **70** (2004) 077701, arXiv:hep-ph/0403004.

[171] P. J. Fox and E. Poppitz, "Leptophilic Dark Matter," *Phys. Rev. D* **79** (2009) 083528, arXiv:0811.0399 [hep-ph].

[172] P. Konar, K. Kong, K. T. Matchev, and M. Perelstein, "Shedding Light on the Dark Sector with Direct WIMP Production," *New J. Phys.* **11** (2009) 105004, arXiv:0902.2000 [hep-ph].

[173] P. J. Fox, R. Harnik, J. Kopp, and Y. Tsai, "LEP Shines Light on Dark Matter," *Phys. Rev. D* **84** (2011) 014028, arXiv:1103.0240 [hep-ph].

[174] C. Bartels, M. Berggren, and J. List, "Characterising WIMPs at a future e^+e^- Linear Collider," *Eur. Phys. J. C* **72** (2012) 2213, arXiv:1206.6639 [hep-ex].

[175] H. Dreiner, M. Huck, M. Krämer, D. Schmeier, and J. Tattersall, "Illuminating Dark Matter at the ILC," *Phys. Rev. D* **87** (2013) no. 7, 075015, arXiv:1211.2254 [hep-ph].

[176] Y. J. Chae and M. Perelstein, "Dark Matter Search at a Linear Collider: Effective Operator Approach," *JHEP* **05** (2013) 138, arXiv:1211.4008 [hep-ph].

[177] M. Habermehl, M. Berggren, and J. List, "WIMP Dark Matter at the International Linear Collider," *Phys. Rev. D* **101** (2020) no. 7, 075053, arXiv:2001.03011 [hep-ex].

[178] J. Kalinowski, W. Kotlarski, K. Mekala, P. Sopicki, and A. F. Zarnecki, "Sensitivity of future e^+e^- colliders to processes of dark matter production with light mediator exchange," arXiv:2107.11194 [hep-ph].

[179] B. Barman, S. Bhattacharya, S. Girmohanta, and S. Jahedi, "Catch 'em all: Effective Leptophilic WIMPs at the $e^+\,e^-$ Collider," arXiv:2109.10936 [hep-ph].

[180] N. Wan, M. Song, G. Li, W.-G. Ma, R.-Y. Zhang, and J.-Y. Guo, "Searching for dark matter via mono-Z boson production at the ILC," *Eur. Phys. J. C* **74** (2014) no. 12, 3219, arXiv:1403.7921 [hep-ph].

[181] Z.-H. Yu, X.-J. Bi, Q.-S. Yan, and P.-F. Yin, "Dark matter searches in the mono-Z channel at high energy e^+e^- colliders," *Phys. Rev. D* **90** (2014) no. 5, 055010, arXiv:1404.6990 [hep-ph].

[182] S. Dutta, D. Sachdeva, and B. Rawat, "Signals of Leptophilic Dark Matter at the ILC," *Eur. Phys. J. C* **77** (2017) no. 9, 639, arXiv:1704.03994 [hep-ph].

[183] B. Grzadkowski, M. Iglicki, K. Mekala, and A. F. Zarnecki, "Dark-matter-spin effects at future e^+e^- colliders," *JHEP* **08** (2020) 052, arXiv:2003.06719 [hep-ph].

[184] J. Kopp, V. Niro, T. Schwetz, and J. Zupan, "DAMA/LIBRA and leptonically interacting Dark Matter," *Phys. Rev. D* **80** (2009) 083502, arXiv:0907.3159 [hep-ph].

[185] M. Beltran, D. Hooper, E. W. Kolb, Z. A. C. Krusberg, and T. M. P. Tait, "Maverick dark matter at colliders," *JHEP* **09** (2010) 037, arXiv:1002.4137 [hep-ph].

[186] J. Goodman, M. Ibe, A. Rajaraman, W. Shepherd, T. M. P. Tait, and H.-B. Yu, "Constraints on Light Majorana dark Matter from Colliders," *Phys. Lett. B* **695** (2011) 185–188, arXiv:1005.1286 [hep-ph].

[187] Y. Bai, P. J. Fox, and R. Harnik, "The Tevatron at the Frontier of Dark Matter Direct Detection," *JHEP* **12** (2010) 048, arXiv:1005.3797 [hep-ph].

[188] J. Goodman, M. Ibe, A. Rajaraman, W. Shepherd, T. M. P. Tait, and H.-B. Yu, "Constraints on Dark Matter from Colliders," *Phys. Rev. D* **82** (2010) 116010, arXiv:1008.1783 [hep-ph].

[189] P. J. Fox, R. Harnik, J. Kopp, and Y. Tsai, "Missing Energy Signatures of Dark Matter at the LHC," *Phys. Rev. D* **85** (2012) 056011, arXiv:1109.4398 [hep-ph].

[190] A. Rajaraman, W. Shepherd, T. M. P. Tait, and A. M. Wijangco, "LHC Bounds on Interactions of Dark Matter," *Phys. Rev. D* **84** (2011) 095013, arXiv:1108.1196 [hep-ph].

[191] F. Kahlhoefer, "Review of LHC Dark Matter Searches," *Int. J. Mod. Phys. A* **32** (2017) no. 13, 1730006, arXiv:1702.02430 [hep-ph].

[192] B. Penning, "The pursuit of dark matter at colliders—an overview," *J. Phys. G* **45** (2018) no. 6, 063001, arXiv:1712.01391 [hep-ex].

[193] **CMS** Collaboration, A. M. Sirunyan *et al.*, "Search for new physics in final states with an energetic jet or a hadronically decaying W or Z boson and transverse momentum imbalance at $\sqrt{s} = 13$ TeV," *Phys. Rev. D* **97** (2018) no. 9, 092005, arXiv:1712.02345 [hep-ex].

[194] **ATLAS** Collaboration, G. Aad *et al.*, "Search for new phenomena in events with an energetic jet and missing transverse momentum in pp collisions at $\sqrt{s}$ =13 TeV with the ATLAS detector," *Phys. Rev. D* **103** (2021) no. 11, 112006, arXiv:2102.10874 [hep-ex].

[195] S. Matsumoto, S. Mukhopadhyay, and Y.-L. S. Tsai, "Effective Theory of WIMP Dark Matter supplemented by Simplified Models: Singlet-like Majorana fermion case," *Phys. Rev. D* **94** (2016) no. 6, 065034, arXiv:1604.02230 [hep-ph].

[196] **XENON** Collaboration, E. Aprile *et al.*, "Dark Matter Search Results from a One Ton-Year Exposure of XENON1T," *Phys. Rev. Lett.* **121** (2018) no. 11, 111302, arXiv:1805.12562 [astro-ph.CO].

[197] **PandaX-4T** Collaboration, Y. Meng *et al.*, "Dark Matter Search Results from the PandaX-4T Commissioning Run," arXiv:2107.13438 [hep-ex].

[198] R. K. Leane, T. R. Slatyer, J. F. Beacom, and K. C. Y. Ng, "GeV-scale thermal WIMPs: Not even slightly ruled out," *Phys. Rev. D* **98** (2018) no. 2, 023016, arXiv:1805.10305 [hep-ph].

[199] I. John and T. Linden, "Cosmic-Ray Positrons Strongly Constrain Leptophilic Dark Matter," arXiv:2107.10261 [astro-ph.HE].

[200] A. Guha, P. S. B. Dev, and P. K. Das, "Model-independent Astrophysical Constraints on Leptophilic Dark Matter in the Framework of Tsallis Statistics," *JCAP* **02** (2019) 032, arXiv:1810.00399 [hep-ph].

[201] **XENON** Collaboration, E. Aprile *et al.*, "Constraining the spin-dependent WIMP-nucleon cross sections with XENON1T," *Phys. Rev. Lett.* **122** (2019) no. 14, 141301, arXiv:1902.03234 [astro-ph.CO].

[202] J. Liu, X. Chen, and X. Ji, "Current status of direct dark matter detection experiments," *Nature Phys.* **13** (2017) no. 3, 212–216, arXiv:1709.00688 [astro-ph.CO].

[203] M. Schumann, "Direct Detection of WIMP Dark Matter: Concepts and Status," *J. Phys. G* **46** (2019) no. 10, 103003, arXiv:1903.03026 [astro-ph.CO].

[204] J. Billard *et al.*, "Direct detection of dark matter—APPEC committee report*," *Rept. Prog. Phys.* **85** (2022) no. 5, 056201, arXiv:2104.07634 [hep-ex].

[205] J. M. Gaskins, "A review of indirect searches for particle dark matter," *Contemp. Phys.* **57** (2016) no. 4, 496–525, arXiv:1604.00014 [astro-ph.HE].

[206] R. K. Leane, "Indirect Detection of Dark Matter in the Galaxy," in *3rd World Summit on Exploring the Dark Side of the Universe*, pp. 203–228. 2020. arXiv:2006.00513 [hep-ph].

[207] T. R. Slatyer, "Les Houches Lectures on Indirect Detection of Dark Matter," *SciPost Phys. Lect. Notes* **53** (2022) 1, arXiv:2109.02696 [hep-ph].

[208] S. Gori *et al.*, "Dark Sector Physics at High-Intensity Experiments," arXiv:2209.04671 [hep-ph].

[209] T. Lagouri, "Review on Higgs Hidden–Dark Sector Physics at High-Energy Colliders," *Symmetry* **14** (2022) no. 7, 1299.

[210] S.-F. Ge, X.-G. He, X.-D. Ma, and J. Sheng, "Revisiting the fermionic dark matter absorption on electron target," *JHEP* **05** (2022) 191, arXiv:2201.11497 [hep-ph].

[211] J. Cao, Z. Heng, D. Li, L. Shang, and P. Wu, "Higgs-strahlung production process $e^+e^- \to Zh$ at the future Higgs factory in the Minimal Dilaton Model," *JHEP* **08** (2014) 138, arXiv:1405.4489 [hep-ph].

[212] M. A. Fedderke, T. Lin, and L.-T. Wang, "Probing the fermionic Higgs portal at lepton colliders," *JHEP* **04** (2016) 160, arXiv:1506.05465 [hep-ph].

[213] Q.-H. Cao, Y. Li, B. Yan, Y. Zhang, and Z. Zhang, "Probing dark particles indirectly at the CEPC," *Nucl. Phys. B* **909** (2016) 197–217, arXiv:1604.07536 [hep-ph].

[214] C. Cai, Z.-H. Yu, and H.-H. Zhang, "CEPC Precision of Electroweak Oblique Parameters and Weakly Interacting Dark Matter: the Fermionic Case," *Nucl. Phys. B* **921** (2017) 181–210, arXiv:1611.02186 [hep-ph].

[215] N. Liu and L. Wu, "An indirect probe of the higgsino world at the CEPC," *Eur. Phys. J. C* **77** (2017) no. 12, 868, arXiv:1705.02534 [hep-ph].

[216] C. Cai, Z.-H. Yu, and H.-H. Zhang, "CEPC Precision of Electroweak Oblique Parameters and Weakly Interacting Dark Matter: the Scalar Case," *Nucl. Phys. B* **924** (2017) 128–152, arXiv:1705.07921 [hep-ph].

[217] Q.-F. Xiang, X.-J. Bi, P.-F. Yin, and Z.-H. Yu, "Exploring Fermionic Dark Matter via Higgs Boson Precision Measurements at the Circular Electron Positron Collider," *Phys. Rev. D* **97** (2018) no. 5, 055004, arXiv:1707.03094 [hep-ph].

[218] J.-W. Wang, X.-J. Bi, Q.-F. Xiang, P.-F. Yin, and Z.-H. Yu, "Exploring triplet-quadruplet fermionic dark matter at the LHC and future colliders," *Phys. Rev. D* **97** (2018) no. 3, 035021, arXiv:1711.05622 [hep-ph].

[219] L.-Q. Gao, X.-J. Bi, J.-W. Wang, Q.-F. Xiang, and P.-F. Yin, "Exploring fermionic multiplet dark matter through precision measurements at the CEPC *," *Chin. Phys. C* **46** (2022) no. 9, 093112, arXiv:2112.02519 [hep-ph].

[220] R. Mahbubani and L. Senatore, "The Minimal model for dark matter and unification," *Phys. Rev. D* **73** (2006) 043510, arXiv:hep-ph/0510064.

[221] T. Cohen, J. Kearney, A. Pierce, and D. Tucker-Smith, "Singlet-Doublet Dark Matter," *Phys. Rev. D* **85** (2012) 075003, arXiv:1109.2604 [hep-ph].

[222] A. Dedes and D. Karamitros, "Doublet-Triplet Fermionic Dark Matter," *Phys. Rev. D* **89** (2014) no. 11, 115002, arXiv:1403.7744 [hep-ph].

[223] **Planck** Collaboration, N. Aghanim *et al.*, "Planck 2018 results. VI. Cosmological parameters," *Astron. Astrophys.* **641** (2020) A6, arXiv:1807.06209 [astro-ph.CO]. [Erratum: Astron.Astrophys. 652, C4 (2021)].

[224] **LZ** Collaboration, S. Haselschwardt, "Status of the lux-zeplin dark matter experiment." https://indico.uchicago.edu/event/427/contributions/1325/.

[225] C. Cheung, L. J. Hall, D. Pinner, and J. T. Ruderman, "Prospects and Blind Spots for Neutralino Dark Matter," *JHEP* **05** (2013) 100, arXiv:1211.4873 [hep-ph].

[226] P. Huang and C. E. M. Wagner, "Blind Spots for neutralino Dark Matter in the MSSM with an intermediate m_A," *Phys. Rev. D* **90** (2014) no. 1, 015018, arXiv:1404.0392 [hep-ph].

[227] R. Essig *et al.*, "Working Group Report: New Light Weakly Coupled Particles," in *Proceedings, Community Summer Study 2013: Snowmass on the Mississippi (CSS2013): Minneapolis, MN, USA, July 29-August 6, 2013*. 2013. arXiv:1311.0029 [hep-ph]. https://inspirehep.net/record/1263039/files/arXiv:1311.0029.pdf.

[228] S. Alekhin *et al.*, "A facility to Search for Hidden Particles at the CERN SPS: the SHiP physics case," *Rept. Prog. Phys.* **79** (2016) no. 12, 124201, arXiv:1504.04855 [hep-ph].

[229] J. Beacham *et al.*, "Physics Beyond Colliders at CERN: Beyond the Standard Model Working Group Report," *J. Phys.* **G47** (2020) no. 1, 010501, arXiv:1901.09966 [hep-ex].

[230] D. Curtin *et al.*, "Long-Lived Particles at the Energy Frontier: The MATHUSLA Physics Case," *Rept. Prog. Phys.* **82** (2019) no. 11, 116201, arXiv:1806.07396 [hep-ph].

[231] C. Antel *et al.*, "Feebly Interacting Particles: FIPs 2022 workshop report," in *Workshop on Feebly-Interacting Particles*. 5, 2023. arXiv:2305.01715 [hep-ph].

[232] **ATLAS** Collaboration, M. Aaboud *et al.*, "Search for photonic signatures of gauge-mediated supersymmetry in 13 TeV *pp* collisions with the ATLAS detector," *Phys. Rev. D* **97** (2018) no. 9, 092006, arXiv:1802.03158 [hep-ex].

[233] **CMS** Collaboration, A. M. Sirunyan *et al.*, "Search for gauge-mediated supersymmetry in events with at least one photon and missing transverse momentum in pp collisions at $\sqrt{s} =$ 13 TeV," *Phys. Lett. B* **780** (2018) 118–143, arXiv:1711.08008 [hep-ex].

[234] **CMS** Collaboration, A. M. Sirunyan *et al.*, "Search for supersymmetry in final states with photons and missing transverse momentum in proton-proton collisions at 13 TeV," *JHEP* **06** (2019) 143, arXiv:1903.07070 [hep-ex].

[235] **CMS** Collaboration, T. C. Collaboration *et al.*, "Search for supersymmetry in proton-proton collisions at 13 TeV in final states with jets and missing transverse momentum," *JHEP* **10** (2019) 244, arXiv:1908.04722 [hep-ex].

[236] **ATLAS** Collaboration, G. Aad *et al.*, "Search for new phenomena in final states with large jet multiplicities and missing transverse momentum using $\sqrt{s} = 13$ TeV proton-proton collisions recorded by ATLAS in Run 2 of the LHC," *JHEP* **10** (2020) 062, arXiv:2008.06032 [hep-ex].

[237] L. Lee, C. Ohm, A. Soffer, and T.-T. Yu, "Collider Searches for Long-Lived Particles Beyond the Standard Model," arXiv:1810.12602 [hep-ph].

[238] J. Alimena *et al.*, "Searching for Long-Lived Particles beyond the Standard Model at the Large Hadron Collider," *J. Phys. G* **47** (2019) no. 9, 090501, arXiv:1903.04497 [hep-ex].

[239] A. De Roeck, "Searching for long-lived particles at the Large Hadron Collider and beyond," *Phil. Trans. Roy. Soc. Lond. A* **377** (2019) no. 2161, 20190047.

[240] D. Acosta *et al.*, "Review of opportunities for new long-lived particle triggers in Run 3 of the Large Hadron Collider," arXiv:2110.14675 [hep-ex].

[241] S. Knapen and S. Lowette, "A guide to hunting long-lived particles at the LHC," arXiv:2212.03883 [hep-ph].

[242] **ATLAS** Collaboration, G. Aad *et al.*, "Observation of a new particle in the search for the Standard Model Higgs boson with the ATLAS detector at the LHC," *Phys. Lett. B* **716** (2012) 1–29, arXiv:1207.7214 [hep-ex].

[243] **CMS** Collaboration, S. Chatrchyan *et al.*, "Observation of a New Boson at a Mass of 125 GeV with the CMS Experiment at the LHC," *Phys. Lett. B* **716** (2012) 30–61, arXiv:1207.7235 [hep-ex].

[244] **CEPC Study Group** Collaboration, "CEPC Conceptual Design Report: Volume 1 - Accelerator," arXiv:1809.00285 [physics.acc-ph].

[245] F. An *et al.*, "Precision Higgs physics at the CEPC," *Chin. Phys. C* **43** (2019) no. 4, 043002, arXiv:1810.09037 [hep-ex].

[246] **CEPC Accelerator Study Group** Collaboration, "CEPC Input to the ESPP 2018 -Accelerator," arXiv:1901.03169 [physics.acc-ph].

[247] G. Aarons *et al.*, "ILC Reference Design Report Volume 3 - Accelerator," arXiv:0712.2361 [physics.acc-ph].

[248] "The International Linear Collider Technical Design Report - Volume 1: Executive Summary," arXiv:1306.6327 [physics.acc-ph].

[249] **ILC** Collaboration, "The International Linear Collider Technical Design Report - Volume 2: Physics," arXiv:1306.6352 [hep-ph].

[250] H. Abramowicz *et al.*, "The International Linear Collider Technical Design Report - Volume 4: Detectors," arXiv:1306.6329 [physics.ins-det].

[251] K. Fujii *et al.*, "Physics Case for the 250 GeV Stage of the International Linear Collider," arXiv:1710.07621 [hep-ex].

[252] **FCC** Collaboration, A. Abada *et al.*, "FCC Physics Opportunities: Future Circular Collider Conceptual Design Report Volume 1," *Eur. Phys. J. C* **79** (2019) no. 6, 474.

[253] **FCC** Collaboration, A. Abada *et al.*, "FCC-hh: The Hadron Collider: Future Circular Collider Conceptual Design Report Volume 3," *Eur. Phys. J. ST* **228** (2019) no. 4, 755–1107.

[254] **FCC** Collaboration, A. Abada *et al.*, "HE-LHC: The High-Energy Large Hadron Collider: Future Circular Collider Conceptual Design Report Volume 4," *Eur. Phys. J. ST* **228** (2019) no. 5, 1109–1382.

[255] L. Linssen, A. Miyamoto, M. Stanitzki, and H. Weerts, "Physics and Detectors at CLIC: CLIC Conceptual Design Report," arXiv:1202.5940 [physics.ins-det].

[256] **CLICdp** Collaboration, J. Klamka, "The CLIC potential for new physics," *PoS* **EPS-HEP2021** (2022) 714, arXiv:2111.04787 [hep-ex].

[257] A. Blondel *et al.*, "Searches for long-lived particles at the future FCC-ee," *Front. in Phys.* **10** (2022) 967881, arXiv:2203.05502 [hep-ex].

[258] Y. Lu, Y.-n. Mao, K. Wang, and Z. S. Wang, "LAYCAST: LAYered CAvern Surface Tracker at future electron-positron colliders," arXiv:2406.05770 [hep-ph].

[259] M. Tian, K. Wang, and Z. S. Wang, "Search for long-lived axions with far detectors at future lepton colliders," arXiv:2201.08960 [hep-ph].

[260] M. Kucharczyk and M. Goncerz, "Search for exotic decays of the Higgs boson into long-lived particles with jet pairs in the final state at CLIC," *JHEP* **03** (2023) 131, arXiv:2212.04147 [hep-ex].

[261] This is true for electric-neutral LLPs; for electric-charged LLPs we assume that they have large enough transverse momentum p_T so that the bending effect of the magnetic field at the MD is unimportant and that the potential ionization effect in material is negligible.

[262] The total invisible decay mode is not considered here.

[263] E. Fuchs, O. Matsedonskyi, I. Savoray, and M. Schlaffer, "Collider searches for scalar singlets across lifetimes," *JHEP* **04** (2021) 019, arXiv:2008.12773 [hep-ph].

[264] M. J. Strassler and K. M. Zurek, "Discovering the Higgs through highly-displaced vertices," *Phys. Lett. B* **661** (2008) 263–267, arXiv:hep-ph/0605193.

[265] J. C. Helo, M. Hirsch, and Z. S. Wang, "Heavy neutral fermions at the high-luminosity LHC," *JHEP* **07** (2018) 056, arXiv:1803.02212 [hep-ph].

[266] D. Dercks, H. K. Dreiner, M. Hirsch, and Z. S. Wang, "Long-Lived Fermions at AL3X," *Phys. Rev.* **D99** (2019) no. 5, 055020, arXiv:1811.01995 [hep-ph].

[267] Y. Kao and T. Takeuchi, "Single-Coupling Bounds on R-parity violating Supersymmetry, an update," arXiv:0910.4980 [hep-ph].

[268] **ATLAS** Collaboration, G. Aad *et al.*, "The ATLAS Experiment at the CERN Large Hadron Collider," *JINST* **3** (2008) S08003.

[269] V. V. Gligorov, S. Knapen, B. Nachman, M. Papucci, and D. J. Robinson, "Leveraging the ALICE/L3 cavern for long-lived particle searches," *Phys. Rev.* **D99** (2019) no. 1, 015023,

arXiv:1810.03636 [hep-ph].

[270] V. V. Gligorov, S. Knapen, M. Papucci, and D. J. Robinson, "Searching for Long-lived Particles: A Compact Detector for Exotics at LHCb," *Phys. Rev.* **D97** (2018) no. 1, 015023, arXiv:1708.09395 [hep-ph].

[271] J. L. Feng, I. Galon, F. Kling, and S. Trojanowski, "ForwArd Search ExpeRiment at the LHC," *Phys. Rev. D* **97** (2018) no. 3, 035001, arXiv:1708.09389 [hep-ph].

[272] D. Croon, G. Elor, R. K. Leane, and S. D. McDermott, "Supernova Muons: New Constraints on Z' Bosons, Axions and ALPs," *JHEP* **01** (2021) 107, arXiv:2006.13942 [hep-ph].

[273] J. Heisig, "Long-lived charged sleptons at the ILC/CLIC," in *3rd Linear Collider Forum*, pp. 398–404. DESY, Hamburg, 11, 2012. arXiv:1211.2195 [hep-ph].

[274] H.-U. Martyn, "Detection of long-lived staus and gravitinos at the ILC," *eConf* **C0705302** (2007) SUS03, arXiv:0709.1030 [hep-ph].

[275] A. Ibarra and S. Roy, "Lepton flavour violation in future linear colliders in the long-lived stau NLSP scenario," *JHEP* **05** (2007) 059, arXiv:hep-ph/0606116.

[276] "http://www.ship-korea.com/SND.html,".

[277] **SHiP** Collaboration, C. Ahdida *et al.*, "SND@LHC," arXiv:2002.08722 [physics.ins-det].

[278] **SND@LHC** Collaboration, G. Acampora *et al.*, "SND@LHC: The Scattering and Neutrino Detector at the LHC," arXiv:2210.02784 [hep-ex].

[279] **FASER** Collaboration, H. Abreu *et al.*, "Detecting and Studying High-Energy Collider Neutrinos with FASER at the LHC," *Eur. Phys. J. C* **80** (2020) no. 1, 61, arXiv:1908.02310 [hep-ex].

[280] **FASER** Collaboration, H. Abreu *et al.*, "Technical Proposal: FASERnu," arXiv:2001.03073 [physics.ins-det].

[281] J. L. Feng *et al.*, "The Forward Physics Facility at the High-Luminosity LHC," *J. Phys. G* **50** (2023) no. 3, 030501, arXiv:2203.05090 [hep-ex].

[282] R. Mammen Abraham *et al.*, "Tau neutrinos in the next decade: from GeV to EeV," *J. Phys. G* **49** (2022) no. 11, 110501, arXiv:2203.05591 [hep-ph].

[283] R. Mammen Abraham *et al.*, "Forward Physics Facility - Snowmass 2021 Letter of Interest,".

[284] L. A. Anchordoqui *et al.*, "The Forward Physics Facility: Sites, experiments, and physics potential," *Phys. Rept.* **968** (2022) 1–50, arXiv:2109.10905 [hep-ph].

[285] B. Batell, J. L. Feng, and S. Trojanowski, "Detecting Dark Matter with Far-Forward Emulsion and Liquid Argon Detectors at the LHC," *Phys. Rev. D* **103** (2021) no. 7, 075023, arXiv:2101.10338 [hep-ph].

[286] **FASER** Collaboration, A. Ariga *et al.*, "FASER: ForwArd Search ExpeRiment at the LHC," arXiv:1901.04468 [hep-ex].

[287] **FASER** Collaboration, H. Abreu *et al.*, "The FASER Detector," arXiv:2207.11427 [physics.ins-det].

[288] J. P. Chou, D. Curtin, and H. J. Lubatti, "New Detectors to Explore the Lifetime Frontier," *Phys. Lett.* **B767** (2017) 29–36, arXiv:1606.06298 [hep-ph].

[289] **MATHUSLA** Collaboration, C. Alpigiani *et al.*, "An Update to the Letter of Intent for MATHUSLA: Search for Long-Lived Particles at the HL-LHC," arXiv:2009.01693 [physics.ins-det].

[290] M. Bauer, O. Brandt, L. Lee, and C. Ohm, "ANUBIS: Proposal to search for long-lived neutral particles in CERN service shafts," arXiv:1909.13022 [physics.ins-det].

[291] S. Cerci *et al.*, "FACET: A new long-lived particle detector in the very forward region of the CMS experiment," *JHEP* **06** (2022) 110, arXiv:2201.00019 [hep-ex].

[292] G. Aielli *et al.*, "Expression of Interest for the CODEX-b Detector," arXiv:1911.00481 [hep-ex].

[293] J. L. Pinfold, "The MoEDAL Experiment at the LHC—A Progress Report," *Universe* **5** (2019) no. 2, 47.

[294] J. L. Pinfold, "The MoEDAL experiment: a new light on the high-energy frontier," *Phil. Trans. Roy. Soc. Lond. A* **377** (2019) no. 2161, 20190382.

[295] J. De Vries, H. K. Dreiner, J. Y. Günther, Z. S. Wang, and G. Zhou, "Long-lived Sterile Neutrinos at the LHC in Effective Field Theory," *JHEP* **03** (2021) 148, arXiv:2010.07305 [hep-ph].

[296] Y.-n. Mao, K. Wang, and Z. S. Wang, "Can we discover lepton number violation with the LHC far detectors?," *Phys. Rev. D* **108** (2023) no. 9, 095025, arXiv:2305.03908 [hep-ph].

[297] M. Chrzaszcz, M. Drewes, and J. Hajer, "HECATE: A long-lived particle detector concept for the FCC-ee or CEPC," *Eur. Phys. J. C* **81** (2021) no. 6, 546, arXiv:2011.01005 [hep-ph].

[298] R. Schäfer, F. Tillinger, and S. Westhoff, "Near or far detectors? A case study for long-lived particle searches at electron-positron colliders," *Phys. Rev. D* **107** (2023) no. 7, 076022, arXiv:2202.11714 [hep-ph].

[299] Y. Sakaki and D. Ueda, "Searching for new light particles at the international linear collider main beam dump," *Phys. Rev. D* **103** (2021) no. 3, 035024, arXiv:2009.13790 [hep-ph].

[300] P. Satyamurthy *et al.*, "Design of an 18-MW vortex flow water beam dump for 500-GeV electrons/positrons of an international linear collider," *Nucl. Instrum. Meth. A* **679** (2012) 67–81.

[301] M. J. Dolan, T. Ferber, C. Hearty, F. Kahlhoefer, and K. Schmidt-Hoberg, "Revised constraints and Belle II sensitivity for visible and invisible axion-like particles," *JHEP* **12** (2017) 094, arXiv:1709.00009 [hep-ph].

[302] J. Jaeckel, P. C. Malta, and J. Redondo, "Decay photons from the axionlike particles burst of type II supernovae," *Phys. Rev. D* **98** (2018) no. 5, 055032, arXiv:1702.02964 [hep-ph].

[303] D. Cadamuro and J. Redondo, "Cosmological bounds on pseudo Nambu-Goldstone bosons," *JCAP* **02** (2012) 032, arXiv:1110.2895 [hep-ph].

[304] B. Doebrich, J. Jaeckel, F. Kahlhoefer, A. Ringwald, and K. Schmidt-Hoberg, "ALPtraum: ALP production in proton beam dump experiments," *JHEP* **02** (2016) 018, arXiv:1512.03069 [hep-ph].

[305] B. Döbrich, J. Jaeckel, and T. Spadaro, "Light in the beam dump. Axion-Like Particle production from decay photons in proton beam-dumps," *JHEP* **05** (2019) 213, arXiv:1904.02091 [hep-ph].

[306] C.-Y. Chen, M. Pospelov, and Y.-M. Zhong, "Muon Beam Experiments to Probe the Dark Sector," *Phys. Rev. D* **95** (2017) no. 11, 115005, arXiv:1701.07437 [hep-ph].

[307] K. Asai, T. Moroi, and A. Niki, "Leptophilic Gauge Bosons at ILC Beam Dump Experiment," *Phys. Lett. B* **818** (2021) 136374, arXiv:2104.00888 [hep-ph].

[308] K. Asai, A. Das, J. Li, T. Nomura, and O. Seto, "Chiral Z' in FASER, FASER2, DUNE, and ILC beam dump experiments," *Phys. Rev. D* **106** (2022) no. 9, 095033,

arXiv:2206.12676 [hep-ph].

[309] **ATLAS** Collaboration, "Snowmass White Paper Contribution: Physics with the Phase-2 ATLAS and CMS Detectors,".

[310] F. Kling and S. Trojanowski, "Forward experiment sensitivity estimator for the LHC and future hadron colliders," *Phys. Rev. D* **104** (2021) no. 3, 035012, arXiv:2105.07077 [hep-ph].

[311] F. Domingo, J. Günther, J. S. Kim, and Z. S. Wang, "A C++ program for estimating detector sensitivities to long-lived particles: Displaced Decay Counter," arXiv:2308.07371 [hep-ph].

[312] M. Ovchynnikov, J.-L. Tastet, O. Mikulenko, and K. Bondarenko, "Sensitivities to feebly interacting particles: Public and unified calculations," *Phys. Rev. D* **108** (2023) no. 7, 075028, arXiv:2305.13383 [hep-ph].

[313] J. P. Delahaye, M. Diemoz, K. Long, B. Mansoulié, N. Pastrone, L. Rivkin, D. Schulte, A. Skrinsky, and A. Wulzer, "Muon Colliders," arXiv:1901.06150 [physics.acc-ph].

[314] K. Long, D. Lucchesi, M. Palmer, N. Pastrone, D. Schulte, and V. Shiltsev, "Muon colliders to expand frontiers of particle physics," arXiv:2007.15684 [physics.acc-ph].

[315] H. Al Ali *et al.*, "The Muon Smasher's Guide," arXiv:2103.14043 [hep-ph].

[316] C. Accettura *et al.*, "Towards a muon collider," *Eur. Phys. J. C* **83** (2023) no. 9, 864, arXiv:2303.08533 [physics.acc-ph].

[317] **Muon Collider** Collaboration, J. de Blas *et al.*, "The physics case of a 3 TeV muon collider stage," arXiv:2203.07261 [hep-ph].

[318] M. Lu, A. M. Levin, C. Li, A. Agapitos, Q. Li, F. Meng, S. Qian, J. Xiao, and T. Yang, "The physics case for an electron-muon collider," *Adv. High Energy Phys.* **2021** (2021) 6693618, arXiv:2010.15144 [hep-ph].

[319] A. O. Bouzas and F. Larios, "Two-to-Two Processes at an Electron-Muon Collider," *Adv. High Energy Phys.* **2022** (2022) 3603613, arXiv:2109.02769 [hep-ph].

[320] J. B. Dainton, M. Klein, P. Newman, E. Perez, and F. Willeke, "Deep inelastic electron-nucleon scattering at the LHC," *JINST* **1** (2006) P10001, arXiv:hep-ex/0603016.

[321] **LHeC Study Group** Collaboration, J. L. Abelleira Fernandez *et al.*, "A Large Hadron Electron Collider at CERN: Report on the Physics and Design Concepts for Machine and Detector," *J. Phys. G* **39** (2012) 075001, arXiv:1206.2913 [physics.acc-ph].

[322] M. Klein, *Future Deep Inelastic Scattering with the LHeC*, pp. 303–347. 2019. arXiv:1802.04317 [hep-ph].

[323] K. Cheung and Z. S. Wang, "Physics potential of a muon-proton collider," *Phys. Rev. D* **103** (2021) 116009, arXiv:2101.10476 [hep-ph].

[324] A. Caliskan, S. O. Kara, and A. Ozansoy, "Excited muon searches at the FCC based muon-hadron colliders," *Adv. High Energy Phys.* **2017** (2017) 1540243, arXiv:1701.03426 [hep-ph].

[325] Y. C. Acar, U. Kaya, and B. B. Oner, "Resonant production of color octet muons at Future Circular Collider-based muon-proton colliders," *Chin. Phys. C* **42** (2018) no. 8, 083108, arXiv:1703.04030 [hep-ph].

[326] **ATLAS** Collaboration, G. Aad *et al.*, "Search for new phenomena in final states with large jet multiplicities and missing transverse momentum using $\sqrt{s} = 13$ TeV proton-proton collisions recorded by ATLAS in Run 2 of the LHC," *JHEP* **10** (2020) 062, arXiv:2008.06032 [hep-ex].

[327] **ATLAS** Collaboration, G. Aad *et al.*, "Search for a scalar partner of the top quark in the all-hadronic $t\bar{t}$ plus missing transverse momentum final state at $\sqrt{s} = 13$ TeV with the ATLAS detector," *Eur. Phys. J. C* **80** (2020) no. 8, 737, arXiv:2004.14060 [hep-ex].

[328] **ATLAS** Collaboration, G. Aad *et al.*, "Search for chargino-neutralino production with mass splittings near the electroweak scale in three-lepton final states in $\sqrt{s}$=13 TeV pp collisions with the ATLAS detector," *Phys. Rev. D* **101** (2020) no. 7, 072001, arXiv:1912.08479 [hep-ex].

[329] **ATLAS** Collaboration, G. Aad *et al.*, "Searches for electroweak production of supersymmetric particles with compressed mass spectra in $\sqrt{s} = 13$ TeV pp collisions with the ATLAS detector," *Phys. Rev. D* **101** (2020) no. 5, 052005, arXiv:1911.12606 [hep-ex].

[330] C. Han, A. Kobakhidze, N. Liu, A. Saavedra, L. Wu, and J. M. Yang, "Probing Light Higgsinos in Natural SUSY from Monojet Signals at the LHC," *JHEP* **02** (2014) 049, arXiv:1310.4274 [hep-ph].

[331] C. Han, L. Wu, J. M. Yang, M. Zhang, and Y. Zhang, "New approach for detecting a compressed bino/wino at the LHC," *Phys. Rev. D* **91** (2015) 055030, arXiv:1409.4533 [hep-ph].

[332] A. Kobakhidze, M. Talia, and L. Wu, "Probing the MSSM explanation of the muon g-2 anomaly in dark matter experiments and at a 100 TeV pp collider," *Phys. Rev. D* **95** (2017) no. 5, 055023, arXiv:1608.03641 [hep-ph].

[333] C. Han, K.-i. Hikasa, L. Wu, J. M. Yang, and Y. Zhang, "Status of CMSSM in light of current LHC Run-2 and LUX data," *Phys. Lett. B* **769** (2017) 470–476, arXiv:1612.02296 [hep-ph].

[334] M. Abdughani, L. Wu, and J. M. Yang, "Status and prospects of light bino–higgsino dark matter in natural SUSY," *Eur. Phys. J. C* **78** (2018) no. 1, 4, arXiv:1705.09164 [hep-ph].

[335] J. Ren, L. Wu, J. M. Yang, and J. Zhao, "Exploring supersymmetry with machine learning," *Nucl. Phys. B* **943** (2019) 114613, arXiv:1708.06615 [hep-ph].

[336] G. H. Duan, W. Wang, L. Wu, J. M. Yang, and J. Zhao, "Probing GeV-scale MSSM neutralino dark matter in collider and direct detection experiments," *Phys. Lett. B* **778** (2018) 296–302, arXiv:1711.03893 [hep-ph].

[337] G. H. Duan, K.-I. Hikasa, J. Ren, L. Wu, and J. M. Yang, "Probing bino-wino coannihilation dark matter below the neutrino floor at the LHC," *Phys. Rev. D* **98** (2018) no. 1, 015010, arXiv:1804.05238 [hep-ph].

[338] M. Abdughani and L. Wu, "On the coverage of neutralino dark matter in coannihilations at the upgraded LHC," *Eur. Phys. J. C* **80** (2020) no. 3, 233, arXiv:1908.11350 [hep-ph].

[339] M. Abdughani, K.-I. Hikasa, L. Wu, J. M. Yang, and J. Zhao, "Testing electroweak SUSY for muon $g-2$ and dark matter at the LHC and beyond," *JHEP* **11** (2019) 095, arXiv:1909.07792 [hep-ph].

[340] Y. Gu, M. Khlopov, L. Wu, J. M. Yang, and B. Zhu, "Light gravitino dark matter: LHC searches and the Hubble tension," *Phys. Rev. D* **102** (2020) no. 11, 115005, arXiv:2006.09906 [hep-ph].

[341] M. Abdughani, Y.-Z. Fan, L. Feng, Y.-L. S. Tsai, L. Wu, and Q. Yuan, "A common origin of muon g-2 anomaly, Galaxy Center GeV excess and AMS-02 anti-proton excess in the NMSSM," *Sci. Bull.* **66** (2021) 2170–2174, arXiv:2104.03274 [hep-ph].

[342] F. Wang, L. Wu, Y. Xiao, J. M. Yang, and Y. Zhang, "GUT-scale constrained SUSY in light of new muon g-2 measurement," *Nucl. Phys. B* **970** (2021) 115486, arXiv:2104.03262 [hep-ph].

[343] Y. Gu, L. Wu, and B. Zhu, "Axion dark radiation: Hubble tension and the Hyper-Kamiokande neutrino experiment," *Phys. Rev. D* **105** (2022) no. 9, 095008, arXiv:2105.07232 [hep-ph].

[344] H. Lv, D. Wang, and L. Wu, "Deep learning jet images as a probe of light Higgsino dark matter at the LHC," *Phys. Rev. D* **106** (2022) no. 5, 055008, arXiv:2203.14569 [hep-ph].

[345] V. V. Flambaum, X. Liu, I. Samsonov, L. Wu, and B. Zhu, "Probing supersymmetry breaking scale with atomic clocks," *Nucl. Phys. B* **993** (2023) 116260, arXiv:2209.03231 [hep-ph].

[346] S. L. Hu, N. Liu, J. Ren, and L. Wu, "Revisiting Associated Production of 125 GeV Higgs Boson with a Photon at a Higgs Factory," *J. Phys. G* **41** (2014) no. 12, 125004, arXiv:1402.3050 [hep-ph].

[347] J. Cao, C. Han, J. Ren, L. Wu, J. M. Yang, and Y. Zhang, "SUSY effects in Higgs productions at high energy e^+e^- colliders," *Chin. Phys. C* **40** (2016) no. 11, 113104, arXiv:1410.1018 [hep-ph].

[348] G. H. Duan, C. Han, B. Peng, L. Wu, and J. M. Yang, "Vacuum stability in stau-neutralino coannihilation in MSSM," *Phys. Lett. B* **788** (2019) 475–479, arXiv:1809.10061 [hep-ph].

[349] C. Han, M. L. López-Ibáñez, A. Melis, O. Vives, L. Wu, and J. M. Yang, "LFV and (g-2) in non-universal SUSY models with light higgsinos," *JHEP* **05** (2020) 102, arXiv:2003.06187 [hep-ph].

[350] P. Athron, C. Balazs, A. Fowlie, H. Lv, W. Su, L. Wu, J. M. Yang, and Y. Zhang, "Global fits of SUSY at future Higgs factories," *Phys. Rev. D* **105** (2022) no. 11, 115029, arXiv:2203.04828 [hep-ph].

[351] T. Leggett, T. Li, J. A. Maxin, D. V. Nanopoulos, and J. W. Walker, "No Naturalness or Fine-tuning Problems from No-Scale Supergravity," arXiv:1403.3099 [hep-ph].

[352] T. Leggett, T. Li, J. A. Maxin, D. V. Nanopoulos, and J. W. Walker, "Confronting Electroweak Fine-tuning with No-Scale Supergravity," *Phys. Lett. B* **740** (2015) 66–72, arXiv:1408.4459 [hep-ph].

[353] G. Du, T. Li, D. V. Nanopoulos, and S. Raza, "Super-Natural MSSM," *Phys. Rev. D* **92** (2015) no. 2, 025038, arXiv:1502.06893 [hep-ph].

[354] T. Li, S. Raza, and X.-C. Wang, "Supernatural supersymmetry and its classic example: M-theory inspired NMSSM," *Phys. Rev. D* **93** (2016) no. 11, 115014, arXiv:1510.06851 [hep-ph].

[355] European Strategy for Particle Physics Preparatory Group, "Physics briefing book," arXiv:1910.11775 [hep-ex].

[356] J.-R. Yuan, H.-J. Cheng, and X.-A. Zhuang, "Prospects for chargino pair production at the CEPC," *Chinese Physics C* **46** (2022) no. 1, 013104.

[357] H. Pagels and J. R. Primack, "Supersymmetry, Cosmology and New TeV Physics," *Phys. Rev. Lett.* **48** (1982) 223.

[358] J. Chen, C. Han, J. M. Yang, and M. Zhang, "Probing a bino NLSP at lepton colliders," *Phys. Rev. D* **104** (2021) no. 1, 015009, arXiv:2101.12131 [hep-ph].

[359] J.-R. Yuan, H.-J. Cheng, and X.-A. Zhuang, "Prospects for slepton pair production in the future e^-e^+ Higgs factories," arXiv:2203.10580 [hep-ex].

[360] W. Ahmed, I. Khan, T. Li, S. Raza, and W. Zhang, "Probing Relatively Heavier Right-Handed Selectron at the CEPC, $\mathbf{FCC_{ee}}$ and ILC," arXiv:2202.11011 [hep-ex].

[361] J. M. Yang, Y. Zhang, P. Zhu, and R. Zhu, "Reconstructing masses for semi-invisibly decaying particles pair-produced at lepton colliders," arXiv:2211.08132 [hep-ph].

[362] T. Li, J. A. Maxin, D. V. Nanopoulos, and X. Yin, "The right-handed slepton bulk region for dark matter in generalized no-scale $\mathcal{F}$-$su(5)$ with effective super-natural supersymmetry," arXiv:2310.03622 [hep-ph].

[363] S. M. Barr, "Phys. lett. b,".

[364] J. Jiang, T. Li, and D. V. Nanopoulos, "Testable flipped $su(5)xu(1)_x$ models," *Nucl. Phys. B* **772** (2007) 49.

[365] J. Jiang, T. Li, D. V. Nanopoulos, and D. Xie, "F-su(5)," *Phys. Lett. B* **677** (2009) 322.

[366] J. Jiang, T. Li, D. V. Nanopoulos, and D. Xie, "Flipped $su(5)xu(1)_x$ models from f-theory," *Nucl. Phys. B* **830** (2010) 195.

[367] J. L. Lopez, D. V. Nanopoulos, and K. J. Yuan, "The search for a realistic flipped su(5) string model," *Nucl. Phys. B* **399** (1993) 654.

[368] J. Yuan, H. Cheng, and X. Zhuang, "Prospects for slepton pair production in the future e^-e^+ Higgs factories," arXiv:2203.10580 [hep-ex].

[369] D. S. Akerib and others [LZ], "Projected wimp sensitivity of the lux-zeplin dark matter experiment," *Phys. Rev. D* **101** (2020) no. 5, 052002, arXiv:1802.06039 [astro-ph.IM].

[370] E. Aprile and others [XENON], "First dark matter search with nuclear recoils from the xenonnt experiment," *Phys. Rev. Lett.* **131** (2023) no. 4, 041003, arXiv:2303.14729 [hep-ex].

[371] J. Aalbers and others [LZ], "First dark matter search results from the lux-zeplin (lz) experiment," *Phys. Rev. Lett.* **131** (2023) no. 4, 041002, arXiv:2207.03764 [hep-ex].

[372] P. N. Bhattiprolu, S. P. Martin, and J. D. Wells, "Statistical significances and projections for proton decay experiments," *Phys. Rev. D* **107** (2023) no. 5, 055016, arXiv:2210.07735 [hep-ph].

[373] S. Antusch, E. Cazzato, M. Drewes, O. Fischer, B. Garbrecht, D. Gueter, and J. Klaric, "Probing leptogenesis at future colliders," *JHEP* **09** (2018) 124, arXiv:1710.03744 [hep-ph].

[374] J. de Blas *et al.*, "The clic potential for new physics," arXiv:1812.02093 [hep-ph].

[375] ATLAS Collaboration, "Search for supersymmetry in final states with charm jets and missing transverse momentum in 13 tev pp collisions with the atlas detector," *Journal of High Energy Physics* **2018** (2018) no. Sep, 50.

[376] T. Zheng, J. Xu, L. Cao, D. Yu, W. Wang, S. Prell, Y.-K. E. Cheung, and M. Ruan, "Analysis of $B_c \to \tau\nu_\tau$ at CEPC," *Chin. Phys. C* **45** (2021) no. 2, 023001, arXiv:2007.08234 [hep-ex].

[377] R. Aleksan, L. Oliver, and E. Perez, "CP violation and determination of the bs "flat" unitarity triangle at FCCee," arXiv:2107.02002 [hep-ph].

[378] R. Aleksan, L. Oliver, and E. Perez, "Study of CP violation in $B^\pm$ decays to $\overline{D^0}(D^0)K^\pm$ at FCCee," arXiv:2107.05311 [hep-ph].

[379] Y. Amhis, C. Helsens, D. Hill, and O. Sumensari, "Prospects for $B_c^+ \to \tau^+\nu_\tau$ at FCC-ee," arXiv:2105.13330 [hep-ex].

[380] J. F. Kamenik, S. Monteil, A. Semkiv, and L. V. Silva, "Lepton polarization asymmetries in rare semi-tauonic $b \to s$ exclusive decays at FCC-ee," *Eur. Phys. J.* **C77** (2017) no. 10, 701, arXiv:1705.11106 [hep-ph].

[381] L. Li and T. Liu, "$b \to s\tau^+\tau^-$ Physics at Future Z Factories," arXiv:2012.00665 [hep-ph].

[382] S. Monteil and G. Wilkinson, "Heavy-quark opportunities and challenges at FCC-ee," arXiv:2106.01259 [hep-ex].

[383] M. Chrzaszcz, R. G. Suarez, and S. Monteil, "Hunt for rare processes and long-lived particles at FCC-ee," *Eur. Phys. J. Plus* **136** (2021) no. 10, 1056, arXiv:2106.15459 [hep-ex].

[384] M. Dam, "Tau-lepton Physics at the FCC-ee circular e^+e^- Collider," *SciPost Phys. Proc.* **1** (2019) 041, arXiv:1811.09408 [hep-ex].

[385] Q. Qin, Q. Li, C.-D. Lü, F.-S. Yu, and S.-H. Zhou, "Charged lepton flavor violating Higgs decays at future e^+e^- colliders," *Eur. Phys. J. C* **78** (2018) no. 10, 835, arXiv:1711.07243 [hep-ph].

[386] T. Li and M. A. Schmidt, "Sensitivity of future lepton colliders to the search for charged lepton flavor violation," *Phys. Rev.* **D99** (2019) no. 5, 055038, arXiv:1809.07924 [hep-ph].

[387] L. Calibbi, X. Marcano, and J. Roy, "Z lepton flavour violation as a probe for new physics at future e^+e^- colliders," *Eur. Phys. J. C* **81** (2021) no. 12, 1054, arXiv:2107.10273 [hep-ph].

[388] W. Altmannshofer, P. Munbodh, and T. Oh, "Probing lepton flavor violation at Circular Electron-Positron Colliders," *JHEP* **08** (2023) 026, arXiv:2305.03869 [hep-ph].

[389] S. L. Glashow, J. Iliopoulos, and L. Maiani, "Weak Interactions with Lepton-Hadron Symmetry," *Phys. Rev. D* **2** (1970) 1285–1292.

[390] C. F. P. S. Group, "Flavor Physics at CEPC: a General Perspective,".

[391] H.-C. Cheng, L. Li, and E. Salvioni, "A theory of dark pions," *JHEP* **01** (2022) 122, arXiv:2110.10691 [hep-ph].

[392] H.-C. Cheng, X.-H. Jiang, L. Li, and E. Salvioni, "Dark showers from Z-dark Z' mixing," arXiv:2401.08785 [hep-ph].

[393] L. Dolan and R. Jackiw, "Symmetry Behavior at Finite Temperature," *Phys. Rev. D* **9** (1974) 3320–3341.

[394] Following the Ehrenfest classification, we distinguish *bona fide* phase transitions, characterized by discontinuities in derivatives of thermodynamic quantities, from smooth crossover transitions devoid of such discontinuities.

[395] K. Kajantie, M. Laine, K. Rummukainen, and M. E. Shaposhnikov, "A Nonperturbative analysis of the finite T phase transition in SU(2) x U(1) electroweak theory," *Nucl. Phys. B* **493** (1997) 413–438, arXiv:hep-lat/9612006.

[396] K. Rummukainen, M. Tsypin, K. Kajantie, M. Laine, and M. E. Shaposhnikov, "The Universality class of the electroweak theory," *Nucl. Phys. B* **532** (1998) 283–314, arXiv:hep-lat/9805013.

[397] M. Laine and K. Rummukainen, "What's new with the electroweak phase transition?," *Nucl. Phys. B Proc. Suppl.* **73** (1999) 180–185, arXiv:hep-lat/9809045.

[398] M. Dine, R. G. Leigh, P. Y. Huet, A. D. Linde, and D. A. Linde, "Towards the theory of the electroweak phase transition," *Phys. Rev. D* **46** (1992) 550–571, arXiv:hep-ph/9203203.

[399] D. E. Morrissey and M. J. Ramsey-Musolf, "Electroweak baryogenesis," *New J. Phys.* **14** (2012) 125003, arXiv:1206.2942 [hep-ph].

[400] M. Joyce, T. Prokopec, and N. Turok, "Electroweak baryogenesis from a classical force," *Phys. Rev. Lett.* **75** (1995) 1695–1698, arXiv:hep-ph/9408339. [Erratum: Phys.Rev.Lett. 75, 3375 (1995)].

[401] L. Fromme and S. J. Huber, "Top transport in electroweak baryogenesis," *JHEP* **03** (2007) 049, arXiv:hep-ph/0604159.

[402] M. Jiang, L. Bian, W. Huang, and J. Shu, "Impact of a complex singlet: Electroweak baryogenesis and dark matter," *Phys. Rev. D* **93** (2016) no. 6, 065032, arXiv:1502.07574 [hep-ph].

[403] C.-W. Chiang, M. J. Ramsey-Musolf, and E. Senaha, "Standard Model with a Complex Scalar Singlet: Cosmological Implications and Theoretical Considerations," *Phys. Rev. D* **97** (2018) no. 1, 015005, arXiv:1707.09960 [hep-ph].

[404] K.-P. Xie, "Lepton-mediated electroweak baryogenesis, gravitational waves and the 4τ final state at the collider," *JHEP* **02** (2021) 090, arXiv:2011.04821 [hep-ph]. [Erratum: JHEP 8, 052 (2022)].

[405] L. Bian, Y. Wu, and K.-P. Xie, "Electroweak phase transition with composite Higgs models: calculability, gravitational waves and collider searches," *JHEP* **12** (2019) 028, arXiv:1909.02014 [hep-ph].

[406] K.-P. Xie, L. Bian, and Y. Wu, "Electroweak baryogenesis and gravitational waves in a composite Higgs model with high dimensional fermion representations," *JHEP* **12** (2020)

047, arXiv:2005.13552 [hep-ph].

[407] N. F. Bell, M. J. Dolan, L. S. Friedrich, M. J. Ramsey-Musolf, and R. R. Volkas, "Two-Step Electroweak Symmetry-Breaking: Theory Meets Experiment," *JHEP* **05** (2020) 050, arXiv:2001.05335 [hep-ph].

[408] L. Bian, H.-K. Guo, and J. Shu, "Gravitational Waves, baryon asymmetry of the universe and electric dipole moment in the CP-violating NMSSM," *Chin. Phys. C* **42** (2018) no. 9, 093106, arXiv:1704.02488 [hep-ph]. [Erratum: Chin.Phys.C 43, 129101 (2019)].

[409] S. Kanemura and Y. Mura, "Electroweak baryogenesis via top-charm mixing," *JHEP* **09** (2023) 153, arXiv:2303.11252 [hep-ph].

[410] K. Enomoto, S. Kanemura, and S. Taniguchi, "The electric dipole moment in a model for neutrino mass, dark matter and baryon asymmetry of the Universe," arXiv:2403.13613 [hep-ph].

[411] D. J. Weir, "Gravitational waves from a first order electroweak phase transition: a brief review," *Phil. Trans. Roy. Soc. Lond. A* **376** (2018) no. 2114, 20170126, arXiv:1705.01783 [hep-ph]. [Erratum: Phil.Trans.Roy.Soc.Lond.A 381, 20230212 (2023)].

[412] A. Mazumdar and G. White, "Review of cosmic phase transitions: their significance and experimental signatures," *Rept. Prog. Phys.* **82** (2019) no. 7, 076901, arXiv:1811.01948 [hep-ph].

[413] P. Athron, C. Balázs, A. Fowlie, L. Morris, and L. Wu, "Cosmological phase transitions: from perturbative particle physics to gravitational waves," arXiv:2305.02357 [hep-ph].

[414] R. Caldwell *et al.*, "Detection of early-universe gravitational-wave signatures and fundamental physics," *Gen. Rel. Grav.* **54** (2022) no. 12, 156, arXiv:2203.07972 [gr-qc].

[415] H.-K. Guo, K. Sinha, D. Vagie, and G. White, "The benefits of diligence: how precise are predicted gravitational wave spectra in models with phase transitions?," *JHEP* **06** (2021) 164, arXiv:2103.06933 [hep-ph].

[416] C. Grojean and G. Servant, "Gravitational Waves from Phase Transitions at the Electroweak Scale and Beyond," *Phys. Rev. D* **75** (2007) 043507, arXiv:hep-ph/0607107.

[417] C. Caprini *et al.*, "Science with the space-based interferometer eLISA. II: Gravitational waves from cosmological phase transitions," *JCAP* **1604** (2016) no. 04, 001, arXiv:1512.06239 [astro-ph.CO].

[418] C. Caprini *et al.*, "Detecting gravitational waves from cosmological phase transitions with LISA: an update," *JCAP* **03** (2020) 024, arXiv:1910.13125 [astro-ph.CO].

[419] **LISA** Collaboration, P. Amaro-Seoane *et al.*, "Laser Interferometer Space Antenna," arXiv:1702.00786 [astro-ph.IM].

[420] **TianQin** Collaboration, J. Luo *et al.*, "TianQin: a space-borne gravitational wave detector," *Class. Quant. Grav.* **33** (2016) no. 3, 035010, arXiv:1512.02076 [astro-ph.IM].

[421] **TianQin** Collaboration, J. Mei *et al.*, "The TianQin project: current progress on science and technology," *PTEP* **2021** (2021) no. 5, 05A107, arXiv:2008.10332 [gr-qc].

[422] W.-R. Hu and Y.-L. Wu, "The Taiji Program in Space for gravitational wave physics and the nature of gravity," *Natl. Sci. Rev.* **4** (2017) no. 5, 685–686.

[423] W.-H. Ruan, Z.-K. Guo, R.-G. Cai, and Y.-Z. Zhang, "Taiji program: Gravitational-wave sources," *Int. J. Mod. Phys. A* **35** (2020) no. 17, 2050075, arXiv:1807.09495 [gr-qc].

[424] M. J. Baker and J. Kopp, "Dark Matter Decay between Phase Transitions at the Weak Scale," *Phys. Rev. Lett.* **119** (2017) no. 6, 061801, arXiv:1608.07578 [hep-ph].

[425] M. J. Baker, M. Breitbach, J. Kopp, and L. Mittnacht, "Dynamic Freeze-In: Impact of Thermal Masses and Cosmological Phase Transitions on Dark Matter Production," *JHEP* **03** (2018) 114, arXiv:1712.03962 [hep-ph].

[426] X.-R. Wong and K.-P. Xie, "Freeze-in of WIMP dark matter," *Phys. Rev. D* **108** (2023) no. 5, 055035, arXiv:2304.00908 [hep-ph].

[427] T. Hambye, A. Strumia, and D. Teresi, "Super-cool Dark Matter," *JHEP* **08** (2018) 188, arXiv:1805.01473 [hep-ph].

[428] A. Azatov, M. Vanvlasselaer, and W. Yin, "Dark Matter production from relativistic bubble walls," *JHEP* **03** (2021) 288, arXiv:2101.05721 [hep-ph].

[429] A. Azatov, M. Vanvlasselaer, and W. Yin, "Baryogenesis via relativistic bubble walls," *JHEP* **10** (2021) 043, arXiv:2106.14913 [hep-ph].

[430] W.-Y. Ai, M. Fairbairn, K. Mimasu, and T. You, "Non-thermal production of heavy vector dark matter from relativistic bubble walls," arXiv:2406.20051 [hep-ph].

[431] I. Baldes, S. Blasi, A. Mariotti, A. Sevrin, and K. Turbang, "Baryogenesis via relativistic bubble expansion," *Phys. Rev. D* **104** (2021) no. 11, 115029, arXiv:2106.15602 [hep-ph].

[432] P. Huang and K.-P. Xie, "Leptogenesis triggered by a first-order phase transition," *JHEP* **09** (2022) 052, arXiv:2206.04691 [hep-ph].

[433] E. J. Chun, T. P. Dutka, T. H. Jung, X. Nagels, and M. Vanvlasselaer, "Bubble-assisted leptogenesis," *JHEP* **09** (2023) 164, arXiv:2305.10759 [hep-ph].

[434] M. J. Baker, J. Kopp, and A. J. Long, "Filtered Dark Matter at a First Order Phase Transition," *Phys. Rev. Lett.* **125** (2020) no. 15, 151102, arXiv:1912.02830 [hep-ph].

[435] D. Chway, T. H. Jung, and C. S. Shin, "Dark matter filtering-out effect during a first-order phase transition," *Phys. Rev. D* **101** (2020) no. 9, 095019, arXiv:1912.04238 [hep-ph].

[436] W. Chao, X.-F. Li, and L. Wang, "Filtered pseudo-scalar dark matter and gravitational waves from first order phase transition," *JCAP* **06** (2021) 038, arXiv:2012.15113 [hep-ph].

[437] S. Jiang, F. P. Huang, and C. S. Li, "Hydrodynamic effects on the filtered dark matter produced by a first-order phase transition," *Phys. Rev. D* **108** (2023) no. 6, 063508, arXiv:2305.02218 [hep-ph].

[438] F. P. Huang and C. S. Li, "Probing the baryogenesis and dark matter relaxed in phase transition by gravitational waves and colliders," *Phys. Rev. D* **96** (2017) no. 9, 095028, arXiv:1709.09691 [hep-ph].

[439] Y. Bai and A. J. Long, "Six Flavor Quark Matter," *JHEP* **06** (2018) 072, arXiv:1804.10249 [hep-ph].

[440] J.-P. Hong, S. Jung, and K.-P. Xie, "Fermi-ball dark matter from a first-order phase transition," *Phys. Rev. D* **102** (2020) no. 7, 075028, arXiv:2008.04430 [hep-ph].

[441] M. J. Baker, M. Breitbach, J. Kopp, and L. Mittnacht, "Primordial Black Holes from First-Order Cosmological Phase Transitions," arXiv:2105.07481 [astro-ph.CO].

[442] K. Kawana and K.-P. Xie, "Primordial black holes from a cosmic phase transition: The collapse of Fermi-balls," *Phys. Lett. B* **824** (2022) 136791, arXiv:2106.00111 [astro-ph.CO].

[443] P. Huang and K.-P. Xie, "Primordial black holes from an electroweak phase transition," *Phys. Rev. D* **105** (2022) no. 11, 115033, arXiv:2201.07243 [hep-ph].

[444] K. Kawana, P. Lu, and K.-P. Xie, "First-order phase transition and fate of false vacuum remnants," *JCAP* **10** (2022) 030, arXiv:2206.09923 [astro-ph.CO].

[445] P. Lu, K. Kawana, and K.-P. Xie, "Old phase remnants in first-order phase transitions," *Phys. Rev. D* **105** (2022) no. 12, 123503, arXiv:2202.03439 [astro-ph.CO].

[446] P. Lu, K. Kawana, and A. Kusenko, "Late-forming primordial black holes: Beyond the CMB era," *Phys. Rev. D* **107** (2023) no. 10, 103037, arXiv:2210.16462 [astro-ph.CO].

[447] T. Kim, P. Lu, D. Marfatia, and V. Takhistov, "Regurgitated Dark Matter," arXiv:2309.05703 [hep-ph].

[448] K.-P. Xie, "Revisiting the fermion-field nontopological solitons," arXiv:2405.01227 [hep-ph].

[449] J. M. Cline, B. Laurent, S. Raby, and J.-S. Roux, "PeV-scale leptogenesis, gravitational waves, and black holes from a SUSY-breaking phase transition," *Phys. Rev. D* **107** (2023) no. 9, 095011, arXiv:2211.00422 [hep-ph].

[450] T. C. Gehrman, B. Shams Es Haghi, K. Sinha, and T. Xu, "Recycled dark matter," *JCAP* **03** (2024) 044, arXiv:2310.08526 [hep-ph].

[451] J. Liu, L. Bian, R.-G. Cai, Z.-K. Guo, and S.-J. Wang, "Primordial black hole production during first-order phase transitions," *Phys. Rev. D* **105** (2022) no. 2, L021303, arXiv:2106.05637 [astro-ph.CO].

[452] K. Hashino, S. Kanemura, and T. Takahashi, "Primordial black holes as a probe of strongly first-order electroweak phase transition," *Phys. Lett. B* **833** (2022) 137261, arXiv:2111.13099 [hep-ph].

[453] K. Kawana, T. Kim, and P. Lu, "PBH formation from overdensities in delayed vacuum transitions," *Phys. Rev. D* **108** (2023) no. 10, 103531, arXiv:2212.14037 [astro-ph.CO].

[454] K. Hashino, S. Kanemura, T. Takahashi, and M. Tanaka, "Probing first-order electroweak phase transition via primordial black holes in the effective field theory," *Phys. Lett. B* **838** (2023) 137688, arXiv:2211.16225 [hep-ph].

[455] M. Lewicki, P. Toczek, and V. Vaskonen, "Primordial black holes from strong first-order phase transitions," *JHEP* **09** (2023) 092, arXiv:2305.04924 [astro-ph.CO].

[456] Y. Gouttenoire and T. Volansky, "Primordial Black Holes from Supercooled Phase Transitions," arXiv:2305.04942 [hep-ph].

[457] S. Kanemura, M. Tanaka, and K.-P. Xie, "Primordial black holes from slow phase transitions: a model-building perspective," *JHEP* **06** (2024) 036, arXiv:2404.00646 [hep-ph].

[458] R.-G. Cai, Y.-S. Hao, and S.-J. Wang, "Primordial black holes and curvature perturbations from false-vacuum islands," arXiv:2404.06506 [astro-ph.CO].

[459] M. Arteaga, A. Ghoshal, and A. Strumia, "Gravitational waves and black holes from the phase transition in models of dynamical symmetry breaking," arXiv:2409.04545 [hep-ph].

[460] W.-Y. Ai, L. Heurtier, and T. H. Jung, "Primordial black holes from an aborted phase transition," arXiv:2409.02175 [astro-ph.CO].

[461] D. Gonçalves, A. Kaladharan, and Y. Wu, "Primordial Black Holes from First-Order Phase Transition in the xSM," arXiv:2406.07622 [hep-ph].

[462] A. D. Linde, "Decay of the False Vacuum at Finite Temperature," *Nucl. Phys. B* **216** (1983) 421. [Erratum: Nucl.Phys.B 223, 544 (1983)].

[463] D. J. H. Chung, A. J. Long, and L.-T. Wang, "125 GeV Higgs boson and electroweak phase transition model classes," *Phys. Rev.* **D87** (2013) no. 2, 023509, arXiv:1209.1819 [hep-ph].

[464] M. J. Ramsey-Musolf, "The electroweak phase transition: a collider target," *JHEP* **09** (2020) 179, arXiv:1912.07189 [hep-ph].

[465] A. Alves, T. Ghosh, H.-K. Guo, K. Sinha, and D. Vagie, "Collider and Gravitational Wave Complementarity in Exploring the Singlet Extension of the Standard Model," *JHEP* **04** (2019) 052, arXiv:1812.09333 [hep-ph].

[466] A. Alves, T. Ghosh, H.-K. Guo, and K. Sinha, "Resonant Di-Higgs Production at Gravitational Wave Benchmarks: A Collider Study using Machine Learning," *JHEP* **12** (2018) 070, arXiv:1808.08974 [hep-ph].

[467] A. Alves, D. Gonçalves, T. Ghosh, H.-K. Guo, and K. Sinha, "Di-Higgs Production in the $4b$ Channel and Gravitational Wave Complementarity," *JHEP* **03** (2020) 053, arXiv:1909.05268 [hep-ph].

[468] A. Alves, D. Gonçalves, T. Ghosh, H.-K. Guo, and K. Sinha, "Di-Higgs Blind Spots in Gravitational Wave Signals," *Phys. Lett. B* **818** (2021) 136377, arXiv:2007.15654 [hep-ph].

[469] W. Liu and K.-P. Xie, "Probing electroweak phase transition with multi-TeV muon colliders and gravitational waves," *JHEP* **04** (2021) 015, arXiv:2101.10469 [hep-ph].

[470] L. Bian, H.-K. Guo, Y. Wu, and R. Zhou, "Gravitational wave and collider searches for electroweak symmetry breaking patterns," *Phys. Rev. D* **101** (2020) no. 3, 035011, arXiv:1906.11664 [hep-ph].

[471] R. Zhou, W. Cheng, X. Deng, L. Bian, and Y. Wu, "Electroweak phase transition and Higgs phenomenology in the Georgi-Machacek model," arXiv:1812.06217 [hep-ph].

[472] F. P. Huang and J.-H. Yu, "Exploring inert dark matter blind spots with gravitational wave signatures," *Phys. Rev. D* **98** (2018) no. 9, 095022, arXiv:1704.04201 [hep-ph].

[473] Y. Wang, C. S. Li, and F. P. Huang, "Complementary probe of dark matter blind spots by lepton colliders and gravitational waves," *Phys. Rev. D* **104** (2021) no. 5, 053004, arXiv:2012.03920 [hep-ph].

[474] T. Ghosh, H.-K. Guo, T. Han, and H. Liu, "Electroweak phase transition with an SU(2) dark sector," *JHEP* **07** (2021) 045, arXiv:2012.09758 [hep-ph].

[475] F. P. Huang, P.-H. Gu, P.-F. Yin, Z.-H. Yu, and X. Zhang, "Testing the electroweak phase transition and electroweak baryogenesis at the LHC and a circular electron-positron collider," *Phys. Rev. D* **93** (2016) no. 10, 103515, arXiv:1511.03969 [hep-ph].

[476] P. Huang, A. J. Long, and L.-T. Wang, "Probing the Electroweak Phase Transition with Higgs Factories and Gravitational Waves," *Phys. Rev. D* **94** (2016) no. 7, 075008, arXiv:1608.06619 [hep-ph].

[477] Q.-H. Cao, F. P. Huang, K.-P. Xie, and X. Zhang, "Testing the electroweak phase transition in scalar extension models at lepton colliders," *Chin. Phys.* **C42** (2018) no. 2, 023103, arXiv:1708.04737 [hep-ph].

[478] N. Chen, T. Li, Y. Wu, and L. Bian, "Complementarity of the future e^+e^- colliders and gravitational waves in the probe of complex singlet extension to the standard model," *Phys. Rev. D* **101** (2020) no. 7, 075047, arXiv:1911.05579 [hep-ph].

[479] W. Su, A. G. Williams, and M. Zhang, "Strong first order electroweak phase transition in 2HDM confronting future Z & Higgs factories," arXiv:2011.04540 [hep-ph].

[480] H. Song, W. Su, and M. Zhang, "Electroweak phase transition in 2HDM under Higgs, Z-pole, and W precision measurements," *JHEP* **10** (2022) 048, arXiv:2204.05085 [hep-ph].

[481] F. P. Huang, Y. Wan, D.-G. Wang, Y.-F. Cai, and X. Zhang, "Hearing the echoes of electroweak baryogenesis with gravitational wave detectors," *Phys. Rev. D* **94** (2016) no. 4,

041702, arXiv:1601.01640 [hep-ph].

[482] Y. Gong, Z. Li, X. Xu, L. L. Yang, and X. Zhao, "Mixed QCD-EW corrections for Higgs boson production at e^+e^- colliders," arXiv:1609.03955 [hep-ph].

[483] Q.-F. Sun, F. Feng, Y. Jia, and W.-L. Sang, "Mixed electroweak-QCD corrections to $e^+e^- \to HZ$ at Higgs factories," arXiv:1609.03995 [hep-ph].

[484] M. Carena, Z. Liu, and Y. Wang, "Electroweak phase transition with spontaneous Z_2-breaking," *JHEP* **08** (2020) 107, arXiv:1911.10206 [hep-ph].

[485] J. Kozaczuk, M. J. Ramsey-Musolf, and J. Shelton, "Exotic Higgs boson decays and the electroweak phase transition," *Phys. Rev. D* **101** (2020) no. 11, 115035, arXiv:1911.10210 [hep-ph].

[486] Y. Gershtein, S. Knapen, and D. Redigolo, "Probing naturally light singlets with a displaced vertex trigger," *Phys. Lett. B* **823** (2021) 136758, arXiv:2012.07864 [hep-ph].

[487] J. de Blas *et al.*, "Higgs Boson Studies at Future Particle Colliders," *JHEP* **01** (2020) 139, arXiv:1905.03764 [hep-ph].

[488] Z. Wang, X. Zhu, E. E. Khoda, S.-C. Hsu, N. Konstantinidis, K. Li, S. Li, M. J. Ramsey-Musolf, Y. Wu, and Y. E. Zhang, "Probing Electroweak Phase Transition at CEPC via Exotic Higgs Decays with 4b Final States," *LHEP* **2023** (2023) 436.

[489] Y. Kato, "Search for Higgs decaying to exotic scalers at the ILC," 11, 2021. https://indico.ihep.ac.cn/event/14938/.

[490] W. Liu, A. Yang, and H. Sun, "Shedding light on the electroweak phase transition from exotic Higgs boson decays at the lifetime frontiers," *Phys. Rev. D* **105** (2022) no. 11, 115040, arXiv:2205.08205 [hep-ph].

[491] M. Cermeño, C. Degrande, and L. Mantani, "Signatures of leptophilic t-channel dark matter from active galactic nuclei," *Phys. Rev. D* **105** (2022) no. 8, 083019, arXiv:2201.07247 [hep-ph].

[492] A. Jueid, S. Nasri, and R. Soualah, "Searching for GeV-scale Majorana Dark Matter: inter spem et metum," *JHEP* **04** (2021) 012, arXiv:2006.01348 [hep-ph].

[493] A. Jueid and S. Nasri, "Phenomenology of Minimal Leptophilic Dark Matter Models at Linear Colliders," in *International Workshop on Future Linear Colliders*. 5, 2021. arXiv:2105.02921 [hep-ph].

[494] X. Chen and Y. Wu, "Search for CP violation effects in the $h \to \tau\tau$ decay with e^+e^- colliders," *Eur. Phys. J. C* **77** (2017) no. 10, 697, arXiv:1703.04855 [hep-ph].

[495] X. Chen and Y. Wu, "Probing the CP-Violation effects in the $h\tau\tau$ coupling at the LHC," *Phys. Lett. B* **790** (2019) 332–338, arXiv:1708.02882 [hep-ph].

[496] S.-F. Ge, G. Li, P. Pasquini, and M. J. Ramsey-Musolf, "CP-violating Higgs Di-tau Decays: Baryogenesis and Higgs Factories," *Phys. Rev. D* **103** (2021) no. 9, 095027, arXiv:2012.13922 [hep-ph].

[497] J. Alonso-González, L. Merlo, and S. Pokorski, "A new bound on CP violation in the τ lepton Yukawa coupling and electroweak baryogenesis," *JHEP* **06** (2021) 166, arXiv:2103.16569 [hep-ph].

[498] S.-P. Li and K.-P. Xie, "Collider test of nano-Hertz gravitational waves from pulsar timing arrays," *Phys. Rev. D* **108** (2023) no. 5, 055018, arXiv:2307.01086 [hep-ph].

[499] S. Antusch, E. Cazzato, and O. Fischer, "Displaced vertex searches for sterile neutrinos at future lepton colliders," *JHEP* **12** (2016) 007, arXiv:1604.02420 [hep-ph].

[500] "Sterile neutrino constraints." https://www.hep.ucl.ac.uk/~pbolton/plots.html.

[501] **Super-Kamiokande** Collaboration, Y. Fukuda *et al.*, "Evidence for oscillation of atmospheric neutrinos," *Phys. Rev. Lett.* **81** (1998) 1562–1567, arXiv:hep-ex/9807003.

[502] **SNO** Collaboration, Q. R. Ahmad *et al.*, "Direct evidence for neutrino flavor transformation from neutral current interactions in the Sudbury Neutrino Observatory," *Phys. Rev. Lett.* **89** (2002) 011301, arXiv:nucl-ex/0204008.

[503] **FASER** Collaboration, H. Abreu *et al.*, "First Direct Observation of Collider Neutrinos with FASER at the LHC," *Phys. Rev. Lett.* **131** (2023) no. 3, 031801, arXiv:2303.14185 [hep-ex].

[504] F. F. Deppisch, P. S. Bhupal Dev, and A. Pilaftsis, "Neutrinos and Collider Physics," *New J. Phys.* **17** (2015) no. 7, 075019, arXiv:1502.06541 [hep-ph].

[505] Y. Cai, T. Han, T. Li, and R. Ruiz, "Lepton Number Violation: Seesaw Models and Their Collider Tests," *Front.in Phys.* **6** (2018) 40, arXiv:1711.02180 [hep-ph].

[506] W.-Y. Keung and G. Senjanovic, "Majorana Neutrinos and the Production of the Right-handed Charged Gauge Boson," *Phys. Rev. Lett.* **50** (1983) 1427.

[507] S. Weinberg, "Baryon and Lepton Nonconserving Processes," *Phys. Rev. Lett.* **43** (1979) 1566–1570.

[508] P. Minkowski, "$\mu \to e\gamma$ at a Rate of One Out of 10^9 Muon Decays?," *Phys. Lett.* **67B** (1977) 421–428.

[509] R. N. Mohapatra and G. Senjanovic, "Neutrino Mass and Spontaneous Parity Nonconservation," *Phys. Rev. Lett.* **44** (1980) 912. [,231(1979)].

[510] T. Yanagida, "Horizontal gauge symmetry and masses of neutrinos, Proceedings: Workshop on the Unified Theories and the Baryon Number in the Universe," *Conf. Proc.* **C7902131** (1979) 95–99.

[511] M. Gell-Mann, P. Ramond, and R. Slansky, "Complex Spinors and Unified Theories," *Conf. Proc.* **C790927** (1979) 315–321, arXiv:1306.4669 [hep-th].

[512] S. L. Glashow, "The Future of Elementary Particle Physics," *NATO Sci. Ser. B* **61** (1980) 687.

[513] J. Schechter and J. W. F. Valle, "Neutrino Masses in SU(2) x U(1) Theories," *Phys. Rev.* **D22** (1980) 2227.

[514] A. Davidson, M. Koca, and K. C. Wali, "U(1) as the Minimal Horizontal Gauge Symmetry," *Phys. Rev. Lett.* **43** (1979) 92.

[515] R. E. Marshak and R. N. Mohapatra, "Quark - Lepton Symmetry and B-L as the U(1) Generator of the Electroweak Symmetry Group," *Phys. Lett. B* **91** (1980) 222–224.

[516] W. Buchmuller, C. Greub, and P. Minkowski, "Neutrino masses, neutral vector bosons and the scale of B-L breaking," *Phys. Lett. B* **267** (1991) 395–399.

[517] R. N. Mohapatra and J. C. Pati, "Left-Right Gauge Symmetry and an Isoconjugate Model of CP Violation," *Phys. Rev. D* **11** (1975) 566–571.

[518] R. N. Mohapatra and J. C. Pati, "A Natural Left-Right Symmetry," *Phys. Rev. D* **11** (1975) 2558.

[519] G. Senjanovic and R. N. Mohapatra, "Exact Left-Right Symmetry and Spontaneous Violation of Parity," *Phys. Rev. D* **12** (1975) 1502.

[520] H. Fritzsch and P. Minkowski, "Unified Interactions of Leptons and Hadrons," *Annals Phys.* **93** (1975) 193–266.

[521] E. Witten, "Neutrino Masses in the Minimal O(10) Theory," *Phys. Lett. B* **91** (1980) 81–84.

[522] W. Konetschny and W. Kummer, "Nonconservation of Total Lepton Number with Scalar Bosons," *Phys. Lett.* **70B** (1977) 433–435.

[523] M. Magg and C. Wetterich, "Neutrino Mass Problem and Gauge Hierarchy," *Phys. Lett.* **94B** (1980) 61–64.

[524] T. P. Cheng and L.-F. Li, "Neutrino Masses, Mixings and Oscillations in SU(2) x U(1) Models of Electroweak Interactions," *Phys. Rev.* **D22** (1980) 2860.

[525] R. N. Mohapatra and G. Senjanovic, "Neutrino Masses and Mixings in Gauge Models with Spontaneous Parity Violation," *Phys. Rev.* **D23** (1981) 165.

[526] G. Lazarides, Q. Shafi, and C. Wetterich, "Proton Lifetime and Fermion Masses in an SO(10) Model," *Nucl. Phys.* **B181** (1981) 287–300.

[527] R. Foot, H. Lew, X. G. He, and G. C. Joshi, "Seesaw Neutrino Masses Induced by a Triplet of Leptons," *Z. Phys.* **C44** (1989) 441.

[528] E. Ma and D. P. Roy, "Heavy triplet leptons and new gauge boson," *Nucl. Phys. B* **644** (2002) 290–302, arXiv:hep-ph/0206150.

[529] A. Zee, "A Theory of Lepton Number Violation, Neutrino Majorana Mass, and Oscillation," *Phys. Lett. B* **93** (1980) 389. [Erratum: Phys.Lett.B 95, 461 (1980)].

[530] A. Zee, "Quantum Numbers of Majorana Neutrino Masses," *Nucl. Phys. B* **264** (1986) 99–110.

[531] K. S. Babu, "Model of 'Calculable' Majorana Neutrino Masses," *Phys. Lett. B* **203** (1988) 132–136.

[532] Y. Cai, J. Herrero-García, M. A. Schmidt, A. Vicente, and R. R. Volkas, "From the trees to the forest: a review of radiative neutrino mass models," *Front. in Phys.* **5** (2017) 63, arXiv:1706.08524 [hep-ph].

[533] P. S. B. Dev, M. J. Ramsey-Musolf, and Y. Zhang, "Doubly-Charged Scalars in the Type-II Seesaw Mechanism: Fundamental Symmetry Tests and High-Energy Searches," *Phys. Rev. D* **98** (2018) no. 5, 055013, arXiv:1806.08499 [hep-ph].

[534] V. Cirigliano, A. Kurylov, M. J. Ramsey-Musolf, and P. Vogel, "Neutrinoless double beta decay and lepton flavor violation," *Phys. Rev. Lett.* **93** (2004) 231802, arXiv:hep-ph/0406199.

[535] A. Abada, C. Biggio, F. Bonnet, M. B. Gavela, and T. Hambye, "Low energy effects of neutrino masses," *JHEP* **12** (2007) 061, arXiv:0707.4058 [hep-ph].

[536] V. Tello, M. Nemevsek, F. Nesti, G. Senjanovic, and F. Vissani, "Left-Right Symmetry: from LHC to Neutrinoless Double Beta Decay," *Phys. Rev. Lett.* **106** (2011) 151801,

arXiv:1011.3522 [hep-ph].

[537] J. Chakrabortty, H. Z. Devi, S. Goswami, and S. Patra, "Neutrinoless double-β decay in TeV scale Left-Right symmetric models," *JHEP* **08** (2012) 008, arXiv:1204.2527 [hep-ph].

[538] J. Barry and W. Rodejohann, "Lepton number and flavour violation in TeV-scale left-right symmetric theories with large left-right mixing," *JHEP* **09** (2013) 153, arXiv:1303.6324 [hep-ph].

[539] P. S. Bhupal Dev, S. Goswami, and M. Mitra, "TeV Scale Left-Right Symmetry and Large Mixing Effects in Neutrinoless Double Beta Decay," *Phys. Rev. D* **91** (2015) no. 11, 113004, arXiv:1405.1399 [hep-ph].

[540] R. L. Awasthi, P. S. B. Dev, and M. Mitra, "Implications of the Diboson Excess for Neutrinoless Double Beta Decay and Lepton Flavor Violation in TeV Scale Left Right Symmetric Model," *Phys. Rev. D* **93** (2016) no. 1, 011701, arXiv:1509.05387 [hep-ph].

[541] G. Bambhaniya, P. S. B. Dev, S. Goswami, and M. Mitra, "The Scalar Triplet Contribution to Lepton Flavour Violation and Neutrinoless Double Beta Decay in Left-Right Symmetric Model," *JHEP* **04** (2016) 046, arXiv:1512.00440 [hep-ph].

[542] D. Borah and A. Dasgupta, "Charged lepton flavour violcxmation and neutrinoless double beta decay in left-right symmetric models with type I+II seesaw," *JHEP* **07** (2016) 022, arXiv:1606.00378 [hep-ph].

[543] G. Li, M. Ramsey-Musolf, and J. C. Vasquez, "Left-Right Symmetry and Leading Contributions to Neutrinoless Double Beta Decay," *Phys. Rev. Lett.* **126** (2021) no. 15, 151801, arXiv:2009.01257 [hep-ph].

[544] G. Li, M. J. Ramsey-Musolf, and J. C. Vasquez, "Unraveling the left-right mixing using $0\nu\beta\beta$ decay and collider probes," *Phys. Rev. D* **105** (2022) no. 11, 115021, arXiv:2202.01789 [hep-ph].

[545] J. de Vries, G. Li, M. J. Ramsey-Musolf, and J. C. Vasquez, "Light sterile neutrinos, left-right symmetry, and $0\nu\beta\beta$ decay," *JHEP* **11** (2022) 056, arXiv:2209.03031 [hep-ph].

[546] G. Li, M. J. Ramsey-Musolf, S. Urrutia Quiroga, and J. C. Vasquez, "Dissecting Lepton Number Violation in the Left-Right Symmetric Model: $0\nu\beta\beta$ decay, Møller scattering, and collider searches," arXiv:2408.06306 [hep-ph].

[547] Y. Gao and K. Wang, "Heavy Neutrino Searches via Same-sign Lepton Pairs at the Higgs Factory," arXiv:2102.12826 [hep-ph].

[548] F. F. Deppisch, W. Liu, and M. Mitra, "Long-lived Heavy Neutrinos from Higgs Decays," *JHEP* **08** (2018) 181, arXiv:1804.04075 [hep-ph].

[549] A. Das, S. Mandal, T. Nomura, and S. Shil, "Heavy Majorana neutrino pair production from Z' at hadron and lepton colliders," *Phys. Rev. D* **105** (2022) no. 9, 095031, arXiv:2202.13358 [hep-ph].

[550] M. Nemevšek, F. Nesti, and J. C. Vasquez, "Majorana Higgses at colliders," *JHEP* **04** (2017) 114, arXiv:1612.06840 [hep-ph].

[551] J. Liao and Y. Zhang, "Constraining nonstandard neutrino interactions at electron colliders," *Phys. Rev. D* **104** (2021) no. 3, 035043, arXiv:2105.11215 [hep-ph].

[552] Y. Zhang and W. Liu, "Probing active-sterile neutrino transition magnetic moments at LEP and CEPC," *Phys. Rev. D* **107** (2023) no. 9, 095031, arXiv:2301.06050 [hep-ph].

[553] P. S. B. Dev, R. N. Mohapatra, and Y. Zhang, "Lepton Flavor Violation Induced by a Neutral Scalar at Future Lepton Colliders," *Phys. Rev. Lett.* **120** (2018) no. 22, 221804, arXiv:1711.08430 [hep-ph].

[554] P. S. Bhupal Dev, R. N. Mohapatra, and Y. Zhang, "Probing TeV scale origin of neutrino mass at future lepton colliders via neutral and doubly-charged scalars," *Phys. Rev. D* **98** (2018) no. 7, 075028, arXiv:1803.11167 [hep-ph].

[555] A. M. Abdullahi *et al.*, "The present and future status of heavy neutral leptons," *J. Phys. G* **50** (2023) no. 2, 020501, arXiv:2203.08039 [hep-ph].

[556] S. Antusch and O. Fischer, "Testing sterile neutrino extensions of the Standard Model at future lepton colliders," *JHEP* **05** (2015) 053, arXiv:1502.05915 [hep-ph].

[557] D. Barducci and E. Bertuzzo, "The see-saw portal at future Higgs factories: the role of dimension six operators," *JHEP* **06** (2022) 077, arXiv:2201.11754 [hep-ph].

[558] L. Rygaard, "Long-Lived Heavy Neutral Leptons at the FCC-ee," other thesis, Uppsala U., 2022.

[559] M. Drewes, "Distinguishing Dirac and Majorana Heavy Neutrinos at Lepton Colliders," *PoS* **ICHEP2022** (2022) 608, arXiv:2210.17110 [hep-ph].

[560] M. Ovchynnikov and J.-Y. Zhu, "Search for the dipole portal of heavy neutral leptons at future colliders," *JHEP* **07** (2023) 039, arXiv:2301.08592 [hep-ph].

[561] **RD-FA** Collaboration, M. Antonello, "IDEA: A detector concept for future leptonic colliders," *Nuovo Cim. C* **43** (2020) no. 2-3, 27.

[562] **SHiP** Collaboration, C. Ahdida *et al.*, "Sensitivity of the SHiP experiment to Heavy Neutral Leptons," *JHEP* **04** (2019) 077, arXiv:1811.00930 [hep-ph].

[563] P. Ballett, T. Boschi, and S. Pascoli, "Heavy Neutral Leptons from low-scale seesaws at the DUNE Near Detector," *JHEP* **03** (2020) 111, arXiv:1905.00284 [hep-ph].

[564] **CHARM** Collaboration, F. Bergsma *et al.*, "A Search for Decays of Heavy Neutrinos in the Mass Range 0.5-GeV to 2.8-GeV," *Phys. Lett. B* **166** (1986) 473–478.

[565] **CMS** Collaboration, A. M. Sirunyan *et al.*, "Search for heavy neutral leptons in events with three charged leptons in proton-proton collisions at $\sqrt{s} = 13$ TeV," *Phys. Rev. Lett.* **120** (2018) no. 22, 221801, arXiv:1802.02965 [hep-ex].

[566] **ATLAS** Collaboration, G. Aad *et al.*, "Search for heavy neutral leptons in decays of W bosons produced in 13 TeV pp collisions using prompt and displaced signatures with the ATLAS detector," *JHEP* **10** (2019) 265, arXiv:1905.09787 [hep-ex].

[567] **DELPHI** Collaboration, P. Abreu *et al.*, "Search for neutral heavy leptons produced in Z decays," *Z. Phys. C* **74** (1997) 57–71. [Erratum: Z.Phys.C 75, 580 (1997)].

[568] **E949** Collaboration, A. V. Artamonov *et al.*, "Search for heavy neutrinos in $K^+ \to \mu^+ \nu_H$ decays," *Phys. Rev. D* **91** (2015) no. 5, 052001, arXiv:1411.3963 [hep-ex]. [Erratum: Phys.Rev.D 91, 059903 (2015)].

[569] **LHCb** Collaboration, R. Aaij *et al.*, "Search for massive long-lived particles decaying semileptonically in the LHCb detector," *Eur. Phys. J. C* **77** (2017) no. 4, 224, arXiv:1612.00945 [hep-ex].

[570] S. Antusch, E. Cazzato, and O. Fischer, "Sterile neutrino searches via displaced vertices at LHCb," *Phys. Lett. B* **774** (2017) 114–118, arXiv:1706.05990 [hep-ph].

[571] **NuTeV, E815** Collaboration, A. Vaitaitis *et al.*, "Search for neutral heavy leptons in a high-energy neutrino beam," *Phys. Rev. Lett.* **83** (1999) 4943–4946, arXiv:hep-ex/9908011.

[572] G. Bernardi *et al.*, "Further Limits On Heavy Neutrino Couplings," *Phys. Lett.* **B203** (1988) 332–334.

[573] A. Boyarsky, M. Ovchynnikov, O. Ruchayskiy, and V. Syvolap, "Improved big bang nucleosynthesis constraints on heavy neutral leptons," *Phys. Rev. D* **104** (2021) no. 2,

023517, arXiv:2008.00749 [hep-ph].

[574] T. Asaka, S. Blanchet, and M. Shaposhnikov, "The nuMSM, dark matter and neutrino masses," *Phys. Lett. B* **631** (2005) 151–156, arXiv:hep-ph/0503065.

[575] T. Asaka and M. Shaposhnikov, "The νMSM, dark matter and baryon asymmetry of the universe," *Phys. Lett. B* **620** (2005) 17–26, arXiv:hep-ph/0505013.

[576] W. Liao and X.-H. Wu, "Signature of heavy sterile neutrinos at CEPC," *Phys. Rev.* **D97** (2018) no. 5, 055005, arXiv:1710.09266 [hep-ph].

[577] J.-N. Ding, Q. Qin, and F.-S. Yu, "Heavy neutrino searches at future Z-factories," *Eur. Phys. J. C* **79** (2019) no. 9, 766, arXiv:1903.02570 [hep-ph].

[578] A. Blondel, A. de Gouvêa, and B. Kayser, "Z-boson decays into Majorana or Dirac heavy neutrinos," *Phys. Rev. D* **104** (2021) no. 5, 055027, arXiv:2105.06576 [hep-ph].

[579] I. M. Shoemaker, K. Petraki, and A. Kusenko, "Collider signatures of sterile neutrinos in models with a gauge-singlet Higgs," *JHEP* **09** (2010) 060, arXiv:1006.5458 [hep-ph].

[580] Y. Gao, M. Jin, and K. Wang, "Probing the Decoupled Seesaw Scalar in Rare Higgs Decay," *JHEP* **02** (2020) 101, arXiv:1904.12325 [hep-ph].

[581] T. Robens, "Constraining Extended Scalar Sectors at Current and Future Colliders—An Update," *Springer Proc. Phys.* **292** (2023) 141–152, arXiv:2209.15544 [hep-ph].

[582] "SiD Letter of Intent," arXiv:0911.0006 [physics.ins-det].

[583] J. Gu, H. Li, Z. Liu, S. Su, and W. Su, "Learning from Higgs Physics at Future Higgs Factories," *JHEP* **12** (2017) 153, arXiv:1709.06103 [hep-ph].

[584] A. Das, P. S. B. Dev, Y. Hosotani, and S. Mandal, "Probing the minimal U(1)X model at future electron-positron colliders via fermion pair-production channels," *Phys. Rev. D* **105** (2022) no. 11, 115030, arXiv:2104.10902 [hep-ph].

[585] A. Das, N. Okada, and D. Raut, "Enhanced pair production of heavy Majorana neutrinos at the LHC," *Phys. Rev. D* **97** (2018) no. 11, 115023, arXiv:1710.03377 [hep-ph].

[586] J. C. Pati and A. Salam, "Lepton Number as the Fourth Color," *Phys. Rev. D* **10** (1974) 275–289. [Erratum: Phys.Rev.D 11, 703–703 (1975)].

[587] A. Djouadi, "The Anatomy of electro-weak symmetry breaking. I: The Higgs boson in the standard model," *Phys. Rept.* **457** (2008) 1–216, arXiv:hep-ph/0503172.

[588] **TLEP Design Study Working Group** Collaboration, M. Bicer *et al.*, "First Look at the Physics Case of TLEP," *JHEP* **01** (2014) 164, arXiv:1308.6176 [hep-ex].

[589] J. Barranco, O. G. Miranda, C. A. Moura, and J. W. F. Valle, "Constraining non-standard neutrino-electron interactions," *Phys. Rev. D* **77** (2008) 093014, arXiv:0711.0698 [hep-ph].

[590] G. Magill, R. Plestid, M. Pospelov, and Y.-D. Tsai, "Dipole Portal to Heavy Neutral Leptons," *Phys. Rev. D* **98** (2018) no. 11, 115015, arXiv:1803.03262 [hep-ph].

[591] **OPAL** Collaboration, R. Akers *et al.*, "Measurement of single photon production in e+ e- collisions near the Z0 resonance," *Z. Phys. C* **65** (1995) 47–66.

[592] **ATLAS** Collaboration, G. Aad *et al.*, "Search for dark matter in association with an energetic photon in pp collisions at $\sqrt{s} = 13$ TeV with the ATLAS detector," *JHEP* **02** (2021) 226, arXiv:2011.05259 [hep-ex].

[593] **CMS** Collaboration, A. M. Sirunyan *et al.*, "Search for supersymmetry in events with a photon, a lepton, and missing transverse momentum in proton-proton collisions at $\sqrt{s} = 13$ TeV," *JHEP* **01** (2019) 154, arXiv:1812.04066 [hep-ex].

[594] At the LHC, the limits for $d_{\mathcal{W}} = 2 \tan\theta_w d_B$ ($d_Z = 0$) for τ flavor are not shown, as τ final states are not considered by the CMS search [593], and we mainly focus on $pp \to Z$ channels for the ATLAS search [592].

[595] R. Barbier *et al.*, "R-parity violating supersymmetry," *Phys. Rept.* **420** (2005) 1–202, arXiv:hep-ph/0406039 [hep-ph].

[596] P. Q. Hung, "A Model of electroweak-scale right-handed neutrino mass," *Phys. Lett. B* **649** (2007) 275–279, arXiv:hep-ph/0612004.

[597] J.-P. Bu, Y. Liao, and J.-Y. Liu, "Lepton Flavor Violating Muon Decays in a Model of Electroweak-Scale Right-Handed Neutrinos," *Phys. Lett. B* **665** (2008) 39–43, arXiv:0802.3241 [hep-ph].

[598] C.-F. Chang, C.-H. V. Chang, C. S. Nugroho, and T.-C. Yuan, "Lepton Flavor Violating Decays of Neutral Higgses in Extended Mirror Fermion Model," *Nucl. Phys. B* **910** (2016) 293–308, arXiv:1602.00680 [hep-ph].

[599] G. C. Branco, P. M. Ferreira, L. Lavoura, M. N. Rebelo, M. Sher, and J. P. Silva, "Theory and phenomenology of two-Higgs-doublet models," *Phys. Rept.* **516** (2012) 1–102, arXiv:1106.0034 [hep-ph].

[600] A. Crivellin, J. Heeck, and P. Stoffer, "A perturbed lepton-specific two-Higgs-doublet model facing experimental hints for physics beyond the Standard Model," *Phys. Rev. Lett.* **116**

(2016) no. 8, 081801, arXiv:1507.07567 [hep-ph].

[601] A. Maiezza, G. Senjanović, and J. C. Vasquez, "Higgs sector of the minimal left-right symmetric theory," *Phys. Rev. D* **95** (2017) no. 9, 095004, arXiv:1612.09146 [hep-ph].

[602] H. Baer, T. Barklow, K. Fujii, Y. Gao, A. Hoang, S. Kanemura, J. List, H. E. Logan, A. Nomerotski, M. Perelstein, *et al.*, "The International Linear Collider Technical Design Report - Volume 2: Physics," arXiv:1306.6352 [hep-ph].

[603] **Particle Data Group** Collaboration, S. Navas *et al.*, "Review of particle physics," *Phys. Rev. D* **110** (2024) no. 3, 030001.

[604] **DELPHI** Collaboration, J. Abdallah *et al.*, "Measurement and interpretation of fermion-pair production at LEP energies above the Z resonance," *Eur. Phys. J. C* **45** (2006) 589–632, arXiv:hep-ex/0512012.

[605] P. Fileviez Perez, T. Han, G.-y. Huang, T. Li, and K. Wang, "Neutrino Masses and the CERN LHC: Testing Type II Seesaw," *Phys. Rev. D* **78** (2008) 015018, arXiv:0805.3536 [hep-ph].

[606] A. Melfo, M. Nemevsek, F. Nesti, G. Senjanovic, and Y. Zhang, "Type II Seesaw at LHC: The Roadmap," *Phys. Rev. D* **85** (2012) 055018, arXiv:1108.4416 [hep-ph].

[607] S. Kanemura, M. Kikuchi, K. Yagyu, and H. Yokoya, "Bounds on the mass of doubly-charged Higgs bosons in the same-sign diboson decay scenario," *Phys. Rev. D* **90** (2014) no. 11, 115018, arXiv:1407.6547 [hep-ph].

[608] P. S. Bhupal Dev and Y. Zhang, "Displaced vertex signatures of doubly charged scalars in the type-II seesaw and its left-right extensions," *JHEP* **10** (2018) 199, arXiv:1808.00943 [hep-ph].

[609] S. Dodelson and L. M. Widrow, "Sterile-neutrinos as dark matter," *Phys. Rev. Lett.* **72** (1994) 17–20, arXiv:hep-ph/9303287.

[610] X.-D. Shi and G. M. Fuller, "A New dark matter candidate: Nonthermal sterile neutrinos," *Phys. Rev. Lett.* **82** (1999) 2832–2835, arXiv:astro-ph/9810076.

[611] K. Abazajian, G. M. Fuller, and M. Patel, "Sterile neutrino hot, warm, and cold dark matter," *Phys. Rev. D* **64** (2001) 023501, arXiv:astro-ph/0101524.

[612] T. Asaka, M. Laine, and M. Shaposhnikov, "Lightest sterile neutrino abundance within the nuMSM," *JHEP* **01** (2007) 091, arXiv:hep-ph/0612182. [Erratum: JHEP 02, 028 (2015)].

[613] M. Laine and M. Shaposhnikov, "Sterile neutrino dark matter as a consequence of nuMSM-induced lepton asymmetry," *JCAP* **06** (2008) 031, arXiv:0804.4543 [hep-ph].

[614] E. K. Akhmedov, V. A. Rubakov, and A. Y. Smirnov, "Baryogenesis via neutrino oscillations," *Phys. Rev. Lett.* **81** (1998) 1359–1362, arXiv:hep-ph/9803255.

[615] J. Liu and G. Segre, "Reexamination of generation of baryon and lepton number asymmetries by heavy particle decay," *Phys. Rev. D* **48** (1993) 4609–4612, arXiv:hep-ph/9304241.

[616] M. Flanz, E. A. Paschos, and U. Sarkar, "Baryogenesis from a lepton asymmetric universe," *Phys. Lett. B* **345** (1995) 248–252, arXiv:hep-ph/9411366. [Erratum: Phys.Lett.B 384, 487–487 (1996), Erratum: Phys.Lett.B 382, 447–447 (1996)].

[617] M. Flanz, E. A. Paschos, U. Sarkar, and J. Weiss, "Baryogenesis through mixing of heavy Majorana neutrinos," *Phys. Lett. B* **389** (1996) 693–699, arXiv:hep-ph/9607310.

[618] L. Covi, E. Roulet, and F. Vissani, "CP violating decays in leptogenesis scenarios," *Phys. Lett. B* **384** (1996) 169–174, arXiv:hep-ph/9605319.

[619] L. Covi and E. Roulet, "Baryogenesis from mixed particle decays," *Phys. Lett. B* **399** (1997) 113–118, arXiv:hep-ph/9611425.

[620] A. Pilaftsis, "CP violation and baryogenesis due to heavy Majorana neutrinos," *Phys. Rev. D* **56** (1997) 5431–5451, arXiv:hep-ph/9707235.

[621] A. Pilaftsis, "Resonant CP violation induced by particle mixing in transition amplitudes," *Nucl. Phys. B* **504** (1997) 61–107, arXiv:hep-ph/9702393.

[622] A. Pilaftsis, "Heavy Majorana neutrinos and baryogenesis," *Int. J. Mod. Phys. A* **14** (1999) 1811–1858, arXiv:hep-ph/9812256.

[623] W. Buchmuller and M. Plumacher, "CP asymmetry in Majorana neutrino decays," *Phys. Lett. B* **431** (1998) 354–362, arXiv:hep-ph/9710460.

[624] A. Pilaftsis and T. E. J. Underwood, "Resonant leptogenesis," *Nucl. Phys. B* **692** (2004) 303–345, arXiv:hep-ph/0309342.

[625] A. Pilaftsis and T. E. J. Underwood, "Electroweak-scale resonant leptogenesis," *Phys. Rev. D* **72** (2005) 113001, arXiv:hep-ph/0506107.

[626] S. Davidson and A. Ibarra, "A Lower bound on the right-handed neutrino mass from leptogenesis," *Phys. Lett. B* **535** (2002) 25–32, arXiv:hep-ph/0202239.

[627] J. Klarić, M. Shaposhnikov, and I. Timiryasov, "Uniting Low-Scale Leptogenesis Mechanisms," *Phys. Rev. Lett.* **127** (2021) no. 11, 111802, arXiv:2008.13771 [hep-ph].

[628] J. Klarić, M. Shaposhnikov, and I. Timiryasov, "Reconciling resonant leptogenesis and baryogenesis via neutrino oscillations," *Phys. Rev. D* **104** (2021) no. 5, 055010, arXiv:2103.16545 [hep-ph].

[629] M. Drewes, Y. Georis, and J. Klarić, "Mapping the Viable Parameter Space for Testable Leptogenesis," *Phys. Rev. Lett.* **128** (2022) no. 5, 051801, arXiv:2106.16226 [hep-ph].

[630] R. Abela, M. Daum, G. H. Eaton, R. Frosch, B. Jost, P. R. Kettle, and E. Steiner, "Search for an Admixture of Heavy Neutrino in Pion Decay," *Phys. Lett. B* **105** (1981) 263–266. [Erratum: Phys.Lett.B 106, 513 (1981)].

[631] T. Yamazaki *et al.*, "Search for Heavy Neutrinos in Kaon Decay," *Conf. Proc. C* **840719** (1984) 262.

[632] A. G. Vaitaitis, *Search for neutral heavy leptons in a high-energy neutrino beam*. PhD thesis, Columbia U., 2000.

[633] **CMS** Collaboration, A. Tumasyan *et al.*, "Search for long-lived heavy neutral leptons with displaced vertices in proton-proton collisions at $\sqrt{s}$ =13 TeV," *JHEP* **07** (2022) 081, arXiv:2201.05578 [hep-ex].

[634] N. Sabti, A. Magalich, and A. Filimonova, "An Extended Analysis of Heavy Neutral Leptons during Big Bang Nucleosynthesis," *JCAP* **11** (2020) 056, arXiv:2006.07387 [hep-ph].

[635] E. Izaguirre and B. Shuve, "Multilepton and Lepton Jet Probes of Sub-Weak-Scale Right-Handed Neutrinos," *Phys. Rev. D* **91** (2015) no. 9, 093010, arXiv:1504.02470 [hep-ph].

[636] A. Das, P. Konar, and A. Thalapillil, "Jet substructure shedding light on heavy Majorana neutrinos at the LHC," *JHEP* **02** (2018) 083, arXiv:1709.09712 [hep-ph].

[637] S. Pascoli, R. Ruiz, and C. Weiland, "Heavy neutrinos with dynamic jet vetoes: multilepton searches at $\sqrt{s} = 14$, 27, and 100 TeV," *JHEP* **06** (2019) 049, arXiv:1812.08750 [hep-ph].

[638] M. Drewes and J. Hajer, "Heavy Neutrinos in displaced vertex searches at the LHC and HL-LHC," *JHEP* **20** (2019) 070, arXiv:1903.06100 [hep-ph].

[639] M. Drewes, J. Hajer, J. Klaric, and G. Lanfranchi, "NA62 sensitivity to heavy neutral leptons in the low scale seesaw model," *JHEP* **07** (2018) 105, arXiv:1801.04207 [hep-ph].

[640] **FASER** Collaboration, A. Ariga *et al.*, "FASER's physics reach for long-lived particles," *Phys. Rev. D* **99** (2019) no. 9, 095011, arXiv:1811.12522 [hep-ph].

[641] D. Gorbunov, I. Krasnov, Y. Kudenko, and S. Suvorov, "Heavy Neutral Leptons from kaon decays in the SHiP experiment," *Phys. Lett. B* **810** (2020) 135817, arXiv:2004.07974 [hep-ph].

[642] S. Antusch, E. Cazzato, M. Drewes, O. Fischer, B. Garbrecht, D. Gueter, and J. Klaric, "Probing Leptogenesis at Future Colliders," *JHEP* **09** (2018) 124, arXiv:1710.03744 [hep-ph].

[643] S. Antusch, E. Cazzato, and O. Fischer, "Sterile neutrino searches at future e^-e^+, pp, and e^-p colliders," *Int. J. Mod. Phys. A* **32** (2017) no. 14, 1750078, arXiv:1612.02728 [hep-ph].

[644] It can also be produced by other mechanisms if the νMSM is extended, e.g. with Higgs inflation [744].

[645] T. Asaka, M. Laine, and M. Shaposhnikov, "On the hadronic contribution to sterile neutrino production," *JHEP* **06** (2006) 053, arXiv:hep-ph/0605209.

[646] T. Venumadhav, F.-Y. Cyr-Racine, K. N. Abazajian, and C. M. Hirata, "Sterile neutrino dark matter: Weak interactions in the strong coupling epoch," *Phys. Rev. D* **94** (2016) no. 4, 043515, arXiv:1507.06655 [astro-ph.CO].

[647] J. Ghiglieri and M. Laine, "Improved determination of sterile neutrino dark matter spectrum," *JHEP* **11** (2015) 171, arXiv:1506.06752 [hep-ph].

[648] J. Ghiglieri and M. Laine, "Sterile neutrino dark matter via GeV-scale leptogenesis?," *JHEP* **07** (2019) 078, arXiv:1905.08814 [hep-ph].

[649] J. Ghiglieri and M. Laine, "Sterile neutrino dark matter via coinciding resonances," *JCAP* **07** (2020) 012, arXiv:2004.10766 [hep-ph].

[650] D. Bodeker and A. Klaus, "Sterile neutrino dark matter: Impact of active-neutrino opacities," *JHEP* **07** (2020) 218, arXiv:2005.03039 [hep-ph].

[651] L. Canetti, M. Drewes, and M. Shaposhnikov, "Sterile Neutrinos as the Origin of Dark and Baryonic Matter," *Phys. Rev. Lett.* **110** (2013) no. 6, 061801, arXiv:1204.3902 [hep-ph].

[652] M. Nemevsek, G. Senjanovic, and Y. Zhang, "Warm Dark Matter in Low Scale Left-Right Theory," *JCAP* **07** (2012) 006, arXiv:1205.0844 [hep-ph].

[653] M. Nemevšek and Y. Zhang, "Anatomy of diluted dark matter in the minimal left-right symmetric model," *Phys. Rev. D* **109** (2024) no. 5, 056021, arXiv:2312.00129 [hep-ph].

[654] S. S. Biswal and P. S. B. Dev, "Probing left-right seesaw models using beam polarization at an e^+e^- collider," *Phys. Rev. D* **95** (2017) no. 11, 115031, arXiv:1701.08751 [hep-ph].

[655] K. A. Urquía-Calderón, "Long-lived heavy neutral leptons at lepton colliders as a probe of left-right-symmetric models," *Phys. Rev. D* **109** (2024) no. 5, 055002, arXiv:2310.17406 [hep-ph].

[656] X.-K. Wen, B. Yan, Z. Yu, and C. P. Yuan, "Single Transverse Spin Asymmetry as a New Probe of Standard-Model-Effective-Field-Theory Dipole Operators," *Phys. Rev. Lett.* **131** (2023) no. 24, 241801, arXiv:2307.05236 [hep-ph].

[657] J. A. Aguilar-Saavedra, "Laboratory-frame tests of quantum entanglement in H→WW," *Phys. Rev. D* **107** (2023) no. 7, 076016, arXiv:2209.14033 [hep-ph].

[658] A. J. Barr, "Testing Bell inequalities in Higgs boson decays," *Phys. Lett. B* **825** (2022) 136866, arXiv:2106.01377 [hep-ph].

[659] Q. Bi, Q.-H. Cao, K. Cheng, and H. Zhang, "New observables for testing Bell inequalities in W boson pair production," arXiv:2307.14895 [hep-ph].

[660] R. D. Peccei and H. R. Quinn *Phys. Rev. Lett.* **38** (1997) 1440.

[661] S. Weinberg *Phys. Rev. Lett.* **40** (1978) 223.

[662] F. Wilczek *Phys. Rev. Lett.* **40** (1978) 279.

[663] P. Svrcek and E. Witten *JHEP* **06** (2006) 051, hep-th/0605206.

[664] A. Arvanitaki, S. Dimopoulos, S.and Dubovsky, N. Kaloper, and J. March-Russell *PRD* **81** (2010) 123530, arXiv:0905.4720 [hep-ph].

[665] M. Cicoli, M. Goodsell, and A. Goodsell *JHEP* **10** (2012) 146, arXiv:1206.0819 [hep-ph].

[666] P. Arias and et al. *JCAP* **06** (2012) 013, arXiv:1201.5902 [hep-ph].

[667] H.-Y. Zhang, C.-X. Yue, Y.-C. Guo, and S. Yang, "Searching for axion-like particles at future electron-positron colliders," *PRD* **104** (2021) 096008, arXiv:2103.05218 [hep-ph].

[668] H.-Y. Zhang, C.-X. Yue, Y.-C. Guo, and S. Yang, "Searching for axionlike particles at future electron-positron colliders," *Phys. Rev. D* **104** (2021) no. 9, 096008, arXiv:2103.05218 [hep-ph].

[669] K. Cheung and C. J. Ouseph, "Axionlike particle search at Higgs factories," *Phys. Rev. D* **108** (2023) no. 3, 035003, arXiv:2303.16514 [hep-ph].

[670] W. Altmannshofer, J. A. Dror, and S. Gori, "New Opportunities for Detecting Axion-Lepton Interactions," *Phys. Rev. Lett.* **130** (2023) no. 24, 241801, arXiv:2209.00665 [hep-ph].

[671] C.-T. Lu, "Lighting Electroweak-Violating ALP-Lepton Interactions at e^+e^- and ep Colliders," arXiv:2210.15648 [hep-ph].

[672] C. D. Roberts, D. G. Richards, T. Horn, and L. Chang, "Insights into the emergence of mass from studies of pion and kaon structure," *Prog. Part. Nucl. Phys.* **120** (2021) 103883, arXiv:2102.01765 [hep-ph].

[673] M. Ding, C. D. Roberts, and S. M. Schmidt, "Emergence of Hadron Mass and Structure," *Particles* **6** (2023) 57–120, arXiv:2211.07763 [hep-ph].

[674] D. Binosi, "Emergent Hadron Mass in Strong Dynamics," *Few Body Syst.* **63** (2022) no. 2, 42, arXiv:2203.00942 [hep-ph].

[675] M. N. Ferreira and J. Papavassiliou, "Gauge Sector Dynamics in QCD," *Particles* **6** (2023) no. 1, 312–363, arXiv:2301.02314 [hep-ph].

[676] Z.-F. Cui, J.-L. Zhang, D. Binosi, F. de Soto, C. Mezrag, J. Papavassiliou, C. D. Roberts, J. Rodríguez-Quintero, J. Segovia, and S. Zafeiropoulos, "Effective charge from lattice QCD," *Chin. Phys. C* **44** (2020) no. 8, 083102, arXiv:1912.08232 [hep-ph].

[677] A. Deur, S. J. Brodsky, and C. D. Roberts, "QCD Running Couplings and Effective Charges," arXiv:2303.00723 [hep-ph].

[678] Z.-Q. Yao, D. Binosi, Z.-F. Cui, and C. D. Roberts, "Semileptonic transitions: $B(s)ßπ(K); DsßK; DßπK; and Kßπ$," *Phys. Lett. B* **824** (2022) 136793, arXiv:2111.06473 [hep-ph].

[679] Z.-Q. Yao, D. Binosi, Z.-F. Cui, and C. D. Roberts, "Semileptonic $B_c \to \eta_c, J/\psi$ transitions," *Phys. Lett. B* **818** (2021) 136344, arXiv:2104.10261 [hep-ph].

[680] T. Aoyama *et al.*, "The anomalous magnetic moment of the muon in the Standard Model," *Phys. Rept.* **887** (2020) 1–166, arXiv:2006.04822 [hep-ph].

[681] D. Hanneke, S. Fogwell, and G. Gabrielse, "New Measurement of the Electron Magnetic Moment and the Fine Structure Constant," *Phys. Rev. Lett.* **100** (2008) 120801, arXiv:0801.1134 [physics.atom-ph].

[682] L. Morel, Z. Yao, P. Cladé, and S. Guellati-Khélifa, "Determination of the fine-structure constant with an accuracy of 81 parts per trillion," *Nature* **588** (2020) no. 7836, 61–65.

[683] S. Borsanyi *et al.*, "Leading hadronic contribution to the muon magnetic moment from lattice QCD," *Nature* **593** (2021) no. 7857, 51–55, arXiv:2002.12347 [hep-lat].

[684] **RBC, UKQCD** Collaboration, T. Blum, P. A. Boyle, V. Gülpers, T. Izubuchi, L. Jin, C. Jung, A. Jüttner, C. Lehner, A. Portelli, and J. T. Tsang, "Calculation of the hadronic vacuum polarization contribution to the muon anomalous magnetic moment," *Phys. Rev. Lett.* **121** (2018) no. 2, 022003, arXiv:1801.07224 [hep-lat].

[685] H. Wittig, "Progress on $(g-2)_\mu$ from Lattice QCD," in *57th Rencontres de Moriond on Electroweak Interactions and Unified Theories*. 6, 2023. arXiv:2306.04165 [hep-ph].

[686] P. Athron, C. Balázs, D. H. J. Jacob, W. Kotlarski, D. Stöckinger, and H. Stöckinger-Kim, "New physics explanations of a_μ in light of the FNAL muon g − 2 measurement," *JHEP* **09** (2021) 080, arXiv:2104.03691 [hep-ph].

[687] **GAMBIT** Collaboration, P. Athron *et al.*, "Combined collider constraints on neutralinos and charginos," *Eur. Phys. J. C* **79** (2019) no. 5, 395, arXiv:1809.02097 [hep-ph].

[688] A. Crivellin, D. Mueller, and F. Saturnino, "Correlating h→μ+μ- to the Anomalous Magnetic Moment of the Muon via Leptoquarks," *Phys. Rev. Lett.* **127** (2021) no. 2, 021801, arXiv:2008.02643 [hep-ph].

[689] F. Wang, W. Wang, and J. M. Yang, "Solving the muon g-2 anomaly in deflected anomaly mediated SUSY breaking with messenger-matter interactions," *Phys. Rev. D* **96** (2017) no. 7, 075025, arXiv:1703.10894 [hep-ph].

[690] X. Ning and F. Wang, "Solving the muon g-2 anomaly within the NMSSM from generalized deflected AMSB," *JHEP* **08** (2017) 089, arXiv:1704.05079 [hep-ph].

[691] X. Du and F. Wang, "NMSSM From Alternative Deflection in Generalized Deflected Anomaly Mediated SUSY Breaking," *Eur. Phys. J. C* **78** (2018) no. 5, 431, arXiv:1710.06105 [hep-ph].

[692] X. K. Du, Z. Li, F. Wang, and Y. K. Zhang, "The muon g−2 anomaly in EOGM with adjoint messengers," *Nucl. Phys. B* **989** (2023) 116151, arXiv:2204.04286 [hep-ph].

[693] S. Akula and P. Nath, "Gluino-driven radiative breaking, Higgs boson mass, muon g-2, and the Higgs diphoton decay in supergravity unification," *Phys. Rev. D* **87** (2013) no. 11, 115022, arXiv:1304.5526 [hep-ph].

[694] Z. Li, G.-L. Liu, F. Wang, J. M. Yang, and Y. Zhang, "Gluino-SUGRA scenarios in light of FNAL muon g – 2 anomaly," *JHEP* **12** (2021) 219, arXiv:2106.04466 [hep-ph].

[695] S. Li, Z. Li, F. Wang, and J. M. Yang, "Explanation of electron and muon g−2 anomalies in AMSB," *Nucl. Phys. B* **983** (2022) 115927, arXiv:2205.15153 [hep-ph].

[696] W. Bernreuther, U. Low, J. P. Ma, and O. Nachtmann, "CP Violation and Z Boson Decays," *Z. Phys. C* **43** (1989) 117.

[697] M. J. Booth, "The Electric dipole moment of the W and electron in the Standard Model," arXiv:hep-ph/9301293.

[698] Y. Yamaguchi and N. Yamanaka, "Quark level and hadronic contributions to the electric dipole moment of charged leptons in the standard model," *Phys. Rev. D* **103** (2021) no. 1, 013001, arXiv:2006.00281 [hep-ph].

[699] **Belle** Collaboration, K. Inami *et al.*, "Search for the electric dipole moment of the tau lepton," *Phys. Lett. B* **551** (2003) 16–26, arXiv:hep-ex/0210066.

[700] **Belle-II** Collaboration, L. Aggarwal *et al.*, "Snowmass White Paper: Belle II physics reach and plans for the next decade and beyond," arXiv:2207.06307 [hep-ex].

[701] J. Bernabeu, G. A. Gonzalez-Sprinberg, and J. Vidal, "Normal and transverse single tau polarization at the Z peak," *Phys. Lett. B* **326** (1994) 168–174.

[702] U. Stiegler, "On the magnetic moment in Z —> tau tau," *Z. Phys. C* **57** (1993) 511–514.

[703] A. Stahl, "Physics with tau leptons," *Springer Tracts Mod. Phys.* **160** (2000) 1–316.

[704] **ALEPH** Collaboration, A. Heister *et al.*, "Search for anomalous weak dipole moments of the tau lepton," *Eur. Phys. J. C* **30** (2003) 291–304, arXiv:hep-ex/0209066.

[705] W. Lohmann, "Electromagnetic and weak moments of the tau-lepton," *Nucl. Phys. B Proc. Suppl.* **144** (2005) 122–127, arXiv:hep-ex/0501065.

[706] W. Bernreuther, L. Chen, and O. Nachtmann, "Electric dipole moment of the tau lepton revisited," *Phys. Rev. D* **103** (2021) no. 9, 096011, arXiv:2101.08071 [hep-ph].

[707] D. Atwood and A. Soni, "Analysis for magnetic moment and electric dipole moment form-factors of the top quark via e+ e- —> t anti-t," *Phys. Rev. D* **45** (1992) 2405–2413.

[708] M. Davier, L. Duflot, F. Le Diberder, and A. Rouge, "The Optimal method for the measurement of tau polarization," *Phys. Lett. B* **306** (1993) 411–417.

[709] M. Diehl and O. Nachtmann, "Optimal observables for the measurement of three gauge boson couplings in e+ e- —> W+ W-," *Z. Phys. C* **62** (1994) 397–412.

[710] P. Poulose and S. D. Rindani, "CP violating dipole form-factors of the top quark and τ lepton in scalar leptoquark models," *Pramana* **51** (1998) 387–403, arXiv:hep-ph/9708332.

[711] T. Huang, W. Lu, and Z.-j. Tao, "Search for nonstandard model CP/T violation at tau charm factory," *Phys. Rev. D* **55** (1997) 1643–1652, arXiv:hep-ph/9609220.

[712] A. Einstein, B. Podolsky, and N. Rosen, "Can quantum mechanical description of physical reality be considered complete?," *Phys. Rev.* **47** (1935) 777–780.

[713] D. Bohm and Y. Aharonov, "Discussion of Experimental Proof for the Paradox of Einstein, Rosen, and Podolsky," *Phys. Rev.* **108** (1957) 1070–1076.

[714] J. S. Bell, "On the Einstein-Podolsky-Rosen paradox," *Physics Physique Fizika* **1** (1964) 195–200.

[715] K. Ma and T. Li, "Testing Bell inequality through $h \to \tau\tau$ at CEPC," *Chinese Phys. C* (2024) .

[716] N. A. Tornqvist, "Suggestion for Einstein-podolsky-rosen Experiments Using Reactions Like $e^+e^- \to \Lambda\bar{\Lambda} \to \pi^- p \pi^+ \bar{p}$," *Found. Phys.* **11** (1981) 171–177.

[717] J. F. Clauser, M. A. Horne, A. Shimony, and R. A. Holt, "Proposed experiment to test local hidden variable theories," *Phys. Rev. Lett.* **23** (1969) 880–884.

[718] R. A. Morales, "Tripartite entanglement and Bell non-locality in loop-induced Higgs boson decays," *Eur. Phys. J. C* **84** (2024) no. 6, 581, arXiv:2403.18023 [hep-ph].

[719] Y. Koide, "Fermion - Boson Two-body Model of Quarks and Leptons and Cabibbo Mixing," *Lett. Nuovo Cim.* **34** (1982) 201.

[720] Y. Koide, "A Fermion - Boson Composite Model of Quarks and Leptons," *Phys. Lett. B* **120** (1983) 161–165.

[721] Y. Koide, "A New View of Quark and Lepton Mass Hierarchy," *Phys. Rev. D* **28** (1983) 252.

[722] **Particle Data Group** Collaboration, R. L. Workman *et al.*, "Review of Particle Physics," *PTEP* **2022** (2022) 083C01.

[723] **Belle-II** Collaboration, I. Adachi *et al.*, "Measurement of the τ-lepton mass with the Belle II experiment," *Phys. Rev. D* **108** (2023) no. 3, 032006, arXiv:2305.19116 [hep-ex].

[724] C. D. Froggatt and H. B. Nielsen, "Hierarchy of Quark Masses, Cabibbo Angles and CP Violation," *Nucl. Phys. B* **147** (1979) 277–298.

[725] Y. Koide, "Charged lepton mass sum rule from U(3) family Higgs potential model," *Mod. Phys. Lett. A* **5** (1990) 2319–2324.

[726] Y. Koide, "Charged Lepton Mass Relations in a Supersymmetric Yukawaon Model," *Phys. Rev. D* **79** (2009) 033009, arXiv:0811.3470 [hep-ph].

[727] Y. Koide and T. Yamashita, "Charged Lepton Mass Relations in a SUSY Scenario," *Phys. Lett. B* **787** (2018) 171–174, arXiv:1805.09533 [hep-ph].

[728] Z. Liang and Z. Sun, "A modified version of the Koide formula from flavor nonets in a scalar potential model and in a Yukawaon model," *Nucl. Phys. B* **972** (2021) 115546, arXiv:2007.05878 [hep-ph].

[729] T. Appelquist and J. Carazzone, "Infrared Singularities and Massive Fields," *Phys. Rev. D* **11** (1975) 2856.

[730] W. Buchmuller and D. Wyler, "Effective Lagrangian Analysis of New Interactions and Flavor Conservation," *Nucl. Phys.* **B268** (1986) 621–653.

[731] B. Grzadkowski, M. Iskrzynski, M. Misiak, and J. Rosiek, "Dimension-Six Terms in the Standard Model Lagrangian," *JHEP* **10** (2010) 085, arXiv:1008.4884 [hep-ph].

[732] A. Falkowski and A. Falkowski, "Higgs Basis: Proposal for an EFT basis choice for LHC HXSWG,". https://cds.cern.ch/record/2001958.

[733] S. Chai, J. Gu, and L. Li, "From optimal observables to machine learning: an effective-field-theory analysis of $e^+e^- \to W^+W^-$ at future lepton colliders," *JHEP* **05** (2024) 292, arXiv:2401.02474 [hep-ph].

[734] J. de Blas, Y. Du, C. Grojean, J. Gu, V. Miralles, M. E. Peskin, J. Tian, M. Vos, and E. Vryonidou, "Global SMEFT Fits at Future Colliders," in *Snowmass 2021*. 6, 2022. arXiv:2206.08326 [hep-ph].

[735] Y. Du and J.-H. Yu, "Neutrino non-standard interactions meet precision measurements of N_{eff}," *JHEP* **05** (2021) 058, arXiv:2101.10475 [hep-ph].

[736] Y. Du, "Neff as a new physics probe in the precision era of cosmology," *Phys. Rev. D* **110** (2024) no. 5, 055030, arXiv:2310.10034 [hep-ph].

[737] **ALEPH, DELPHI, L3, OPAL, SLD, LEP Electroweak Working Group, SLD Electroweak Group, SLD Heavy Flavour Group** Collaboration, S. Schael *et al.*, "Precision electroweak measurements on the Z resonance," *Phys. Rept.* **427** (2006) 257–454, arXiv:hep-ex/0509008 [hep-ex].

[738] N. Chen, T. Han, S. Su, W. Su, and Y. Wu, "Type-II 2HDM under the Precision Measurements at the Z-pole and a Higgs Factory," *JHEP* **03** (2019) 023, arXiv:1808.02037 [hep-ph].

[739] H. Li, H. Song, S. Su, W. Su, and J. M. Yang, "MSSM at future Higgs factories," *Chin. Phys. C* **45** (2021) no. 4, 045106, arXiv:2010.09782 [hep-ph].

[740] **GAMBIT** Collaboration, P. Athron *et al.*, "GAMBIT: The Global and Modular Beyond-the-Standard-Model Inference Tool," *Eur. Phys. J. C* **77** (2017) no. 11, 784, arXiv:1705.07908 [hep-ph]. [Addendum: Eur.Phys.J.C 78, 98 (2018)].

[741] **GAMBIT** Collaboration, P. Athron *et al.*, "Global fits of GUT-scale SUSY models with GAMBIT," *Eur. Phys. J. C* **77** (2017) no. 12, 824, arXiv:1705.07935 [hep-ph].

[742] **GAMBIT** Collaboration, P. Athron *et al.*, "A global fit of the MSSM with GAMBIT," *Eur. Phys. J. C* **77** (2017) no. 12, 879, arXiv:1705.07917 [hep-ph].

[743] A. Arbey, M. Battaglia, A. Djouadi, F. Mahmoudi, M. Muhlleitner, and M. Spira, "Higgs boson properties and supersymmetry: Constraints and sensitivity from the LHC to an e+e- collider," *Phys. Rev. D* **106** (2022) no. 5, 055002, arXiv:2201.00070 [hep-ph].

[744] F. L. Bezrukov and M. Shaposhnikov, "The Standard Model Higgs boson as the inflaton," *Phys. Lett. B* **659** (2008) 703–706, arXiv:0710.3755 [hep-th].